AD NUMBER

AD846668

LIMITATION CHANGES

TO:

Approved for public release; distribution is unlimited.

FROM:

Distribution authorized to U.S. Gov't. agencies and their contractors; Critical Technology; SEP 1968. Other requests shall be referred to Air Force Materials Laboratory, Wright-Patterson AFB, 45433. This document contains export-controlled technical data.

AUTHORITY

AFML per DTIC form 55

AFML-TR-68-309

STUDY OF GRINDING PROCESS AS APPLIED TO HIGH-STRENGTH AND THERMAL-RESISTANT ALLOYS

K. Okamura, T. Nakajima, N. DesRuisseaux, J. Lemon
D. Brown, J. Gerhardt, R. Snoeys
UNIVERSITY OF CINCINNATI

TECHNICAL REPORT AFML-TR-68-309

October 1968

Air Force Materials Laboratory
Air Force Systems Command
Wright-Patterson Air Force Base, Ohio

NOTICES

When U.S. Government drawings, specifications, or other data are used for any purpose other than a definitely related Government procurement operation, the Government thereby incurs no responsibility nor any obligation whatsoever; and the fact that the Government may have formulated, furnished, or in any way supplied the said drawings, specifications, or other data is not to be regarded by implication or otherwise, as in any manner licensing the holder or any other person or corporation, or conveying any rights or permission to manufacture, use, or sell any patented invention that may in any way be related thereto.

DDC release to CFSTI not authorized. The distribution of this report is limited because it contains technology identifiable with items on the strategic embargo lists excluded from export or re-export under U.S. Export Control Act of 1949 (63 STAT. 7), as amended (50 U.S.C. App. 2020, 2031), as implemented by AFR 400-10.

Qualified requesters may obtain copies from Defense Documentation Center, Cameron Station, Alexandria, Virginia 22314. Orders will be expedited if placed through the librarian or other person designated to request documents from DDC.

Copies of this report should not be returned to the Research and Technology Division unless return is required by security considerations, contractual obligations, or notice on a specific document.

This document is subject to special export controls and each transmittal to foreign governments or foreign nationals may be made only with prior approval of the Manufacturing Technology Division, MATF, Air Force Materials Laboratory, Wright-Patterson Air Force Base, Ohio 45433.

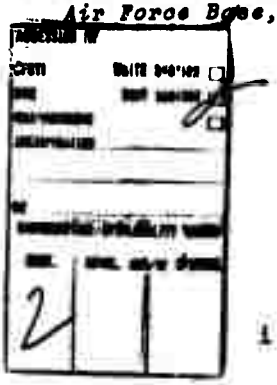

Blank Page

FOREWORD

This Final Technical Report covers the work performed under Contract AF33(615)-5412 from 1 July 1966 to 30 September 1968. The manuscript was released by the authors in September 1968 for publication.

This contract with the University of Cincinnati, Cincinnati, Ohio was initiated under the Manufacturing Methods Project 9-711, "Study of Grinding Process as Applied to High-Strength and Thermal-Resistance Alloys". The work has been accomplished under the technical direction of Mr. E. Smith, Mr. F.L. Whitney, and Mr. M. Guenther of the Advanced Fabrication Techniques Branch (MATF), Manufacturing Technology Division, Air Force Materials Laboratory, Wright-Patterson Air Force Base, Ohio.

The following investigators have been assigned to this project: Dr. K. Okamura, Visiting Professor; Dr. J.R. Lemon, Associate Professor; Dr. R. Snoeys, Visiting Professor; Dr. R. Zerkle, Associate Professor; Mr. T. Nakajima and Dr. N. DesRuisseaux, Junior Research Associates; and Mr. D. Brown and Mr. J. Gerhardt, Research Assistants.

Metallurgical tests were conducted by Metcut Research Associates, 3980 Rosslyn Drive, Cincinnati, Ohio 45209.

This project has been accomplished as part of the Air Force Manufacturing Methods Program, the primary objective of which is to develop, on a timely basis, manufacturing processes, techniques and equipment for use in economical production of USAF materials and components.

Your comments are solicited on the potential utilization of the information contained herein as applied to your present and/or future production programs. Suggestions concerning additional manufacturing methods development required on this or other subjects will be appreciated.

This technical report has been reviewed and is approved.

Jack R. Marsh

JACK R. MARSH, Chief
Advanced Fabrication Techniques Branch
Manufacturing Technology Division

ABSTRACT

This project is engaged in a program which is directed towards the study of the basic understanding of the grinding process as applied to high-strength thermal-resistant alloys. Analytical methods and testing and specification techniques have been developed that should enable significant improvements in grinding efficiency and finished surface integrity to be accomplished.

Grinding is an extremely complex process with many interrelated phenomena occurring simultaneously. For this reason an attempt is made to look at all aspects of grinding processes with the wheel-work interaction analysis taken as the basic standpoint for all of the analyses. The group of investigators is organized from many specialists in various technologies such as manufacturing, heat transfer, metallurgy and vibration.

The chip formation mechanism in the grinding process has been clarified and the relationship between working conditions and grinding results are discussed from a scientific viewpoint.

Thermal analyses have been presented which can be used to investigate the heat effect upon the finished surface.

A set of scientific grinding wheel characteristics have been defined such that a better understanding of the grinding process when used as a cutting operation can be gained.

The machine tool-grinding system has been investigated using vibrational analysis techniques to determine the effects of machine dynamics and to improve the grinding efficiency for HSTRA materials.

In conclusion, new high efficiency grinding techniques which yield extremely high production rates for grinding HSTRA materials have been recommended from this study.

TABLE OF CONTENTS

TABLE OF CONTENTS (Continued)

TABLE OF CONTENTS (Continued)

TABLE OF CONTENTS (Continued)

TABLE OF CONTENTS (Continued)

TABLE OF CONTENTS (Continued)

TABLE OF CONTENTS (Continued)

LIST OF ILLUSTRATIONS

LIST OF ILLUSTRATIONS (Continued)

LIST OF ILLUSTRATIONS (Continued)

LIST OF ILLUSTRATIONS (Continued)

LIST OF ILLUSTRATIONS (Continued)

LIST OF ILLUSTRATIONS (Continued)

LIST OF ILLUSTRATIONS (Continued)

LIST OF ILLUSTRATIONS (Continued)

LIST OF ILLUSTRATIONS (Continued)

LIST OF ILLUSTRATIONS (Continued)

LIST OF TABLES

LIST OF TABLES (Continued)

Blank Page

INTRODUCTION

The following is the FINAL TECHNICAL REPORT on a "Study of Grinding Process as Applied to High-Strength and Thermal-Resistant Alloys" and covers the work performed under Contract No. AF33(615)-5412 from 1 July to 30 September 1968. In this final report the results of the work performed for the purpose of finding techniques to grind high-strength and thermal-resistant alloys (HSTRA) with high efficiency and good finished surface integrity are summarized and improvements of HSTRA grinding are clearly indicated.

Data and theories have been presented in detail in the six interim engineering progress reports.

Each interim report has been divided into nine sections. The results on a specific subject for a reporting period have been described under the same section number of each interim report. In this reporting system it is convenient to follow the development of progress on a specific subject in each interim report.

In the final report all results of this contract work are divided into eight sections. The subject matter appears, in some cases, under a different section number than was used in the interim reports. The purpose of this reorganization is to provide better continuity and more logical relationships between the interrelated sections.

In Section I the fundamental policy and method of study under this contract are outlined. The purpose and organization

of the areas of investigation and the interrelation between each section are generally described.

In Section II the analysis of wheel-work interaction, which is one of the most important basic considerations, is summarized. The following are presented: the theoretical and experimental analyses on rubbing and ploughing in transitional cutting operation, the cutting model used to analyze the grinding mechanism, the geometrical analysis of wheel-work conformity, and the contact stiffness consideration where the relation between chip formation mechanism and finished surface integrity are analyzed.

In Section III thermal analysis of the effect of cooling is presented. Furthermore, relations are developed which indicate the effect of temperature occurring on the surface being ground to the surface which remains after grinding.

In Section IV grinding wheel characteristics are discussed. Several physical properties of grinding wheels are described based on the consideration of scientific grinding wheel characteristics. Furthermore, new dressing methods for obtaining optimum cutting edges for high efficiency grinding are presented.

In Section V dynamic characteristics of grinding systems are described. New vibration theories for the grinding process are summarized. The stiffness of several grinders and the relation between the stiffness and grinding results are discussed.

In Section VI the application of the fundamental theories to HSTRA grinding are reported. Practical grinding for HSTRA materials are carried out. The grinding conditions are

selected considering the fundamental analysis and the inputs which essentially affect the wheel-work interaction are studied.

In Section VII new recommended high efficiency grinding processes are proposed. The background for the recommended grinding and the improvement predicted by the new recommended high efficiency grinding are discussed. Furthermore, the difficulties of applying the recommended high efficiency grinding are considered.

General conclusions obtained from the efforts under this contract are summarized in Section VIII.

SECTION I

GENERAL DESCRIPTION

I.1 Introduction

The main purpose of this contract is to conduct HSTRA grinding development. The specific objectives of the program of study outlined in this report are: to fully develop the mechanism of grinding as applied to very high-strength and thermal-resistant alloys within a dynamic machine tool-grinding system; to organize and execute and analytical and experimental program aimed at investigating, controlling and minimizing the detrimental effects of grinding variables on metal removal rate, surface integrity, etc.; and therefrom create criteria which will form the basis for development of significantly improved capabilities and economies in precision grinding of difficult-to-machine materials.

This type of work was started about 15 years ago and much has been written on the subject. At present, HSTRA materials are ground under specifications which came from past reports. For example, titanium alloy (Ti-4A-6V) is ground under the conditions which are shown in Table I-1.

TABLE I-1 - SPECIFICATION OF TITANIUM GRINDING CONDITIONS

Grinding Wheel	A 60 J V
Wheel Speed (fpm)	1500 - 2500
Work Speed (fpm)	50
Infeed Rough (in/pass)	.001
Finish (in/pass)	.0005 max.

Usually the roughness, the accuracy and/or the grinding ratio are checked to obtain the best grinding condition. It is not as difficult to obtain desired surface roughness and accuracy as it is to minimize the production time and to improve the surface integrity of HSTRA grinding.

In most studies on HSTRA grinding to the present time, results have been obtained by changing easily-varied parameters within a range available on a specific grinding machine. Recommendations therefore are based on data obtained within the confinements of the machine in use. Consequently all papers[1-9] which have been published during these fifteen years describe almost the same conclusions. Grinding conditions recommended for HSTRA were as follows see Figure I-1 :

(1) Do reduce wheel speed (V_s)

(2) Do increase work speed (V_w)

Grinding techniques have hardly been improved in spite of much work on grinding because most of the research, not only on HSTRA grinding but also on grinding of conventional steel, has been performed in manner discussed above. The main purpose of production engineering efforts is to increase production efficiency. Over the past ten years cutting speeds in turning have almost doubled while relative cutting speeds in grinding have been almost constant and therefore productivity in grinding has shown little improvement. The reason may not be due to the number of personnel on grinding, but rather the approach of the personnel.

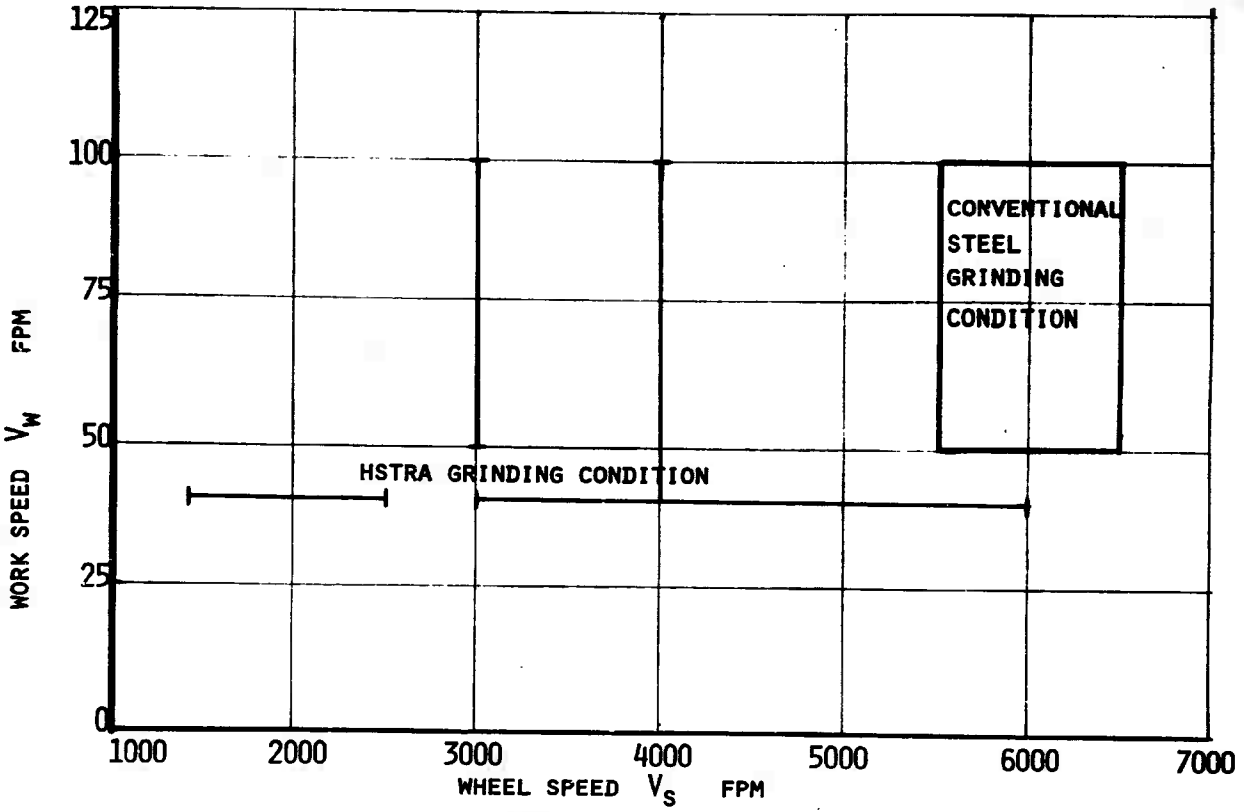

FIGURE I-1 - RECOMMENDED GRINDING CONDITIONS

In order to significantly improve techniques in the field of engineering, optimum conditions for a process should be determined after clearly describing the actual phenomena in the process and the relations between results and input parameters. In other words, the best way to improve a process is to clarify the *mechanisms* of the process. For example in air travel, speeds have been increased substantially in the past half century. The reason is that the understanding of fluid mechanics has been extensively developed.

Under this contract, AF33(615)-5412, the mechanisms of grinding have been developed in order to relate input and output variables in grinding, and indicate the direction of improvement of productivity in HSTRA grinding more clearly than any of the reports published to the present time.

I.2 Basic Consideration of Grinding Process

In order to ascertain the quality of grinding, many kinds of grinding results have been used. However, the relation (wheel-work interaction) between input (working conditions) and output (grinding results) should be discussed in detail to find real grinding results with which grinding efficiency and surface integrity can properly be estimated.

Figure I-2 shows the process for investigating an ideal machining process. All machining processes such as single point tool cutting, milling, grinding, honing and lapping are chip formation processes which possess relative motion

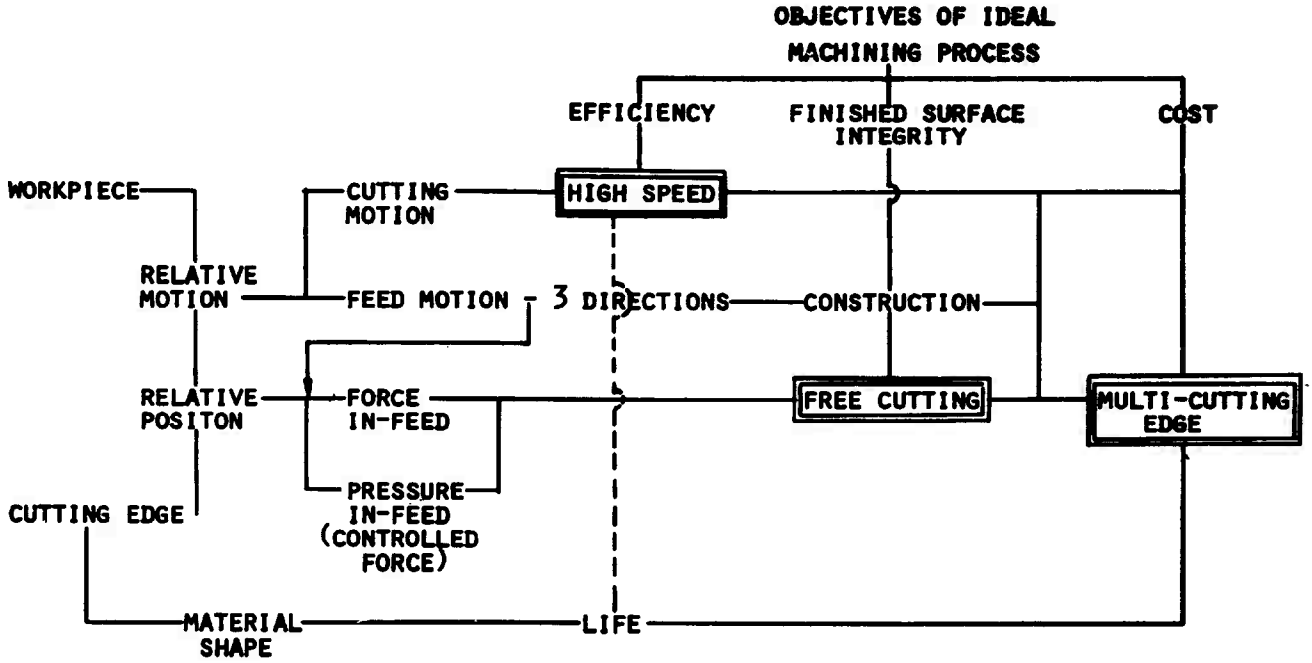

FIGURE I-2 - CONSIDERATION OF IDEAL MACHINING OPERATIONS

between cutting edge and workpiece and have some relative position.

Improvements in machining are aimed at higher efficiency, better surface integrity and lower costs. Therefore an ideal machining process is one in which the operating conditions yield higher efficiency, better surface integrity and lower cost. In other words, an ideal machining process implies free cutting at high cutting speeds with multi-cutting edged tools as can be seen in Figure I-2. The grinding process is operated at the highest cutting speed with the greatest number of cutting edges of all machining processes. It is, however, uncertain whether or not the grinding process is a free cutting operation which yields metal removal without adverse effects upon the finished surface.

Therefore grinding processes should aim at means of obtaining free cutting at high cutting speeds for high efficiency and good surface integrity. It is therefore necessary to determine the chip formation mechanism in the wheel-work interaction zone.

The most difficult problem of conducting grinding studies from above-mentioned point of view is that the boundary conditions (input) are so abundant and so complicated that they have not yet been defined scientifically. For example, the studies on single point tool cutting should be conducted after completely investigating the geometry of the cutting edge. For grinding, the cutting edge conditions are represented by grain material, grain size, grade, bond material, structure of grinding wheel and dressing condition. These values are

not adequate to determine the cutting edge condition, which is one of the basic boundary conditions in wheel-work interaction.

Therefore, the definition for scientific boundary conditions which have a direct relation to the cutting phenomena in wheel-work interference zone is considered instead of the old commercial and expedient input conditions.

First, the basic conditions which influence the wheel-work interaction can be classified into five categories as follows:

1. Cutting edge condition - wheel condition and dressing condition
2. Work material condition
3. Machine tool condition
4. Geometrical condition - working condition
5. Atmospheric condition - grinding fluid

In Figure I-3 , the interrelation between various basic categories and grinding results are shown schematically. These categories are explained abstractly. It is necessary to show the physical quantities which have a direct effect on the grinding results corresponding to these categories. Thus it is necessary to consider the relation between practical grinding conditions and the most basic variables or parameters which can be most directly used to describe the grinding mechanism. These basic variables are obtained from the analytical studies which are presented in the following sections.

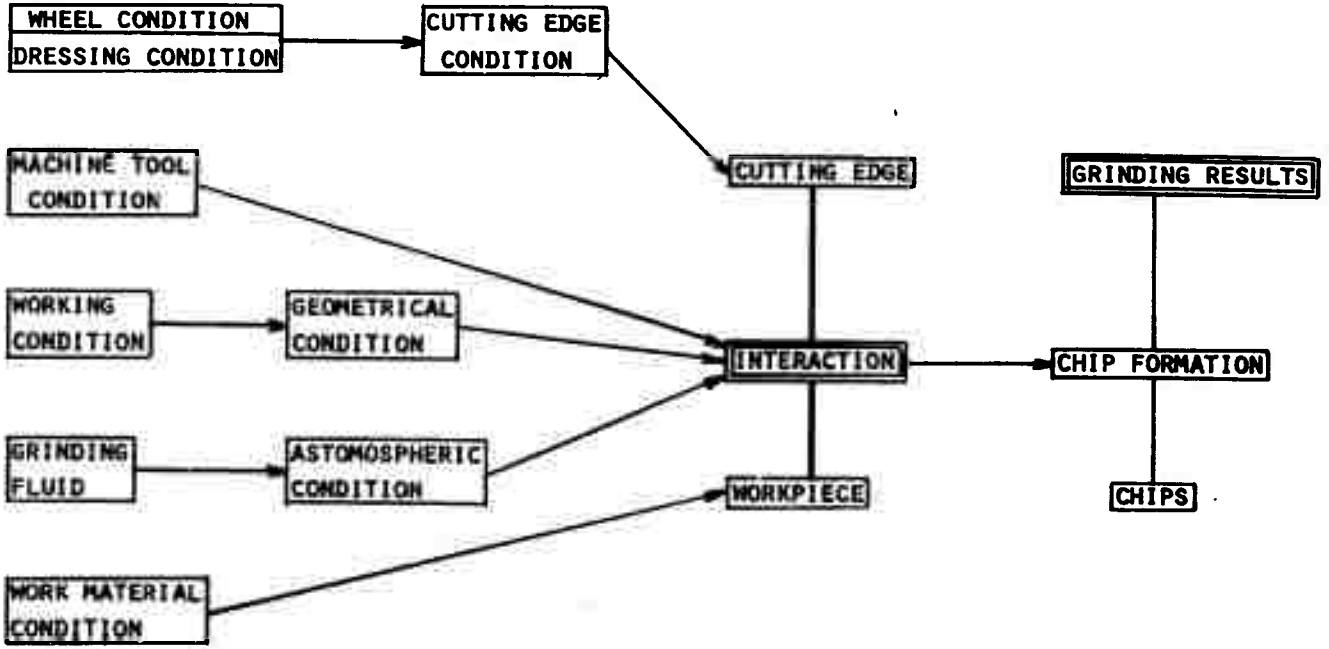

FIGURE I-3 - INTERRELATION BETWEEN VARIOUS BASIC BOUNDARY CONDITIONS AND GRINDING RESULTS

From these considerations, each of the basic categories should be subdivided into a number of physical values as shown in Figure I-4 . It is the purpose of this diagram to clarify the relation between grinding results and each physical parameter of the basic conditions is shown in Figure I-3 . The physical meaning and the influence of each parameter as shown in Figure I-4 will be explained in the following sections.

It is impossible under this contract to describe the effects of all parameters (input) shown in Figure I-4 upon HSTRA grinding. In order to find the best grinding condition for HSTRA materials for the purpose of optimizing efficiency and surface integrity, the efforts under this contract has been conducted with special attention paid to several important parameters which may significantly affect the HSTRA grinding results. The important parameters can be found by simplifying and analyzing important phenomena in the wheel-work interaction.

I.3 Interrelation Between Following Sections

Optimum condition for HSTRA grinding can be found by analyzing the phenomena in wheel-work interference zone and clarifying how the inputs that control the phenomena affect efficiency and surface integrity. For this purpose the work under this contract has been divided into five groups as follows:

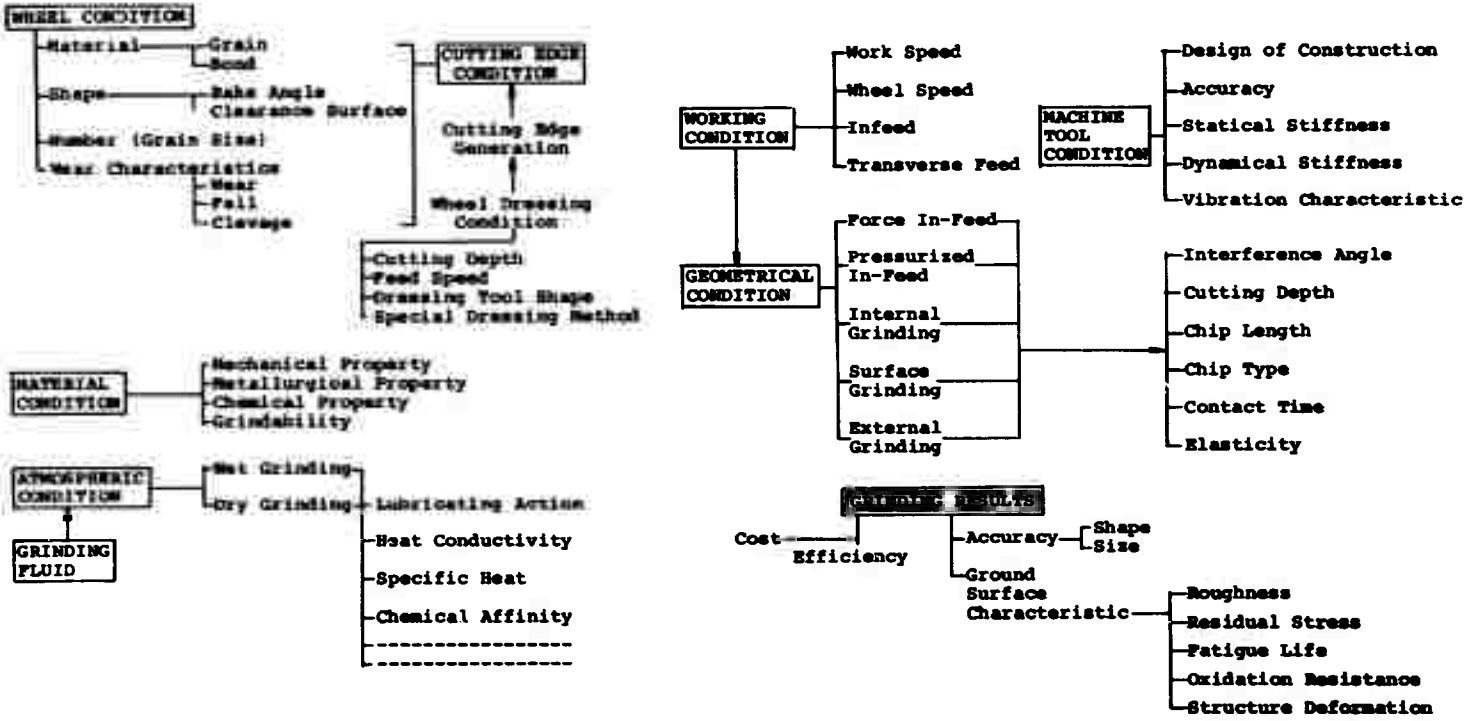

FIGURE I-4 - SUBDIVISIONS OF BASIC BOUNDARY CONDITIONS
(PHYSICAL PARAMETER)

GROUP 1 - CHIP FORMATION PHYSICS:

The purpose of this work is to determine how grinding chips are generated. First, rubbing and ploughing phenomena in transitional cutting have been analyzed with elastic and plastic theory and experimentally verified. These theories have provided information on the difference of the ground surface properties in the elastic, plastic and cutting regions. Next, it has been pointed out that the two dimensional cutting model cannot be applied to an analysis of grinding process. A new cutting model has been proposed in order to clarify the transitional cutting process. Important parameters for analyzing the grinding process have been related to working conditions through geometrical analysis of wheel-work conformity. Furthermore, contact stiffness considerations have been established by combining the elastic and plastic deformation theories with the wheel-work conformity theory. These considerations have laid the foundation for the stock removal rate equation in grinding and described the relation between the chip formation physics and ground surface integrity which traditional theories on cutting mechanisms of abrasive grain have never been able to do. The work in this group is of primary importance in this contract and forms the basis of the recommendation for high efficiency grinding.

GROUP 2 - THERMAL ANALYSIS IN GRINDING:

In any process of generating a chip and forming a new surface, energy must be supplied, part of which is converted

to heat. The heat generated results in high-temperatures which affect finished surface integrity. Thermal analysis of the grinding process includes the determination of the effect of surface cooling on grinding temperatures. Conditions approximating surface grinding and cylindrical plunge grinding are discussed. New considerations presented in this report consider the effect of grinding geometry and temperature in the vicinity of a single grain on the temperature of the workpiece surface which remains after grinding.

GROUP 3 - GRINDING WHEEL CHARACTERISTICS:

The work material (HSTRA) and the grinding wheel characteristics determine the effects of wheel-work interaction. The traditional grinding wheel characteristics which are represented by the five parameters of grain material, grain size, grade, bond material and wheel structure, are convenient for the manufacturers of grinding wheels. However these are not sufficient to indicate the cutting edge conditions which affect the wheel-work interaction. In group 3, grinding wheel characteristics which are essential for the analysis of wheel-work interaction have been described, based upon the wheel wear mechanism. The vibration dressing procedure has been experimentally investigated. The results of the new dressing procedure indicate greatly improved cutting ability and reduced damage.

GROUP 4 - DYNAMIC ANALYSIS IN GRINDING:

The analyses on wheel-work interaction are basic theories which do not consider machine dynamics or gross wheel and work

deformations, and therefore assume that the relative position between the wheel and workpiece is fixed. In practical grinding, the relative position varies cyclically due to dynamic characteristics of the machine tool-work system and therefore the basic boundary condition for the analysis of the grinding process is different from the geometrical one. The dynamic characteristics of a grinding machine should be analyzed in order to better apply high efficiency grinding recommended under this contract. In group 4, a new theory has been developed to analyze the vibration resulting from grinding. The relation between the vibration and grinding results has been discussed theoretically and experimentally.

GROUP 5 - HSTRA GRINDING TESTS

In this group, selection of grinding test conditions with which relations between working conditions and grinding results can be analyzed has been discussed, based upon the theoretical and experimental results of the previous four groups. Consequently a set of standard grinding test conditions has been proposed. HSTRA grinding has been systematically carried out under the standard grinding conditions. Work materials in the grinding tests are HSTRA (titanium Ti-4Al-4V, Rene'41 and Waspalloy) and heat treated 4340 steel.

Figure I-5 schematically shows the interrelation between the groups and clearly indicates work considered and the purpose of the efforts under this contract. The work under this contract also indicates a method to develop and

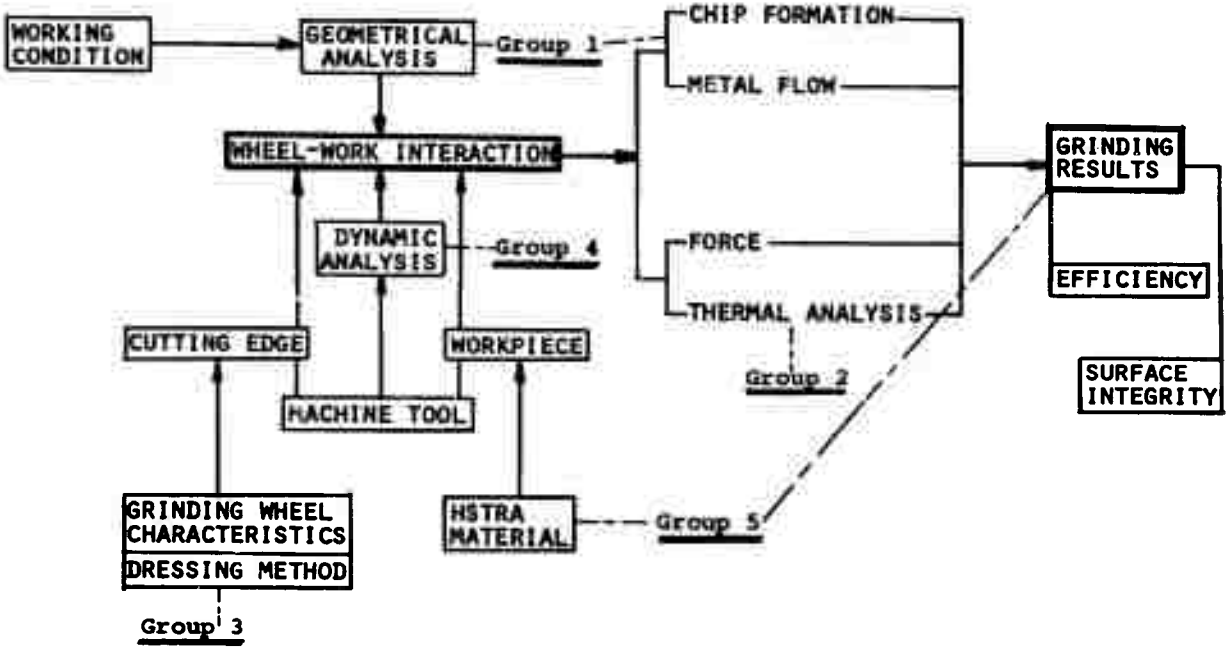

FIGURE I-5 - INTERRELATION BETWEEN RESEARCH TASKS

significantly improve HSTRA grinding. Recommended HSTRA grinding yielding suprisingly high grinding efficiency and good surface integrity is discussed in detail in Section VII.

I.4 Future Development

The fundamental and academic studies performed during the two year duration of this contract have clearly defined the important phenomena of the wheel-work interaction in grinding and indicated how to greatly improve the efficiency of HSTRA grinding. The grinding theories and experimental data under this contract can be further developed in order to provide additional advancement to grinding process technology.

The latest grinding machines and measuring equipment have been utilized at U.C. under this contract. These grinding machines and equipment are, however, not good enough to verify the recommended methods for improving the efficiency and surface integrity in grinding under this contract. If the results of the work under this contract are applied to high efficiency grinders which are being developed in Norton Company, Cincinnati Milling Machine Company, Europe and Japan, significant improvements of HSTRA grinding can be made in the near future.

SECTION II

CHIP FORMATION PHYSICS

II.1 Introduction

All the mechanical machining operations utilize the chip formation process where the relative motion and position between the tool and workpiece produce the chip. Practical development of machining cannot, therefore, be made until the chip formation physics is clearly understood. This is clear from the fact that the two-dimensional cutting theory has played a great role in the analysis of the cutting mechanism for a single cutting edge such as in turning and milling and aided significantly in their development. Most investigations on grinding to the present time has been conducted by varying the easily measurable quantities such as grain size, grade, depth setting and feed rate. This approach has not been significantly useful in developing grinding processes. The reason is that these easily varied parameters are not basic factors which affect the cutting mechanism in grinding. These parameters are more useful for specifying the configuration of the machine or in the manufacture of the grinding wheel. In order to significantly develop grinding, it should be made clear which essential factors affect the cutting mechanism in grinding; that is, what the transfer function is between grinding results (output) and grinding conditions (input) which have a direct effect upon the grinding results.

The following factors describe the grinding operation, but do not apply to two-dimensional cutting:

1. Transitional cutting operation.
2. Cutting edge geometry (multi-cutting edges, large negative rake angle, large contact area as compared with the depth of cut).
3. High cutting velocity
4. Small depth of cut of individual cutting edges.

Due to these differences, grinding is remarkably complicated as compared with conventional machining. In the cutting by an abrasive grain in grinding, the depth of cut increases linearly from zero to a maximum and then decreases to zero. Therefore there are two regions, the elastic and plastic regions, at the beginning of contact between the abrasive grain and workpiece which are very important. In the elastic region the workpiece is only elastically deformed and in the plastic region grooves are produced by plastic deformation without any chip formation. The elastic and plastic regions have a direct effect upon the grinding efficiency and surface integrity and play a very significant role in the formation of the surface even in cases where these two regions are very small as compared with the whole length of contact between cutting edge and workpiece. The metal deformed elastically and plastically at the beginning of contact forms the remaining surface in grinding.

The elastic and plastic regions always exist ahead of the cutting region and therefore the cutting process of each

grain in grinding is transitional. Much grinding work is based upon the assumption that the two-dimensional cutting theory is applicable for each moment that the cutting grain is in contact with the workpiece.

This is incorrect from the standpoint that the complete deformation process is considered to be only a shear phenomenon and does not give any information concerning the surface integrity during grinding. This approach, however, is better than the trial and error approach basically taken when the easily varied parameters are utilized.

In order to significantly develop the grinding process, the chip formation physics should be analyzed from the new viewpoint that the cutting process in grinding is transitional.

In Subsection II.2 deformation processes in transitional cutting operation will be analyzed with elastic and plastic theories and a clear understanding of the significant effects during the transitional cutting processes developed. In Subsection II.3, the deformation theories will be verified experimentally and the differences between the deformation process in each region will be discussed. In Subsection II.4, conformity theory, fundamental for determining what happens during grinding, will be developed, and the manner in which the undeformed chip shape is changed with working conditions such as wheel speed, work speed, and depth setting will be discussed.

The conformity theory will be combined with the deformation theory in Subsection II.5 and the grinding process will be described as the transitional cutting process.

Conclusions obtained in each subsection will be summarized in Subsection II.6 and it will be shown that the chip formation physics approach presented in this report is very useful for developing significant grinding results.

II.2 Deformation Theory

II.2.1 Introduction

The cutting process of an abrasive grain in grinding is transitional. In other words chips are not generated from the beginning of the contact between the workpiece and cutting edge since the cutting edge has a finite mounting spring constant, large contact area and the cutting edge cuts into the workpiece at a very small angle. There are always two regions, elastic and plastic regions, ahead of the cutting region. In the elastic region the cutting edge slides on the surface of workpiece and in the plastic region a groove is produced by plastic deformation without producing a chip. Therefore, there are three completely different deformation processes between the cutting edge and workpiece during contact instead of just the cutting process as often considered. The elastic and plastic regions have a close relationship to the stock removal, wear of the clearance surface of the abrasive grain, induced grinding temperature and/or temperature gradients,

and properties of the ground surface. In order to analyze the cutting process of the abrasive grain from the viewpoint of transitional cutting, the deformation processes in the elastic and plastic regions should be made clear initially.

In this subsection the deformation processes at the beginning of the contact zone where the depth of cut increases linearly from zero, will be analyzed with the elastic and plastic theories. The parameters that affect the transitional cutting process will be determined. In the analysis of elastic deformation, elastic sliding length and critical normal force, under which the workpiece begins to be deformed plastically, will be analyzed as a function of the relative cutting velocity, interference angle, properties of the workpiece (yielding stress) and cutting edge conditions (spring constant and wear area of the clearance surface) based upon the assumption that the deformation under the clearance surface plays a leading role in the elastic region because of its larger wear area as compared with the depth of cut. On the other hand, the effects of the frictional coefficient and the rake angle upon the plastic deformation process will be discussed on the assumption that the deformation under the rake surface plays a leading role in the plastic region. Furthermore, typical results of the elastic and plastic deformation theories and essential factors which affect the transitional cutting will be discussed.

II.2.2 Elastic Deformation Theory

(1) FUNDAMENTAL EQUATIONS

A simplified model for describing an elastic deformation process is shown in Figure II-1. An abrasive grain is considered as a rigid body resiliently mounted with a mounting spring constant k_s and in contact between the clearance surface and the workpiece with a wear width of 2a. The workpiece is considered as a semi-infinite elastic space under the boundary surface. The cutting edge slides over the surface of the workpiece with a relative velocity v and an interference angle i_g to the surface. However, because of the displacement of the workpiece and the cutting edge, the real cut-in angle i_w is smaller than the geometrical angle i_g shown in Figure II-1.

Since the depth of cut is very small in the elastic region, effects of the rake surface are negligible in the analysis of the elastic deformation. From the above considerations , fundamental equations and boundary conditions can be introduced by the theory of elasticity. The dynamic equilibrium equations for a two-dimensional elastic body can be expressed as

$$(\lambda+\mu)\frac{\partial e}{\partial x} + \mu\nabla^2 u - \delta\frac{\partial^2 u}{\partial t^2} = 0$$

$$(\lambda+\mu)\frac{\partial e}{\partial x} + \mu\nabla^2 v - \delta\frac{\partial^2 v}{\partial t^2} = 0 \qquad \text{(II.2.1)}$$

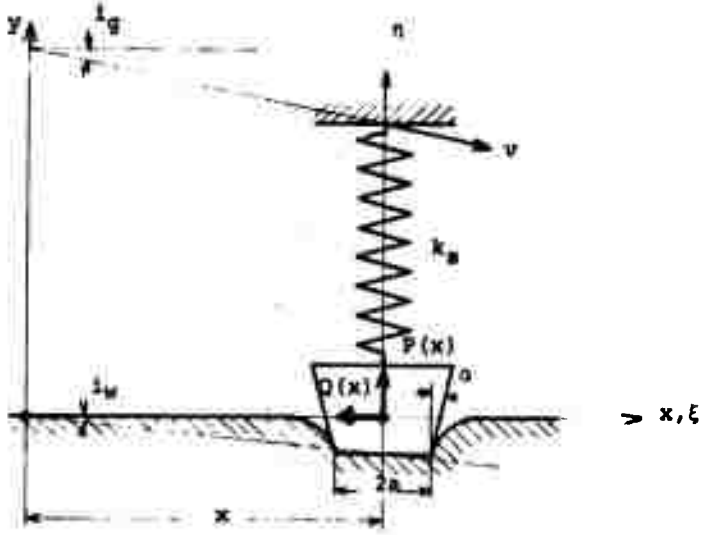

FIGURE II-1 - TWO-DIMENSIONAL ELASTIC CONTACT MODEL

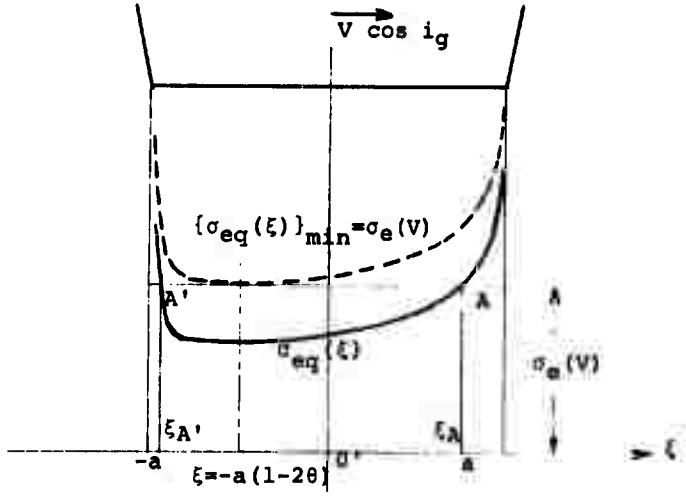

FIGURE II-2 - EQUIVALENT STRESS DISTRIBUTIONS UNDER THE ABRASIVE GRAIN

If the frictional force in the contact region between the cutting edge and the workpiece surface obeys Coulomb's law of friction, the boundary conditions are:

$$\text{(i)}\quad (\sigma_\eta)_{\eta=0} = 0,\ (\tau_{\xi\eta})_{\eta=0} = 0 \quad (-\infty<\xi<-a \text{ and } a<\xi<\infty)$$

$$\text{(ii)}\quad (\tau_{\xi\eta})_{\eta=0} = \rho(\sigma_\eta)_{\eta=0} \quad (-a<\xi<a) \qquad \text{(II.2.2)}$$

(2) CRITICAL NORMAL FORCE IN THE ELASTIC REGION

Now, the condition under which the workpiece surface is elastically deformed below the clearance surface of the cutting edge is investigated. Solving the Equations (II.2.1) so that the boundary conditions (II.2.2) can be satisfied, we find the components of stresses at the surface of workpiece in the form

$$(\sigma_\xi)_{\eta=0} = -\frac{MF-NK}{GN-MH}\cdot\frac{\sin\pi\theta}{\pi}\cdot\frac{P(x)}{(a+\xi)^{\theta}(a-\xi)^{1-\theta}}$$

$$(\delta_\eta)_{\eta=0} = -\frac{\sin\pi\theta}{\pi}\cdot\frac{P(x)}{(a+\xi)^{\theta}(a-\xi)^{1-\theta}}$$

$$(\tau_{\xi\eta})_{\eta=0} = -\rho\frac{\sin\pi\theta}{\pi}\cdot\frac{P(x)}{(a+\xi)^{\theta}(a-\xi)^{1-\theta}} \qquad \text{(II.2.3)}$$

where C, D, G, H, F, K, M, N are constants which can be determined by the cutting velocity, modulus of elasticity and density of the workpiece and θ can be given in the form

$$\theta = \frac{1}{\pi}\tan^{-1}(CN-DM)/\rho(DG-CH) \qquad \text{(II.2.4)}$$

Now, using Tresca's criterion of yielding for the workpiece and assuming that the workpiece is an ideal plastic-elastic

body. The equivalent stress $\sigma_{eq}(\xi)$ is given as a function of ξ only and has the minimum value when $\xi = -a(1-2\theta)$.

$$\sigma_{eq}(\xi) = \frac{\sin \pi\theta}{\pi} \cdot \sqrt{\left(\frac{MF-NK}{GN-MH} - 1\right)^2 + 4\rho^2} \quad \frac{P(x)}{(a+\xi)^{\theta}(a-\xi)^{1-\theta}} \tag{II.2.5}$$

The distribution of the equivalent stress $\sigma_{eq}(\xi)$ with a given normal force P(x) is shown as the solid line in Figure II-2. The expression of the yielding stress of the metal being cut is remarkably influenced by the rate of strain, $\sigma_e(V)$. The metal being cut is deformed plastically in the regions $-a \leq \xi \leq \xi_A'$ and $\xi_A \leq \xi \leq a$ as shown in Figure II-2, where the equivalent stress $\sigma_{eq}(\xi)$ is larger than the yielding stress $\sigma_e(V)$. Now, supposing that the cutting surface of the metal changes from the region of elastic deformation into that of plastic, while the minimum value of the equivalent stress $\{\sigma_{eq}(\xi)\}_{min}$ becomes equal to the yielding stress of the workpiece (see border line in Figure II-2). The critical normal force $P(x_e)$, the point where the workpiece begins to be plastically deformed can be given as

$$P(x_e) = \sigma_e(V) \cdot G(\rho,V) \cdot 2a \tag{II.2.6}$$

where

$$G(\rho,V) = \pi \operatorname{cosec} \pi\theta \cdot g(\theta) \Big/ \sqrt{\left(\frac{MG-NK}{GN-MH} - 1\right)^2 + 4\rho^2}$$

$$g(\theta) = (\theta)^{\theta}(1-\theta)^{1-\theta} \tag{II.2.7}$$

It can be seen that the critical normal force $P(x_e)$ is a function of the cutting velocity V, the properties of workpiece, frictional coefficient ρ and the contact width 2a.

(3) ELASTIC SLIDING LENGTH OF THE CUTTING EDGE ON THE WORKPIECE SURFACE:

The workpiece is only deformed elastically because of the small normal force at the beginning of contact where the depth of cut increases linearly from zero. The metal being cut begins to be deformed plastically when the increasing normal force P(x) caused by the increasing depth of cut becomes equal to the critical normal force $P(x_e)$.

In the following discussion the distance from the beginning of the contact to the critical point, the elastic sliding length x_e, will be analyzed to determine the length of the elastic region.

Displacement v in the y-direction of the workpiece at the surface is given with normal force P(x) acting on the cutting in the equation

$$v = P(x)/J(\rho,V) \qquad \text{(II.2.8)}$$

where

$$\frac{1}{J(\rho,V)} = \frac{1}{\pi E}\left[\ln\left(\frac{2d}{a}\right)^2 - (1+\nu)\right] - 2\rho\,\frac{CH-DG}{GN-MH}$$

$$\frac{d}{a} = 1/\left[1 - \left(2\rho^{-(1+\nu)/2} - 1\right)^2\right]^{1/2} \qquad \text{(II.2.9)}$$

Putting $P(x) = P(x_e)$ in Equation (II.2.8), the depth of cut y_e at the elastic critical point can be given in the form

$$y_e = P(x_e)/J(\rho,V) \qquad \text{(II.2.10)}$$

The displacement Δn_e of the cutting edge at the same point can be expressed as:

$$\Delta n_e = P(x_e)/k_s \qquad \text{(II.2.11)}$$

On the other hand, from the geometrical relations shown in Figure II-1 the following can be obtained:

$$x_e \cdot \tan i_g = y_e + \Delta\eta_e \qquad \text{(II.2.12)}$$

Substituting Equations (II.2.10) and (II.2.11) into the relation (II.2.12) the elastic sliding length of the cutting edge can be determined as:

$$x_e = \frac{k_s + J(\rho,V)}{k_s \cdot J(\rho,V)} \cdot G(\rho,V) \cdot \sigma(V) \cdot 2a \cdot \cot i_g \qquad \text{(II.2.13)}$$

where $J(\rho,V)$, $G(\rho,V)$ and $\sigma_e(V)$ are characteristic values of the workpiece which are determined by cutting velocity and frictional coefficient between the cutting edge and workpiece. Then

$$x_e = f(k,\rho,V) \cdot \frac{2a}{i_g} \qquad \text{(II.2.13')}$$

From this equation it should be noted that the elastic sliding length is proportional to the contact width of cutting edge, 2a, and inversly proportional to the interference angle, i_g.

II.2.3 Typical Results of Elastic Deformation Theory

(1) VALUES OF PARAMETERS IN COMPUTATION OF THE THEORY:

Each equation of the elastic deformation theory in Subsection II.2.2 is so complicated and composed of so many parameters that it is difficult to determine from the equation which factors appreciably affect the elastic deformation region. In order to clearly determine the effect of each parameter upon the critical normal force, the critical depth

of cut and the elastic sliding length; numerical calculation using the elastic deformation theory was performed for titanium (Ti-6Al-4V) and 4340 steel. Values of the parameters used in the calculations of the theory are shown in Table II-1. The constants for the mechanical properties of the workpiece are selected from a conventional table and are, therefore, static values. It should be noted, however, that in grinding the metal is being deformed under very high strain rate temperature, and pressure. Typical trends predicted by the theory will be illustrated and the implications of these trends indicated.

(2) THE EFFECT OF FRICTIONAL COEFFICIENT, CUTTING VELOCITY AND CONTACT WIDTH ON CRITICAL NORMAL FORCE:

Force constants $G(\rho,V)$ which determine the critical normal forces are summarized in Table II-2 for titanium and in Table II-3 for 4340. Figure II-3 shows the effect of the frictional coefficient ρ and the relation of cutting speed V on the critical normal force $P(x_e)$ for titanium and Figure II-4 shows that of ρ and the contact width 2a on $P(x_e)$ for 4340. It should be noted from these tables and figures that the critical normal force decreases significantly with the increase of the frictional coefficient between the cutting edge and workpiece and slightly with the increase of cutting velocity. Furthermore, the critical normal force increases linearly with the increase of contact width. The critical

TABLE II-1 - VALUES OF PARAMETERS IN COMPUTATION

			MATERIAL	
	PARAMETERS	DIMENSION	TITANIUM	4340
E	Young's Modulus	lbs/in^2	1.60×10^7	2.5×10^7
ν	Poison's Ratio	-	0.25	0.3
γ	Density	lbs/in^3	0.15	0.3
$\sigma_e(V)$	Yield Stress	lbs/in^2	1.30×10^5	3.0×10^4
ρ	Frictional Coefficient	-	0, 0.2, 0.4, 0.6, 0.8, 1.0	
V	Cutting Velocity	feet/min	1000, 5000, 10000, 20000, 30000	
2a	Contact Length	in	10^{-4}, $5x10^{-4}$, 10^{-3}, 10^{-2}, $2x10^{-2}$	
i_g	Interference Angle	rad.	$5x10^{-5}$, 10^{-4}, 10^{-3}, 10^{-2}, $2x10^{-2}$	
k	Spring Constant	lbs/in/in	$5x10^5$, 10^6, $5x10^6$, 10^7	

TABLE II-2 - FORCE CONSTANTS $G(\rho,V)$ FOR TITANIUM

	$G(\rho,V)$				
	V			f/min	
	1000	5000	10000	20000	30000
$\rho = 0$	1.5708	1.5705	1.5696	1.5661	1.5601
$\rho = 0.2$	1.4687	1.4684	1.4677	1.4643	1.4595
$\rho = 0.4$	1.2608	1.2606	1.2601	1.2577	1.2538
$\rho = 0.6$	1.0682	1.0680	1.0675	1.0655	1.0621
$\rho = 0.8$	0.9236	0.9234	0.9229	0.9208	0.9173
$\rho = 1.0$	0.8209	0.8207	0.8201	0.8179	0.8140

TABLE II-3 - FORCE CONSTANTS $G(\rho,V)$ FOR 4340

	$G(\rho,V)$				
	V		f/min		
	1000	5000	10000	20000	30000
$\rho = 0$	1.3930	1.3925	1.3912	1.3857	1.3764
$\rho = 0.2$	1.3226	1.3222	1.3210	1.3162	1.3080
$\rho = 0.4$	1.1698	1.1695	1.1686	1.1648	1.1584
$\rho = 0.6$	1.0170	1.0167	1.0159	1.0127	1.0073
$\rho = 0.8$	0.8956	0.8959	0.8946	0.8915	0.8863
$\rho = 1.0$	0.8064	0.8062	0.8053	0.8021	0.7966

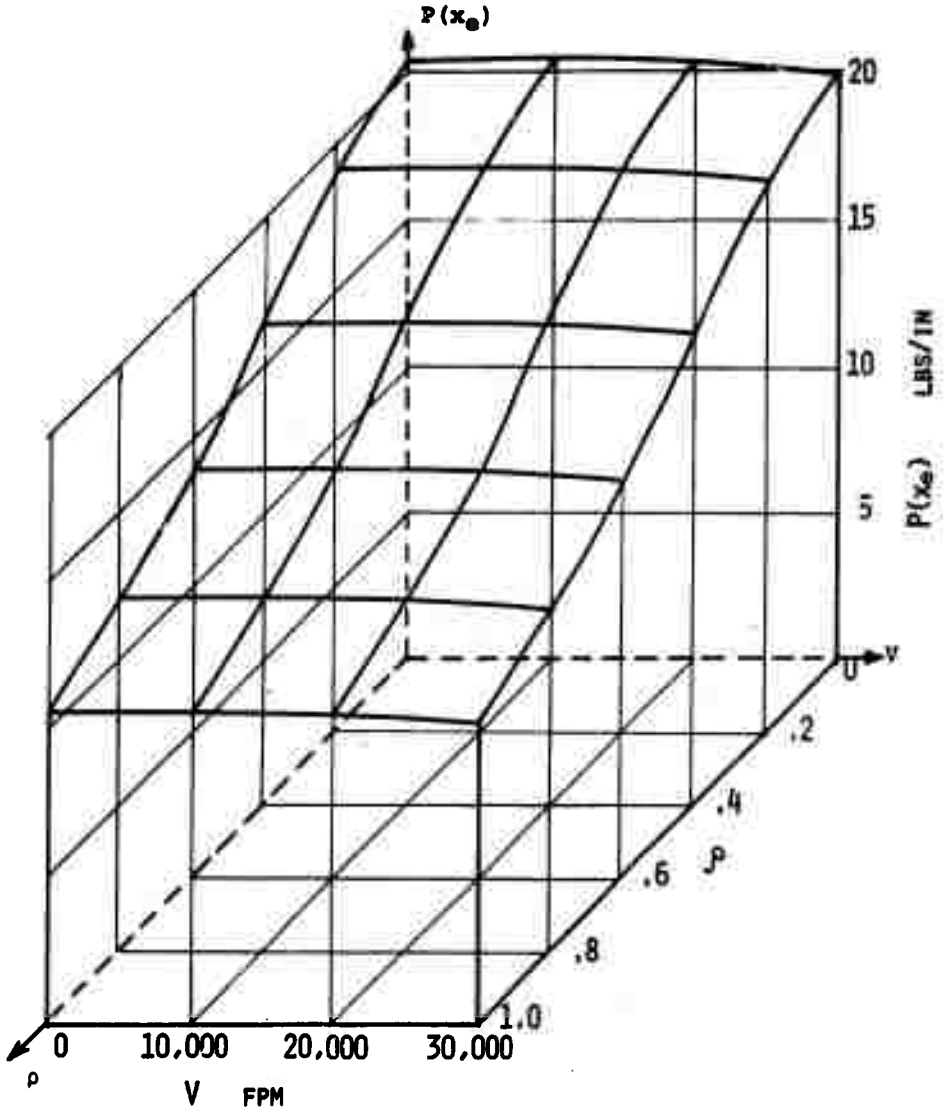

FIGURE II-3 - EFFECTS OF ρ AND V ON $P(x_e)$
FOR TITANIUM ($2a = 10^{-4}$ in.)

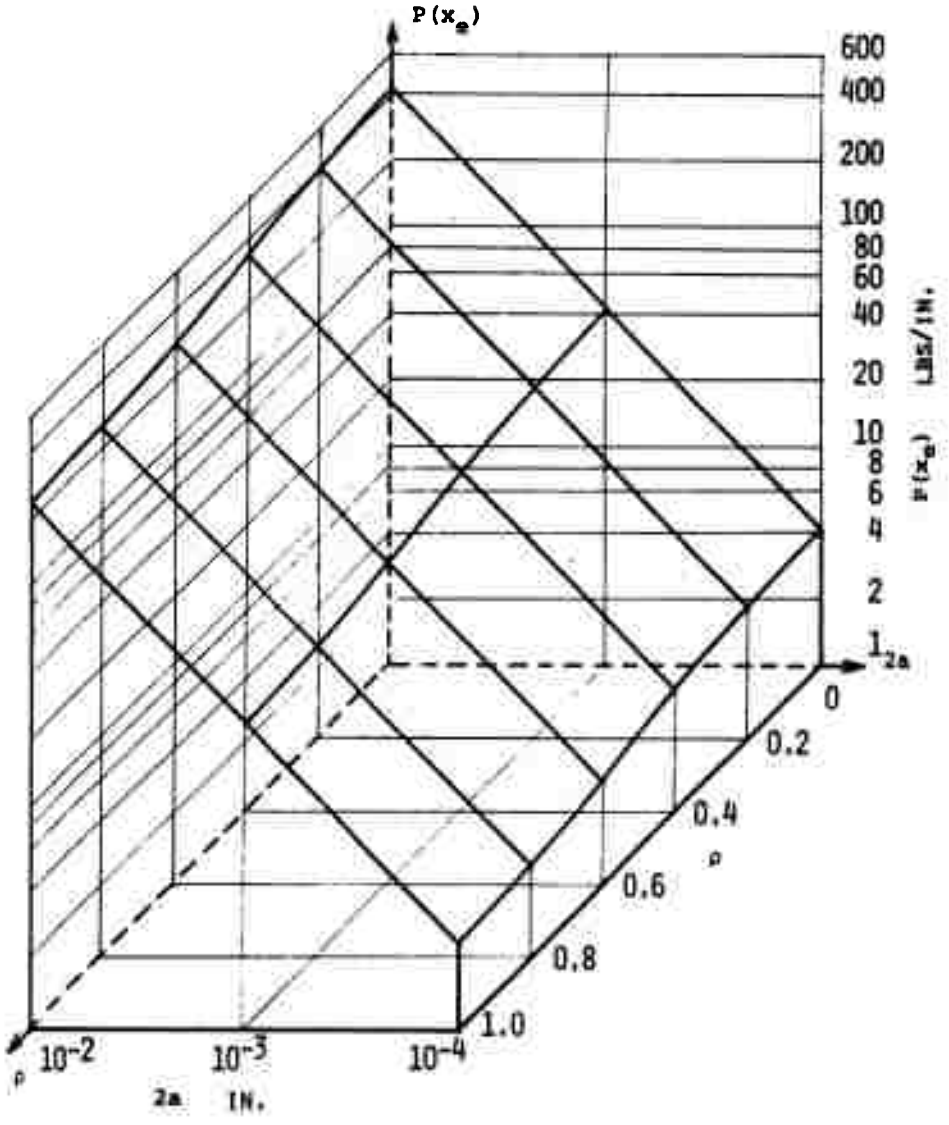

FIGURE II-4 - EFFECTS OF ρ AND 2a ON $P(x_e)$ FOR 4340 (V=5000 f/min)

TABLE II-4 - DEFORMATION CONSTANTS $J(\rho,V)$ FOR TITANIUM

	$J(\rho,V)$ lbs/in^2 x10^7				
	V feet/min				
	1000	5000	10000	20000	30000
$\rho = 0$	35.5786	35.5786	35.5786	35.5786	35.5786
$\rho = 0.2$	4.2295	4.2311	4.2364	4.2577	4.2946
$\rho = 0.4$	2.2484	2.2493	2.2523	2.2644	2.2852
$\rho = 0.6$	1.5312	1.5318	1.5339	1.5423	1.5568
$\rho = 0.8$	1.1609	1.1614	1.1637	1.1694	1.1805
$\rho = 1.0$	0.9348	0.9352	0.9365	0.9417	0.9507

TABLE II-5 - DEFORMATION CONSTANTS $J(\rho,V)$ FOR 4340

	$J(\rho,V)$ lbs/in^2 x10^7				
	V feet/min				
	1000	5000	10000	20000	30000
$\rho = 0$	89.0067	89.0067	89.0067	89.0067	89.0067
$\rho = 0.2$	7.2634	7.2668	7.2774	7.3205	7.3958
$\rho = 0.4$	3.7862	3.7880	3.7938	3.8173	3.8582
$\rho = 0.6$	2.5604	2.5617	2.5656	2.5817	2.6098
$\rho = 0.8$	1.9342	1.9352	1.9382	1.9505	1.9718
$\rho = 1.0$	1.5541	1.5549	1.5573	1.5672	1.5845

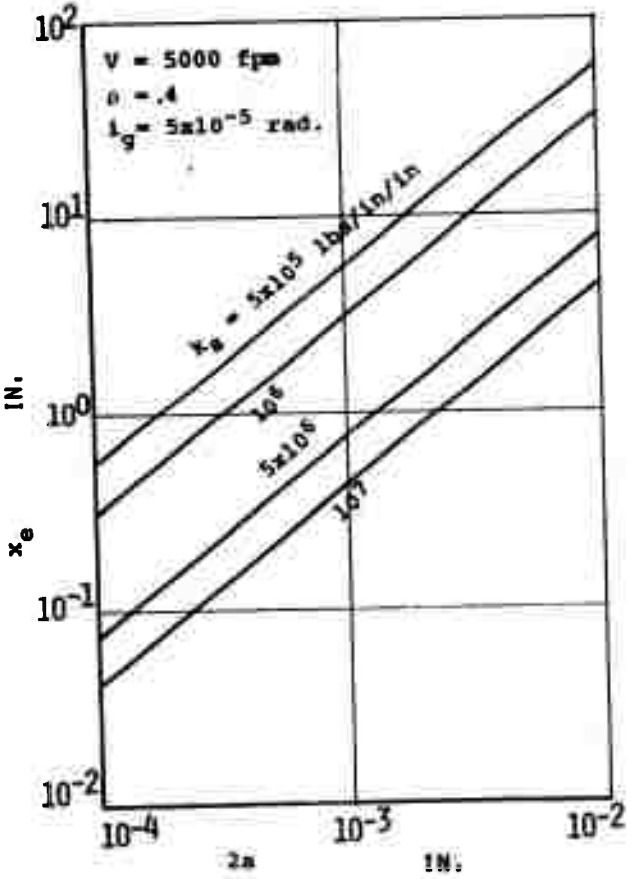

FIGURE II-5 - EFFECTS OF 2a ON x_e FOR TITANIUM

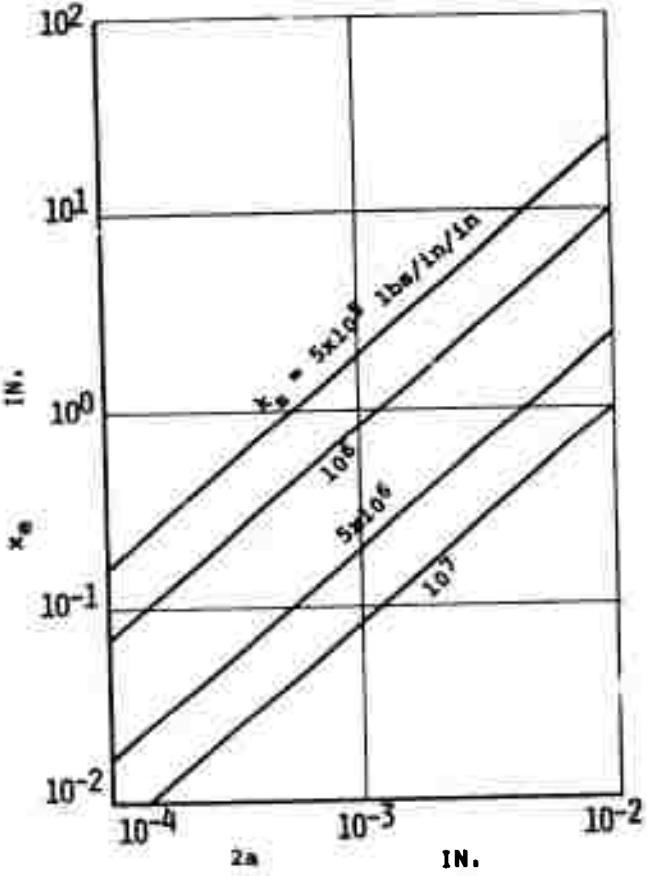

FIGURE II-6 - EFFECTS OF 2a ON x_e FOR 4340

normal force for titanium is about five times as large as that for 4340.

(3) THE EFFECT OF FRICTIONAL COEFFICIENT AND CUTTING VELOCITY ON CRITICAL DEPTH OF CUT:

Deformation constants $J(\rho,V)$ which determine the deformation of workpiece are summarized in Table II-4 for titanium and in Table II-5 for 4340 respectively. These deformation constants correspond to the spring constant of workpiece and indicate the stiffness of workpiece.

It should be noted from these that the spring constant of workpiece becomes slightly stiffer with the increase of cutting velocity and weaker with the increase of frictional coefficient between the cutting edge and workpiece. Therefore the critical depth of cut which can be given as a ratio of the critical normal force to the deformation constant, decreases with increasing cutting velocity and decreasing frictional coefficient.

(4) THE EFFECT OF CONTACT WIDTH ON ELASTIC SLIDING LENGTH:

Figure II-5 and II-6 show the effect of contact width upon the elastic sliding length for titanium and 4340 respectively. It can be seen from these figures that the elastic sliding length of the cutting edge increases linearly with the increase of contact width both for titanium and 4340.

(5) THE EFFECT OF FRICTIONAL COEFFICIENT ON THE ELASTIC SLIDING LENGTH:

As can be seen in Equation (II.2.13), the elastic sliding length is a complicated function of the frictional coefficient. For practical grinding the frictional coefficient between the cutting edge and workpiece will change with different kinds of coolant. As the coolant affects the cutting mechanism of the abrasive grain both physically and chemically, the effect of the coolant on the elastic sliding length cannot be completely understood from the elastic deformation theory. In this paragraph, the physical aspect of the effect of the coolant on the cutting process, that is, the effect of frictional coefficient on the elastic sliding length, is discussed. Figure II-7 shows the effect of frictional coefficient on the elastic sliding length for titanium for the spring constant $k_s = 10^6$ lbs/in/in. It can be easily seen in this figure that the elastic sliding length decreases with the increase of frictional coefficient for any interference angle. Figure II-8 shows the effect of frictional coefficient on the elastic sliding length with a different spring constant for the cutting edge mounting for 4340. It can be seen that the effect of frictional coefficient on the sliding length should be discussed in relation to the spring constant. As seen in Equation (II.2.13), the elastic sliding length is proportional to the value $\frac{k_s+J(\rho,V)}{k_s\ J(\rho,V)}\ G(\rho,V)$. The value $\frac{k_s+J(\rho,V)}{k_s\ J(\rho,V)}$ becomes nearly equal to $1/k_s$ when $k_s \ll J(\rho,V)$ and to $1/J(\rho,V)$ when $k_s \gg J(\rho,V)$.

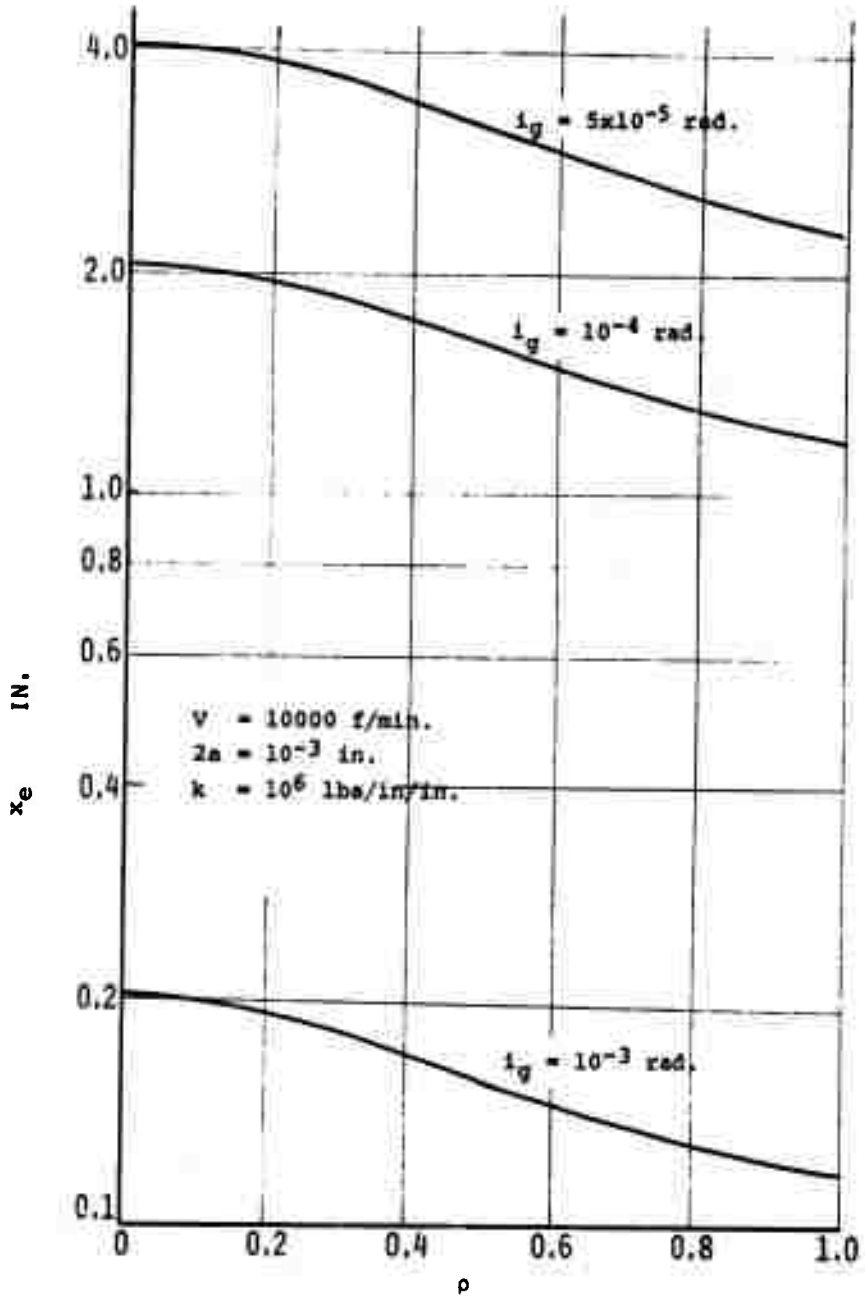

FIGURE II-7 - EFFECTS OF ρ ON x_e FOR TITANIUM

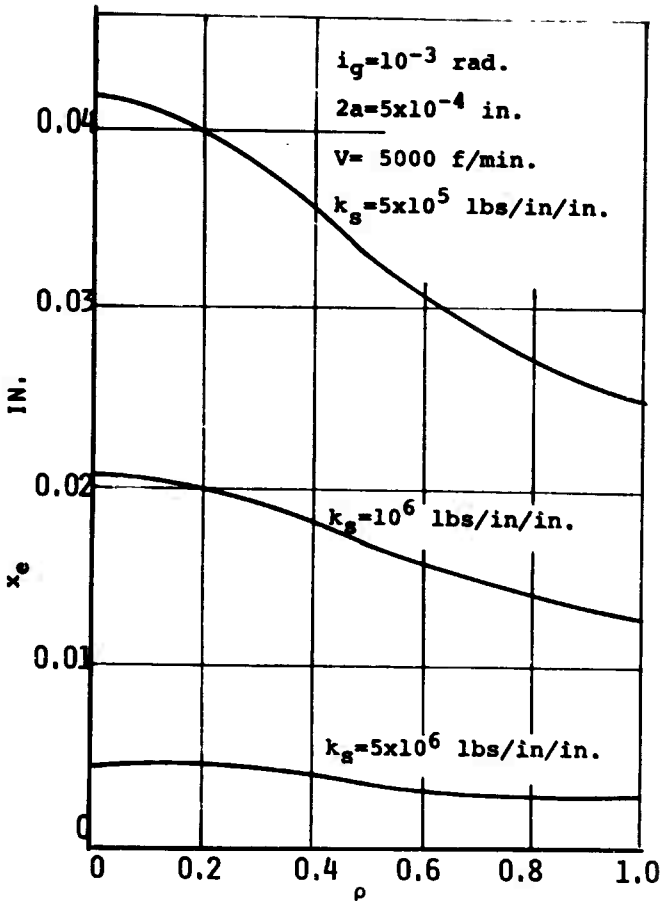

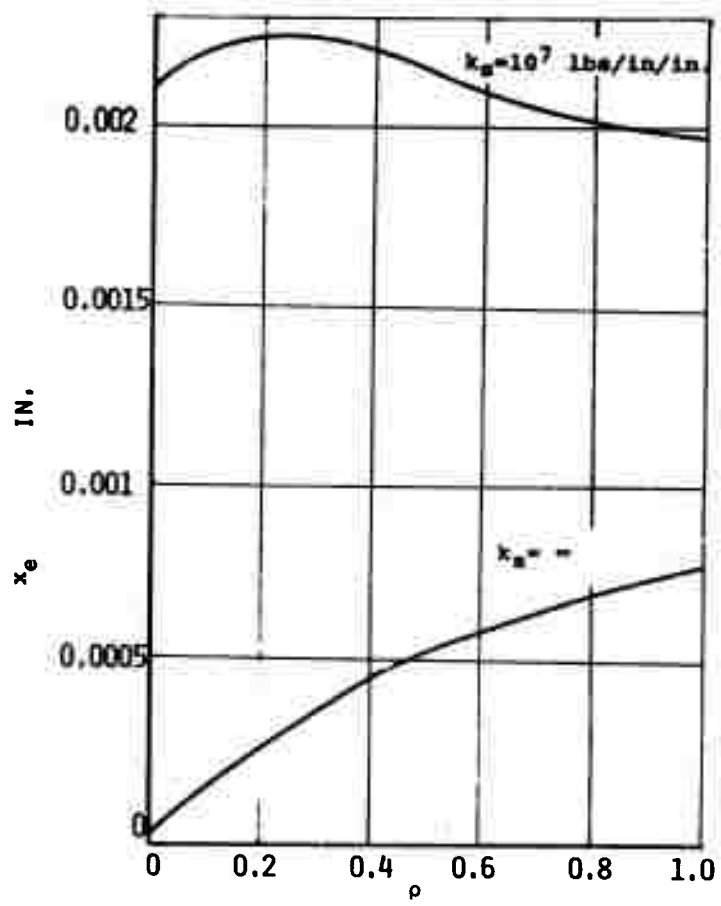

FIGURE II-8 - EFFECTS OF ρ ON x_e WITH DIFFERENT SPRING CONSTANTS FOR 4340

The effect of frictional coefficient on the elastic sliding length is, therefore, controlled by the value $G(\rho,V)/k_s$ when $k_s << J(\rho,V)$ and by the value $G(\rho,V)/J(\rho,V)$ when $k_s >> J(\rho,V)$. As seen in Tables II-4 and II-5, the deformation constant $J(\rho,V)$ is of the order of 10^7 for both titanium and 4340. Therefore, the elastic sliding length decreases simply with the increase of frictional coefficient for small values of the spring constant (example: $k_s = 5 \times 10^5$ and 10^6 lbs/in/in) because the value $G(\rho,V)$ decreases with the increase of frictional coefficient. The elastic sliding length increases simply with the increase of the frictional coefficient for large values of the spring constant because the value $G(\rho,V)/J(\rho,V)$ increases with increasing frictional coefficient.

For spring constants of the same order ($k_s = 10^7$ lbs/in/in) as the value of $J(\rho,V)$, the elastic sliding length becomes a maximum near $\rho = 0.2$.

(6) THE EFFECT OF CUTTING VELOCITY ON THE ELASTIC SLIDING LENGTH:

The effects of cutting velocity on the elastic sliding length are summarized in Tables II-6 and II-7 for titanium and 4340 respectively. As seen in these tables, the effects of cutting velocity on the elastic sliding length are not great because the value of yield stress is taken as a constant, although actually the yield stress is a function of the cutting velocity.

TABLE II-6 - EFFECTS OF v ON x_e FOR TITANIUM

i_g rad.	2a in.	x_e in. V = 1000 f/min	V = 5000 f/min	V = 10000 f/min	V = 20000 f/min	V = 30000 f/min
$5x10^{-5}$	10^{-4}	0.3424	0.3423	0.3422	0.3415	0.3403
	$5x10^{-4}$	1.7120	1.7117	1.7108	1.7073	1.7013
	10^{-3}	3.4239	3.4234	3.4216	3.4146	3.4026
	$5x10^{-3}$	17.1195	17.1167	17.1080	17.0730	17.0130
	10^{-2}	34.2391	34.2335	34.2160	34.1454	34.0260
10^{-4}	10^{-4}	0.1712	0.1712	0.1711	0.1707	0.1701
	$5x10^{-4}$	0.8560	0.8558	0.8554	0.8536	0.8507
	10^{-3}	1.7120	1.7117	1.7108	1.7078	1.7013
	$5x10^{-3}$	8.5598	8.5584	8.5540	8.5363	8.5065
	10^{-2}	17.1195	17.1167	17.1080	17.0730	17.0130
10^{-3}	10^{-4}	0.0171	0.0171	0.0171	0.0171	0.0170
	$5x10^{-4}$	0.0856	0.0856	0.0855	0.0854	0.0851
	10^{-3}	0.1712	0.1712	0.1711	0.1707	0.1701
	$5x10^{-3}$	0.8560	0.8558	0.8554	0.8536	0.8507
	10^{-2}	1.7120	1.7117	1.7108	1.7073	1.7013
10^{-2}	10^{-4}	0.001712	0.001712	0.001711	0.001707	0.001701
	$5x10^{-4}$	0.008559	0.008558	0.008554	0.008536	0.008506
	10^{-3}	0.017120	0.017116	0.017107	0.017072	0.017012
	$5x10^{-3}$	0.085601	0.085580	0.085537	0.085361	0.085062
	10^{-2}	0.171212	0.171160	0.171040	0.170720	0.170124
$2x10^{-2}$	10^{-4}	0.000856	0.000856	0.000855	0.000854	0.000851
	$5x10^{-4}$	0.004279	0.004279	0.004276	0.004268	0.004253
	10^{-3}	0.008559	0.008557	0.008553	0.008535	0.008505
	$5x10^{-3}$	0.042793	0.042786	0.042764	0.042676	0.042527
	10^{-2}	0.085586	0.085572	0.085529	0.085352	0.085054

TABLE II-7 - EFFECTS OF RELATIVE CUTTING SPEED ON SLIDING LENGTH FOR 4340

i_g	2a	X_e in.				
rad.	in.	V = 1000 f/min	V = 5000 f/min	V = 10000 f/min	V = 20000 f/min	V = 30000 f/min
5×10^{-5}	10^{-4}	0.07201	0.07201	0.07196	0.07172	0.07130
	5×10^{-4}	0.36020	0.36011	0.35980	0.35858	0.35652
	10^{-3}	0.72041	0.72021	0.71961	0.71717	0.71303
	5×10^{-3}	3.60203	3.60106	3.59804	3.58585	3.56516
	10^{-2}	7.20406	7.20213	7.19608	7.17169	7.13032
10^{-4}	10^{-4}	0.03602	0.03601	0.03598	0.03586	0.03565
	5×10^{-4}	0.18010	0.18005	0.17990	0.17929	0.17826
	10^{-3}	0.36020	0.36011	0.35980	0.35859	0.35652
	5×10^{-3}	1.80101	1.80053	1.79902	1.79292	1.78258
	10^{-2}	3.60203	3.60106	3.59804	3.58585	3.56516
10^{-3}	10^{-4}	0.00360	0.00360	0.00359	0.00359	0.003565
	5×10^{-4}	0.01801	0.01801	0.01799	0.01793	0.017826
	10^{-3}	0.03602	0.03601	0.03598	0.03586	0.035652
	5×10^{-3}	0.18010	0.18005	0.17990	0.17929	0.178258
	10^{-2}	0.36020	0.36011	0.35980	0.35859	0.356516
10^{-2}	10^{-4}	0,000360	0.000360	0.000359	0.003588	0.000357
	5×10^{-4}	0.001801	0.001800	0.001798	0.001793	0.001783
	10^{-3}	0.003602	0.003601	0.003598	0.003586	0.003565
	5×10^{-3}	0.018010	0.018005	0.017990	0.017929	0.017825
	10^{-2}	0.036019	0.036009	0.035979	0.035853	0.035650
2×10^{-2}	10^{-4}	0.000180	0.000180	0.0001799	0.0001793	0.0001782
	5×10^{-4}	0.000900	0.000900	0.0008994	0.0008963	0.0008912
	10^{-3}	0.001801	0.001800	0.0017991	0.0017930	0.0017823
	5×10^{-3}	0.009004	0.009001	0.0089943	0.0089630	0.0089117
	10^{-2}	0.018008	0.018003	0.0179881	0.0179270	0.0178232

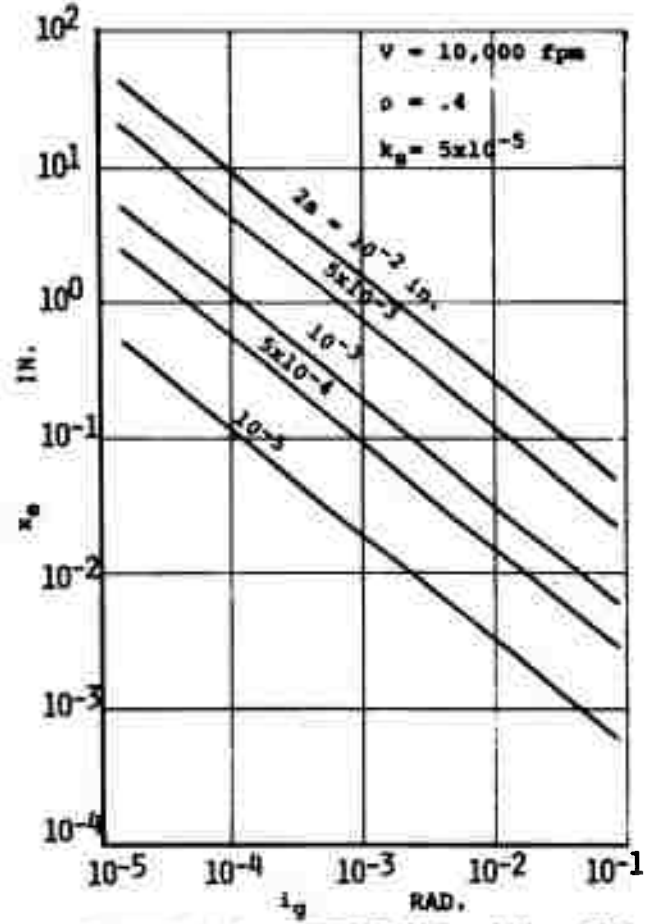

FIGURE II-9 - EFFECTS OF i_g ON x_e FOR TITANIUM

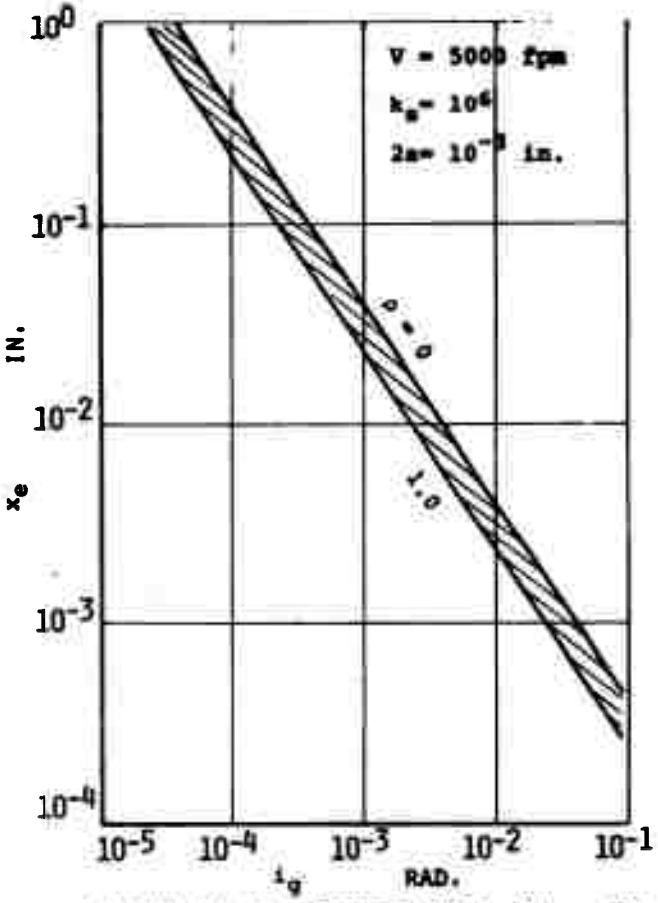

FIGURE II-10 - EFFECTS OF i_g ON x_e FOR 4340

(7) THE EFFECT OF INTERFERENCE ANGLE ON THE ELASTIC SLIDING LENGTH:

Figure II-9 and II-10 show the effects of the interference angle on the elastic sliding length for different values of contact width and frictional coefficient respectively. It should be noted from these figures that the elastic sliding length decreases linearly with the increase of interference angles.

(8) THE EFFECT OF SPRING CONSTANT ON THE ELASTIC SLIDING LENGTH:

Figure II-11 shows the effects of spring constant of the cutting edge mounting on the elastic sliding length for titanium. It can be easily seen that the elastic sliding length decreases with the increase of spring constant, although the slope of the curve decreases with the increase of spring constant.

II.2.4 Plastic Deformation Theory

(1) FUNDAMENTAL EQUATIONS AND BOUNDARY CONDITIONS:

In the analysis of the deformation process in the plastic region the deformation under the rake surface plays a leading role, whereas the deformation under the clearance surface was important in the analysis of the elastic region. Therefore only the deformation under the rake surface will be considered in the plastic region, as is shown in Figure II-12.

There are two stages in plastic deformation process under the rake surface for the model of a cutting edge with

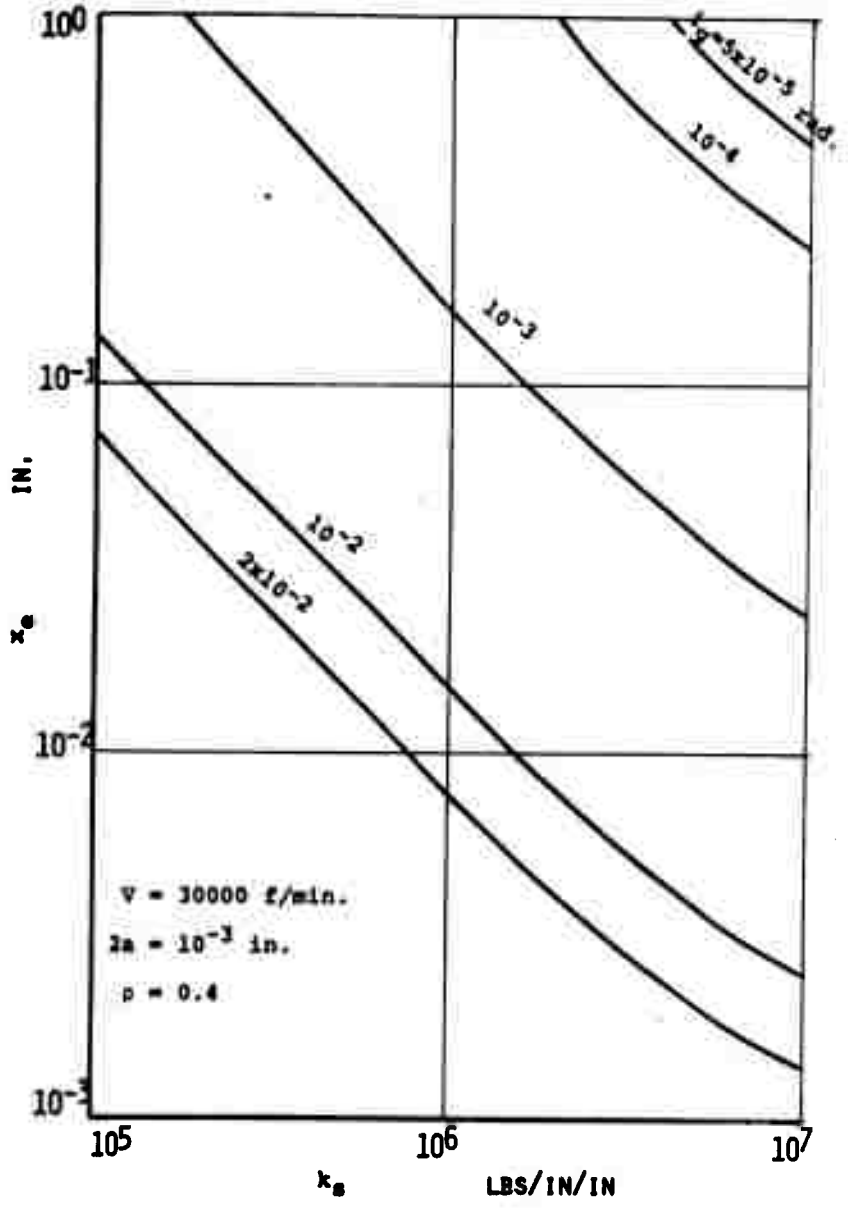

FIGURE II-11 - EFFECTS OF k_s ON x_e FOR TITANIUM

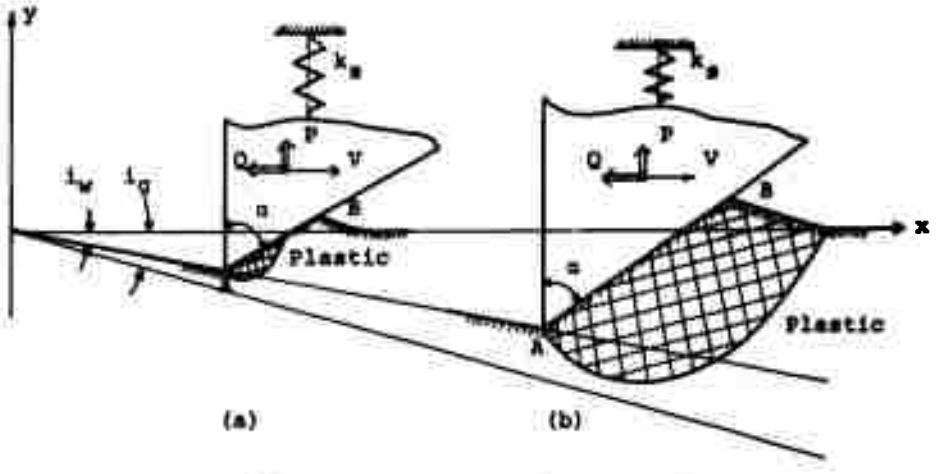

FIGURE II-12 - MODEL OF PLASTIC DEFORMATION PROCESS

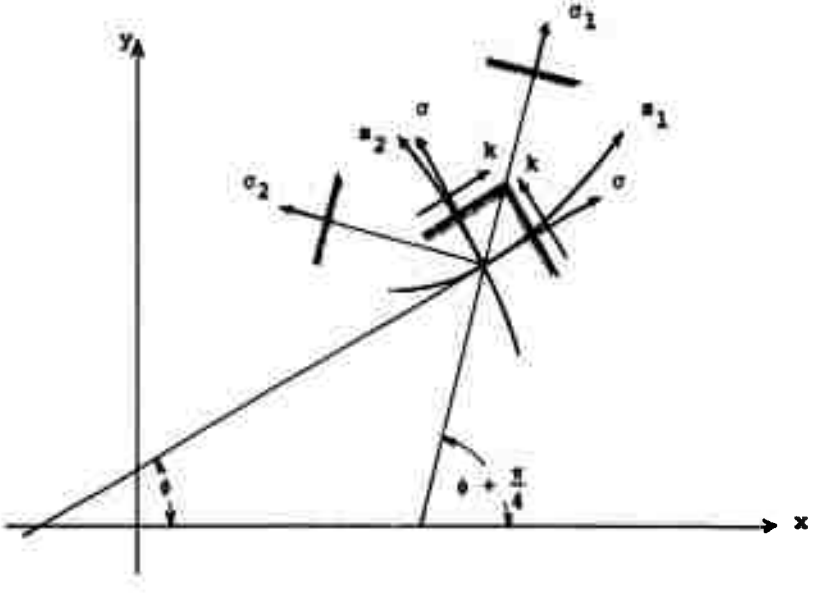

FIGURE II-13 - DEFINITION OF THE FIRST AND SECOND SLIP LINES

rake angle and the spring constant entering the surface at the interference angle i_g.

In stage (a) there is elastic and plastic deformation under the rake surface, and the plastic deformation is developing from point A with increasing values of the depth of cut. Even in this stage a groove will be produced by the partial plastic deformation. In stage (b) there is only plastic deformation under the rake surface and a groove will be produced without chip generation.

It is very difficult to analyze the deformation process corresponding to stage (a), but it is fortunately obvious from experiments that stage (a) is very short and the greatest part of the plastic region is stage (b). Therefore in this subsection the deformation for the stage (b) case will be analyzed two-dimensionally. Also the theory assumes that the metal being cut is ideally plastic and that initial strain is large enough to neglect the work-hardening effect of the plastic deformation. On the assumption that inertia forces are small as compared with the forces required to produce plastic deformation, fundamental equations (yielding criterion, strain increment relations and equilibrium equations) are:

$$(\sigma_x-\sigma_y)^2 + 4\tau_{xy}^2 = 4k^2$$

$$\frac{\partial \sigma_x}{\partial x} + \frac{\partial \tau_{xy}}{\partial y} = 0 \quad , \quad \frac{\partial \sigma_y}{\partial y} + \frac{\partial \tau_{xy}}{\partial x} = 0$$

$$\frac{\partial u_x}{\partial x} + \frac{\partial v_y}{\partial y} = 0$$

(Continued)

$$\frac{\frac{\partial u_x}{\partial x} - \frac{\partial v_y}{\partial y}}{\sigma_x - \sigma_y} = \frac{\frac{\partial u_x}{\partial y} + \frac{\partial v_y}{\partial x}}{2\tau_{xy}} = \lambda \geq 0 \qquad \text{(II.2.14)}$$

where k is the yielding stress in shear of the workpiece, u_x and v_y are velocity components parallel to the corresponding axis and λ is a parameter which represents the rate of strain.

For the slip line field defined by the angle ϕ and the hydrostatic pressure σ, the fundamental equations become (see Figure II-13):

$$\sigma + 2k\phi = \text{const (along } s_1\text{-line)}$$

$$\sigma - 2k\phi = \text{const (along } s_2\text{-line)} \qquad \text{(II.2.15)}$$

$$du - vd\phi = 0 \text{ (along } s_1\text{-line)}$$

$$dv + ud\phi = 0 \text{ (along } s_2\text{-line)} \qquad \text{(II.2.16)}$$

The stress components are given in the equations

$$\sigma_x = \sigma - k \sin 2\phi$$

$$\sigma_y = \sigma + k \sin 2\phi$$

$$\tau_{xy} = k \cos 2\phi \qquad \text{(II.2.17)}$$

An important parameter and boundary conditions for this problem are:

(a) the velocity V in x-direction.

(b) the frictional force on the rake surface which obeys Coulomb's law of friction.

(c) the pile up volume ahead of the rake surface equal to the volume of the groove produced.

(2) PLASTIC DEFORMATION UNDER THE RAKE SURFACE:

Plastic deformation under the given boundary condition is non-linear. However, the theory can assume that the plastic deformation occurs with a similar shape with increasing depth of cut. Figure II-14 shows a slip line field useful for analyzing the plastic deformation below the rake surface under the given boundary conditions. This deformation process may take place in practical grinding and therefore is called a normal type (N-type) deformation process.

Denoting by β_c (pile up profile angle) the angle between x-axis and free surface BC of the pile up ahead of the rake surface, stress components $\sigma_n|_{BC}$ and $\tau|_{BC}$ in normal and tangential directions to the surface BC can be given from Equation (II.2.17) in the form

$$\sigma_n|_{BC} = \sigma + k \sin (2\phi + 2\beta_c)$$

$$\tau|_{BC} = - k \cos (2\phi + 2\beta_c) \qquad \text{(II.2.18)}$$

There is no external force on BC and the stresses on BC are compressive. Consequently, the hydrostatic pressure σ and the angle ϕ between the first slip line s_1 and x-axis can be given as:

$$\sigma = - k$$

on BC

$$\phi = \frac{\pi}{4} - \beta_c \qquad \text{(II.2.19)}$$

σ and ϕ are given from Equation (II.2.15) on the contact line AB between the cutting edge and workpiece in the form

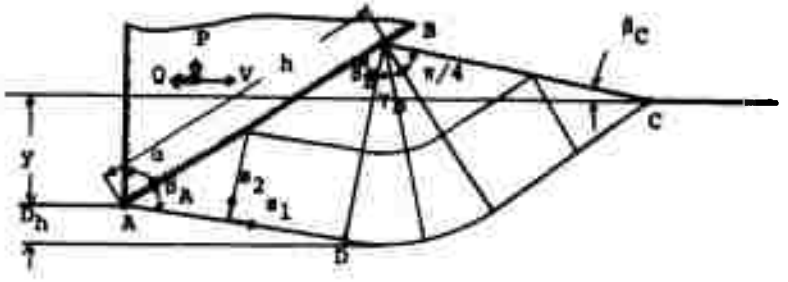

FIGURE II-14 - N-TYPE SLIP LINE FIELD

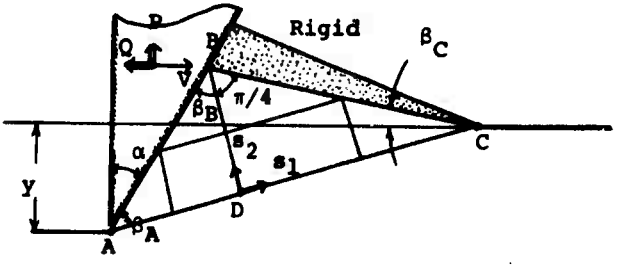

FIGURE II-15 - L-TYPE SLIP LINE FIELD

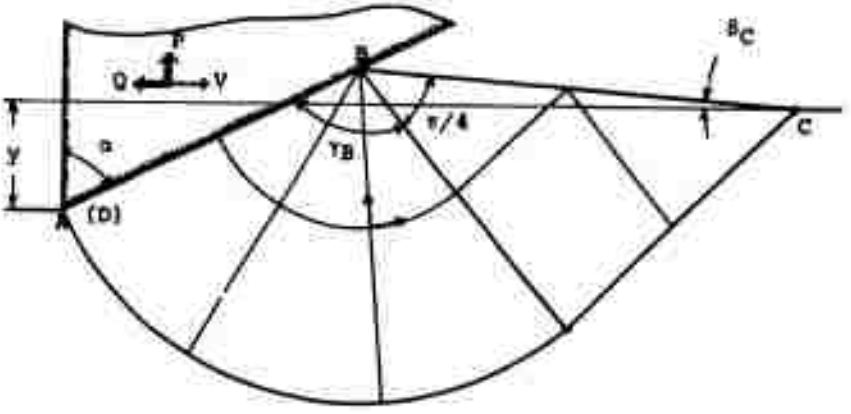

FIGURE II-16 - C-TYPE SLIP LINE FIELD

$$\sigma = -k(1 + 2\gamma_B)$$

on AB

$$\phi = \frac{\pi}{4} - \beta_C - \gamma_B \qquad \text{(II.2.20)}$$

From Equation (II.2.20) and Coulomb's law of friction we get

$$\rho[(1 + 2\gamma_B) + \sin 2\beta_A] + \cos 2\beta_A = 0 \qquad \text{(II.2.21)}$$

The relation between the depth of cut y and the contact length h on the rake surface is:

$$h[\cos\alpha - \sqrt{2}\cos\beta_B \sin\beta_C] = y \qquad \text{(II.2.22)}$$

From the boundary condition that the volume of pile up ahead of the rake surface is equal to that of the groove produced, the following results can be obtained:

$$\sqrt{2}\, h \sin\beta_A \sin\beta_C[\sqrt{2}\, h \sin\beta_A \cos\beta_C + h\sin\alpha - y\tan\alpha] = \frac{y^2}{i_w}$$

(II.2.23)

Geometrical relations between each angle are:

$$\beta_A + \beta_B = \pi/2$$

$$\beta_B + \gamma_B + \beta_C - \alpha = \pi/4 \qquad \text{(II.2.24)}$$

By Equations (II.2.21) to (II.2.24) the plastic deformation under the rake surface is analyzed by checking if this slip line field satisfies the condition for the velocity components. The velocity component v along the s_2-line is zero and u along s_1-line is, from Equation (II.2.16),

$$u = V \cdot \frac{\cos\alpha}{\sin\beta_A} \qquad \text{(II.2.25)}$$

In infinitesimal time dt, the incremental volume deformed plastically under the rake surface is $V\,dt \cdot h \cos \alpha$ and that of the pile up is $\sqrt{2}\, h \sin \beta_A \cdot u \cdot \sin \frac{\pi}{4}$. Both values are equal. Therefore this slip line satisfies the condition of the velocity components.

It should be noted here that the plastic deformation processes change with the rake angle α and the frictional coefficient ρ between workpiece and the cutting edge.

For smaller rake angle α and frictional coefficient ρ, the pressure angle β_B could possibly be equal to zero. In this case the hydrostatic pressure σ on the contact line AB becomes equal to -k as seen in Equation (II.2.20). In other words, the hydrostatic pressure is uniform for the complete plastic deformation zone under the rake surface and, therefore, the slip line field for this case is composed of only straight lines (L-type slip line field) as shown in Figure II-15.

For larger rake angle α and frictional coefficient ρ, the stress in the tangential direction on the contact line AB can possibly equal the yielding stress k and then the contact line AB itself becomes a slip line (C-type slip line field) as shown in Figure II-16. Therefore, there are three different types of deformation processes (N, L and C type) depending on the rake angle and the frictional coefficient. The boundary between N and L type is $\gamma_B = 0$ and that between N and L type is $\beta_A = \pi/2$. The Equations (II.2.21) to (II.2.24) obtained for N-type are effective for L and C types with $\gamma_B = 0$ or $\beta_A = \pi/2$.

(3) FORCES REQUIRED TO PRODUCE THE PLASTIC DEFORMATION AND PLASTIC FLOW LAYER:

For each type of deformation process (L, N and C), stresses σ_n and τ on the contact line AB in the normal and tangential direction to the rake surface can be given in the following equations:

$$\frac{\sigma_n}{k} = (1 + 2\gamma_B) + \sin 2\beta_A$$

$$\frac{\tau}{k} = -\cos 2\beta_A \qquad \text{(II.2.26)}$$

Then pressures q and p in x and y direction which act on the rake surface are

$$p = \sigma_n \sin \alpha - \tau \cos \alpha$$

$$q = \sigma_n \cos \alpha + \tau \sin \alpha \qquad \text{(II.2.27)}$$

From Equations (II.2.26) and (II.2.27) forces P(x) and Q(x) acting on the cutting edge in y and x direction, respectively, are given in the equation

$$P(x) = [(1 + 2\gamma_B) \sin \alpha + \cos (2\beta_A - \alpha)] \cdot k\, h \sin \alpha$$

$$Q(x) = [(1 + 2\gamma_B) \cos \alpha + \sin (2\beta_A - \alpha)] \cdot k\, h \cos \alpha \qquad \text{(II.2.28)}$$

The relation between the depth of cut and normal force P(x) in the plastic region are from Equation (II.2.22)

$$y = P(x)/J_p(\rho,\alpha) \qquad \text{(II.2.29)}$$

where $J_p(\rho,\alpha)$ is a constant which can be determined by yielding stress k, the rake angle α and the frictional coefficient ρ and is expressed as

$$J_p(\rho,\alpha) = k \cdot \frac{[(1+2\gamma_B)\sin\alpha+\cos(2\beta_A-\alpha)]\sin\alpha}{\cos\alpha - \sqrt{2}\sin\beta_A \sin\beta_C} \qquad \text{(II.2.30)}$$

It should be noted from Equation (II.2.29) that the normal force P(x) is proportional to the depth of cut in the plastic region. On the other hand, the depth of the plastic flow layer can be given from Figure II-14 to II-16

$$D_h = 0 \qquad \text{for L-type}$$

$$D_h = h \sin\beta_A[1- \sqrt{2}\sin\beta_C] - y$$

$$\text{for N and C-type} \qquad \text{(II.2.31)}$$

(4) DISCUSSION ON THE DETERMINATION OF THE BOUNDARY POINT BETWEEN THE PLASTIC AND CUTTING REGIONS:

The metal which piles up ahead of the rake surface increases with increasing depth of cut in the plastic region and should finally be removed as a chip. It is very hard at the present time to determine quantitatively the boundary point between the plastic and cutting regions and more experimental and theoretical investigation is required. However, the following qualitative consideration may be useful to determine the boundary point.

Figure II-17 shows a slip line field in two dimensional cutting by E.H. Lee and B.W. Shaffer and this may be effective in the cutting region for this cutting problem.

At the boundary point L - type deformation process should change into the slip line field in Figure II-17(a) and N and C type into that in Figure II-17(b). Upon changing of

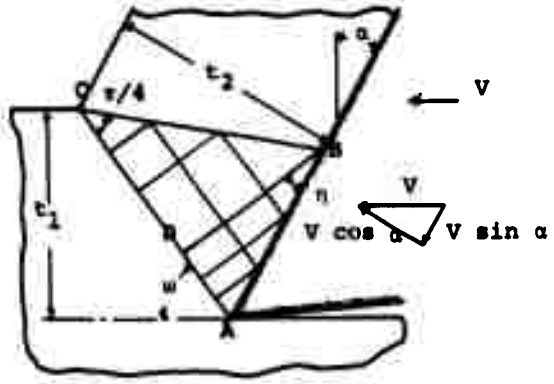

(A) SLIP LINE FIELD CONFIGURATION WITH NO BUILT-UP NOSE

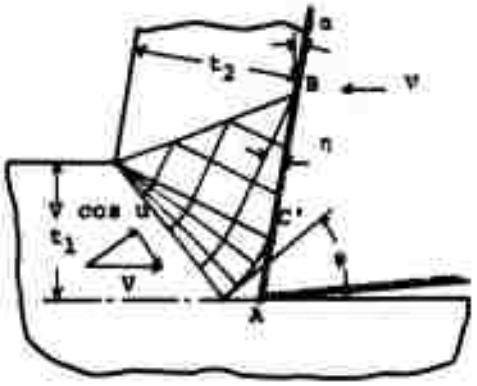

(B) SLIP LINE CONFIGURATION WITH A BUILT-UP NOSE

FIGURE II-17 - SLIP LINE FIELD IN CUTTING REGION (LEE & SHAFFER)

the slip line field from N and C types into that in Figure II-17(b), the built-up nose may be formed by the stress released due in part to the initiation of micro-cracks at point A. Therefore a relation between the strength of metal being cut and the stresses at point A may be useful to determine the boundary point.

Furthermore the pile up phenomena ahead of the rake surface has a close relation to the plastic deformation processes. From the above mentioned point of view the boundary point will be determined in the near future.

II.2.5 Typical Results of the Plastic Deformation Theory

(1) DEFORMATION PROCESS IN THE PLASTIC REGION:

For the plastic region in the transitional cutting process where the cutting edge (with rake angle α and spring constant of mounting k_s) cuts with increasing linear depth of cut into the metal at an angle i_g to the surface, a groove is produced by plastic deformation without the formation of a chip. In this case the form of pile up ahead of the rake surface and of the plastic deformation under the rake surface is a strong function of the rake angle α and the frictional coefficient ρ. In other words, there are three different plastic deformation processes (L, N and C type) depending on the rake angle α and the frictional coefficient ρ. Figure II-18 shows the effective region of each type of the deformation process in the plastic region.

It should be noted from this figure that the L type deformation process occurs for smaller rake angle and frictional coefficient and that C type deformation process occurs for larger rake angle and frictional coefficient. In practical grinding the average rake angle of abrasive grain is about 1 radian and the frictional coefficient ρ is about .2. Then the plastic deformation process of an abrasive grain in grinding should be the N type. From Figure II-19 to II-22, the relations are shown between angles which determine the deformation process, and the rake angle, with the frictional coefficient as a parameter. In these figures the changing ranges of each angle in the L, N and C - type are shown. However the C - type can be represented by a line, because each value of the C - type is independent of the frictional coefficient.

As an example, the pile up profile angle β_c shown in Figure II-22 is explained in case of $\rho = .3$.

The deformation process is L type for rake angle smaller than .3 and the profile angle β_c increases with increasing rake angle. At point B the deformation process changes from L into N type and the profile angle β_c decreases with increasing rake angle. Then at point C the deformation process changes again from N into C type and the profile angle β_c decreases with increasing rake angle, independent of the frictional coefficient.

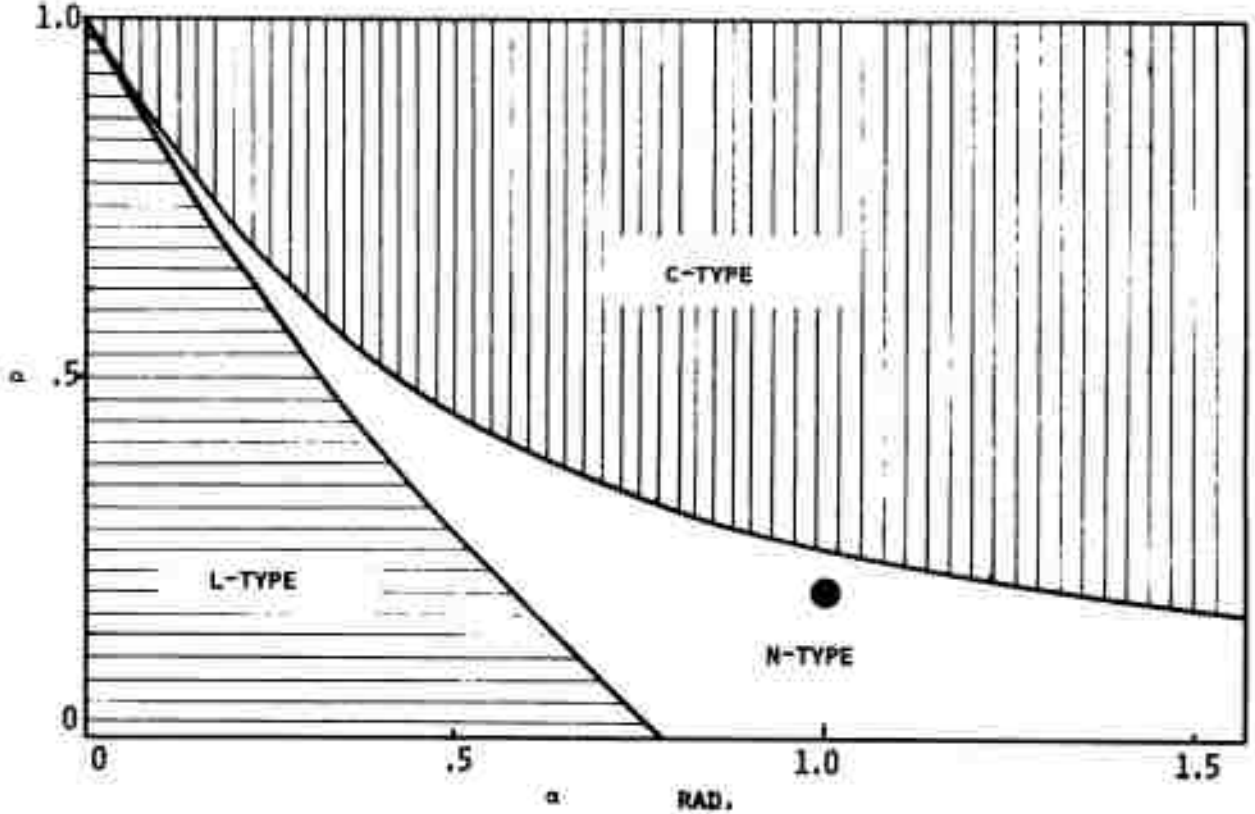

FIGURE II-18 - EFFECTIVE REGION OF EACH TYPE OF DEFORMATION PROCESS

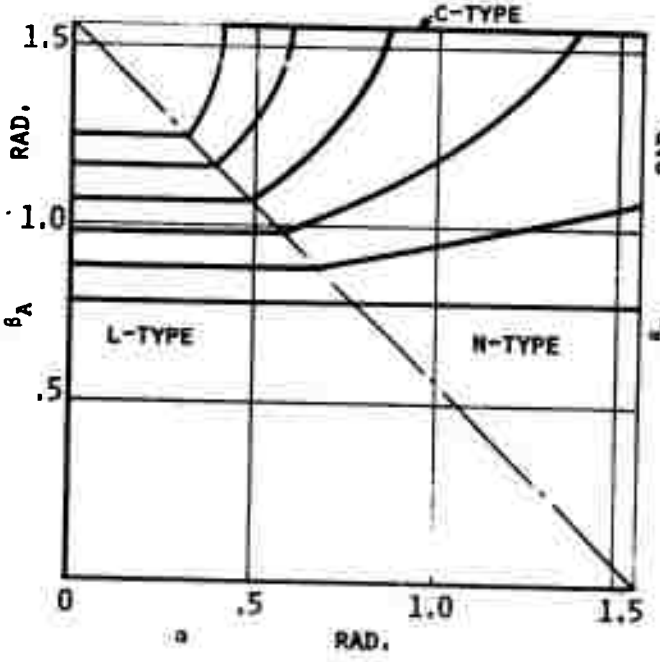

FIGURE II-19 - ANGLE β_A

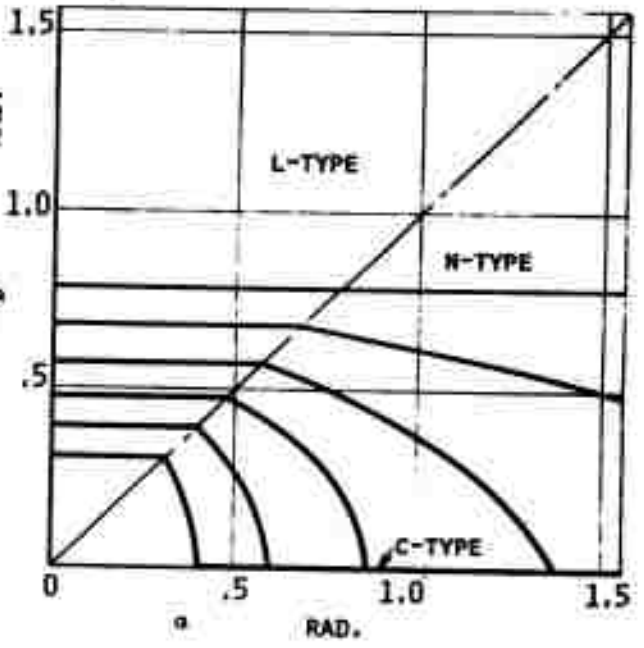

FIGURE II-20 - ANGLE β_B

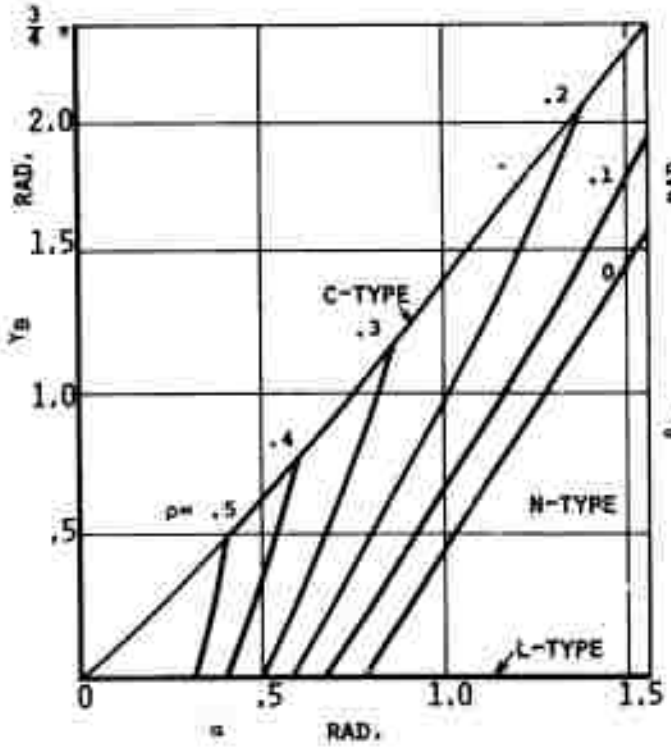

FIGURE II-21 - PRESSURE ANGLE γ_B

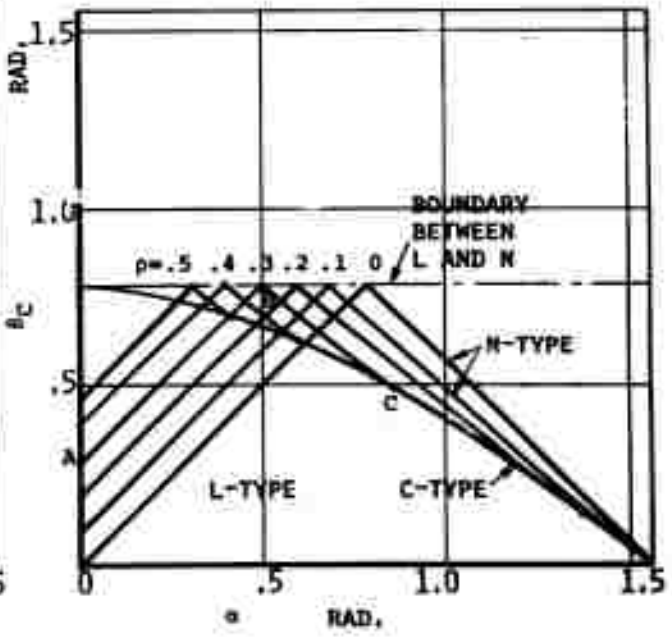

FIGURE II-22 - PROFILE ANGLE β_C

(2) CONTACT LENGTH h ON THE RAKE SURFACE:

Contact length h on the rake surface is greater than y/cos α because of the pile up ahead of the rake surface. This contact length h has a close relation to the total forces acting upon the cutting edge and therefore is very important. Figure II-23 shows the relation for a unit depth of cut between the contact length and the rake angle with ρ as a parameter. It can be seen from this figure that the contact length increases with increasing rake angle and frictional coefficient in the L - type plastic deformation process, and that in type N and C it decreases with increasing frictional coefficient and becomes minimum for a certain rake angle.

(3) PROFILE OF THE PILE-UP AHEAD OF THE RAKE SURFACE:

The pile-up phenomena ahead of the rake surface has a close relation to the plastic deformation process and therefore is very important in the analysis of the transitional cutting process. Figures II-24 and II-25 show variation with rake angle of the heights and width of the pile up ahead of the rake surface for a unit depth of cut. For the N type, which may be a plastic deformation process in practical grinding, it should be noted that the rake height coefficient C_s decreases with increasing rake angle α and frictional coefficient ρ. This indicates that the plastic deformation under the rake surface occurs in a more local region with decreasing rake angle and frictional coefficient.

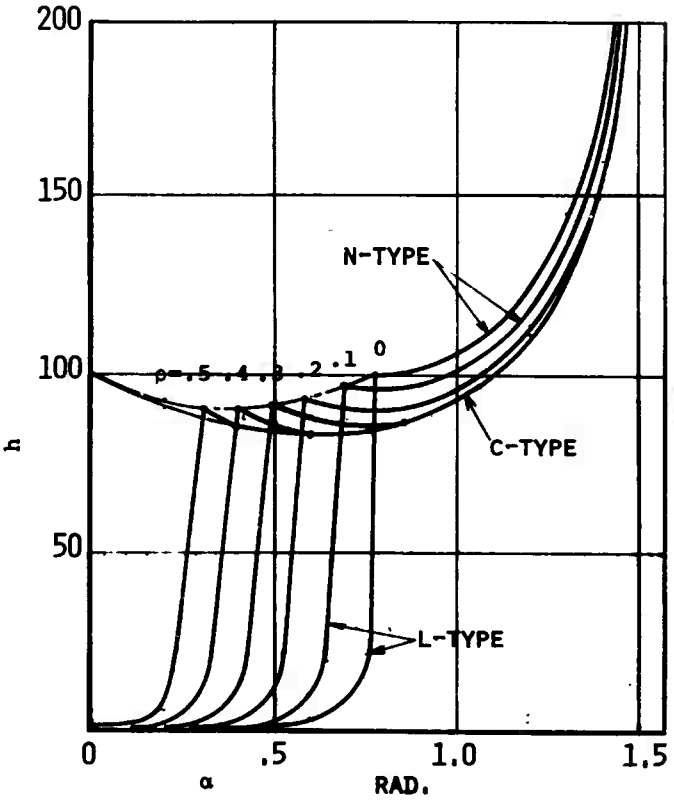

FIGURE II-23 - CONTACT LENGTH ON THE RAKE SURFACE OF CUTTING EDGE
H(ρ,α)

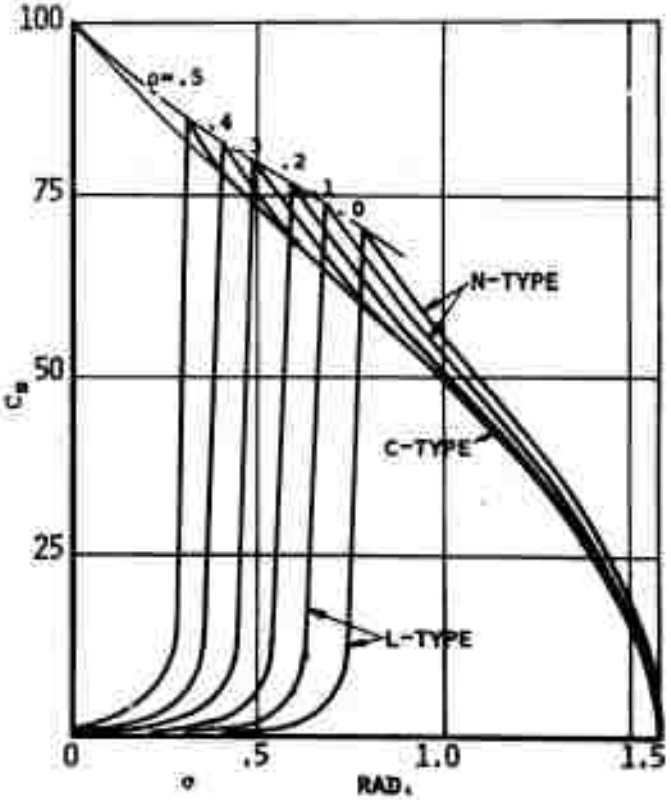

FIGURE II-24 - RAKE HEIGHT COEFFICIENT

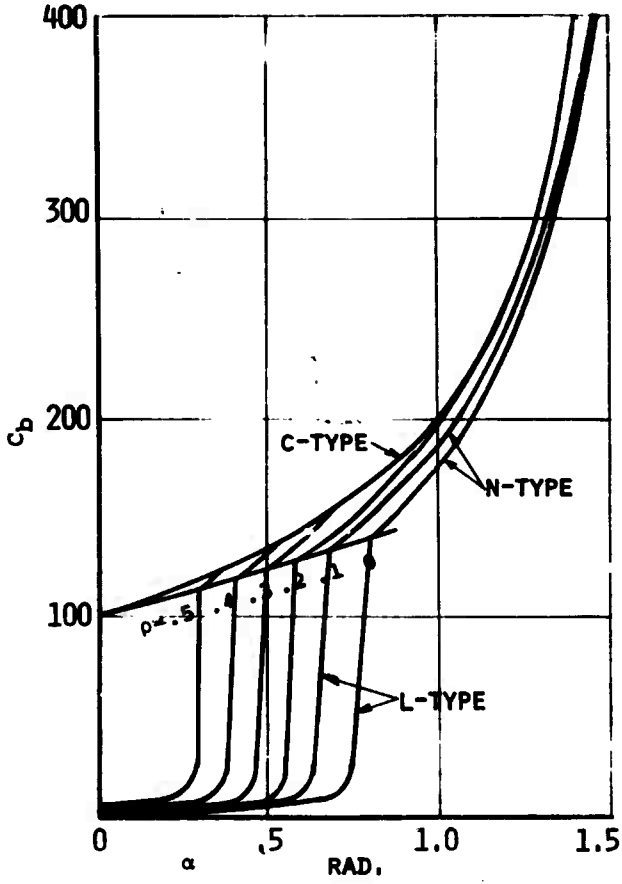

FIGURE II-25 - RAKE WIDTH COEFFICIENT

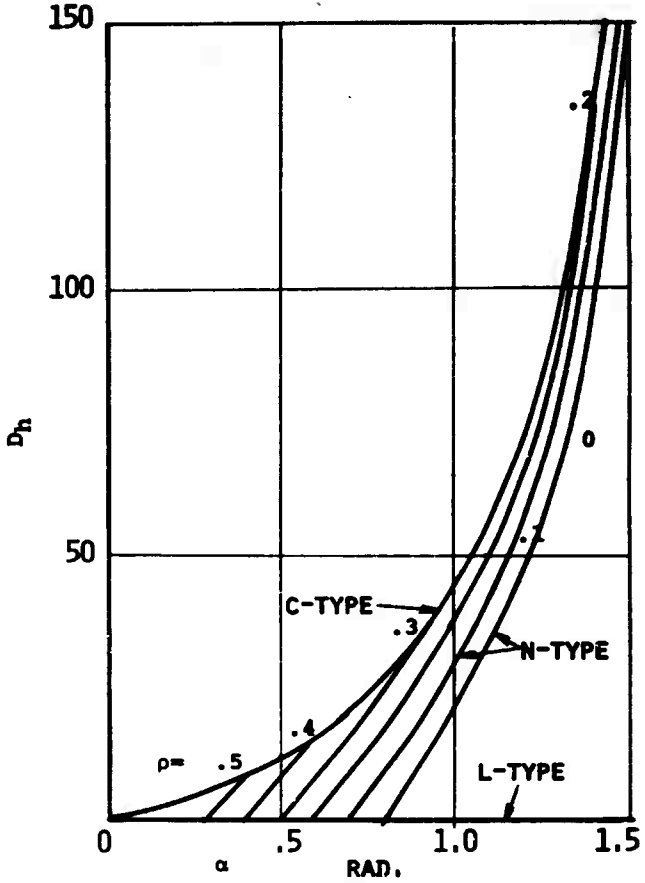

FIGURE II-26 - PLASTIC FLOW LAYER

(4) PLASTIC FLOW LAYER:

It is obvious that the plastic flow layer on the ground surface has a close relation to the surface integrity. Figure II-26 shows variation of the depth D_h of plastic flow layer for unit depth of cut with rake angle. D_h is theoretically zero for the L type plastic deformation process. The depths D_h of plastic flow layer for N and C types increase with increasing rake angle and frictional coefficient. Figures II-27 and II-28 show the variation with rake angle of the pressure q_n in the normal direction to the rake surface and shear stress τ on the rake surface. Figures II-29 and II-30 show variation of normal force P(x) and tangential force Q(x) with with rake angle α and frictional coefficient ρ. It should be noted from these figures that the normal force increases with increasing rake angle and frictional coefficient and that the tangential force increases with increasing frictional coefficient and has a maximum for a certain rake angle.

(5) FORCES ACTING ON THE CUTTING EDGE IN PLASTIC REGION:

Forces acting on a cutting edge have a very close relation to the deformation process in the elastic, plastic and cutting regions and are proportional to the depth of cut in the elastic and plastic regions, although the proportionality constant is different in each region. In other words, the slope of the force variations with the cutting distance changes at the transition point of each region. This indicates that it is incorrect to assume the two dimensional cutting theory is valid for all depths of cut, as is often done.

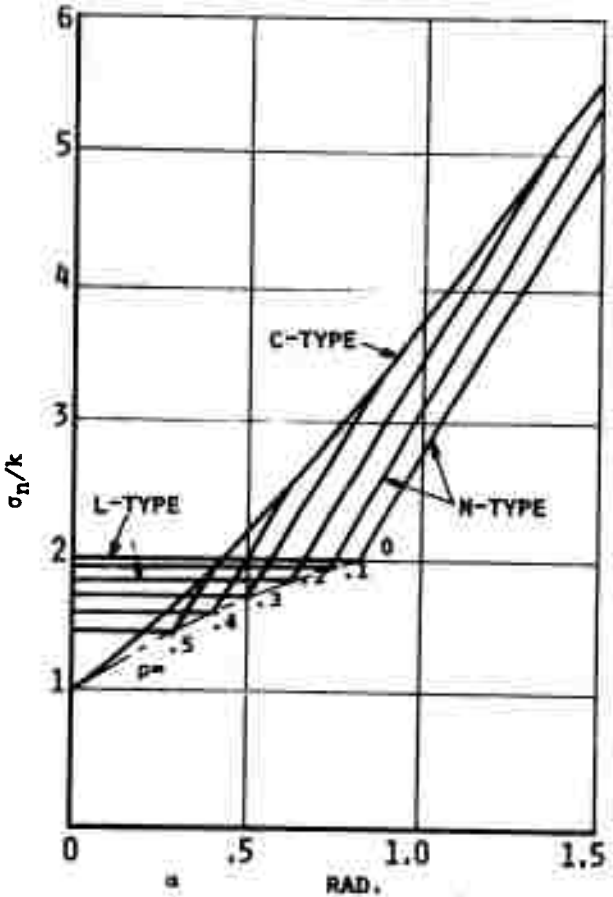

FIGURE II-27 - PRESSURE IN NORMAL DIRECTION TO THE RAKE SURFACE

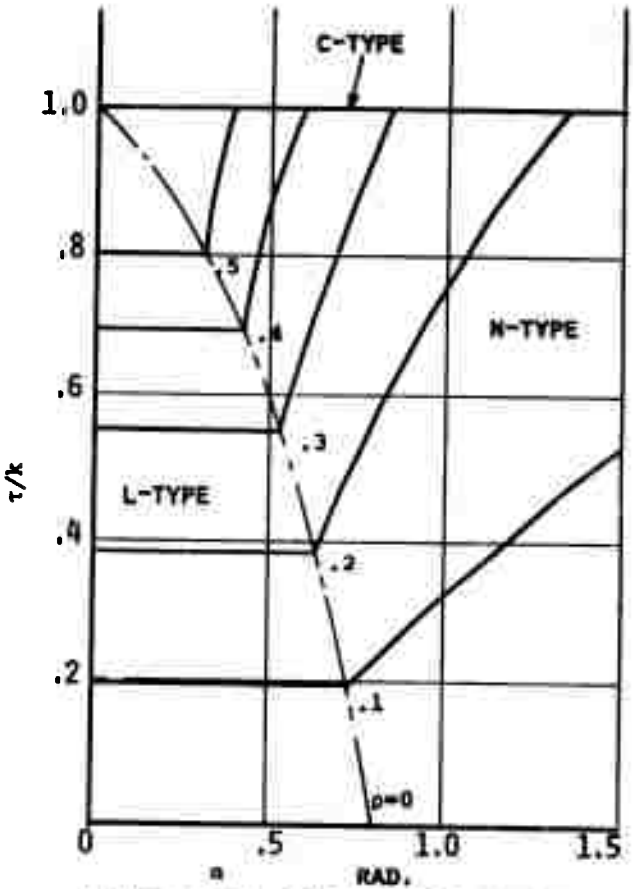

FIGURE II-28 - SHEAR STRESS ON THE RAKE SURFACE

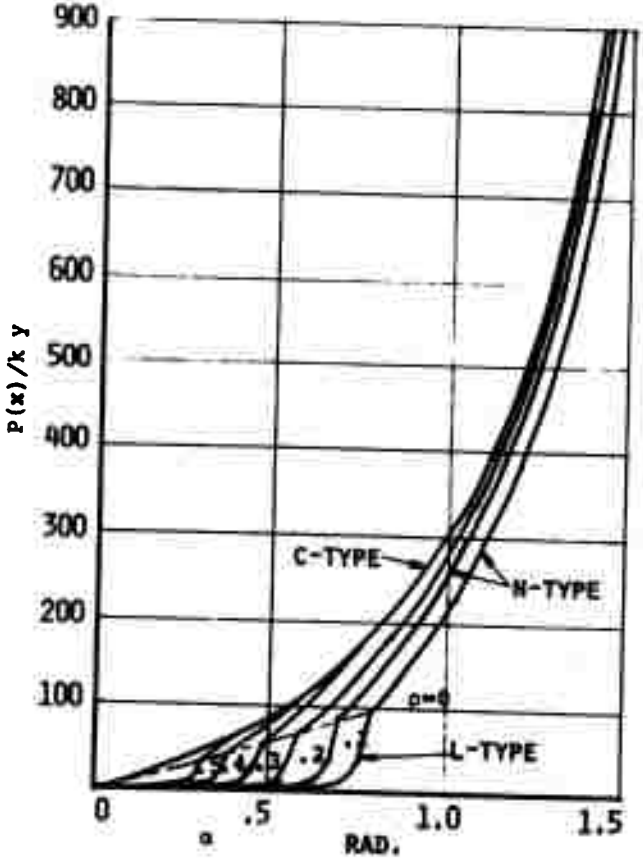

FIGURE II-29 - NORMAL FORCE

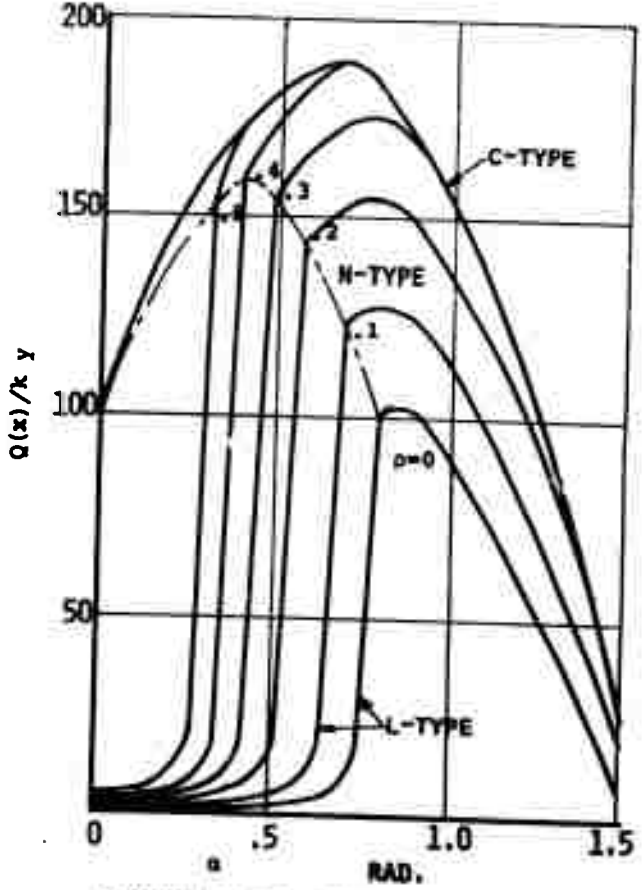

FIGURE II-30 - TANGENTIAL FORCE

II.3 Experimental Analysis of Deformation Process in Transitional Cutting.

II.3.1 Introduction

The elastic and plastic deformations near the beginning of contact were analyzed in Subsection II.2 and essential parameters or factors which affect these transitional cutting regions were clearly defined. In this subsection the transitional cutting process will be examined experimentally, based upon the information obtained from the theoretical analysis so that a clear understanding can be developed. In order to examine the transitional cutting process under circumstances similar to practical grinding, a circular cutting method where the depth of cut becomes maximum at a certain point is used.

Various phenomena such as elastic and plastic sliding length, critical depth of cut, critical normal force, pile-up at the sides of grooves, plastic flow layer and the workhardened layer, which is a measure of the surface integrity, will be discussed in each region of this experimental research.

II.3.2 Experimental Method and Equipment

The experimental equipment used in this study is shown in Figure II-31. It consists of a disc which is attached to the main shaft of a grinder. Fixed upon the peripheral surface of this disc is a pyramidal diamond indentor with one of the pyramidal faces used as the rake surface. A specimen mounted upon a dynamometer is then cut by the cutting edge. Both the

FIGURE II-31 - PHOTOGRAPH OF SINGLE GRAIN CUTTING APPARATUS

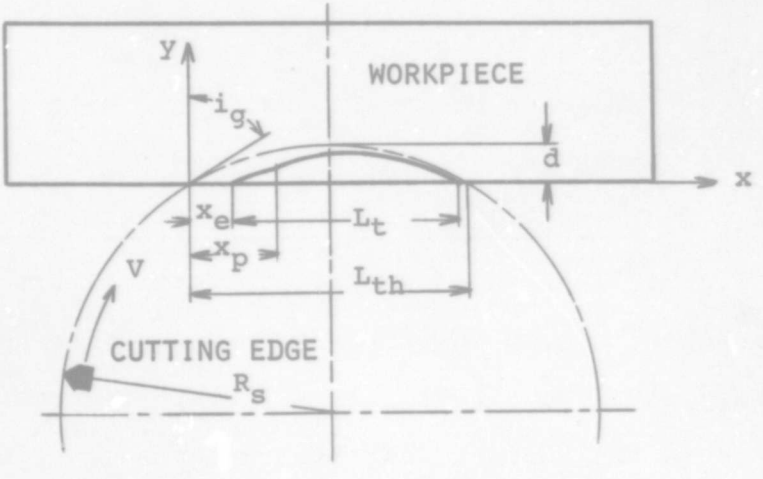

FIGURE II-32 - SCHEMATIC DIAGRAM OF SINGLE GRAIN CUTTING SET-UP

normal component and the tangential component of the cutting force are measured by the dynamometer and recorded using an oscilloscope.

The schematic diagram of this experiment is shown in Figure II-32 and the following experimental condition were utilized;

Cutting velocity	V = 4800 - 12,000 ft/min
Interference angle	i_g = 10' ~ 120'
Rake Angle	α = -68°
Workpiece	mild steel

In order to estimate the elastic and plastic length it is necessary to determine two critical points; that is, the location of initial plastic deformation and the location at which cutting begins. These critical points are estimated from geometrical considerations and from the following information:

(a) Variation of cutting forces with cutting distance

(b) Observation of grooves

(c) Variation of the pile-up stock with cutting distance

(d) Pictures taken by high speed camera

II.3.3 The Elastic and Plastic Sliding Length

Figure II-33 shows variation of the elastic and plastic sliding length with the interference angle for a cutting velocity equal to 5100 ft/min. In this figure the line L_{th} represents the contact length between the cutting edge and the workpiece and the line y_{max} represents the location of

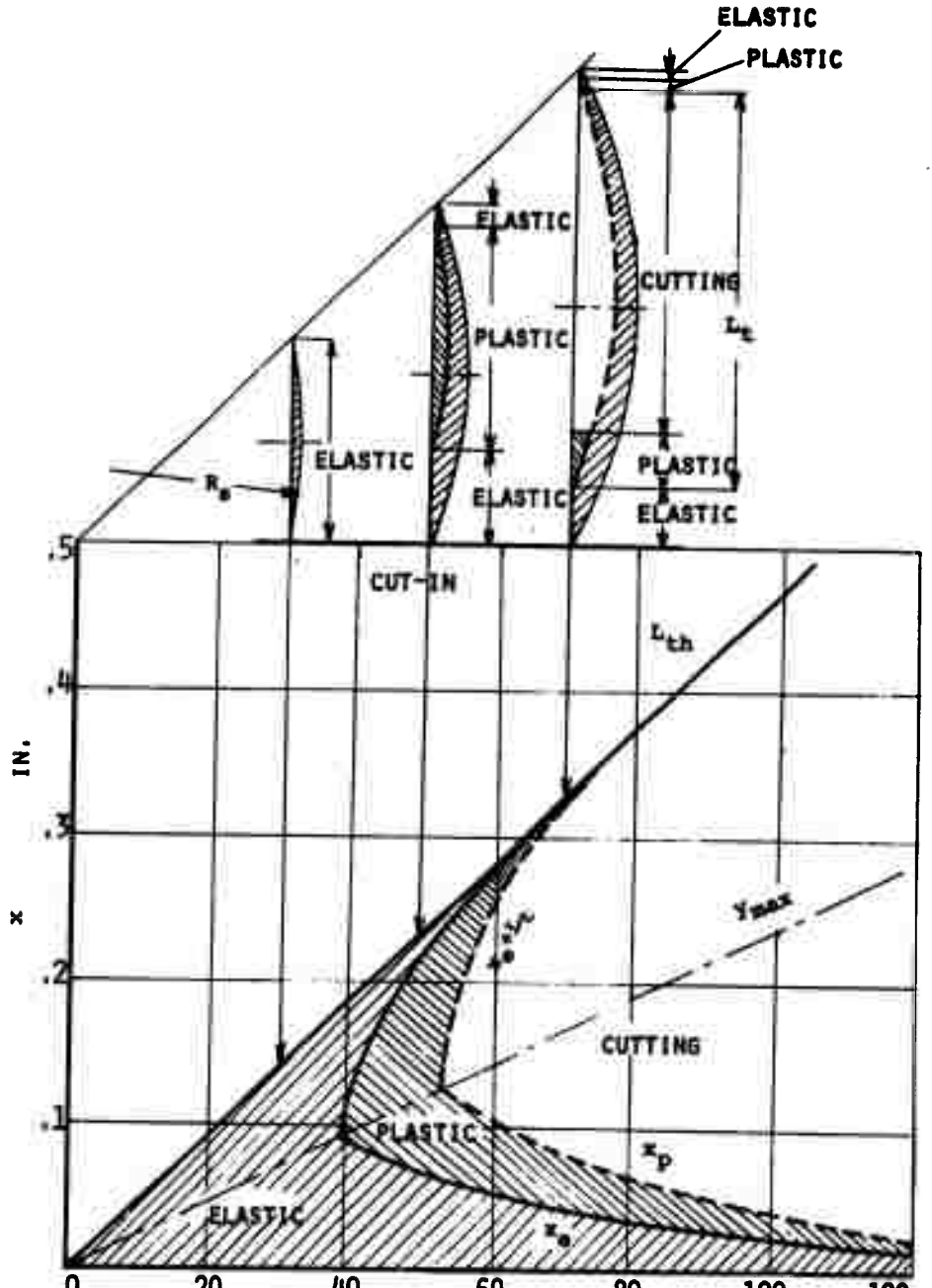

FIGURE II-33 - VARIATION OF ELASTIC AND PLASTIC SLIDING LENGTH (V=5100 fpm)

the maximum theoretical depth of cut. Furthermore, the x_e and x_p curves represent the critical points for the elastic and plastic regions respectively and the curve $(x_e + L_t)$ represents the summation of the elastic sliding length and the length of the groove produced. The region from the i_g axis to the x_e curve would correspond to the elastic region. The region from the x_e curve to the x_p curve corresponds to the plastic region and from the x_p curve to the $(x_e + L_t)$ curve the cutting region. The actual length of the produced groove L_t is therefore equal to the distance between the x_e curve and $(x_e + L_t)$ curve. In order to better illustrate the various regions, several typical cutting grooves are shown at the top of this figure. For cutting under condition I, (i_g=30') the cutting groove is not observed, even though the cutting forces are measured. This indicates that the cutting edge slides elastically throughout the entire contact length between the cutting edge and the workpiece. For cutting under condition II (i_g=50') the cutting groove is produced by only the plastic deformation and no chip is generated. In this case the elastic sliding length at the beginning of contact is longer than that at the end of contact even though the geometry is similar at both the beginning and the end of contact.

For cutting under condition III (i_g=70'), there are five different processes of deformation through the contact length. They are elastic, plastic and cutting at the beginning

of contact and then smaller plastic and elastic at the end of contact. The results indicate that the interference angle should be increased to decrease the elastic and plastic sliding length and therefore to increase the cutting region.

II.3.4 Critical Depth of Cut and Critical Cutting Forces at Critical Points of the Elastic and Plastic Regions.

Figure II-34 shows the relationship between the critical depths of cut y_e, y_p and the interference angle i_g. In this figure, the 2d-curve represents the maximum value of the theoretical depth of cut.

As can easily be seen in Figure II-34, the critical depths of cut y_e and y_p do not depend upon the interference angle i_g but do decrease with increasing cutting velocity V.

Curves of the variation of the critical normal forces $P(x_e)$ and $P(x_p)$ with the interference angle i_g are shown in Figure II-35. In this figure it can be seen that the cutting velocity and the interference angle have the same effect upon the critical normal forces as they did upon the critical depths of cut.

II.3.5 Pile-up Phenomena

A great deal of metal piles up at the sides of the cutting groove instead of being removed as a chip and this pile-up phenomena has a close relation to the deformation process during transitional cutting.

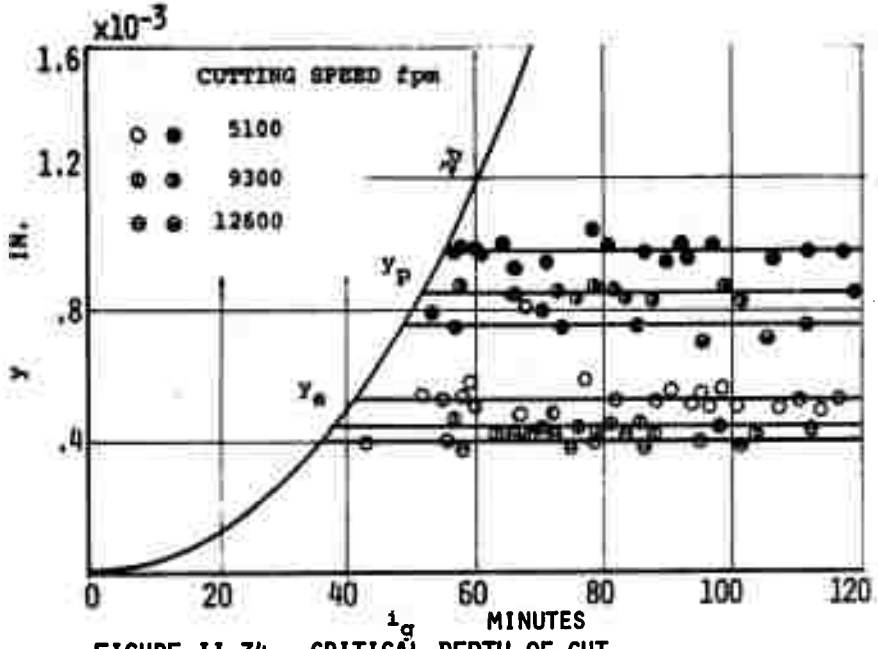

FIGURE II-34 - CRITICAL DEPTH OF CUT

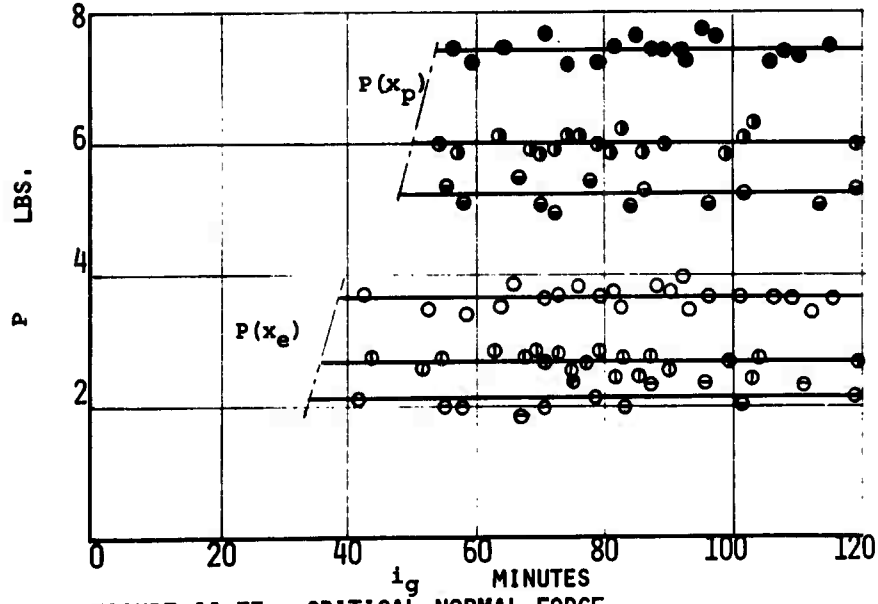

FIGURE II-35 - CRITICAL NORMAL FORCE

The relationship between the cutting distance, which has a relation with cutting depth, and the height coefficient γ_b for the case where there is no cutting region (V = 5100 ft/min, i_g = 46.5), is shown in Figure II-36. As can be seen in Figure II-36, both γ_s and γ_b are equal to zero in the elastic region and both increase very rapidly in the plastic region. In the mid-region, γ_s and γ_b are nearly constant with increasing tendencies near the end of the plastic region. The variation of γ_s and γ_b for the case where all three regions exist (V = 5100 ft/min, i_g = 59.2') is shown in Figure II-37. In the elastic region γ_s and γ_b are again equal to zero as expected. These values increase very rapidly in the plastic region with a sudden decrease at the critical point where the chip begins to be produced. The same increasing tendency can be noted near the end of contact. Furthermore the height coefficient $(\gamma_s)_p$ and the width coefficient $(\gamma_b)_p$ at the elastic critical point are not dependent upon the interference angle and decrease with the increase of the cutting velocity.

II.3.6 Work Hardening

Figure II-38 shows the relation between the depth of cut and the depth of work hardened layer, which is one of the factors that determine the surface integrity. It can be seen from this figure that work hardening doesn't exist in the elastic region and increases with increasing depth of cut in both the plastic and cutting. In other words,

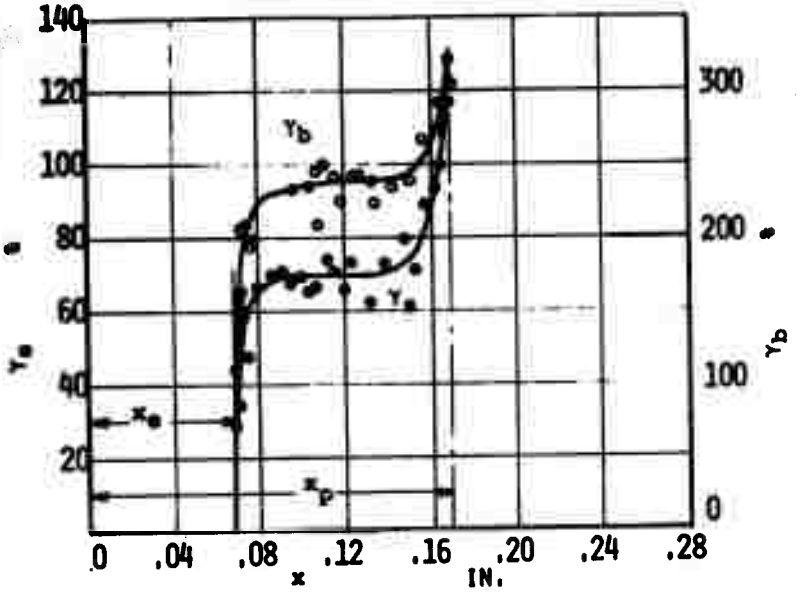

FIGURE II-36 - VARIATION OF PILE-UP STOCK FOR PLASTIC REGION

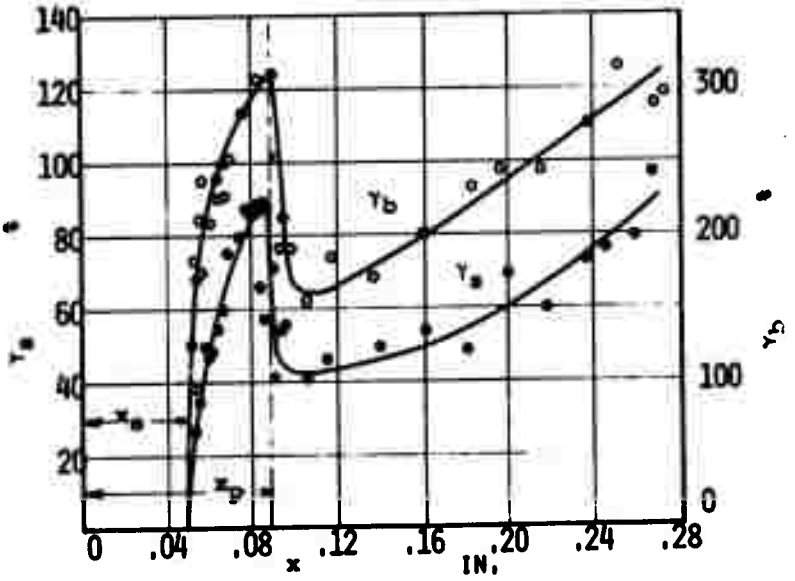

FIGURE II-37 - VARIATION OF PILE-UP STOCK FOR EACH REGION

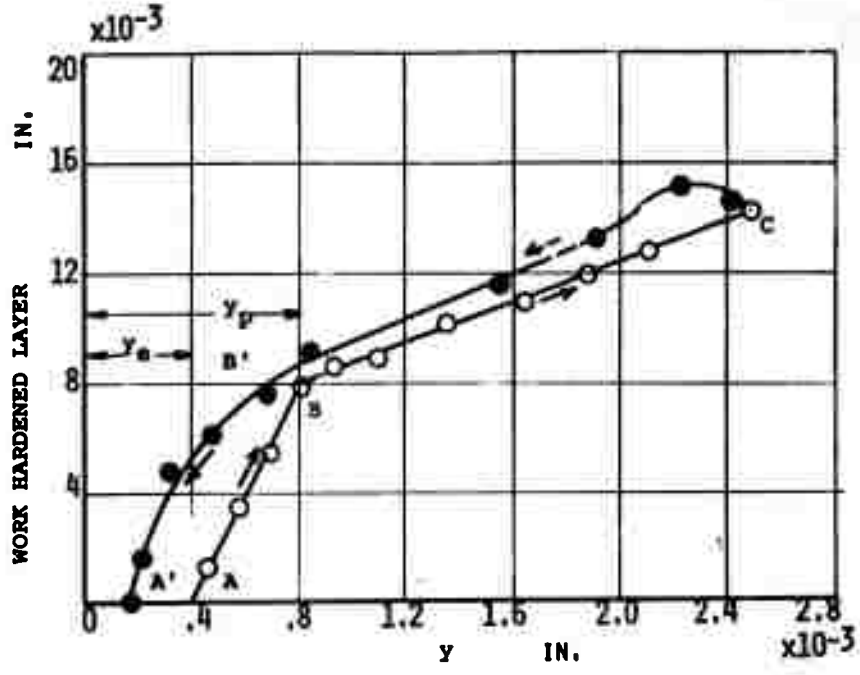

FIGURE II-38 - WORK HARDENED LAYER

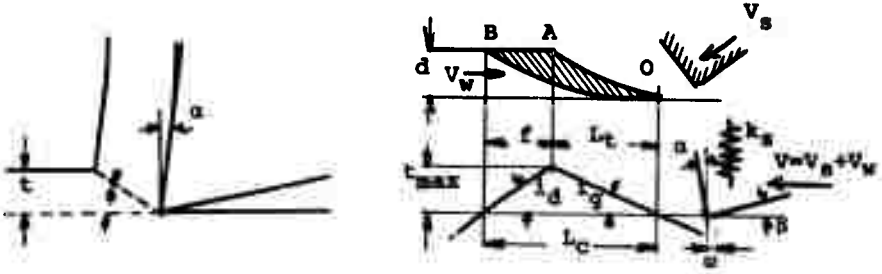

(A) FOR TWO-DIMENSIONAL CUTTING

(B) FOR GRINDING

FIGURE II-39 - CUTTING MODEL

the depth of work hardened layer increases in the plastic region along the line AB with increasing depth of cut and in the cutting region along the line BC, which has a smaller slope than of the plastic region. In the last half of the contact the depth of work hardened layer decreases along the curve CB'A' which depends on the interference angle. The slopes of the lines AB and BC in the first half of contact are independent of the interference angle and also an inverse function of the relative cutting speed. The fact that the slope of the work hardening line AB in the plastic region is larger than that of the line BC in the cutting region, indicates that the increment of the depth of work hardened layer in the plastic region is larger than that in cutting region for a unit increase of the depth of cut. It should be noted from this data that the plastic region should be decreased to improve the integrity of ground surface and therefore the interference angle and the relative cutting velocity should be increased.

II.4 Conformity Theory in Grinding

II.4.1 Introduction

Two dimensional cutting theory has played a great role in developing a clear understanding of the chip formation physics for the cutting of a single grain and therefore was important in developing machining with a single cutting edge such as turning. Consequently, there has been much information

reported using the wrong assumption that the two dimensional cutting theory is applicable for every moment of the cutting process even for cutting during grinding.

As can easily be seen in the traditional analysis of the undeformed chip shape, the depth of cut in grinding increases from zero, becomes maximum at a certain point and then decreases to zero. In such a cutting process the chip is not formed from the beginning of contact, but after the elastic and plastic deformation region as was described in Section II.2. The elastic and plastic sliding lengths occupy a great part of the contact length between a cutting edge and workpiece and for some cases there is only the elastic region or the elastic and plastic regions without chip generation. Thus there are three different types of deformation processes which significantly affect the grinding process and therefore the grinding results. For example, the integrity of the ground surface is largely determined by the elastic and plastic regions, because it is the elastically and plastically deformed metal which forms the ground surface.

Therefore a different cutting model from that of the two dimensional cutting model should be required in grinding for analyzing the transitional cutting process.

From the above point of view, the most convenient model for analyzing the grinding process will be proposed. The basic boundary conditions in grinding will be developed in

this subsection based upon the essential factors which affect grinding processes. These factors were discussed theoretically and experimentally in Subsections II.2 and II.3. Furthermore, the undeformed chip shape will be analyzed to discuss how the working conditions affect the basic boundary conditions in grinding.

II.4.2 Cutting Model in Grinding

The cutting model in grinding corresponds to a two-dimensional cutting model as shown in Figure II-39(b). In other words, a cutting edge with a rake angle α and wear width 2a cuts into the surface at the small angle i_g at very high relative velocity V, a summation of wheel velocity V_s and work velocity V_w. The depth of cut increases linearly from zero, becoming maximum (t_{max}) at a certain point (L_t) and then decreasing to zero (cutting-out angle i_d). In this cutting all of the triangle OAB is not removed as a chip, because there is always the elastic and plastic region before the cutting due to displacement of the cutting edge and the metal being cut (contact stiffness k_s). Therefore, all parameters shown in Figure II-39(b) are very important in analyzing the grinding process since the cutting process in grinding is transitional. Thus the number of the basic boundary conditions for the cutting model in grinding is more than in the two-dimensional cutting model, which can be described by the rake angle α and the depth of cut t.

The difference between the models is that the effects of the continuously changing depth of cut, wear area in the clearance surface, contact stiffness and relative velocity upon the cutting process should be taken into consideration. The grinding model will clearly show the finished surface characteristics which can not be obtained from the two-dimensional cutting theory.

II.4.3 Undeformed Chip Shape in Grinding

(1) THE LOCUS OF A CUTTING EDGE ON THE WORKPIECE SURFACE:

The locus of a cutting edge of the wheel relative to the workpiece is a trochoidal curve. Since the arc of contact between the wheel and work is normally very small, the equation of this locus can be given approximately as (See Figure II-40)

$$\frac{Y}{R_s} = \frac{A \cdot B}{2}\left(\frac{x}{R_s}\right)^2 \qquad \text{(II.4.1)}$$

where $A = \dfrac{1}{(K_v + 1)^2}$, $B = \left[1 - \dfrac{K_v}{DK_R}(K_v + 2)\right]$

D = +1 : external grinding

D = -1 : internal grinding

where $K_v = \dfrac{V_w}{V_s}$, $K_R = \dfrac{R_w}{R_s}$

From the fundamental Equation (II.4.1), the relations between undeformed chip shape (basic geometrical boundary conditions) and working conditions such as work speed V_w, wheel speed V_s,

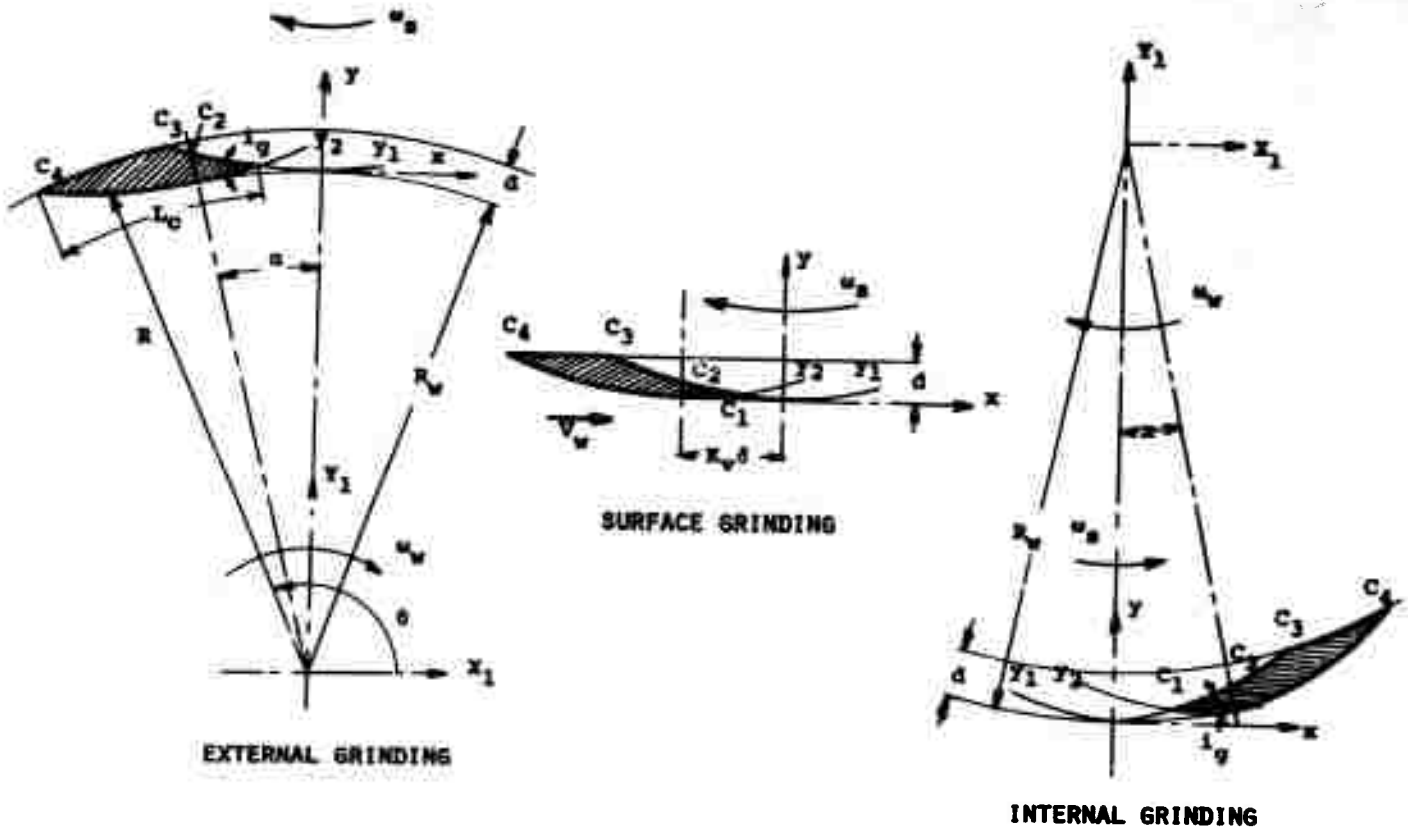

FIGURE II-40 - GRINDING CHIP GEOMETRY

work radius R_w, wheel radius R_s, successive cutting edge spacing δ, and the wheel cutting depth d can be obtained.

(2) INTERFERENCE ANGLE i_g:

As mentioned in detail in Subsections II.2 and II.3, the interference angle i_g is very important for developing a clear understanding of the transitional cutting process.

From the fundamental equation (II.4.1), the equation for the interference angle i_g can be obtained for external and internal grinding as follows:

$$i_g = 2D \tan^{-1} \left| \frac{1}{\tan(\frac{\gamma}{2})} \left[1 - \sqrt{1-2DABK_R \tan^2(\frac{\gamma}{2})} \right| + D\gamma \right. \qquad \text{(II.4.2)}$$

where $$\gamma = \frac{K_V \cdot \delta}{R_w} = \frac{K_V \cdot K_D}{K_R}$$

For surface grinding the interference angle i_g is

$$i_g = 2 \tan^{-1} \left| \frac{AK_V \cdot K_D}{2} \right| \qquad \text{(II.4.3)}$$

From the Equations (II.4.2) and (II.4.3) it should be noted that the interference angle i_g is a function of the radius ratio K_R, the velocity ratio K_V and the successive cutting edge spacing δ and that it is not dependent upon the cutting depth of wheel d.

(3) CHIP LENGTH L_C

The approximate chip length L_c (See Figure II-40) can be given in the equation for external and internal grinding:

$$\frac{L_c}{R_s} = K_R \cdot \cos^{-1} \left[\frac{D}{AB(K_R + DK_D/K_d)} (-1 + D\sqrt{1+e}) + \frac{K_R \gamma}{2} \right. \qquad \text{(II.4.4)}$$

where

$$e = (A \cdot B)^2 (K_R + D\,K_p/K_d)^2 + 2D\,K_R\,AB$$

For surface grinding

$$\frac{L_c}{R_s} = \frac{1}{2} K_V K_p + \sqrt{\frac{2K_p}{AK_d}} \qquad \text{(II.4.5)}$$

It can be seen from the Equations (II.4.4) and II.4.5) the chip length L_c is a function of the radius ratio K_R, the velocity ratio K_V, the successive cutting edge spacing δ and the cutting depth of wheel d.

(4) MAXIMUM CHIP THICKNESS t_{max}

The maximum chip thickness can be given for external and internal grinding in the following equation:

$$\frac{t_{max}}{R_s} = D[D\,\frac{K_p}{K_d} - K_R\,\{\frac{1}{2}(DK_R AB+1)(\beta-\gamma)^2\}] \qquad \text{(II.4.6)}$$

where

$$\beta = \cos^{-1}[\frac{D}{AB(K_R+DK_p/K_d)}\,(-1 + D\sqrt{1+e})]$$

For surface grinding

$$\frac{t_{max}}{R_s} = \frac{K_p}{K_d} - \frac{A}{2}[\sqrt{\frac{2 \cdot K_p}{A \cdot K_d}} - K_V \cdot K_p]^2 \qquad \text{(II.4.7)}$$

It can be seen from the Equations (II.4.6) and (II.4.7) that the maximum chip thickness t_{max} is also a function of the radius ratio K_R, the velocity ratio K_V, the successive cutting edge spacing δ and the depth of the wheel d.

(5) THE ANGLE i_d AT THE END OF CONTACT:

The interference angle i_g is the angle at the beginning of contact between the cutting edge and the workpiece and is an important value for analyzing the transitional cutting process during up-grinding. However, the angle i_d at the end of contact will become important for analyzing down-grinding as mentioned later in more detail. It is be given by the following equation:

$$i_d = \sqrt{2DK_d(AB+\frac{1}{DK_R})} \qquad \text{(II.4.8)}$$

From this equation it should be noted that the angle i_d is a function of the radius ratio K_R, the velocity ratio K_V, the successive cutting edge spacing δ and the depth of wheel d, although the interference angle i_g is independent of the depth of wheel.

II.4.4 Typical Example of Undeformed Chip Shape

In the previous paragraph the fundamental and important equations concerning wheel-work conformity have been developed. However, these equations are very complicated functions of the grinding conditions and it is difficult to see from the equations how the grinding conditions affect the basic boundary conditions such as the interference angle, the chip length, the maximum chip thickness and the angle at the end of contact.

In this paragraph typical trends predicted by these equations will, therefore, be illustrated and the implications of these trends indicated.

(1) THE INTERFERENCE ANGLE i_g:

The effects of the various working conditions upon the interference angle i_g are shown in Figures II-41, II-42, and II-43. As can be seen in Figures II-41 and II-42, the interference angle i_g is greater for external grinding, for decreasing values of the radius ratio K_R, and is increased widely simply by increasing the values of the speed ratio K_V. It is a maximum at K_V=1. As indicated by Figure II-43, the interference angle i_g is a very strong function of the successive cutting edge spacing ratio K_p, increasing with increasing K_p. Ordinarily, there is little control over the value of K_R because of the machine and workpiece geometry, however there is some control over the value of K_p obtained by changing the dressing condition. The best way to increase the interference angle i_g, however, is to increase the speed ratio K_V.

(2) THE MAXIMUM CHIP THICKNESS

In Figures II-44 and II-45, typical variations of the maximum chip thickness t_{max} with speed ratio K_V and the ratio of successive cutting edge spacing to cutting depth of wheel K_d are shown for typical values of K_R and K_p. The interesting feature is that the thickness increases with increasing K_V or the cutting depth of the wheel d.

(3) THE ANGLE i_d AT THE END OF CONTACT

The effects of the grinding conditions upon i_d are shown in Figure II-46 to II-48. As can be seen from these figures

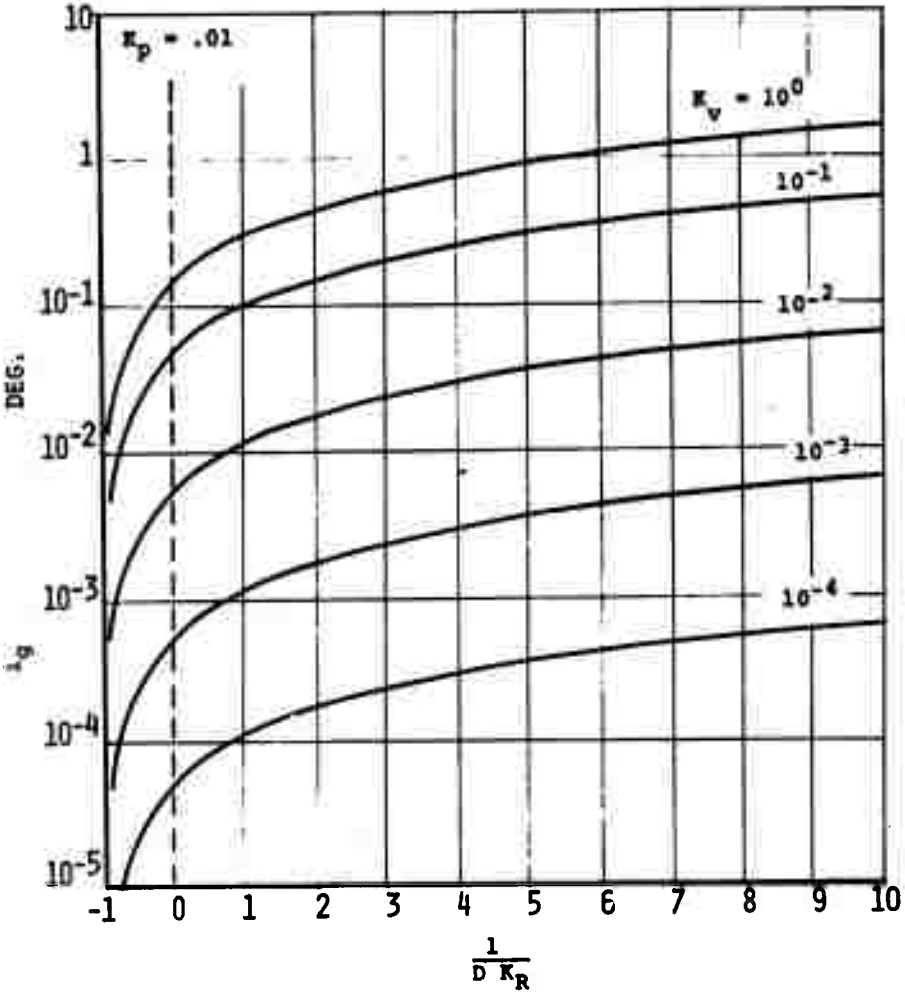

FIGURE II-41 - EFFECTS OF K_R ON i_g

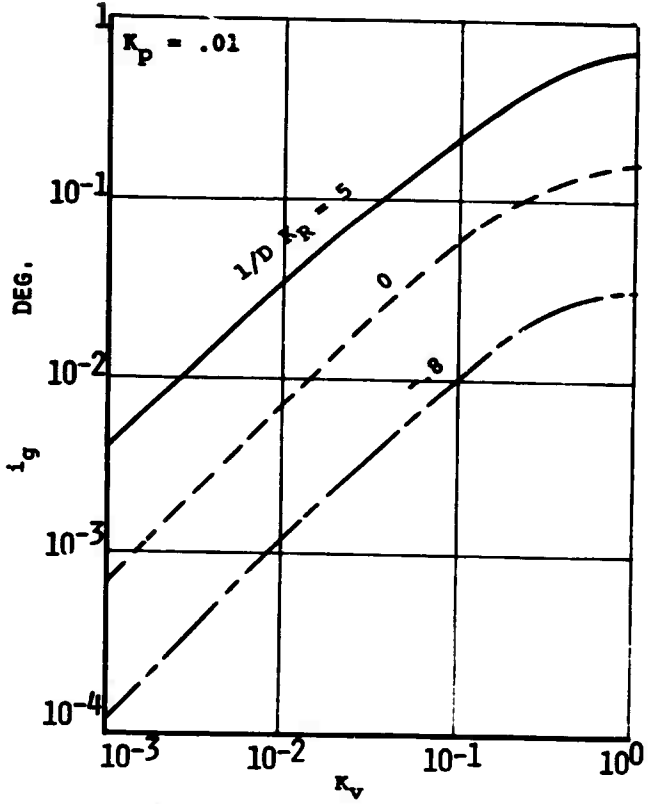

FIGURE II-42 - EFFECTS OF K_v ON i_g

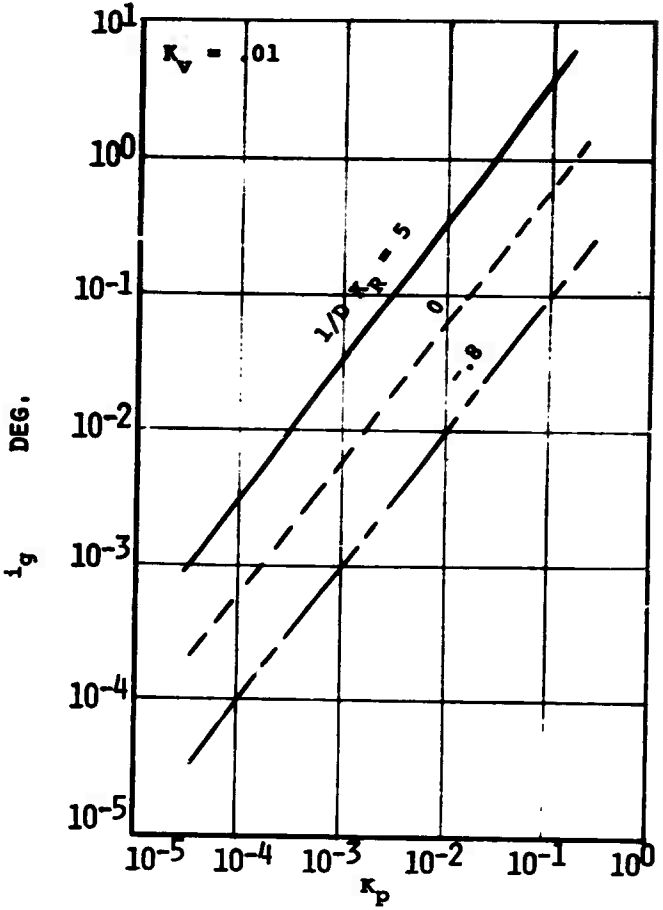

FIGURE II-43 - EFFECTS OF K_p ON i_g

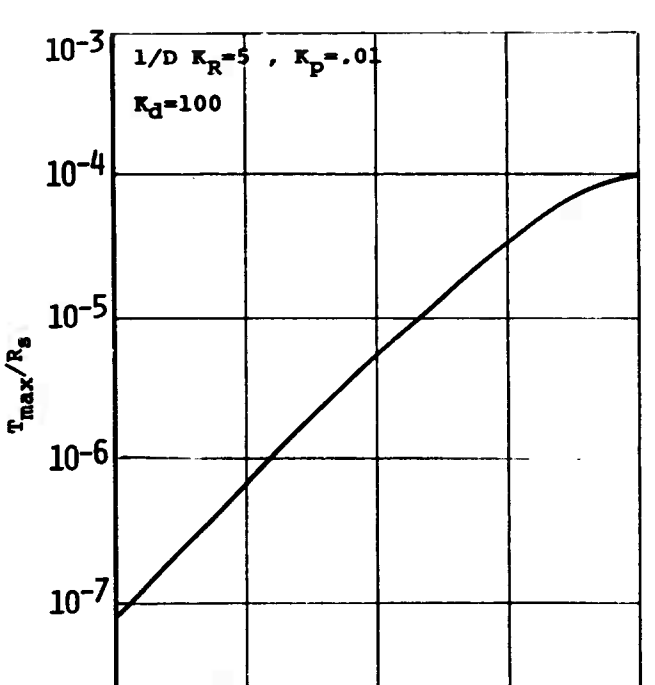

FIGURE II-44 - TYPICAL VARIATION OF T_{max}/R_s WITH K_v

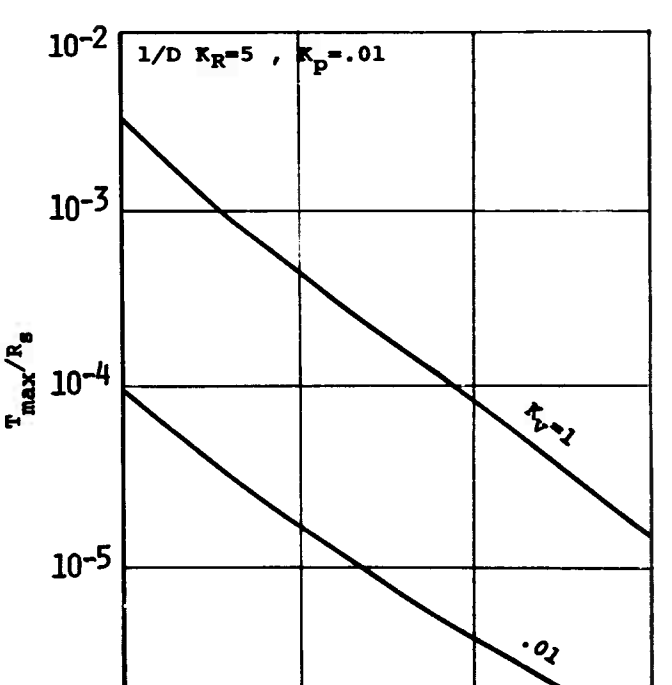

FIGURE II-45 - VARIATION OF T_{max}/R_s WITH K_d

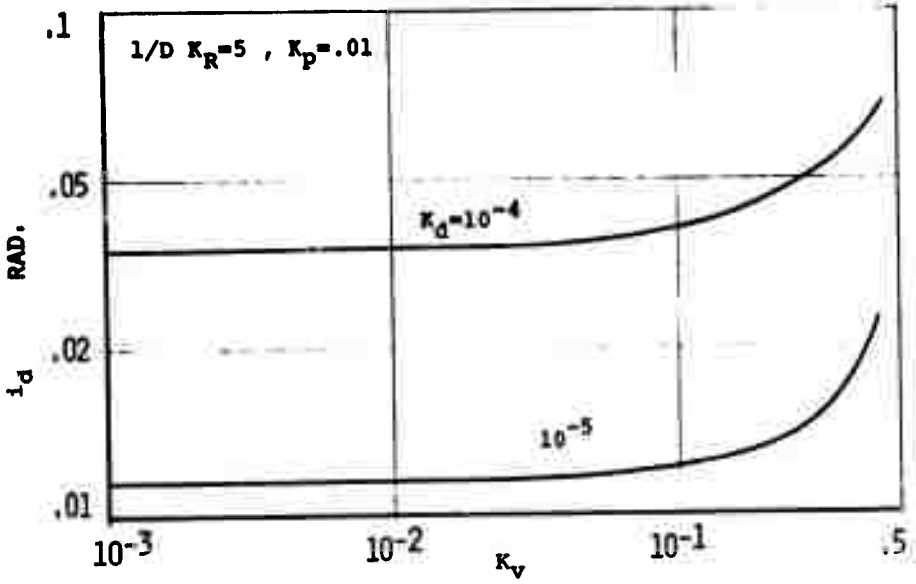

FIGURE II-46 - EFFECTS OF K_v ON i_d

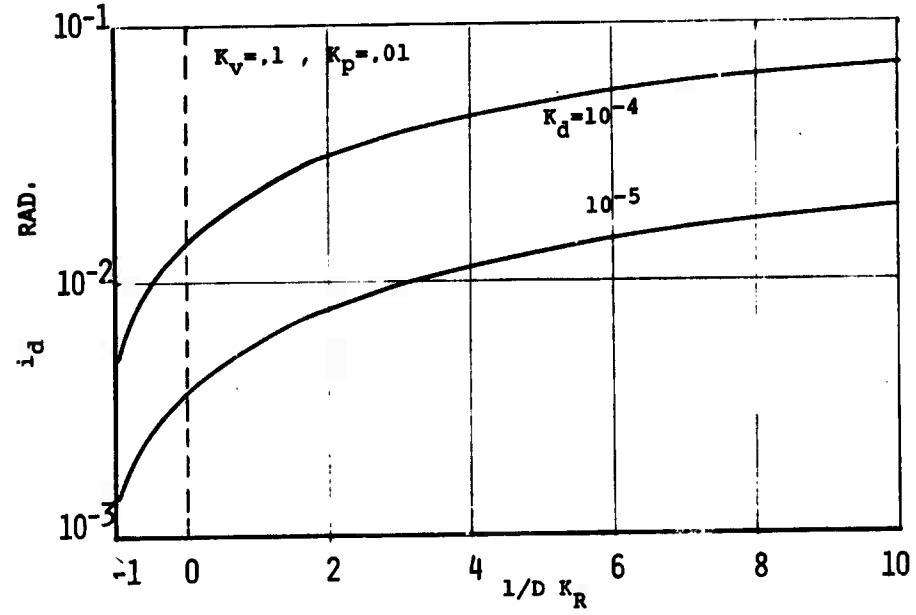

FIGURE II-47 - EFFECTS OF K_R ON i_d

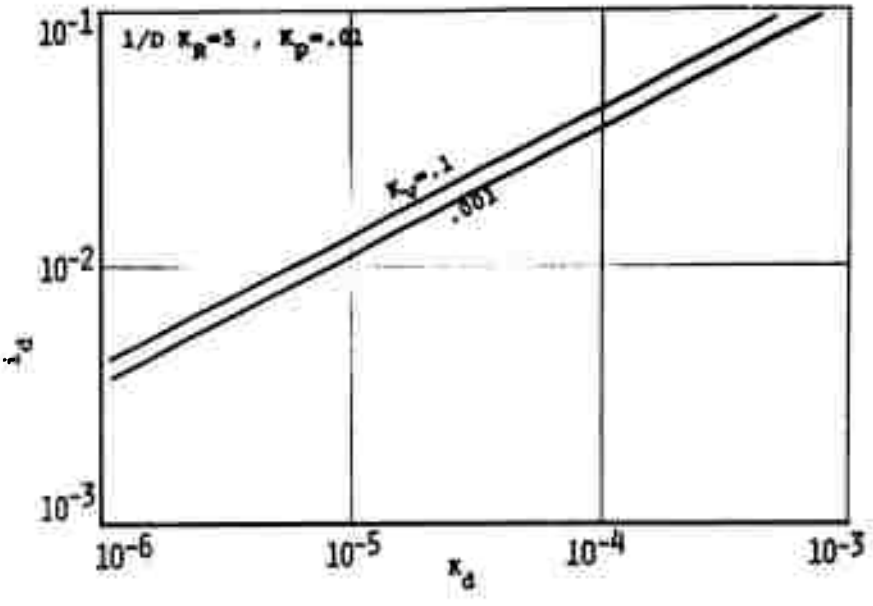

FIGURE II-48 - EFFECTS OF K_d ON i_d

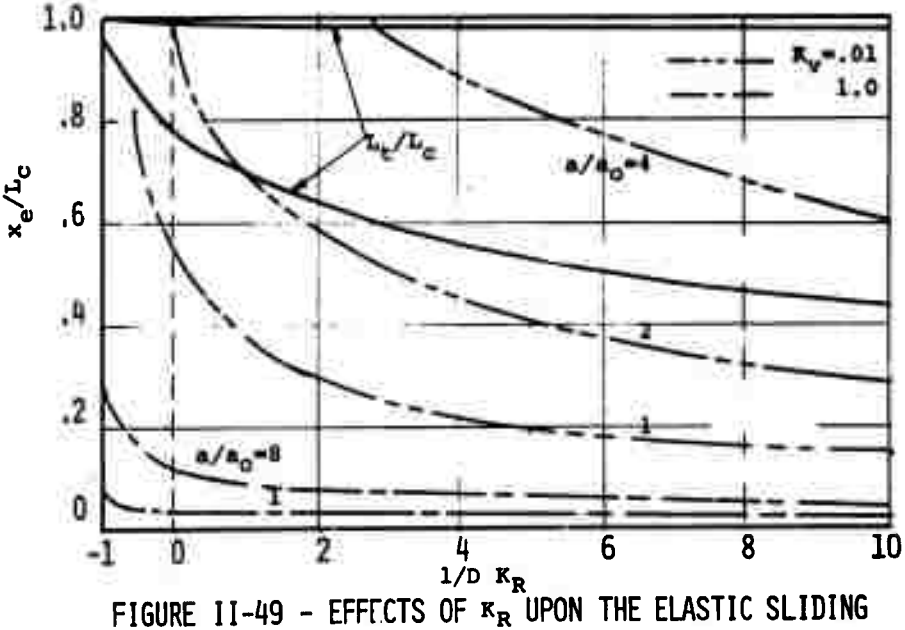

FIGURE II-49 - EFFECTS OF K_R UPON THE ELASTIC SLIDING RATIO

the value of the angle i_d is nearly constant at small values of K_V and increases rapidly at high value of K_V. Furthermore the value of i_d increases with increasing values of $1/DK_R$ and with the square root of K_d.

It should be noted that the main difference between i_g and i_d is that the value of i_g is a function of K_V, K_R and K_p while i_d is a function of K_V, K_R and K_d. Also, for small values of K_V, the value of i_d is nearly constant while i_g is a drastically changing function.

II.5 Contact Stiffness Consideration

II.5.1 Introduction

In Subsection II.2 the deformation processes in the elastic and plastic region were analyzed theoretically for the transitional cutting process where the depth of cut is increased linearly. A discussion of how the interference angle, the wear width of the clearance surface, spring constant of grain mounting and relative cutting velocity affect the deformation process was presented. In Subsection II.3 the transitional cutting process was examined by using a circular cutting test and from this test it was found that the cutting edge slides elastically or plastically throughout the entire length of contact unless the plastic deformation or cutting occurs before the point where the depth of cut becomes a maximum. In Subsection II.4 the cutting model in grinding and the basic boundary conditions were proposed to analyze the transitional

cutting process in grinding, based upon the theoretical and experimental analysis of the transitional cutting process. In this subsection the deformation theory will be combined with the conformity theory to analyze the grinding process. Furthermore, a discussion of the affect of the grinding conditions on the elastic and plastic regions is presented. Optimum grinding conditions for increasing the cutting region by reducing the sliding length of the cutting edges are discussed.

II.5.2 Elastic Sliding Length Ratio In Up Grinding

As described in Subsection II.4, the chip can be divided into two regions (A and B). In region A the chip thickness is linear to the distance from the leading edge of chip and can be given by the following equation

$$\frac{t}{R_s} = i_g \left(\frac{x}{R_s}\right) \qquad \text{(II.5.1)}$$

Region B is a parabolic region and the chip thickness in this region can be given by the equation

$$\frac{t}{R_s} = D\left[C_1\left(\frac{x}{R_s}\right)^2 + C_2\left(\frac{x}{R_s}\right) + C_3\right] \qquad \text{(II.5.2)}$$

where

$$C_1 = -i_g/2\ L_\alpha$$

$$C_2 = i_g/2$$

$$C_3 = -i_g \cdot L_\alpha/8 + D\ \underline{K}_d$$

$$L_\alpha = K_V \cdot K_p\ ,\ \underline{K}_d = K_d/K_p$$

On the other hand, a certain amount of normal force $P(x_e)$ is required for the metal being cut to be deformed plastically

under the cutting edge, and the normal force is given by Equation (II.2.8). The displacement of the cutting edge is Δn_e which is given in Equation (II.2.11) and that at the surface of workpiece y_e is given by Equation (II.2.10), when the normal $P(x_e)$ acts upon the cutting edge.

Therefore the metal being cut begins to be deformed plastically under the cutting edge at the point where the chip thickness given in Equations (II.5.1) and (II.5.2) becomes equal to the summation $(\Delta n_e + y_e)$ of the displacement of the cutting edge and that of the workpiece. Then the critical depth of cut can be given by the equation

$$t_e = P(x_e)/k_{cs} \qquad \text{(II.5.3)}$$

where k_{cs} is a contact stiffness in the elastic region and given by the following relation:

$$\frac{1}{k_{cs}} = \frac{1}{k_s} + \frac{1}{J(\rho, V)}$$

From Equation (II.5.3) and Equation (II.5.1) or Equation (II.5.2), the elastic sliding length of abrasive grain in grinding can be given by the equations

$$\frac{x_e}{R_s} = \frac{1}{I_g}\,\frac{1}{R_s}\,\left(\frac{P(x_e)}{k_{cs}}\right) \qquad \text{(II.5.4)}$$

or

$$\frac{x_e}{R_s} = \frac{L_a}{2} - \sqrt{\frac{2L_a}{I_g}\left[\bar{K}_d - \frac{1}{R_s}\left(\frac{P(x_e)}{k_{cs}}\right)\right]} \qquad \text{(II.5.5)}$$

Therefore the ratio of the sliding length to the total undeformed chip length can be obtained as:

$$\frac{x_e}{L_c} = \frac{\frac{1}{K_s}\left(\frac{P(x_e)}{k_{cs}}\right)}{\left[i_g L_a\left(\frac{1}{2} + \sqrt{\frac{2}{i_g L_a}\,K_d}\right)\right]} \qquad \text{(II.5.6)}$$

or

$$\frac{x_e}{L_c} = \frac{\frac{1}{2} - \sqrt{\frac{2}{i_g L_a}\left[K_d - \frac{1}{K_s}\cdot\frac{P(x_e)}{k_{cs}}\right]}}{\frac{1}{2} + \sqrt{\frac{2}{i_g \cdot L_a}\,K_d}} \qquad \text{(II.5.7)}$$

Equation (II.5.6) should be effective for the case where the metal begins to be deformed plastically in the linear region and Equation (II.5.7) for the parabolic region.

Furthermore, it should be noted that the cutting edge slides throughout the whole contact length between the cutting edge and workpiece unless the plastic deformation occurs before the point where the chip thickness becomes a maximum, as was described in detail in Subsection II.2.

II.5.3 Effects of Grinding Conditions Upon the Elastic Sliding Ratio In Up Grinding

It is very important to discuss the effects of working conditions upon the elastic sliding ratio to determine optimum grinding conditions, because one of the means to get optimum grinding results is to reduce the elastic sliding length.

(1) THE EFFECTS OF THE RADIUS RATIO K_R

Figure II-49 shows variation of the elastic sliding length ratio with the radius ratio K_R. In this figure it can be seen that the sliding length ratio decreases with increasing value of $1/DK_R$ and that internal grinding has extremely poor conformity. This figure exemplifies the difficulty of using

internal grinding. External grinding for the same grinding condition has the lowest values of the elastic sliding length ratio and should give improved grinding results. This is consistent with general grinding knowledge.

(2) THE EFFECTS OF THE VELOCITY RATIO K_V

The effect of the velocity ratio upon the elastic sliding length is extremely important because the velocity ratio and wheel cutting depth are the most controllable parameters.

Figure II-50 shows a typical example of the effects of K_V upon the sliding length ratio. It should be noted from this figure that the sliding length ratio decreases with increasing value of the velocity ratio K_V and becomes minimum at $K_V=1$ where i_g is a maximum for the case where the plastic deformation occurs in the linear region (Region A, Figure II-39(b)). This region is the important one for most practical grinding conditions.

However, for some cases of extreme grinding conditions the plastic deformation occurs in the parabolic region, and then it is possible that the optimum value of K_V is different from one. In order to better indicate this point, Figure II-51 is shown. In this figure K_{Vc} represents the critical velocity ratio and in grinding with velocity ratio K_V smaller than K_{Vc} the cutting edge slides through the whole contact length. It should be noted from this figure that the sliding length ratio is equal to one if $K_V<K_{Vc}$, decreases to a minimum value at K_{Vo} and then increases with increasing K_V.

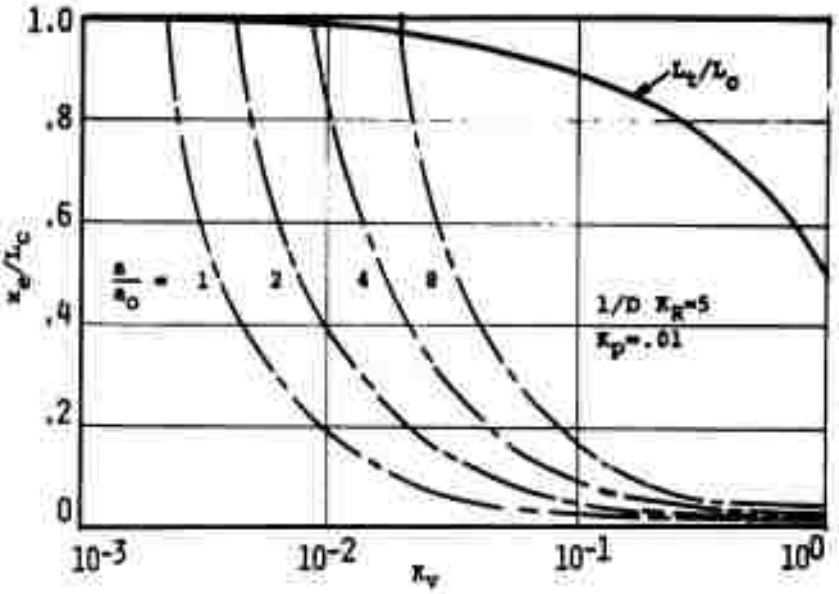

FIGURE II-50 - TYPICAL EXAMPLE FOR THE EFFECT OF K_v UPON THE ELASTIC SLIDING LENGTH RATIO

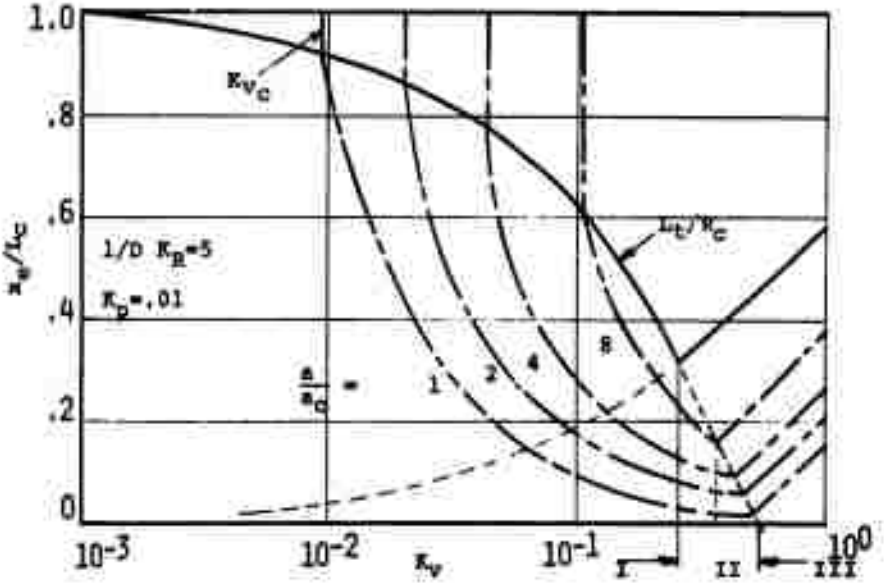

FIGURE II-51 - EFFECTS OF K_v UPON THE SLIDING LENGTH RATIO

Therefore the optimum operating condition would be at K_{V_o} for minimum sliding length ratio. For almost all of the practical grinding the optimum velocity ratio K_{V_o} is, however, equal to one, because the parabolic region rarely exists before the point where the chip thickness is maximum.

(3) THE EFFECTS OF THE SUCCESSIVE CUTTING EDGE PARAMTER K_p

Since the cutting edge spacing is significantly influenced by the dressing condition, one indication of the relative importance of the dressing condition can be obtained by studying the effects of the successive cutting edge spacing upon the elastic sliding length ratio. The effect of the successive cutting edge spacing parameter K_p is shown in Figure II-52 for a typical value of K_V =.01. It should be noted from this figure that the elastic sliding length ratio decreases with increasing value of K_p. However an optimum successive cutting edge spacing exists for the case where plastic deformation occurs in the parabolic region before the point where the chip thickness is maximum, as described previously.

(4) THE EFFECT OF THE DEPTH OF CUT OF THE WHEEL

The depth of cut of the wheel is another variable which can be very easily controlled during grinding and, therefore, is very important. The effect of the depth of cut of wheel upon the elastic sliding ratio is shown in Figure II-53 for K_V=.01.

The elastic sliding length ratio decreases with increasing cutting depth of wheel and therefore it appears that for

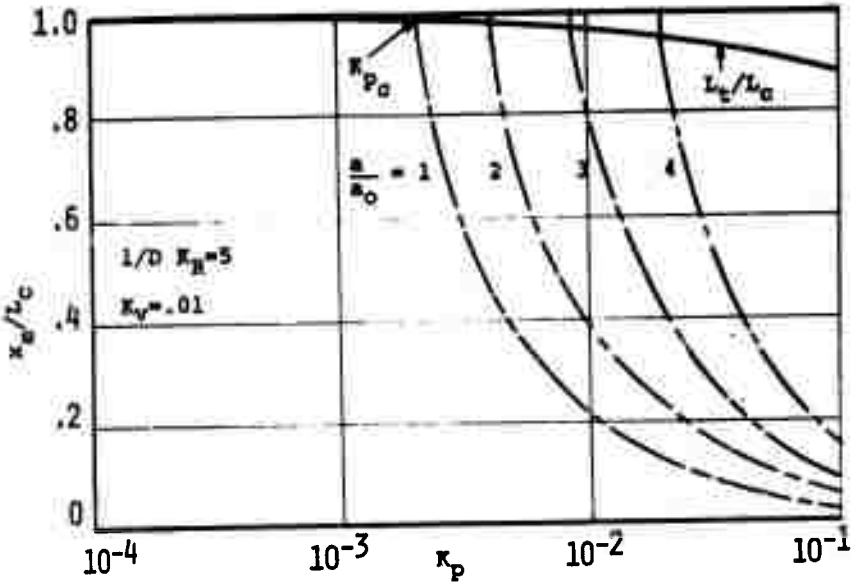

FIGURE II-52 - EFFECTS OF K_p UPON THE SLIDING LENGTH RATIO

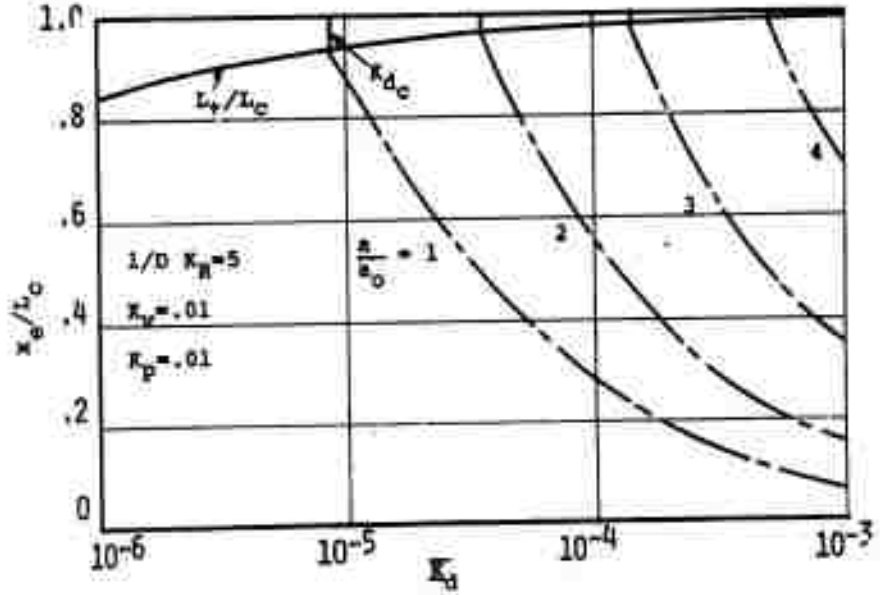

FIGURE II-53 - EFFECTS OF K_d UPON THE SLIDING LENGTH RATIO

larger values of cutting depth better grinding results can be obtained based upon the elastic sliding length consideration.

(5) EFFECT OF THE CONTACT AREA

A typical variation of the sliding length ratio with the contact area is shown in Figure II-54 for several typical cases.

In all cases the sliding length ratio increases with increasing contact area as predicted in the equation for the elastic sliding length. The contact area increases due to wheel wear during grinding and, therefore, the sliding length ratio will increase with time during grinding.

(6) EFFECT OF THE GRAIN MOUNTING SPRING CONSTANT

Cutting edges are mounted resiliently by a bond which has an elastic property and therefore cutting edges can deflect causing the sliding region to increase. The effect of the spring constant is shown in Figure II-55. From this figure the elastic sliding region can be reduced by using a harder wheel.

II.5.4 Elastic Sliding Length Ratio In Down Grinding

As described in Subsection II.4, the cutting-out angle i_d is larger than the cutting-in angle i_g for nearly all of the practical grinding conditions. Therefore, if the grinding wheel is operated in the opposite direction (down grinding), better grinding results can be expected because of the decrease of the sliding length of cutting edges as in down milling.

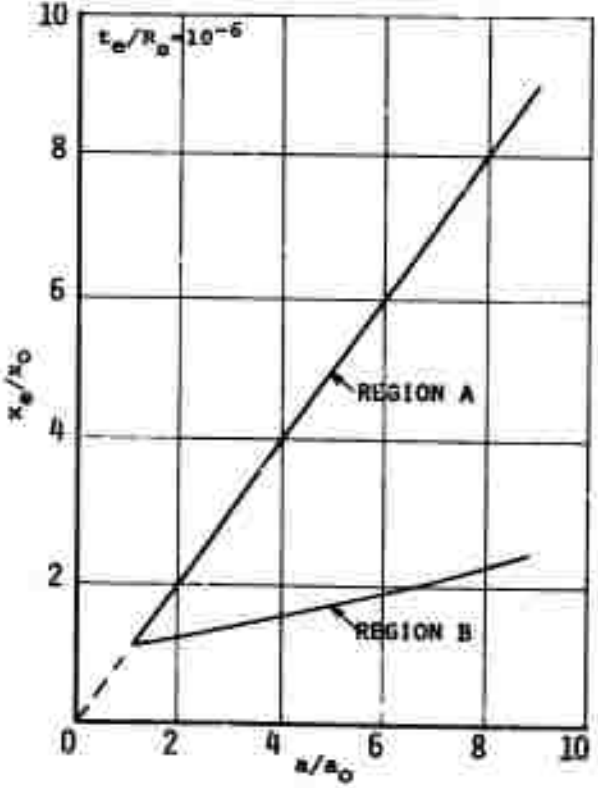

FIGURE II-54 - EFFECTS OF CONTACT AREA UPON THE SLIDING LENGTH RATIO

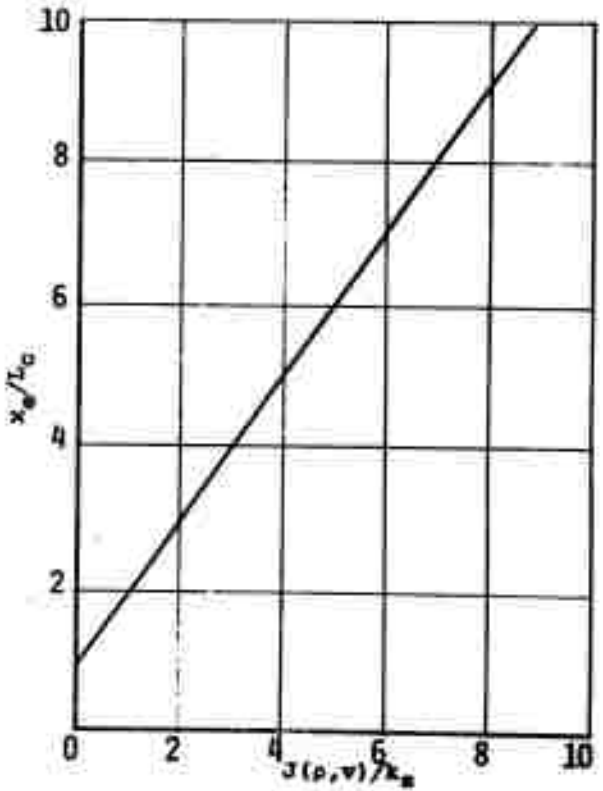

FIGURE II-55 - EFFECTS OF THE SPRING CONSTANT UPON THE SLIDING LENGTH RATIO

The down-grinding chip geometry is basically the same as the up-grinding geometry. The chip is divided into two regions: A linear region and a parabolic region. For up-grinding the cutting edge enters the linear region, then the parabolic region but in down-grinding the cutting edge enters the parabolic region first. Therefore the elastic sliding length ratio for down-grinding can be determined in the same way as in up-grinding:

$$\left(\frac{X_e}{L_c}\right)_{down} = \frac{\frac{2}{i_d \cdot L_a}\left[K_d\sqrt{\frac{1}{K_p}} - \sqrt{K_d\left(\underline{K}_d - \frac{P(x_e)}{R_s k_{cs}}\right)}\right]}{\frac{1}{2} + \frac{2K_d}{L_a \cdot i_d}\sqrt{\frac{1}{K_p}}} \qquad \text{(II.5.8)}$$

In Figures II-56 to II-59, the effects of the grinding conditions upon the sliding length ratio are shown. It should be noted from these figures that the effects of the velocity ratio K_V, the radius ratio K_R and the successive cutting edge spacing parameter K_p upon the elastic sliding length ratio are very small for down-grinding. The important point is that in general the elastic sliding length ratio is much smaller for down-grinding than that for up-grinding.

II.5.5 Consideration of Sliding Phenomena on the Ground Surface

In the previous paragraph the ratio of sliding length to the whole length of contact between cutting edge and workpiece was discussed. However the greatest part of the contact is removed by the successive cutting edges and therefore

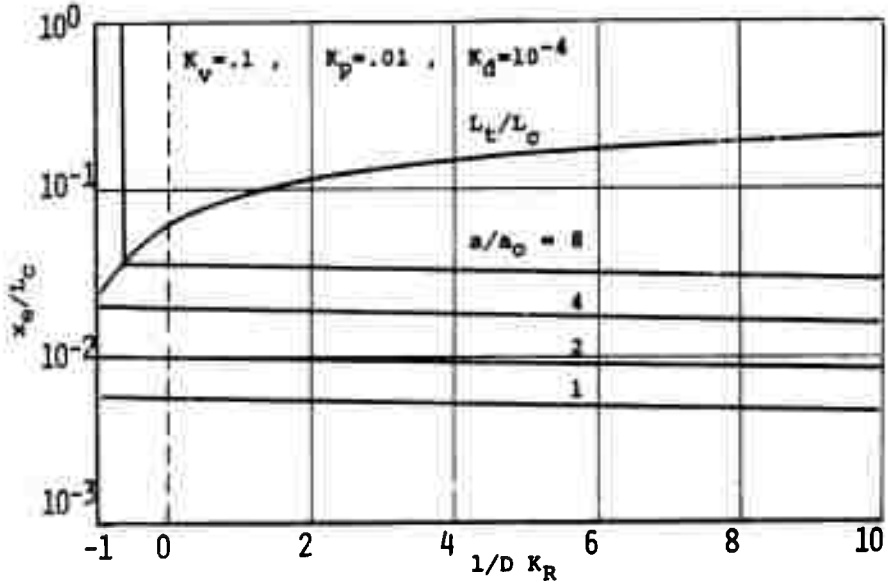

FIGURE II-56 - EFFECTS OF K_R ON x_e/L_c FOR DOWN GRINDING

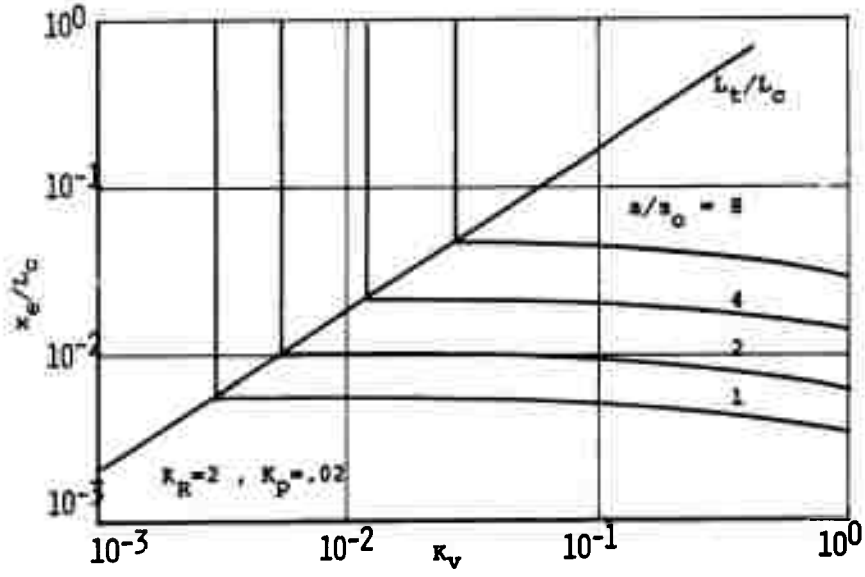

FIGURE II-57 - EFFECTS OF K_v ON x_e/L_c FOR DOWN GRINDING

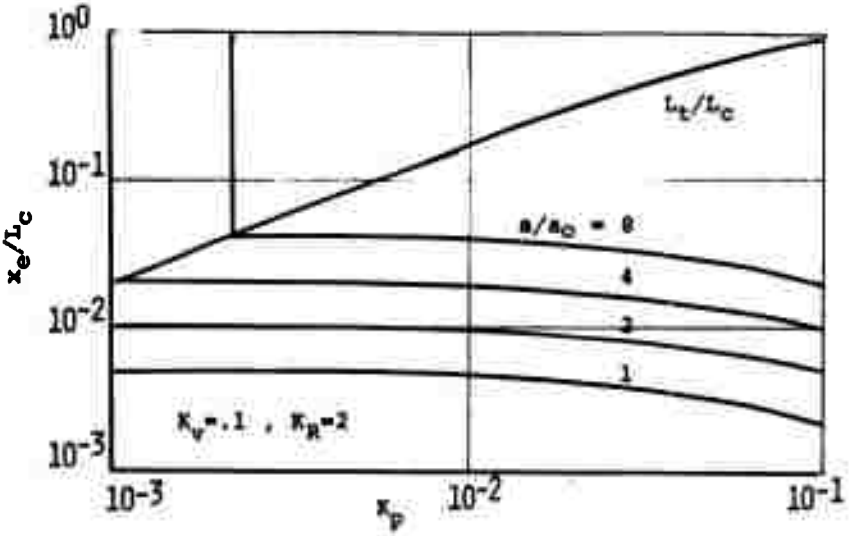

FIGURE II-58 - EFFECTS OF K_p ON x_e/L_c FOR DOWN GRINDING

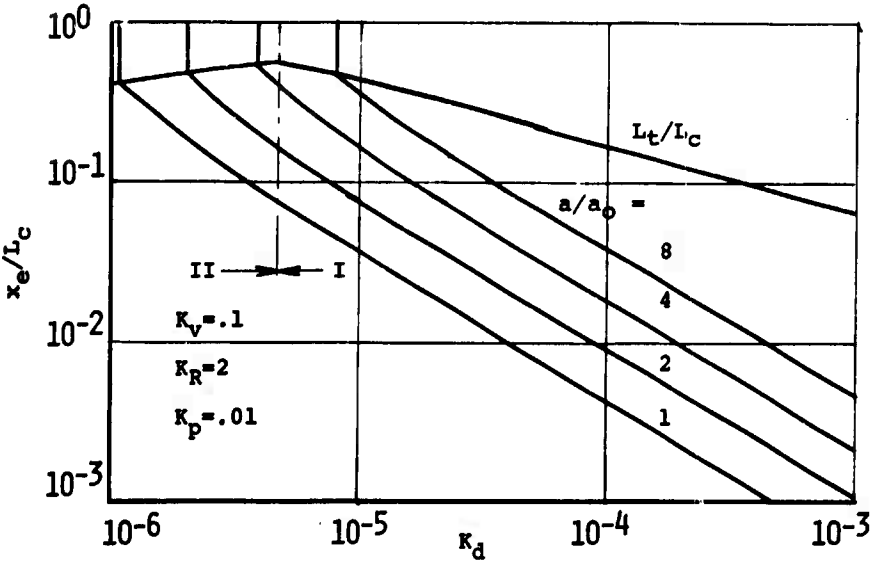

FIGURE II-59 - EFFECTS OF K_d ON x_e/L_c FOR DOWN GRINDING

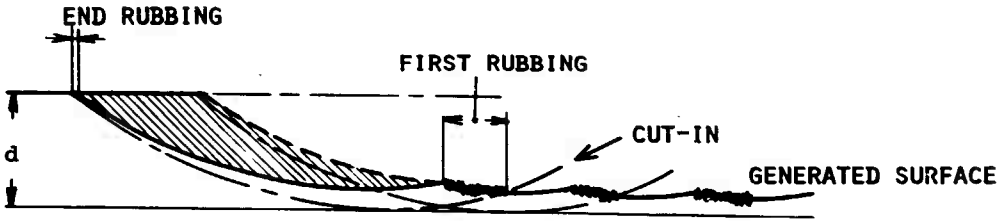

FIGURE II-60 - SURFACE FORMATION IN GRINDING

the final surface will be formed from the initial part of contact (See Figure II-60).

Therefore, in order to evaluate effects upon the ground surface, a parameter which relates the ratio of the elastic sliding length to the length of contact which remains on the ground surface, should be used. For some cases of grinding this parameter is possibly equal to one. This doesn't necessarily mean that the cutting edge will slide through the entire length of contact, but the successive cutting edge removes the cutting region of the previous cutting edge leaving only the sliding region. Therefore the sliding phenomena may play a greater role upon the formation of the surface in grinding even for cases when the ratio of the sliding length to the whole length of contact is very small.

II.6 Conclusions

In this section the deformations in the elastic and plastic regions, which exist near the beginning of contact during transitional cutting, have first been analyzed theoretically and experimentally from the viewpoint that the cutting process in grinding is transitional.

Basic boundary conditions that affect the transitional cutting in grinding have been clearly defined by the proposed cutting model in grinding. The relationship between these basic boundary conditions and the grinding conditions have been discussed by analyzing the geometrically undeformed chip shape in grinding.

Furthermore, various phenomena in the wheel-work interference zone have been analyzed from the deformation theories and the conformity theory.

Consequently it has been discovered that the "free cut" of each grain is required for increasing the grinding efficiency and improving the ground surface integrity. The conditions for the free cut of each cutting edge are:

(1) To increase relative cutting velocity

(2) To increase the ratio of work velocity to wheel velocity

(3) To increase contact stiffness

(4) To use sharper cutting edges.

II.7 Nomenclature

A = $1/(K_v + 1)^2$

$2a$ = Contact length in clearance surface

B = $1 - K_v(K_v+2)/DK_R$

C_b = Rake width coefficient of pile up

C_s = Rake height coefficient of pile up

D = Selection parameter D = +1; external grinding
D = -1; internal grinding

d = Depth of cut of grinding wheel

D_h = Depth of plastic flow layer

G = Grinding ratio

$G(\rho,V)$ = Force constant

h = Contact length on the rake surface in plastic region

H_{max} = Surface roughness

i_d = Interference angle in down grinding

i_g = Interference angle in up grinding

$J(\rho,V)$ = Displacement constant in elastic region

$J_p(\rho,\alpha)$ = Displacement constant in plastic region

K_d = δ/d = ratio of successive cutting edge spacing to depth of wheel

$\underline{K}_d$ = K_d/K_p

K_p = δ/R_s = ratio of successive cutting edge spacing to wheel radius

K_R = R_w/R_s = radius ratio

K_V = V_w/V_s = velocity ratio

k = Yielding stress in shear

k_s = Spring constant of grain mounting

k_{cs} = Contact stiffness in elastic region

L_c = Undeformed chip length

$P(x)$ = Normal force

$P(x_e)$ = Critical normal force

$Q(x)$ = Tangential force

R_s = Wheel radius

R_w = Workpiece radius

t_{max} = Maximum chip thickness

V = Relative cutting speed

V_s = Wheel surface speed

V_w = Work surface speed

x,y = Fixed rectangular coordinates

x_e = Elastic sliding length

x_p = Plastic sliding length

y = Real cutting depth

y_e = Critical depth of cut of elastic region

y_f = Depth of plastic flow layer

y_{hd} = Depth of hardened layer

y_p = Critical depth of cut of plastic region

α = Rake angle

β_c = Profile angle of pile up ahead of rake surface

δ = Successive cutting edge spacing

γ_b = Width coefficient of pile up at sides of cutting groove

γ_s = Height coefficient of pile up at sides of cutting groove

ξ, η = Moving rectangular coordinates

$\Delta\eta_e$ = Displacement of cutting edge at critical point of elastic region

λ, μ = Lame's constant

ν = Poison's ratio

σ, τ = Stress

$\sigma_e(V)$ = Yielding stress in tension

ρ = Frictional coefficient between cutting edge and workpiece

SECTION III

THERMAL ANALYSIS IN GRINDING

III.1 Introduction

The purpose of Section III of this Final Report is to summarize the methods for calculating grinding temperatures which were presented in the Interim Engineering Reports (I.E.R. IV-VI). Some new considerations are also discussed in this section.

The effect of temperature in grinding is discussed in a qualitative manner in Section III.1. A brief literature review is presented in Section III.2. In Section III.3 several methods of calculating grinding temperature are summerarized from previous reports. In Section III.4 temperature in the region of a single grain is related, through wheel-work contact geometry, to temperature of the workpiece surface which remains after grinding. Conclusions and recommendations are discussed in Section III.5.

In considering the effects of the grinding process on the condition of the finished workpiece it is necessary to discuss thermal conditions to which the workpiece and wheel may be subjected. The total energy expended during grinding is usually more than that required to raise the volume of metal removed to its melting temperature. It has been determined that 60 to 80 percent of the total grinding energy can enter the workpiece as heat for dry grinding (1,2). The

heat is generated on the workpiece surface by grain-workpiece friction, and in regions of workpiece deformation. Because of large rates of heat generation in the grinding process, high temperatures can be reached in the workpiece surface layers and in the abrasive grains of the wheel.

The condition of the wheel during grinding is determined to some extent by the temperature encountered by the grains. Accelerated wear of the abrasive and "loading" due to chemical reaction between grain and workpiece material can result from high temperatures. These effects cause dulling of the wheel and decreased cutting capability. On the other hand, high temperature and rapid cooling cycles may cause sufficient thermal stressing of grain and bond to result in grain fracture and the generation of new sharp cutting edges.

The quality of the finished workpiece is determined to a great extent by the temperatures encountered during grinding. The final dimensional accuracy of the workpiece will be diminished if significant expansion occurs during the grinding process and contraction occurs after grinding.

The thermal history of the workpiece affects the physical structure, or surface integrity, of workpiece material. Under metallographic examination hardened steels can exhibit martensitic surface layer if grinding has generated sufficient heat to cause rehardening. Below the surface a region of over tempering, or softening, is frequently detected. In some instances a hardness lost is present at the surface.

These factors can affect the useful life of a workpiece if hardness loss is sufficient to limit allowable loads or reduce the ability of a production part to withstand wear.

Plastic deformation during the cutting process, permanent deformations due to volumetric expansion or contraction caused by phase change, and permanent deformations caused by volumetric expansion and contraction during heating and cooling all contribute to the resultant residual stress distribution of the ground surface, which may ultimately affect the useful life of the part. These factors can also cause cracks in the surface of the part. Surface cracks may result either in scrappage, or, if undetected, in catastrophic failure during service.

Because of the importance of grinding temperatures it is necessary to extend the methods for predicting temperatures and to examine the effect of such things as workpiece cooling by grinding fluids.

III.2 Literature Review

Several investigators have considered grinding temperature from a theoretical and experimental viewpoint. The thermal analysis of Jaeger (3) has been used for calculations of grinding temperature which appear in the literature. The work of Jaeger is reviewed in Section III.3.3. His analysis considers a moving heat source on the surface of a semi-infinite body. The results of that investigation were utilized

by other investigators to determine grinding process temperatures, although the cooling effect of grinding fluids was not considered.

The temperature of a chip shear plane has been calculated to be in the range of 2000°F to 3000°F by several investigators (1, 4, 5) in the case of the surface grinding of steel. Outwater and Shaw (4) measured temperatures by using a wheel-workpiece thermocouple and obtained temperatures in this range. The measured temperature in this case is some average temperature of all places of contact between the rake faces of the grains and chips in the process of being cut, and between the clearance faces of the grains and the workpiece material.

In further experiments Shaw and Mayer (5) used a photo-conducting lead sulfide cell to sight through a hole in the grinding wheel to the radiating surface of the ground workpiece. Qualitative agreement between calculated shear plane temperatures and measured temperatures was obtained, but the calculated temperatures are greater by a factor of three to five.

Littman (6) and Takazawa (7) used thermocouples embedded beneath the workpiece surface to measure temperatures at various depths as material was removed from the workpiece surface in successive grinding passes. In both cases there was no attempt to correlate experimental temperatures to theoretically calculated temperatures. However, the effect of measured temperatures on hardness changes of the workpiece material was discussed.

Takazawa determined a semi-empirical expression to predict the effect of grinding conditions (V_s, V_w, and d) on the workpiece surface temperatures. This expression was used to recommend ways to reduce grinding temperature and its effects on workpiece metallurgy. He recommends reduction in depth of cut and wheel speed and he implies that workpiece speed should be increased at least up to a point.

Opitz and Guhring (8) measured temperatures in high wheel speed plunge grinding by embedding an insulated platinum foil in the surface of a steel workpiece, and allowing the grains to break the insulation and cause welds to form between the foil and workpiece, producing a thermocouple. It is not clear which temperatures were measured in this case.

Malkin (1) theoretically determined the shear plane temperature distribution, temperature under the wear flat of an individual grain, and the average interference zone surface temperature.

III.3 Methods for Calculating Grinding Temperatures

III.3.1 Introduction

In order to more clearly understand thermal problems in grinding it is necessary to extend theoretical methods for determining temperatures. A summary of theoretical analyses which can be applied for predicting grinding temperatures is presented in this section.

In Subsection III.3.2 thermal models which can be used in calculating temperatures in grinding are discussed. In Subsection III.3.3 the thermal analysis of Jaeger (3) is reviewed. This analysis considers a moving heat source on the adiabatic surface of a semi-infinite body. In Subsection III.3.4 the thermal analysis of the semi-infinite body with a moving heat source and with convective cooling is summarized from I.E.R.IV. The analysis of a rotating cylindrical body with a heat source on the surface and with convective cooling is summarized in Subsection III.3.5 from I.E.R.VI.

III.3.2 Thermal Models

In order to estimate temperatures in grinding it is necessary to hypothesize idealized thermal models which can be mathematically analyzed and which provide a reasonable approximation to the conditions occuring in grinding. Two such models are shown in Figures III-1 and III-2.

Figure III-1 shows a heat source on the surface of a moving semi-infinite body. The heat source $\bar{q}_B$ represents the fraction of grinding energy which enters the workpiece as heat per unit time over the wheel-work contact zone. In this case it is assumed that the heat flux is uniformly distributed over the interference zone area. Therefore, the heat flux is given by

$$\bar{q}_B = \frac{C_1 F_H (V_w + V_s)}{bL_c} \qquad \text{(III.3.1)}$$

where C_1 is the fraction of the total grinding energy $F_H (V_w + V_s)$ which enters as heat.

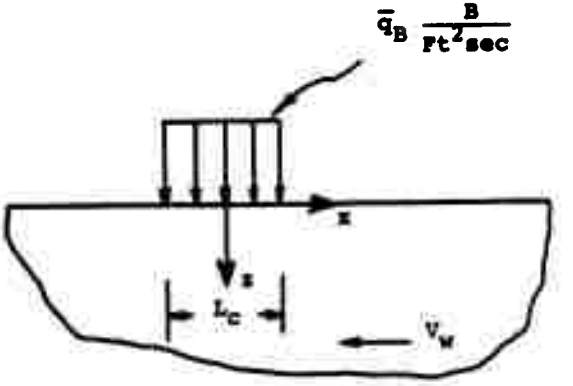

FIGURE III-1 - INTERFERENCE ZONE HEAT SOURCE

TYPICAL VALUES

$L_c \sim 0.1$ in.	$t_2 \sim 10^{-4}$in.
$K_v \equiv \frac{V_w}{V_s} \sim .01$	$w \sim 10^{-3}$in.
$\delta \sim 0.05$ in.	$L_c/t_{1max} \sim 10^4$
$d \sim 0.001$ in.	$d/t_{1max} \sim 10^2$
$t_{1max} \sim 10^{-5}$in.	

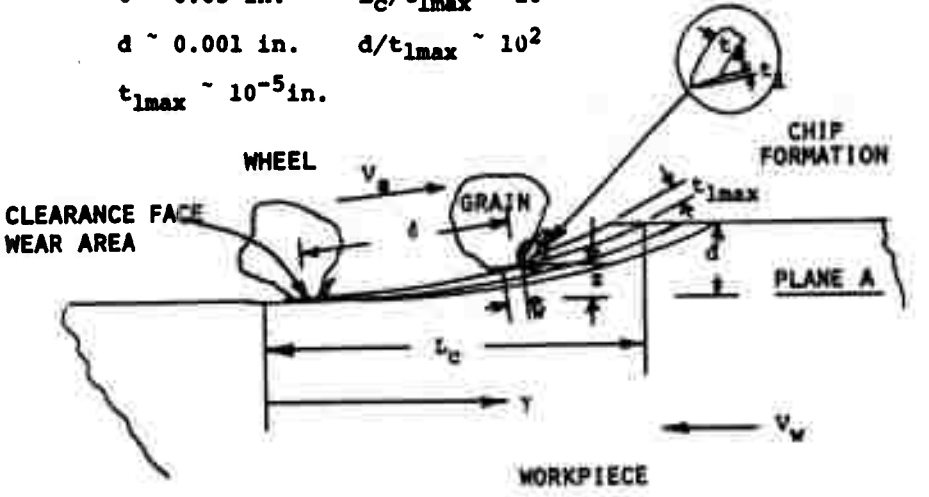

FIGURE III-2 - SINGLE-GRAIN HEAT SOURCE

Figure III-2 shows the cutting process which results in heat generation by friction of a single grain on the workpiece material and by deformation in the region of a chip. It is assumed that the heat flux is uniformly distributed over some contact area which can include grain clearance face contact area and an area over which chip deformation occurs. In this case the heat flux is given by

$$q_g = \frac{C_1 F_H (V_w+V_s)}{bL_c C \text{ [contact area]}} \qquad \text{(III.3.2)}$$

where C is the number of cutting edges per unit area of wheel surface. Therefore the product $C_1F_H(V_w+V_s)/bL_cC$ is the heat per unit time per cutting edge which enters the workpiece material over the grain - chip - workpiece contact area on the surface of the interference zone.

The temperature rise due to an overall interference zone heat source (See Figure III-1) or the temperature rise in the region of a single grain (Figure III-2) can be determined by applying the thermal analysis of Jaeger (3) for a specified grinding process. Jaeger's analysis is reviewed briefly in Subsection III.3.3.

III.3.3 Adiabatic Semi-Infinite Body

The two-dimensional temperature distribution due to a heat source of uniform strength q_B which moves on the surface of an adiabatic, semi-infinite body with relative velocity V is given by

$$\frac{\pi kVu(X,Z)}{2aq_B} = \int_{X-L}^{X+L} e^{-p} K_o ([Z^2+p^2]^{1/2})dp \qquad \text{(III.3.3)}$$

This solution provides the steady-state dimensionless temperature distribution in a body of initially zero temperature. The temperature is due to a heat source of dimensionless width 2L, and is referred to coordinate axes which move with the heat source. Dimensionless quantities are defined by

$$X = \frac{xV}{2\alpha} , \quad Z = \frac{zV}{2\alpha} , \quad L = \frac{\ell V}{2\alpha} \qquad \text{(III.3.4)}$$

In applying the results to the overall interference zone model (Figure III-1) the quantities of Jaeger's solution are related to those of the grinding process by

$$q_B = \bar{q}_B , \quad V = V_w , \quad 2\ell = L_c \qquad \text{(III.3.5)}$$

In considering the single grain model (Figure III-2) the appropriate relations are

$$q_B = q_g , \quad V = (V_s + V_w) , \quad 2\ell = w \qquad \text{(III.3.6)}$$

In either case discussed above, temperatures obtained are those relative to a zero ambient temperature of the body.

Some typical results obtained from Equation III.3.3 are shown in Figures III-3, III-4, and III-5. Equation III.3.3 can be evaluated from Table III-1 for specified values of X, Z, and L. Figure III-3 shows the dimensionless temperature distribution for several values of dimensionless depth Z. Figure III-4 shows the dimensionless surface temperature distribution for several values of heat source dimensionless half-width L. In Figure III-5 the maximum

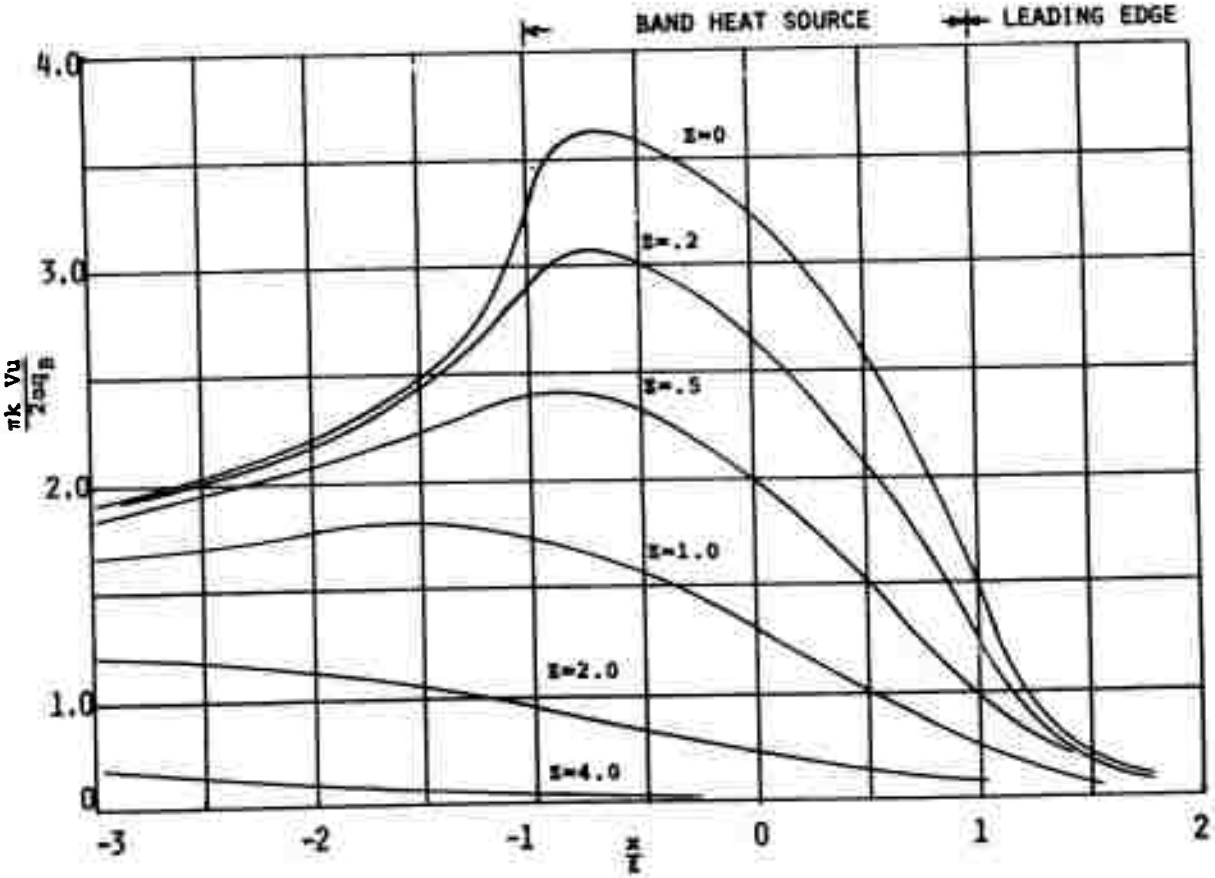

FIGURE III-3 - DIMENSIONLESS TEMPERATURE DISTRIBUTION, L = 1

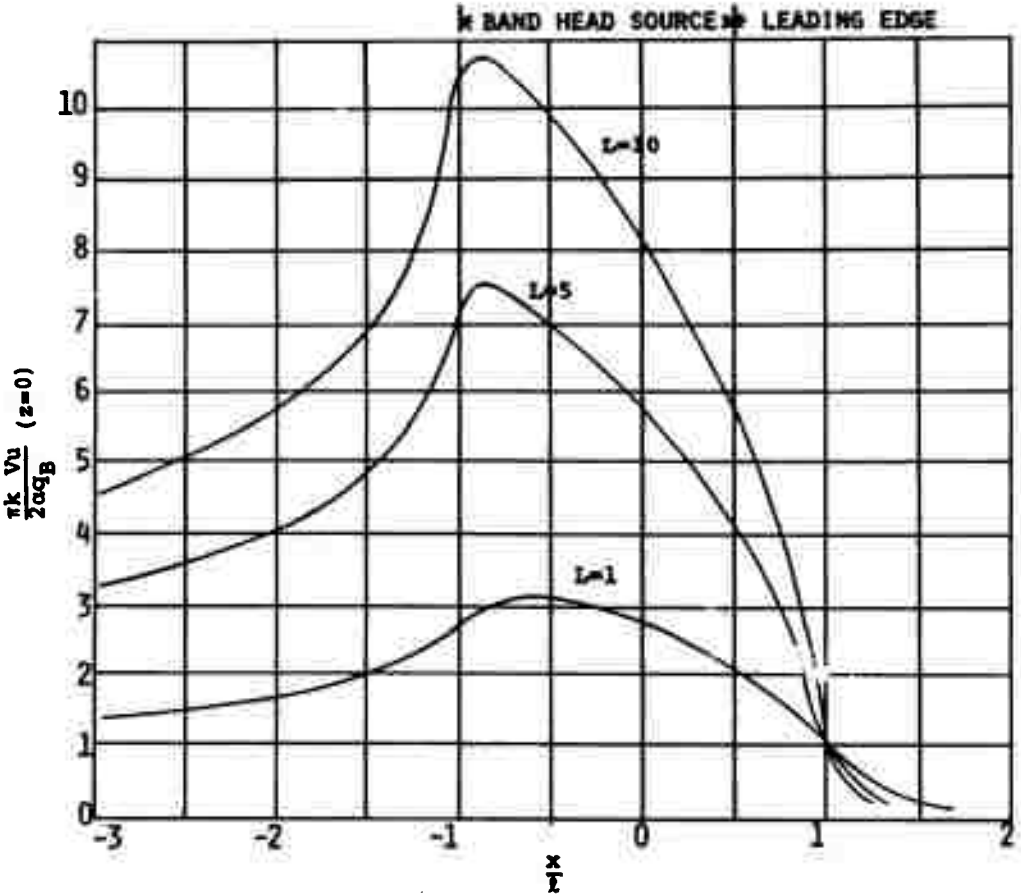

FIGURE III-4 - SURFACE TEMPERATURE DISTRIBUTION

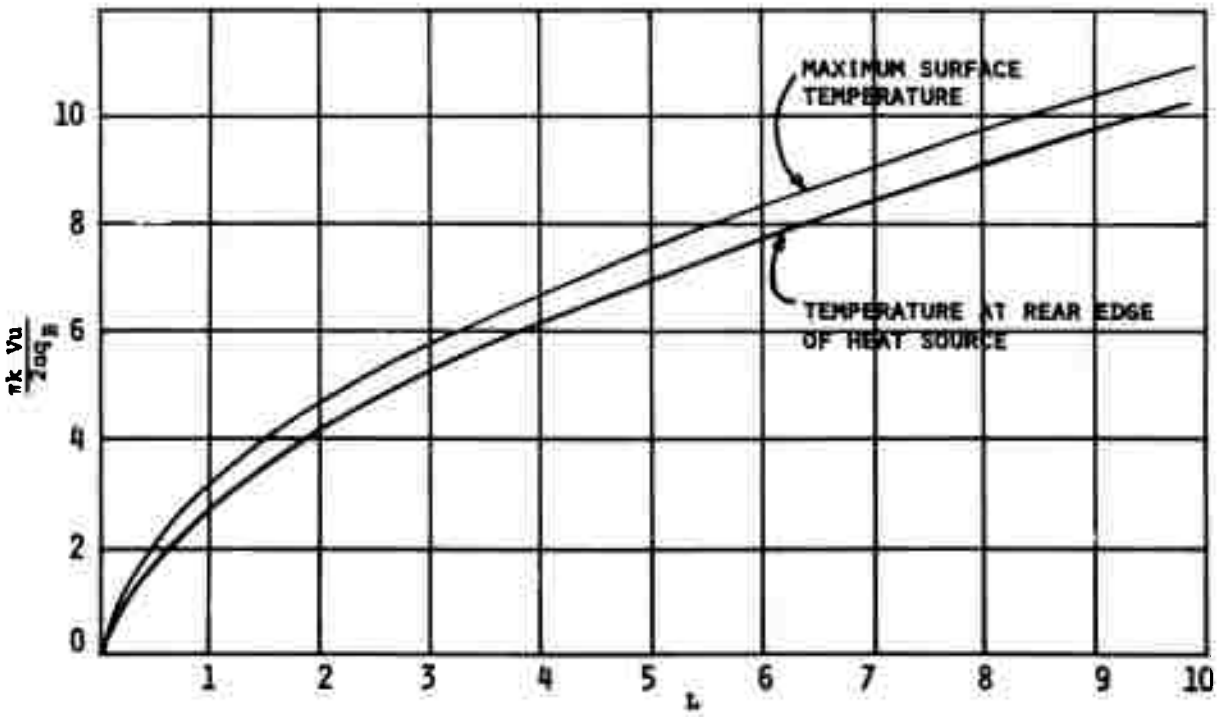

FIGURE III-5 - DIMENSIONLESS TEMPERATURE ON THE SURFACE vs. DIMENSIONLESS HEAT SOURCE HALF-WIDTH

TABLE III-1

Values of $I(\xi,Z) = \int_0^{\xi} e^{-p} K_o([Z^2+p^2]^{1/2})dp$

ξ	$I(\xi,0)$	$I(\xi,.2)$	$I(\xi,.5)$	$I(\xi,1.0)$	$I(\xi,2.0)$	$I(\xi,4.0)$
-20.0	-10.277	-9.903	-9.263	-8.136	-6.011	-2.919
-15.0	-8.789	-8.422	-7.792	-6.697	-4.694	-1.991
-10.0	-7.024	-6.661	-6.047	-5.006	-3.204	-1.078
-9.0	-6.623	-6.260	-5.651	-4.626	-2.881	-.906
-8.0	-6.199	-5.837	-5.233	-4.228	-2.550	-.741
-7.0	-5.748	-5.388	-4.790	-3.808	-2.209	-.585
-6.0	-5.265	-4.906	-4.317	-3.363	-1.859	-.441
-5.0	-4.741	-4.385	-3.806	-2.888	-1.502	-.313
-4.0	-4.164	-3.811	-3.247	-2.377	-1.141	-.203
-3.0	-3.513	-3.164	-2.622	-1.823	-.785	-.117
-2.0	-2.750	-2.409	-1.904	-1.218	-.451	-.055
-1.9	-2.665	-2.325	-1.825	-1.155	-.420	-.051
-1.8	-2.578	-2.239	-1.745	-1.091	-.390	-.046
-1.7	-2.489	-2.151	-1.663	-1.026	-.360	-.042
-1.6	-2.397	-2.060	-1.579	-.962	-.331	-.038
-1.5	-2.302	-1.967	-1.494	-.897	-.302	-.034
-1.4	-2.205	-1.872	-1.406	-.831	-.275	-.030
-1.3	-2.105	-1.773	-1.317	-.766	-.248	-.027
-1.2	-2.001	-1.671	-1.226	-.700	-.222	-.024
-1.1	-1.893	-1.566	-1.132	-.635	-.198	-.021
-1.0	-1.781	-1.457	-1.037	-.570	-.174	-.018
-.9	-1.664	-1.344	-.939	-.505	-.151	-.016
-.8	-1.541	-1.225	-.838	-.441	-.130	-.013
-.7	-1.412	-1.101	-.735	-.378	-.109	-.011
-.6	-1.275	-.970	-.630	-.316	-.090	-.009
-.5	-1.128	-.832	-.523	-.257	-.072	-.0072
-.4	-.969	-.685	-.415	-.199	-.056	-.0054
-.3	-.794	-.528	-.307	-.144	-.040	-.0039
-.2	-.595	-.359	-.200	-.092	-.025	-.0025
-.1	-.357	-.180	-.097	-.044	-.012	-.0012
0	0	0	0	0	0	0
.1	.328	.163	.088	.040	.011	.0011
.2	.505	.296	.164	.076	.021	.0020
.3	.626	.399	.229	.107	.029	.0029
.4	.713	.477	.283	.134	.037	.0037
.5	.778	.537	.327	.158	.044	.0044
.6	.827	.583	.363	.178	.050	.0050
.7	.864	.619	.391	.195	.055	.0055
.8	.892	.647	.414	.209	.060	.0060
.9	.914	.668	.433	.220	.064	.0064
1.0	.932	.685	.447	.230	.067	.0068
1.1	.945	.699	.459	.238	.070	.0072
1.2	.956	.709	.468	.245	.073	.0075
1.3	.965	.718	.476	.250	.075	.0077
1.4	.972	.724	.482	.254	.076	.0079
1.5	.977	.730	.487	.258	.078	.0081
1.6	.981	.734	.491	.261	.079	.0083
1.8	.987	.740	.496	.265	.081	.0086
2.0	.991	.744	.500	.268	.083	.0088
∞	1.0	.751	.506	.274	.086	.0094

dimensionless temperature and the dimensionless temperature at the trailing edge of the heat source (X = -L) as a function of heat source dimensionless half-width L is presented.

The solution given by Equation III.3.3 can be used to determine temperatures for the more general case of a heat source of non-uniform strength $q_B(x)$, as shown in Figure III-6.

Approximating the non-uniform heat source by a number of heat sources of uniform strength $(q_B)_n$ and width $(2\ell)_n$, temperature distributions due to each uniform source can be determined from Equation III.3.3. The superposition of each temperature $\{u(x,z)\}_n$ approximates the temperature distribution resulting from the non-uniform heat source $q_B(x)$.

III.3.4 Semi-Infinite Body With Convective Surface Cooling

In order to indicate the effect of cooling by grinding fluids on workpiece temperature, an analysis of a semi-infinite body with a moving heat source and convective cooling from the surface was presented in I.E.R.IV. The model for analysis is the same as that shown in Figure III-1, except that convective cooling takes place everywhere on the surface. The convective heat flux at a point on the surface to an environment at zero temperature is assumed to be proportional to the surface temperature as given by

$$hu(x,0) = k\frac{\partial u}{\partial z}(x,0)$$

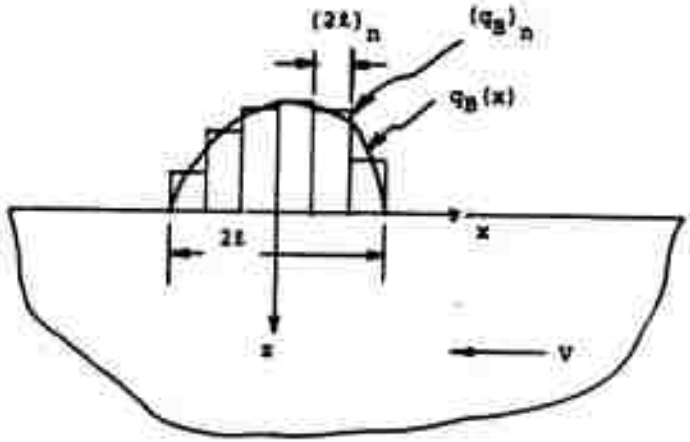

FIGURE III-6 - HEAT SOURCE OF NON-UNIFORM STRENGTH

The dimensionless temperature is given by

$$\frac{\pi k V u(X,Z)}{2\alpha q_B} = I(\xi = X+L,Z) - I(\xi = X-L,Z) - I_H(\xi = X+L,Z) + I_H(\xi = X-L,Z) \qquad \text{(III.3.7)}$$

Where $I(\xi,Z)$ is determined from Table III-1 for specified values of X, L, and Z and is defined by

$$I(\xi,z) = \int_0^{\xi} e^{-p} K_o([Z^2 + p^2]^{1/2})dp \qquad \text{(III.3.8)}$$

and where $I_H(\xi,Z)$ is defined by

$$I_H(\xi,Z) = H\pi e^{HZ} \int_0^{\infty} e^{H^2\tau^2} \tau \operatorname{erfc}(\frac{Z}{2\tau} + \tau) [\operatorname{erf}(\frac{\xi}{2\tau} + \tau) - \operatorname{erf}(\tau)]d\tau \qquad \text{(III.3.9)}$$

Dimensionless quantities are defined by

$$X = \frac{xV}{2\alpha}, \quad Z = \frac{zV}{2\alpha}, \quad L = \frac{\ell V}{2\alpha}, \quad H = \frac{2\alpha}{V}\frac{h}{k} \qquad \text{(III.3.10)}$$

Values of I_H are presented in Tables III-2 and III-3 for the dimensionless heat transfer coefficient H = 1.0 and H = 0.1, respectively.

The dimensionless temperature distribution can be determined from Equation III.3.7 with Equations III.3.8 and III.3.9 for specified values of X, Z, L, and H.

For a value of H = 0, this system of equations reduces to the adiabatic solution by Jaeger, Equation III.3.3.

Some results are presented in Figures III-7 through III-10. These figures illustrate the influence of surface cooling on temperatures, and approximate conditions which would occur

TABLE III-2 VALUES OF $I_H(\xi,Z)$ FOR H = 1.0

$$I_H(\xi,Z) = He^{HZ}\int_0^\infty e^{H^2\tau^2}\,\tau\,\mathrm{erfc}\left(\frac{Z}{2\tau}+\tau\right)\left[\mathrm{erf}\left(\frac{\xi}{2\tau}+\tau\right)-\mathrm{erf}(\tau)\right]d(\tau)$$

ξ	$I_{1.}(\xi,0)$	$I_{1.}(\xi,.2)$	$I_{1.}(\xi,.5)$	$I_{1.}(\xi,1.0)$	$I_{1.}(\xi,2.0)$	$I_{1.}(\xi,4.0)$
-4.0	-2.657	-2.3603	-1.9467	-1.3694	-.6230	-.1051
-3.0	-2.1227	-1.8514	-1.4827	-.9906	-.4071	-.05828
-2.0	-1.5286	-1.2942	-.9896	-.6127	-.2209	-.02685
-1.9	-1.4650	-1.2353	-.9387	-.5756	-.2045	-.02448
-1.8	-1.4005	-1.1757	-.8876	-.5389	-.1886	-.02224
-1.7	-1.3351	-1.1155	-.8362	-.5024	-.1733	-.02013
-1.6	-1.2686	-1.0546	-.7847	-.4662	-.1584	-.01815
-1.5	-1.2011	-.9930	-.7329	-.4305	-.1440	-.01628
-1.4	-1.1326	-.9306	-.6810	-.3952	-.1303	-.01454
-1.3	-1.0628	-.8676	-.6289	-.3605	-.1170	-.01290
-1.2	-.9919	-.8037	-.5769	-.3264	-.1044	-.01138
-1.1	-.9196	-.7391	-.5248	-.2929	-.09235	-.009956
-1.0	-.8460	-.6738	-.4728	-.2603	-.08091	-.008636
-.9	-.7708	-.6077	-.4209	-.2285	-.07007	-.007412
-.8	-.6941	-.5408	-.3694	-.1976	-.05986	-.006281
-.7	-.6156	-.4732	-.3184	-.1679	-.05026	-.005236
-.6	-.5353	-.4050	-.2681	-.1394	-.04129	-.004275
-.5	-.4529	-.3363	-.2187	-.1122	-.03293	-.003391
-.4	-.3682	-.2672	-.1706	-.08647	-.02518	-.002582
-.3	-.2811	-.1982	-.1242	-.06229	-.01803	-.001843
-.2	-.1910	-.1297	-.07994	-.03977	-.01146	-.001169
-.1	-.09754	-.06307	-.03836	-.01899	-.00546	-.000556
0	0	0	0	0	0	0
.1	.08847	.05709	.03472	.01719	.00494	.0005031
.2	.1579	.1065	.06553	.03258	.00939	.0009573
.3	.2126	.1481	.09240	.04625	.01337	.001366
.4	.2560	.1824	.1155	.05826	.01692	.001733
.5	.2905	.2106	.1351	.06873	.02007	.002062
.6	.3130	.2335	.1515	.07779	.02286	.002356
.7	.3399	.2521	.1652	.08557	.02531	.002618
.8	.3575	.2672	.1766	.09221	.02745	.002852
.9	.3715	.2795	.1861	.09784	.02932	.003058
1.0	.3828	.2894	.1938	.1026	.03094	.003242
1.1	.3918	.2974	.2002	.1066	.03234	.003403
1.2	.3991	.3039	.2054	.1100	.03355	.003546
1.3	.4049	.3091	.2097	.1128	.03459	.003671
1.4	.4096	.3134	.2132	.1151	.03548	.003781
1.5	.4134	.3168	.2161	.1171	.03624	.003877
1.6	.4164	.3196	.2184	.1187	.03688	.003961
1.7	.4189	.3218	.2203	.1200	.03743	.004034
1.8	.4209	.3237	.2219	.1211	.03790	.004098
1.9	.4225	.3251	.2231	.1220	.03829	.004153
2.0	.4238	.3263	.2242	.1228	03862	.004206
10.0	.4292	.3314	.2287	.1262	.04031	.004490
20.0	.4292	.3314	.2287	.1262	.04031	.004490

TABLE III-3 VALUES OF $I_H(\xi,Z)$ FOR H = 0.1

ξ	$I_{.1}(\xi,0)$	$I_{.1}(\xi,.2)$	$I_{.1}(\xi,.5)$	$I_{.1}(\xi,1.0)$	$I_{.1}(\xi,2.0)$	$I_{.1}(\xi,4.0)$
-4.0	-.5564	-.4870	-.3944	-.2708	-.1193	-.01948
-3.0	-.4220	-.3630	-.2859	-.1872	-.07511	-.01058
-2.0	-.2849	-.2385	-.1802	-.1102	-.03936	-.004784
-1.9	-.2710	-.2261	-.1699	-.1030	-.03633	-.004356
-1.8	-.2571	-.2136	-.1596	-.09596	-.03341	-.003953
-1.7	-.2432	-.2012	-.1494	-.08402	-.03059	-.003573
-1.6	-.2292	-.1888	-.1393	-.08221	-.02788	-.003217
-1.5	-.2152	-.1764	-.1292	-.07554	-.02529	-.002883
-1.4	-.2012	-.1641	-.1193	-.06902	-.02281	-.002571
-1.3	-.1871	-.1517	-.1095	-.06265	-.02044	-.002280
-1.2	-.1730	-.1394	-.09971	-.05646	-.01819	-.002008
-1.1	-.1589	-.1271	-.09011	-.05045	-.01606	-.001756
-1.0	-.1447	-.1149	-.08064	-.04464	-.01404	-.001522
-.9	-.1304	-.1027	-.07133	-.03903	-.01214	-.001306
-.8	-.1161	-.09057	-.06220	-.03363	-.01035	-.001106
-.7	-.1018	-.07853	-.05328	-.02848	-.008679	-.0009213
-.6	-.08743	-.06659	-.04460	-.02357	-.007120	-.0007518
-.5	-.07301	-.05478	-.03619	-.01892	-.005673	-.0005962
-.4	-.05853	-.04314	-.02809	-.01455	-.004334	-.0004539
-.3	-.04400	-.03172	-.02037	-.01046	-.003101	-.0003239
-.2	-.02940	-.02062	-.01307	-.006671	-.001970	-.0002054
-.1	-.01475	-.009970	-.006261	-.003183	-.000938	-.0000977
0	0	0	0	0	0	0
.1	.01336	.009026	.005666	.002880	.0008490	.0000884
.2	.02424	.01692	.01071	.005465	.001614	.0001682
.3	.03311	.02366	.01514	.007765	.002300	.0002400
.4	.04034	.02934	.01898	.009795	.002912	.0003046
.5	.04624	.03408	.02228	.01157	.003456	.0003625
.6	.05105	.03802	.02508	.01312	.003938	.0004143
.7	.05497	.04128	.02745	.01446	.004363	.0004605
.8	.05817	.04397	.02944	.01561	.004737	.0005016
.9	.06079	.04618	.03111	.01660	.005063	.0005382
1.0	.06292	.04801	.03250	.01744	.005348	.0005706
1.1	.06466	.04951	.03367	.01815	.005595	.0005993
1.2	.06608	.05074	.03463	.01875	.005809	.0006246
1.3	.06724	.05176	.03543	.01926	.005994	.0006468
1.4	.06819	.05259	.03609	.01969	.006153	.0006664
1.5	.06896	.05327	.03664	.02005	.006290	.0006836
1.6	.06959	.05383	.03709	.02035	.006407	.0006986
1.7	.07011	.05429	.03747	.02060	.006507	.0007118
1.8	.07053	.05466	.03778	.02081	.006592	.0007233
1.9	.07088	.05497	.03803	.02099	.006604	.0007332
2.0	.07116	.05522	.03824	.02113	.006726	.0007419
10.0	.07241	.05636	.03921	.02184	.007052	.0007953
20.0	.07241	.05636	.03921	.02184	.007052	.0007953

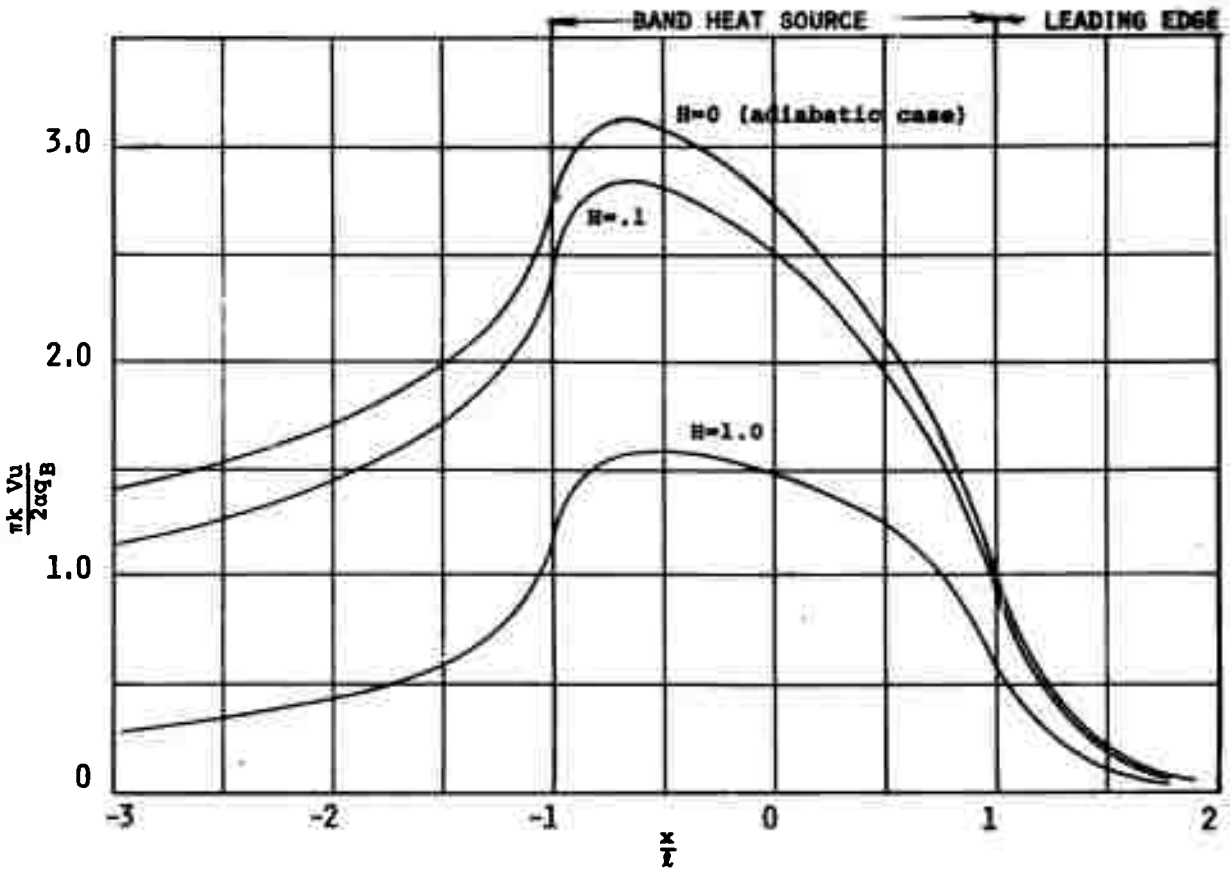

FIGURE III-7 - DIMENSIONLESS TEMPERATURE DISTRIBUTION WITH CONVECTIVE COOLING, L=1, z=0

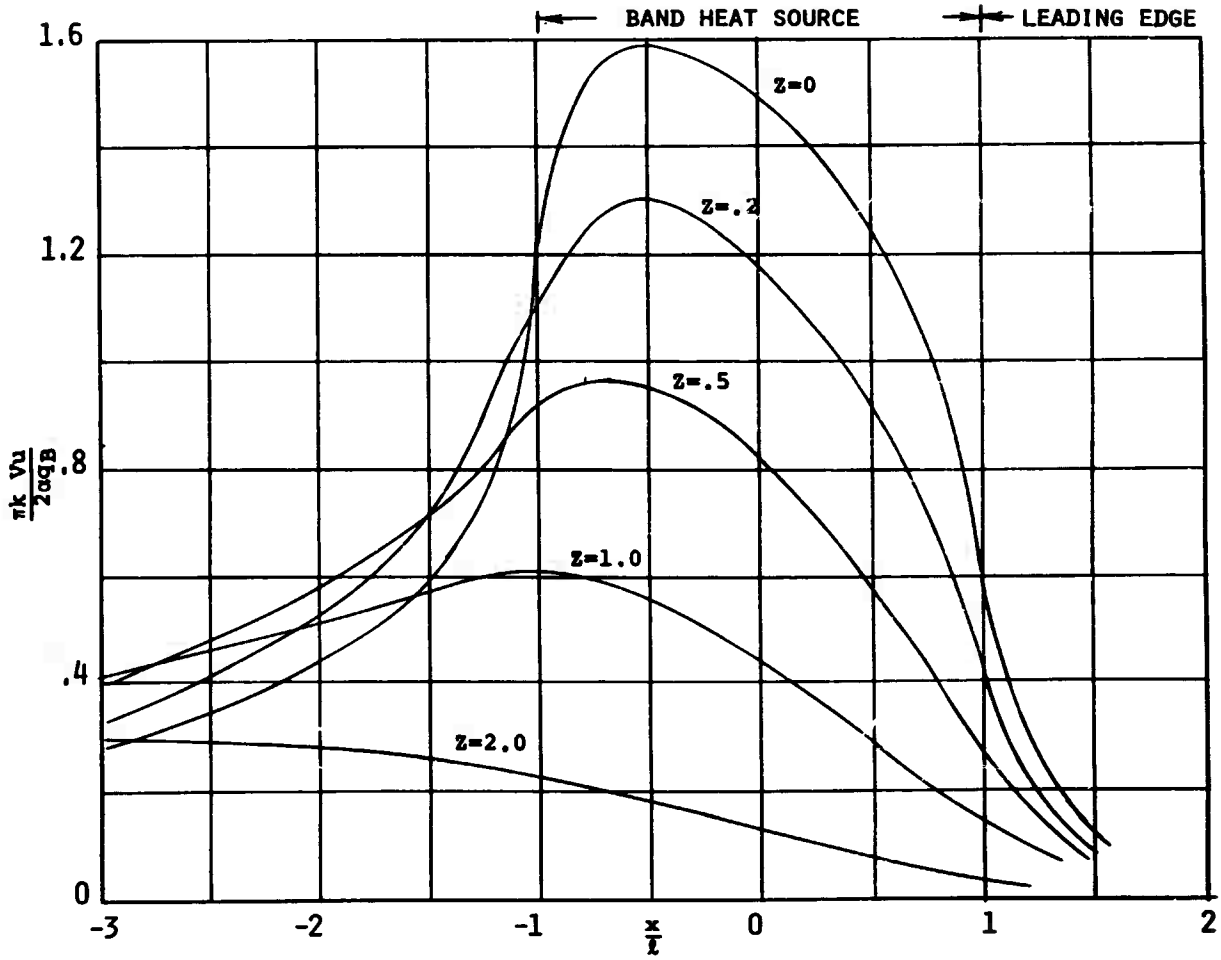

FIGURE III-8 - DIMENSIONLESS TEMPERATURE DISTRIBUTION, L=1, H=1.0

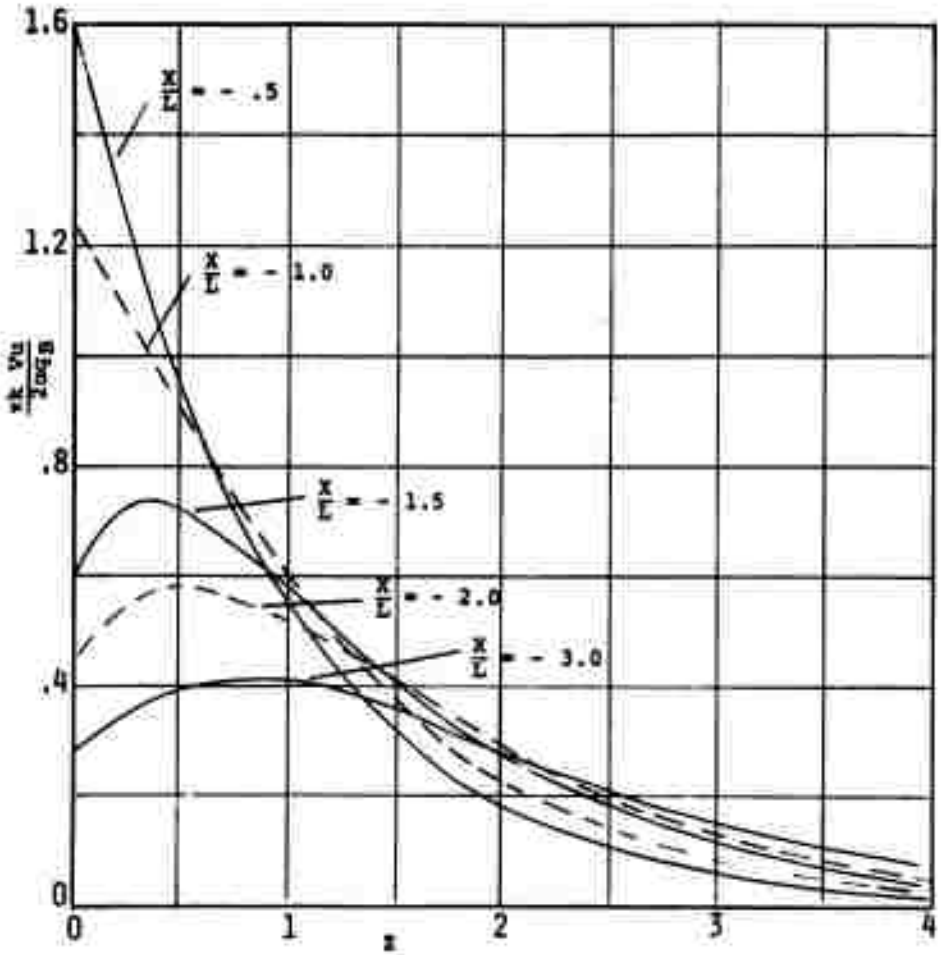

FIGURE III-9 - DIMENSIONLESS TEMPERATURE AS A FUNCTION OF DIMENSIONLESS DEPTH L=1, H=1.0

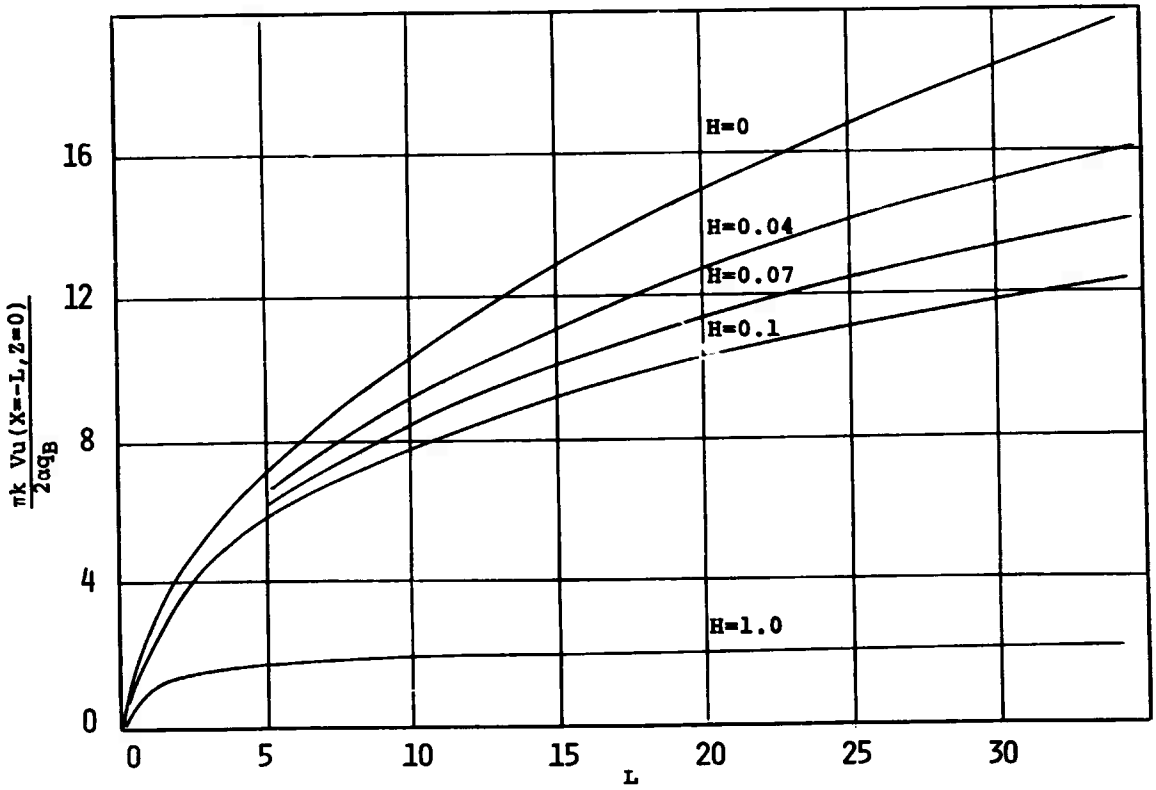

FIGURE III-10 - DIMENSIONLESS TEMPERATURE AT TRAILING EDGE OF HEAT SOURCE vs. DIMENSIONLESS HEAT SOURCE HALF-WIDTH

during one pass in a surface grinding process if coolant is applied over the entire workpiece surface and in the wheel-work interference zone.

Figure III-7 shows the steady-state surface temperature for H = 0, H = 0.1, and H = 1.0. It is seen that the dimensionless temperature decreases everywhere on the surface (Z=0) with increasing dimensionless heat transfer coefficient, H. The effect of increasing H is to establish a more nearly uniform surface temperature.

Figure III-8 shows the dimensionless temperature distribution at various dimensionless depths Z for H = 1.0. From this figure it is seen that at locations (X<-L) beyond the trailing edge of the heat source the maximum temperature occurs at some depth 0 < Z. The dimensionless temperatures of Figure III-8 are plotted in Figure III-9, and it is seen that heat is being conducted toward the surface and into the semi-infinite body.

In Figure III-10 the dimensionless surface temperature at the trailing edge of the heat source is shown as a function of L for several values of H. With increasing L, the increase in temperature at X = -L is less for larger values of H.

The heat transfer coefficient is given by (see Equation III.3.10)

$$h = \frac{HV\,k}{2a}$$

For surface grinding of stainless steel, with V_w = 5 fpm, *dimensionless* heat transfer coefficients of H = 0.1 and 1.0

correspond to heat transfer coefficients of h = 880 $\frac{B}{Ft^2 hr^\circ F}$ and h = 8800 $\frac{B}{Ft^2 hr^\circ F}$. The range of coefficients corresponds to very effective liquid cooling to liquid vaporization cooling. For significant temperature reduction in the overall interference zone, these results indicate that relatively large heat transfer coefficients are required. Heat transfer coefficients of this magnitude may be difficult to obtain in grinding practice.

III.3.5 Cylindrical Body With Cooling

In this section of the analysis of a rotating cylindrical body with a surface heat source and convective cooling is summarized from I.E.R.VI. This analysis approximately corresponds to the case of cylindrical plunge grinding.

Significant differences between semi-infinite and cylindrical bodies are the following:

(1) A steady-state solution is obtainable for the case of an adiabatic semi-infinite body. For the cylinder a steady-state condition is only possible if convective cooling is assumed to exist.

(2) In the case of the cylinder, the material passes repeatedly under the heat source in reaching steady-state, but for the case of the semi-infinite body one pass has been considered.

(3) At large distances from the heat source the temperature is equal to the initial ambient workpiece material in the case of the semi-infinite body. This is not the case for a cylinder.

Theoretical temperature distributions were obtained for the model shown in Figure III-11.

The resulting derivations are summarized from I.E.R.VI for the two-dimensional temperature due to a continuously-acting band heat source

TRANSIENT TEMPERATURE

The transient temperature, $v(r,\theta,t)$, is determined from

$$v^{\#} = v^{\#}_{\text{periodic}} - 2\xi \sum_{j=1}^{\infty} \frac{J_o(\mu_{0,j}r)\ e^{-\mu_{0,j}^2 a^2 \frac{\alpha t}{a^2}}}{J_o(\mu_{0,j}a)[(\frac{ha}{k})^2 + (\mu_{0,j}a)^2]}$$

$$+ 4 \sum_{n=1}^{\infty} \sum_{j=1}^{\infty} \frac{\frac{\sin n\xi}{n}\, a^2\mu_{n,j}^2[a^2\mu_{n,j}^2 \cos n\theta - a^2\omega^2 \sin n\theta]e^{-\mu_{n,j}^2 a^2 \frac{\alpha t}{a^2}} J_n(\mu_{n,j}r)}{[(a\mu_{n,j})^4+(a\omega_n)^4]\, J_n(\mu_{n,j}a)[n^2-(\mu_{n,j}a)^2-(\frac{ha}{k})^2]} \qquad \text{(III.3.11)}$$

$$v^{\#} = \frac{\pi k}{q_B a}\ v(r,\theta,t) \qquad \text{(III.3.12)}$$

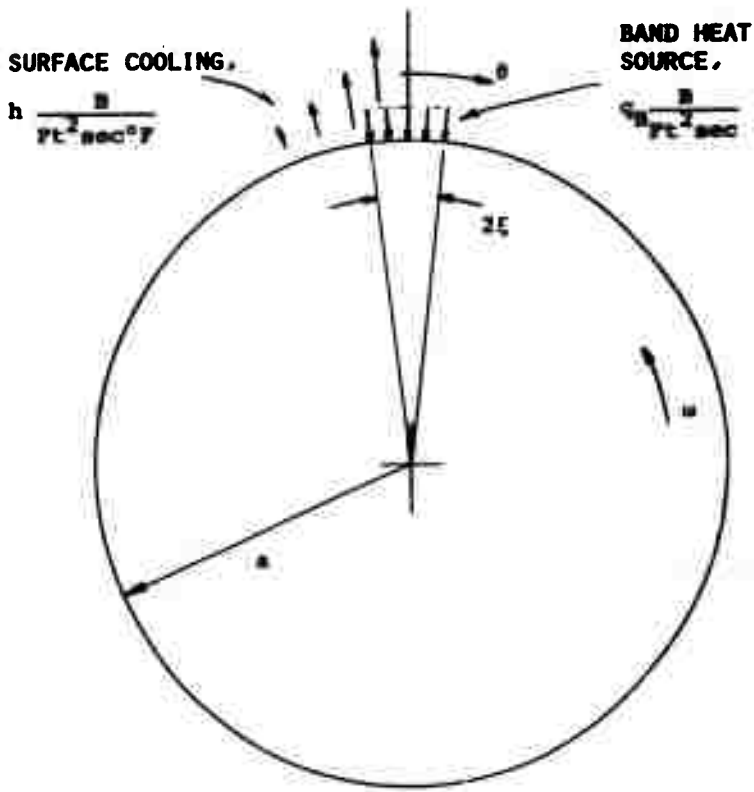

FIGURE III-11 - ROTATING CYLINDRICAL BODY WITH SURFACE HEAT SOURCE AND CONVECTIVE COOLING

$$v^*_{periodic} = \left[\frac{k}{ah}\xi + 2\sum_{n=1}^{\infty}\right.$$

$$\left.\frac{M_1 \frac{\sin n\xi}{n}\left(a\omega_n M_2 \cos[n(\omega t-\theta)+\phi_1-\phi_2] + \frac{ha}{k} M_3 \cos[n(\omega t-\theta)+\phi_1-\phi_3]\right)}{a^2\omega_n{}^2 M_2{}^2 + \frac{h^2a^2}{k^2} M_3{}^2 + a\omega_n M_2 \frac{ha}{k} M_3\, 2\cos(\phi_3-\phi_2)}\right]$$

(III.3.13)

$$M_1 = \sqrt{ber_n{}^2(\omega_n r) + bei_n{}^2(\omega_n r)}$$

$$M_2 = \sqrt{ber_n'{}^2(\omega_n a) + bei_n'{}^2(\omega_n a)}$$

$$M_3 = \sqrt{ber_n{}^2(\omega_n a) + bei_n{}^2(\omega_n a)}$$

$$\phi_1 = \tan^{-1}\frac{bei_n(\omega_n r)}{ber_n(\omega_n r)}$$

$$\phi_2 = \tan^{-1}\frac{bei_n'(\omega_n a)}{ber_n'(\omega_n a)}$$

$$\phi_3 = \tan^{-1}\frac{bei_n(\omega_n a)}{ber_n(\omega_n a)}$$

$$\omega_n = \sqrt{\frac{n\omega}{\alpha}}$$

and the $\mu_{n,j}$ are roots of

$$\mu_{n,j} J_n'(\mu_{n,j}a) + \frac{h}{k} J_n(\mu_{n,j}a) = 0 \qquad \text{(III.3.15)}$$

Approximate Periodic Solution

For the case of steady-state temperatures with respect to a fixed heat source (periodic with respect to a point in the cylinder), an approximate expression is determined (See Reference 9) from Equation III.3.13 to be

$$v^*_{periodic} = \frac{\pi k}{q_B a} v_{periodic} =$$

(Continued)

$$\frac{k}{ah}\,\xi + 2\sqrt{\frac{a}{r}} \sum_{n=1}^{\infty} e^{-\frac{\omega_n}{\sqrt{2}}(a-r)} \frac{\sin n\xi}{n} \cdot$$

$$\frac{\{a\omega_n \cos[n(\omega t-\theta) - \frac{\omega_n}{\sqrt{2}}(a-r) - \frac{\pi}{4}] + \frac{ha}{k}\cos[n(\omega t-\theta) - \frac{\omega_n}{\sqrt{2}}(a-r)]\}}{[a^2\omega_n^2 + \frac{h^2a^2}{k^2} + \frac{2}{\sqrt{2}}a\omega_n\frac{ha}{k}]}$$

(III.3.16)

This expression approximates Equation III.3.13 if $a\sqrt{\frac{\omega}{\alpha}}$, $r\sqrt{\frac{\omega}{\alpha}}$ are large.

Transient Center Temperature

From Equations III.3.11 and III.3.13 the transient center temperature v(r=0,t) is determined as

$$v^*(r=0,t) = \frac{\pi k\, v\ (r=0,t)}{q_B a}$$

$$= [\frac{k}{ah} - 2 \sum_{j=1}^{\infty} \frac{e^{-\mu_{0,j}^2 a^2 \frac{\alpha t}{a^2}}}{J_0(\mu_{0,j}a)[\frac{h^2a^2}{k^2} + \mu_{0,j}^2 a^2]}$$

(III.3.17)

This equation does not involve the approximation.

RESULTS

Equation III.3.16 is evaluated for the case of

$a = .5$ ft.

$k = 10 \frac{B}{\text{Ft hr } ^\circ F}$

$\omega = 10\pi$ rad/sec

$\alpha = .172 \frac{Ft^2}{hr}$

$\frac{ha}{k} = 1, 10, 100, 1000$

$\xi = .01$

to give the approximate periodic surface temperature distribution. In Figure III-12 the temperature distribution is shown for $\frac{ha}{k}$ = 1, 10, and in Figure III-13 for $\frac{ha}{k}$ = 100, 1000.

These figures indicate that if long grinding times are required, then the surface temperature everywhere will be nearly equal to the temperature under the heat source for small values of $\frac{ha}{k}$. For large values of $\frac{ha}{k}$ the surface temperature at regions outside the source will be an order of magnitude lower than the temperature under the heat source.

In Figure III-14 the periodic temperature at the rear edge of the heat source is shown as a function of dimensionless heat transfer coefficient $\frac{ha}{k}$, for two different widths of the heat source ξ, and for two different depths (a-r). The effect of increasing heat transfer coefficients is to reduce the temperature. The greatest reduction is obtained by increasing from h = 20 to h = 200 $\frac{B}{hr\ Ft^{2o}F}$ ($\frac{ha}{k}$ = 1 to 10). This range of heat transfer coefficients corresponds to changing from dry grinding to grinding with a reasonably effective cooling liquid.

Transient surface temperatures are determined from Equation III.3.11 and are shown in Figures III-15, III-16 and III-17. It is seen that the transient condition exists for a longer time ($\frac{at}{a^2}$) with lower values of $\frac{ha}{k}$, and at any particular value of time, the temperature is higher for the lower values of $\frac{ha}{k}$.

The dimensionless quantity $\frac{ha}{k}\frac{v(r=o,t)}{\xi}$ (Equation III.3.17) is shown in Figure III-18 as a function of time ($\frac{at}{a^2}$). From this

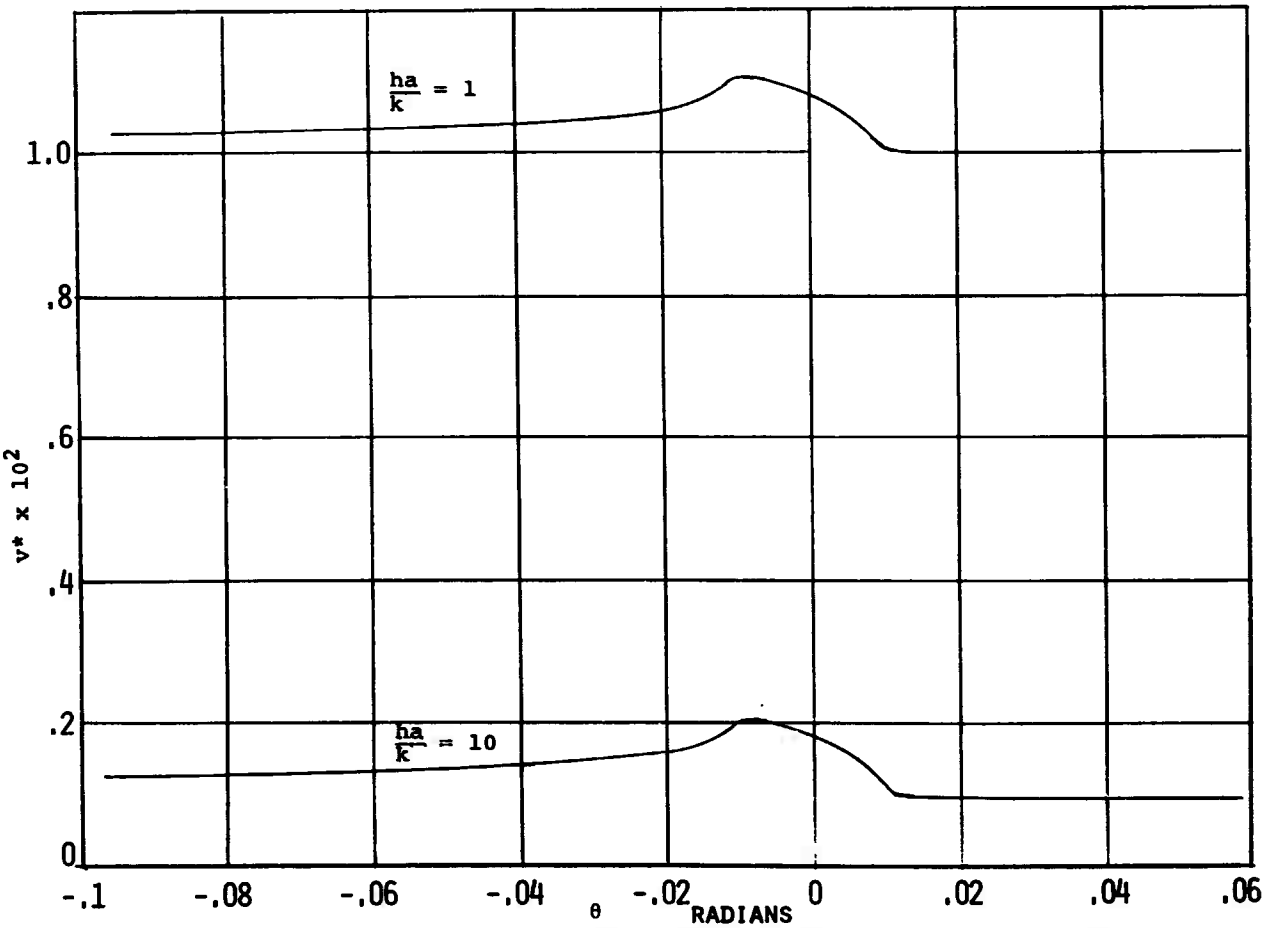

FIGURE III-12 - DIMENSIONLESS TEMPERATURE vs. THETA; ξ=.01, a-r=0; $\frac{ha}{k}$ =1,10

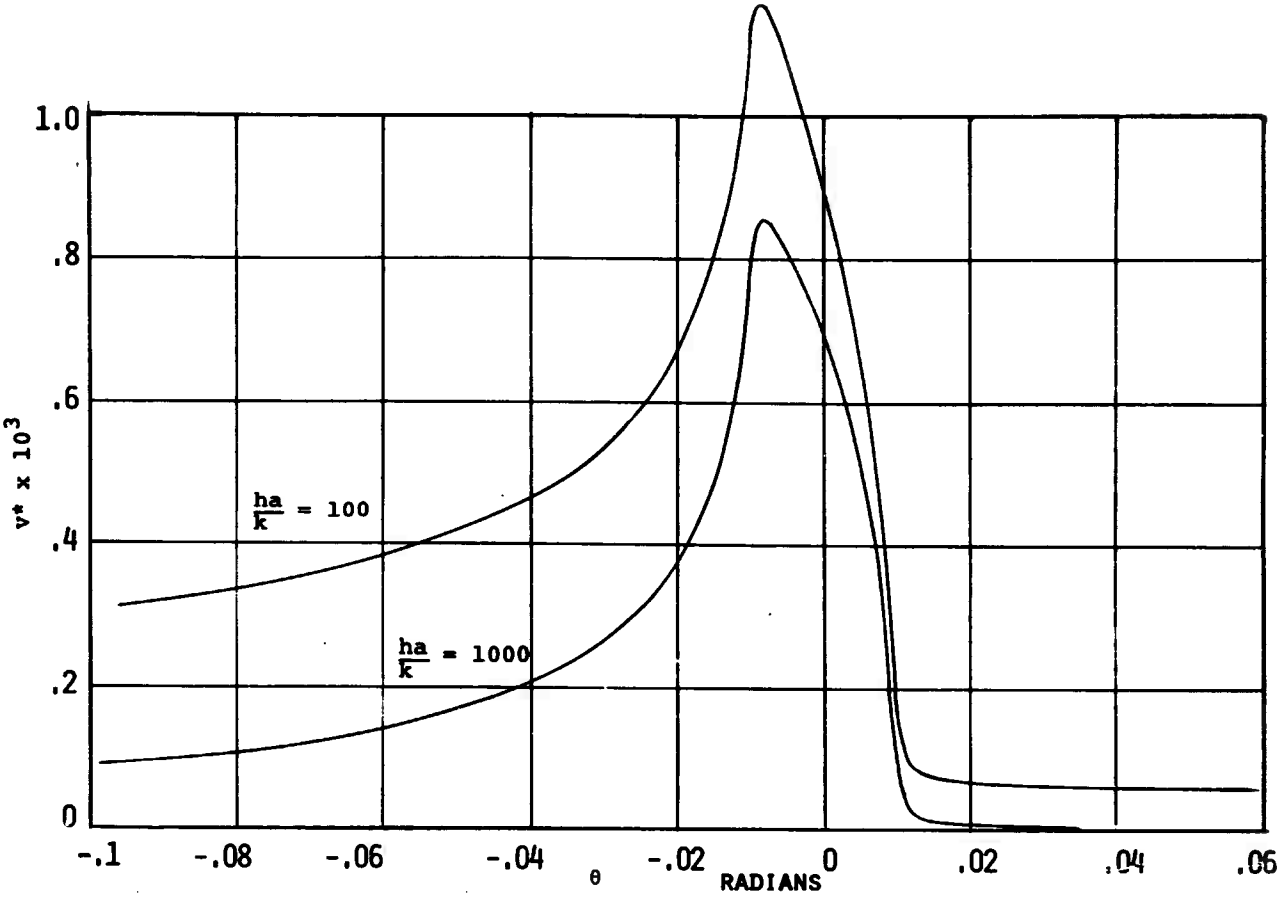

FIGURE III-13 - DIMENSIONLESS TEMPERATURE vs. THETA; ξ=.01, a-r=0; $\frac{ha}{k}$ =100,1000

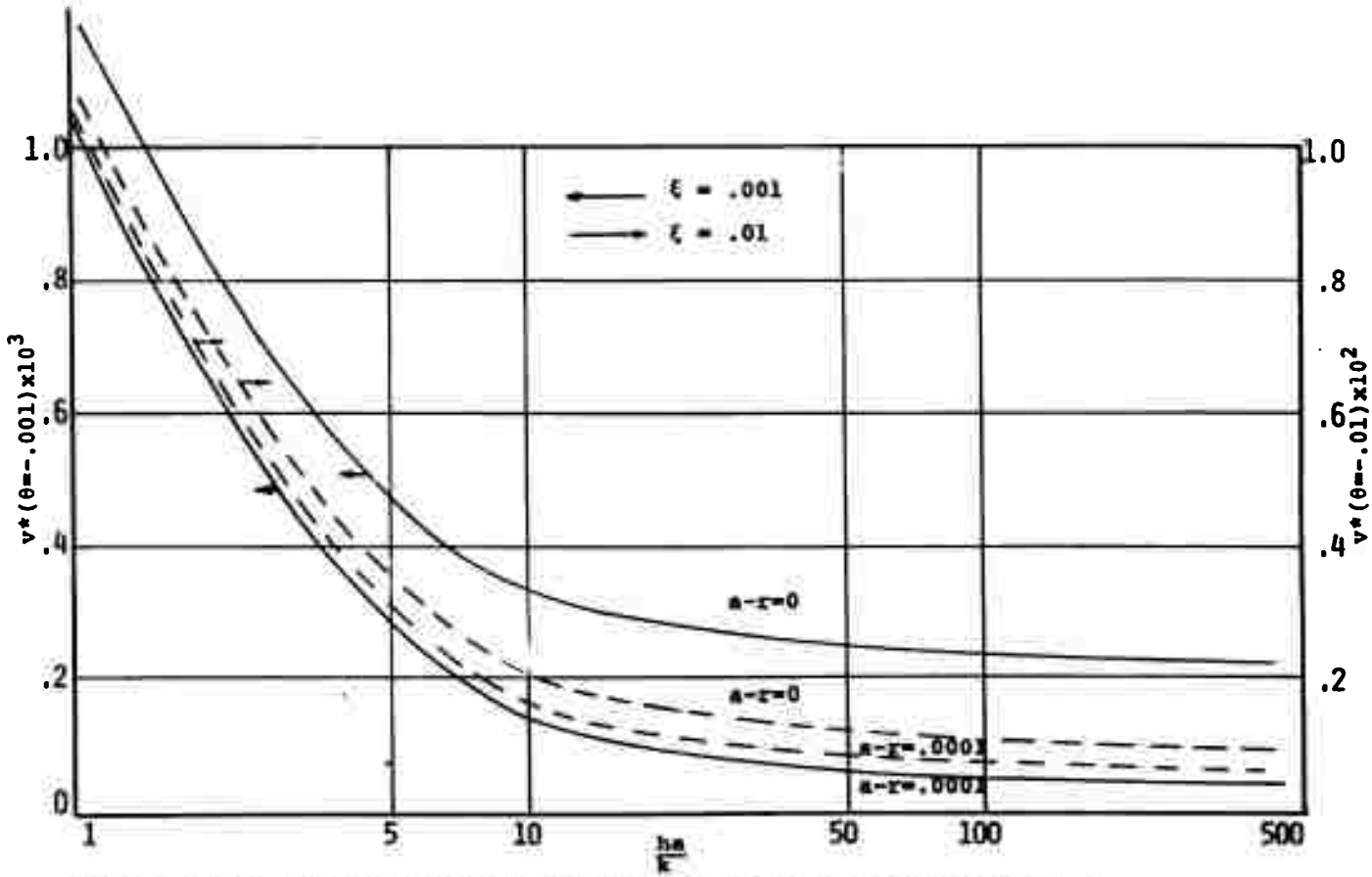

FIGURE III-14 - DIMENSIONLESS TEMPERATURE AT REAR EDGE OF HEAT SOURCE vs. $\frac{ha}{k}$ FOR a-r=0, .0001 Ft.

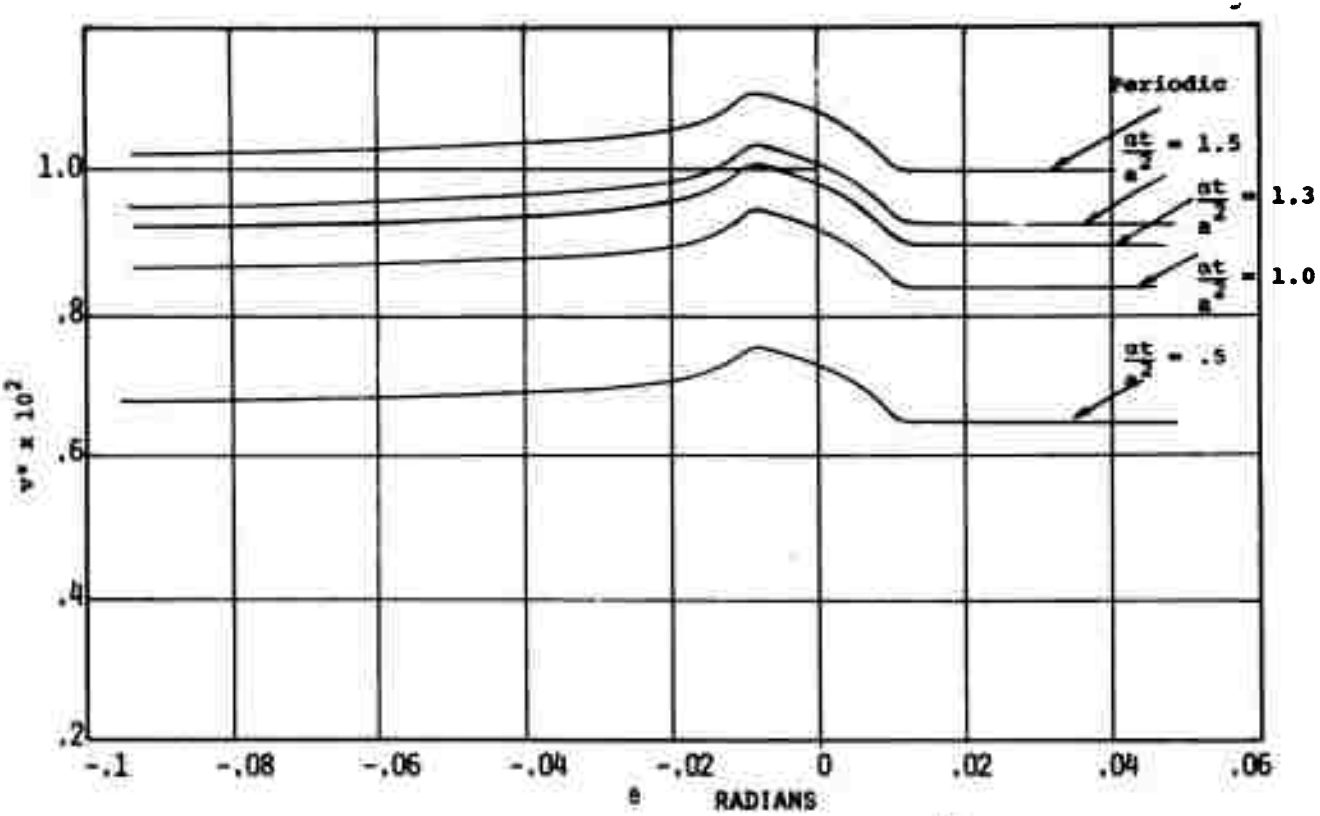

FIGURE III-15 - TRANSIENT SURFACE TEMPERATURE $\varepsilon=.01$, $\frac{ha}{k}=1.0$

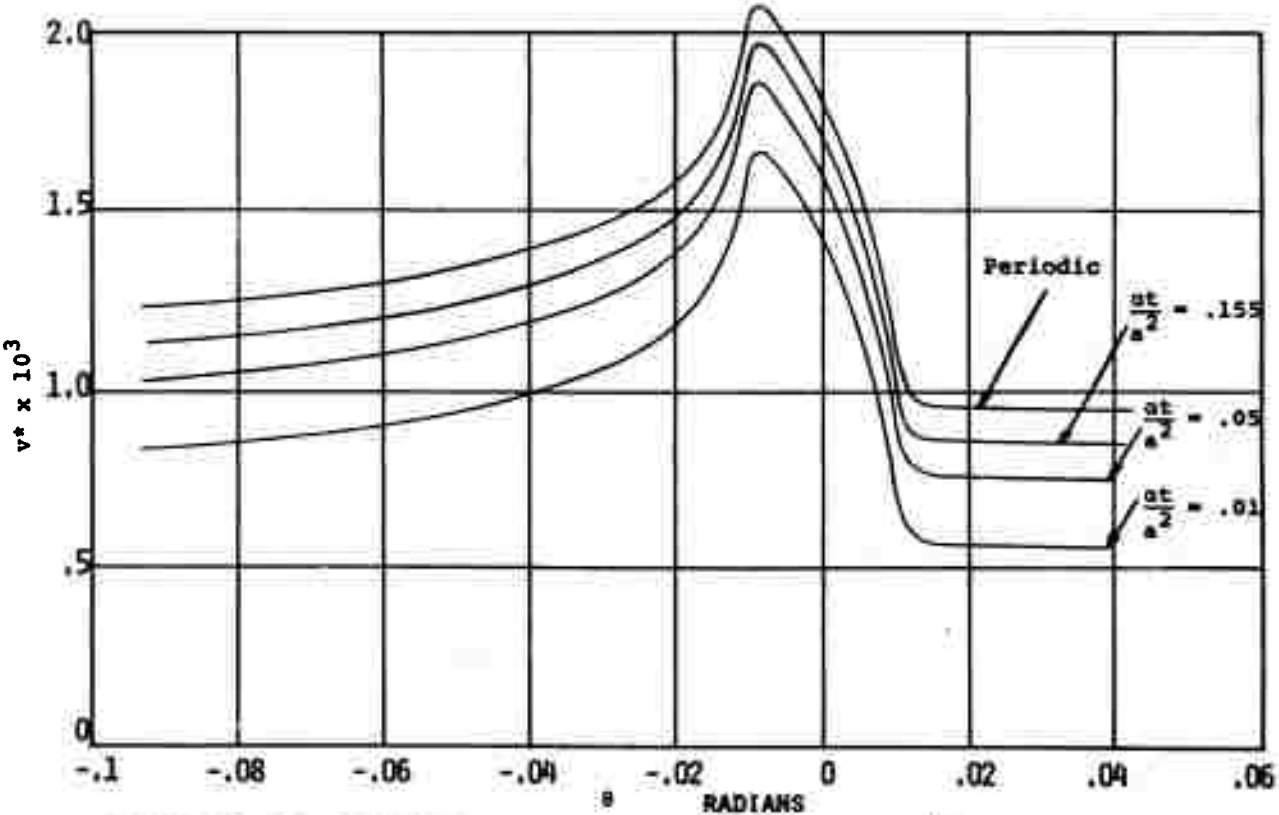

FIGURE III-16 - TRANSIENT SURFACE TEMPERATURE ζ=.01, $\frac{ha}{k}$ =10.0

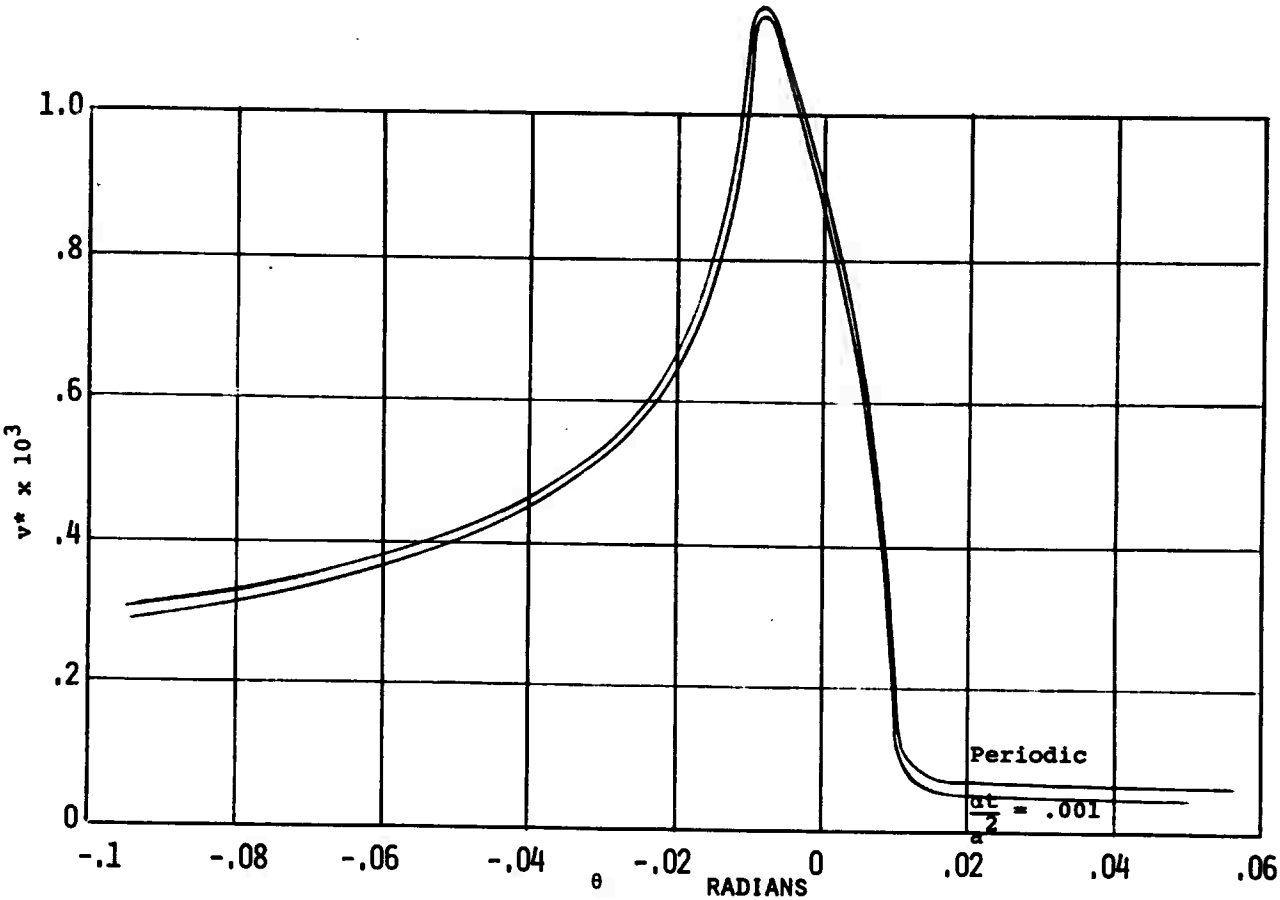

FIGURE III-17 - TRANSIENT SURFACE TEMPERATURE ξ=.01, $\frac{ha}{k}$ =100.0

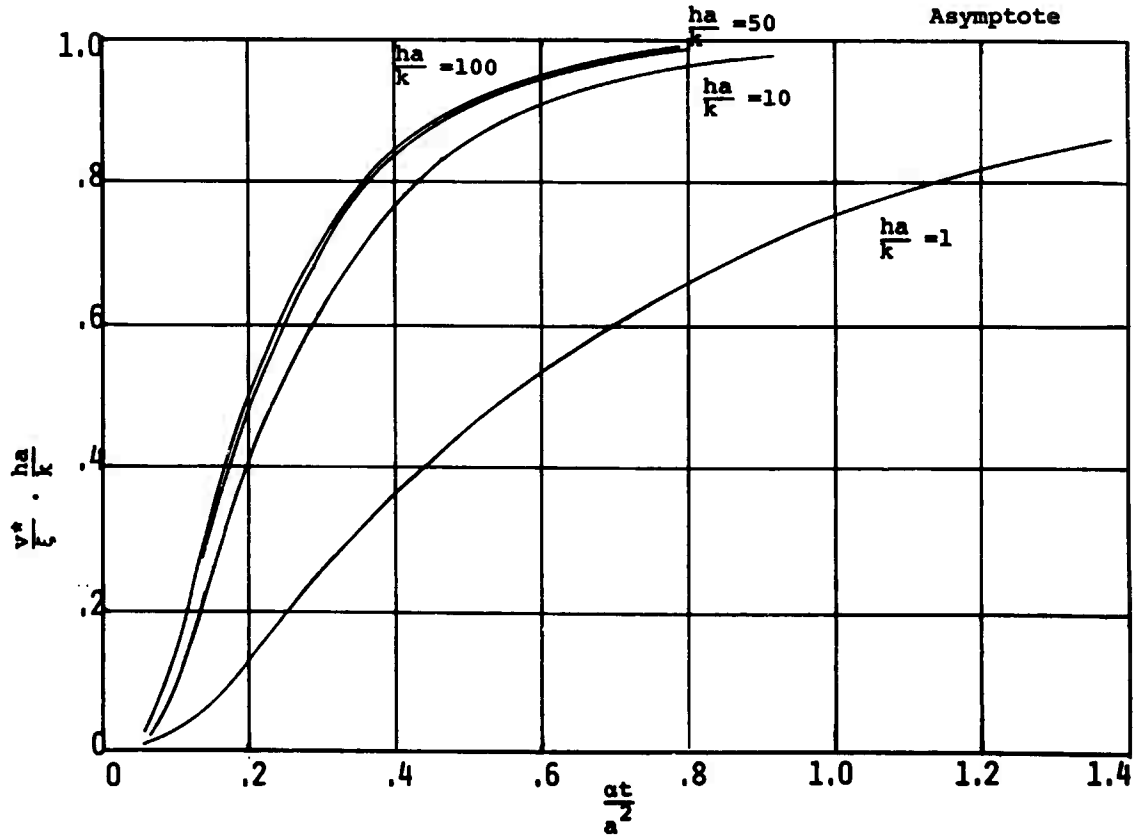

FIGURE III-18 - DIMENSIONLESS CENTER TEMPERATURE vs. DIMENSIONLESS TIME

plot the transient dimensionless center temperature can be determined for a cylinder of any diameter. It is seen that for any specified time, the center temperature is less for larger values of $\frac{ha}{k}$, and also that the steady-state center temperature is approached more rapidly for larger values of $\frac{ha}{k}$.

III.4 Temperature of the Finished Workpiece Surface

III.4.1 Introduction

In Subsection III.2 heat generation in the overall wheel-work interference zone and heat generation by a single grain were discussed. It is expected that both of these heat sources can affect the temperature of the workpiece material which remains after grinding. The workpiece which remains after grinding is designated as "Plane A" in Figure III-2. Since a single grain, sliding on the workpiece and cutting a chip, results in heat generation on material which is subsequently removed by grinding, it is expected that temperatures at Plane A are related through grinding geometry to temperatures on the surface being ground. In this subsection the effect of overall interference zone temperature and temperature resulting from single grain heat generation are related to the temperature at Plane A (Figure III-2.) The analysis is similar to that presented in reference (10).

III.4.2 Geometrical and Force Considerations

For the case of $d << R_s, L_c$ it is determined that the distance above Plane A of a grain heat source located at

γ from the beginning of the interference zone is approximately given by

$$z = \left(\frac{\gamma}{L_c}\right)^2 d \qquad \text{(III.4.1)}$$

It is assumed that the horizonal force per grain varies linearly as the grain passes over the interference zone,

$$F_{H/g} = \frac{\gamma}{L_c} F_{H/g\ max} \qquad \text{(III.4.2)}$$

$$F_{H/g\ ave} = 1/2\ F_{H/g\ max} \qquad \text{(III.4.3)}$$

$$F_{H/g\ ave} = \frac{F_H}{b\ L_c\ C} \qquad \text{(III.4.4)}$$

Equation III.4.4 gives the average horizontal force per grain in the interference zone; that is, the total horizontal force divided by the product of the interference zone area with the number of active cutting edges per unit area of wheel surface.

III.4.3 Temperature Due To A Single Grain

If the energy generated by a single grain is assumed to be uniform over the contact area, w^2, then combining Equations III.4.2,3,4, with III.3.2 gives the heat flux as

$$q_g = R_c 2 \frac{\gamma}{L_c} \frac{F_H}{b\ L_c\ C} \frac{(V_s+V_w)}{w^2} \qquad \text{(III.4.5)}$$

The steady-state temperature distribution can be calculated for a grain located at γ. It is assumed that, although q_g is a function of position γ, the temperature distribution due to a

grain at γ, is the temperature due to a moving heat source of width w and constant strength $q_g(\gamma)$.

The non-dimensional heat source half-width, the distance from the center of the heat source, and depth from the surface are given by

$$L = \frac{w}{2}\frac{(V_w+V_s)}{2\alpha} \; ; \quad X = \frac{x(V_w+V_s)}{2\alpha} \; ; \quad Z = \frac{z(V_w+V_s)}{2\alpha} \tag{III.4.6}$$

From Equation III.3.3

$$\frac{k(V_s+V_w)T}{2\alpha q_g} = \int_{X-L}^{X+L} e^{-P} K_o\left([Z^2 + p^2]^{1/2}\right) dp$$

The maximum value of the integral on the right side is given by an expression by Takazawa (7).

$$I_{max} = 3.1\, L^{.53}\, e^{-.69\, L^{-.37}\, Z} \tag{III.4.7}$$

With Equations III.4.1,5,6,7, the maximum temperature is

$$T_{max} = \left\{\frac{2\alpha}{\pi k}(V_s+V_w) \cdot \frac{2\gamma}{L_c}\frac{C_1 F_H}{(\delta L_c C)} \frac{(V_s+V_w)}{w^2} \cdot 3.1\left[\frac{w}{2}\frac{(V_s+V_w)}{2\alpha}\right]^{.53}\right\} \exp\left\{-.69\left[\frac{w}{2}\frac{(V_w+V_s)}{2\alpha}\right]^{-.37}\left[\left(\frac{\gamma}{L_c}\right)^2 d\,\frac{(V_w+V_s)}{2\alpha}\right]\right\} \tag{III.4.8}$$

The coefficient of the exponential gives the maximum temperature on the surface under the grain (ie. Z=0), and the entire expression gives the maximum temperature at plane A. It would appear from Equation III.4.8 that increasing the grain contact area, w^2, would decrease the temperature, but

actually if contact area is increased then the force F_H is also increased, approximately proportional to contact area w^2 (1).

Equation III.4.8 is evaluated for the following assumed values of grinding parameters.

$$\alpha = .172 \frac{Ft^2}{hr}$$

$$k = 10 \frac{B}{hrFt^\circ F}$$

$$V_s + V_w = 6000 \text{ ft/min}$$

$$w = 0.001"$$

$$C_1 F_H = 2 \text{ lbf}$$

$$b = 0.5"$$

$$L_c = 0.1"$$

$$d = 0.001"$$

$$C = 1500 \text{ cutting edges/in}^2$$

$$V_w = 10 \text{ f.p.m.}$$

III.4.4 Results

The maximum temperature under the grain on the surface of the material being ground is shown in Figure III-19. This temperature increases linearly with the position of the heat source $\frac{\gamma}{L_c}$.

The maximum temperature at Plane A is shown in Figure III-20. It is seen that this temperature is a maximum at $\frac{\gamma}{L_c} = .18$, and is equal to 276 $^\circ$F.

These figures clearly indicates that although very high temperatures can be reached under a grain, the layer of

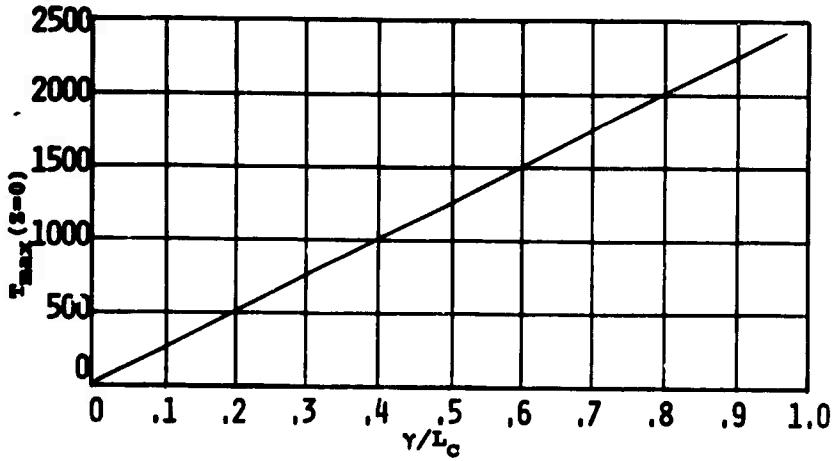

FIGURE III-19 - MAXIMUM TEMPERATURE UNDER GRAIN vs. LOCATION OF GRAIN

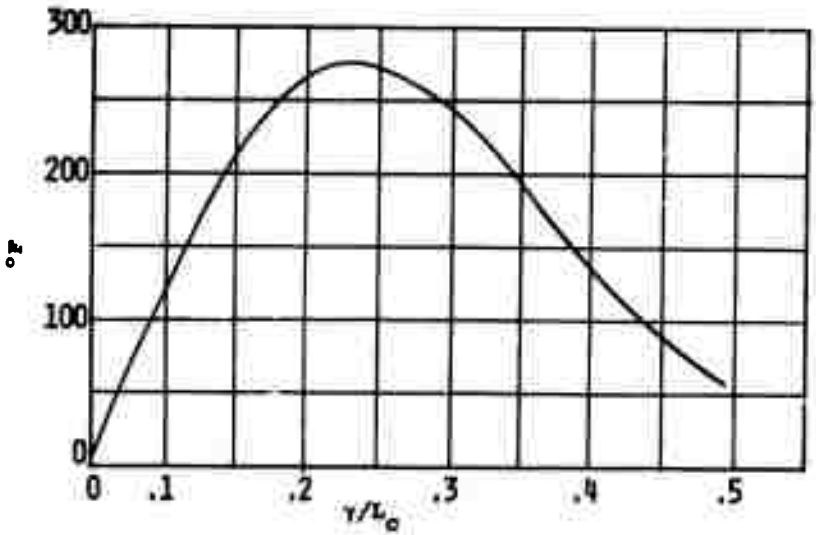

FIGURE III-20 - MAXIMUM TEMPERATURE AT PLANE A vs. LOCATION OF GRAIN

material which is subsequently removed in grinding can act as a thermal insulator between the grain heat source and the material which remains after grinding (Plane A).

The temperature due to a single grain heat source, as shown in Figures III-19 and 20, is the temperature rise above a zero ambient workpiece temperature. Any grain which enters the interference zone encounters a workpiece at a temperature which resulted from previous grinding. This overall interference zone temperature is determined from Equations III.3.1, III.3.4, III.3.5 and III.3.3 or III.4.7

$$q_B = \frac{C_1 F_H (V_w + V_s)}{b\, L_c} = \frac{2\ \text{Lbf}(6000\frac{\text{Ft}}{\text{min}})}{(.5)(.1)\ \text{in}^2} = \frac{240{,}000\ \text{FtLbf}}{\text{min in}^2}$$

$$L = \frac{L_c}{2}\frac{V_w}{2\alpha} = \frac{.1}{2 \cdot 12}\frac{100 \cdot 60}{.344} = 7.27$$

The surface temperature is

$$T_{max} = \frac{2\alpha q_B}{\pi k V_w}\ 3.1\ (7.27)^{.53}$$

$$\text{or } T_{max} = 431\ ^{\circ}\text{F}$$

The maximum overall interference zone temperature occurs near the trailing edge of the interference zone heat source. There is negligible insulating effect for the case of the interference zone heat source because of the low work speed; that is

$$Z = z\frac{V_w}{2\alpha}$$

Thus, for the example discussed here, material in Plane A is expected to reach a maximum temperature of

$$T_{max\ A} = 431 + 276 = 707\ ^{\circ}F.$$

For low work speeds every point in Plane A will experience a temperature rise from overall interference zone temperatures and also from the temperature caused by individual grains.

III.5 Conclusions

Several new considerations have been investigated in the thermal analysis of grinding processes and important conclusions can be drawn from this study.

The cooling effect of grinding fluids was theoretically determined. In the case of a semi-infinite body it was shown that usual cooling methods will not significantly reduce the temperature rise in the wheel-work contact zone for the case of one pass of the workpiece under the wheel. It is therefore desirable, from this point of view, to increase lubrication in the contact zone in order to reduce grinding forces and temperatures.

However, from the analysis of a cylindrical body it was shown that surface cooling is important in order to keep the overall temperature of the body at lower levels when the workpiece makes many revolutions.

Therefore, if lubrication properties of the grinding fluid are improved at the cost of cooling properties, the temperature

rise in the wheel-work contact zone may be less during one grinding pass because of lower grinding force. However, during a large number of grinding passes (surface grinding) or many workpiece revolutions (cylindrical plunge grinding) the overall temperature of the body may be much greater because of the less effective cooling. The level of the overall temperature will effect the dimensional accuracy of the finished workpiece, and if the temperature is sufficiently high the surface integrity of the workpiece may be affected. In some instances a grinding fluid with a good combination of lubrication and cooling properties is therefore required. An optimum condition would seem to be possible, depending on grinding time. Conclusions are summarized as follows:

(1) For short grinding time lubrication is most important.

(2) For long grinding time cooling can be more important than lubrication.

(3) For long grinding time refrigerated grinding fluids may provide a good combination of lubrication and cooling properties.

(4) Grinding fluids should be applied not only to the interference zone, but to the entire workpiece surface. In the case of surface grinding, the workpiece

should be cooled even when not in contact with the wheel so that maximum cooling time is utilized.

III.6 Nomenclature

a radius of cylinder

b width of workpiece

c specific heat

C number of active cutting edges per unit area on grinding wheel surface

C_1 fraction of grinding energy which enters workpiece as heat

d wheel depth of cut

F_H horizontal grinding force

$F_{H/g}$ horizontal grinding force per cutting edge

h convective heat transfer coefficient $\frac{B}{Ft^2 hr\ ^\circ F}$

J_n Bessel function of order n

K_o modified Bessel function of second kind, order 0.

k thermal conductivity

ℓ heat source half-width

L_c wheel-work contact length

q_B band heat source, $\frac{B}{Ft^2 sec}$

$\bar{q}_B$ interference zone band heat source, $\frac{B}{Ft^2 sec}$

q_g single grain heat source, $\frac{B}{Ft^2 sec}$

r radial coordinate

$t_{1\ max}$ maximum undeformed chip thickness

u temperature

V velocity

V_s wheel speed

V_w work speed

w length of single-grain clearance face wear flat

x,z cartesian coordinates

α thermal diffusivity $\alpha = \frac{k}{\rho c}$

γ location from initial point of contact of grain with workpiece

θ angular coordinate

ω angular velocity

ρ density

SECTION IV

GRINDING WHEEL CHARACTERISTICS

IV.1 Introduction

Grinding wheel characteristics (G.W.C.) are very important in the determination of the cutting edge conditions which affect the cutting process in grinding.

The grinding wheel characteristics have been represented by parameters which include grain material, grain size, grade, bond material and structure. Corresponding to these parameters simple letter and number symbols convenient to the wheel manufacturer have been used to represent properties of a grinding wheel. These traditional G.W.C. are called standard grinding wheel characteristics (S.G.W.C.). Efforts to represent the grinding wheel characteristics with scientific values instead of these simple ones have been continuing for a long time. For example, many proposals have been made to represent the grade of the wheel with values measured by various methods. Many reports have described practical grinding tests which were carried out to clarify the relation between G.W.C. and grinding performance.

It is known for grinding under the same grinding conditions that the grade of grinding wheel used for different jobs must be carefully selected in order to obtain optimum conditions. Also the cutting performance of a grinding wheel changes significantly with dressing conditions. Therefore

the present representation for G.W.C. cannot predict grinding results and therefore cannot give the proper information necessary to develop and improve the grinding process.

From the study of chip formation physics it is seen that certain cutting edge conditions are important. The relation between these cutting edge conditions and grinding wheel characteristics will be discussed in this section. In a short duration program it is very hard to basically improve the traditional G.W.C. which have commercially important meanings.

In this section, a scientific definition for G.W.C. will be proposed and then several grinding wheel properties which have physical meaning will be investigated. Furthermore a dressing procedure to obtain the most ideal cutting edges for high efficiency HSTRA grinding on existing grinding wheels will be discussed.

IV.2 New Definition of Grinding Wheel Characteristics

IV.2.1 Introduction

A new scientific definition should be made to properly represent cutting edge conditions on the working surface of a grinding wheel. As known from practical experience, the cutting edge conditions change significantly with dressing conditions, working conditions and machine stiffness, and are not constant on a wheel. There are two categories that need to be considered in order to made a new definition for G.W.C.

(1) Instantaneous Grinding Wheel Characteristics (I.G.W.C.)

I.G.W.C. indicates values which can represent the cutting edge conditions in a specified moment of grinding.

(2) Fixed Grinding Wheel Characteristics (F.G.W.C.)

F.G.W.C., indicating permanent physical properties of the grinding wheel independent of various boundary conditions, can represent the range of I.G.W.C.

One underlying consideration is the wheel wear mechanism which causes a change of the cutting edge conditions and makes it harder to understand G.W.C.

In this subsection the definition I.G.W.C. and F.G.W.C. will be outlined based on the wear mechanism of the grinding wheel.

IV.2.2 Wear Mechanism of Grinding Wheel

Special attention has been paid to the selection of the grade of a wheel because the grade of a wheel and consequently the strength is closely related to the wheel wear mechanism. The wear mechanism of the grinding wheel is quite complicated as compared with that of a conventional tool and is classified into three categories as follows:

(1) Attritious wear of grain (cutting edge wear)
   (a) chipping (b) plastic wear (c) chemical wear

(2) Mechanical fracture of grains (cleavage)

(3) Fracture of bond bridges (fallout)

First consider the relationship between (1) attritious wear and (2) cleavage and the influence of the cutting edge shape. To discuss the relationship entirely in terms of a force magnitude would be taking the wrong viewpoint. For example, a very sharp cutting edge which has no wear area merely chips or obtains a flat. Gross cleavage does not occur. An increase in the contact area due to the attritious wear increases the probability that a cleavage can occur. Cleavage occurs when the stress on a grain due to the compressive stress caused by the load on the contact surface exceeds the cleavage strength of the grain.

Next consider a simple relation between (2) cleavage and (3) fallout which is as follows: If

$f_B > f_G$ (2) occurs , $f_B < f_G$ (3) occurs.

where f_B = bond strength, f_G = cleavage strength. The effect of grade on the relative magnitudes of f_B and f_G are shown in Figure IV-1 . In this figure it was assumed that the value of f_B increases linearly with grade of wheel. Since the grain strength is independent of the bonding agent, f_G has no relation with grade. To the left of point A $f_B < f_G$ therefore wear of type (3) occurs. Above and to the right of point A $f_B > f_G$, therefore wear of type (2) occurs. The solid line OAB indicates a wheel wear mechanism of a combination of types (2) and (3). From these considerations of the wear mechanism, the grade of wheel is shown to be important only in the region where $f_B < f_G$.

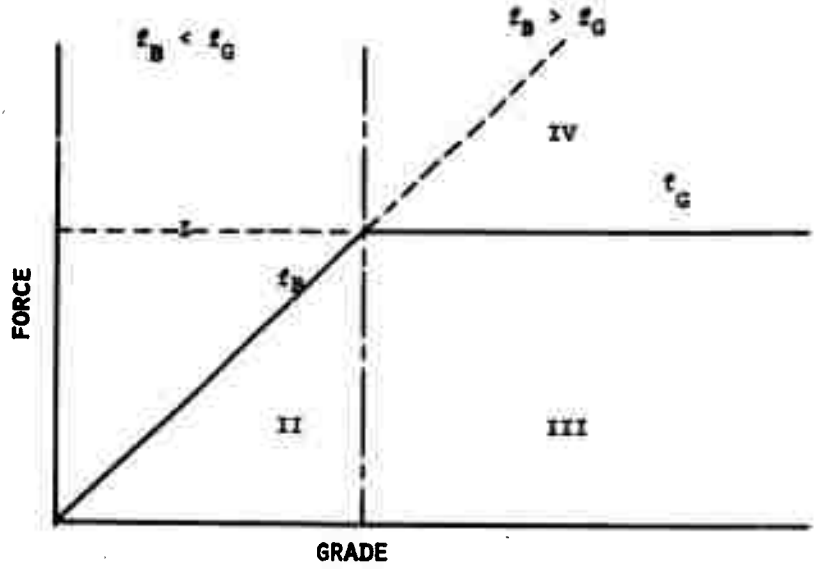

FIGURE IV-1 - GRINDING WHEEL WEAR MECHANISM

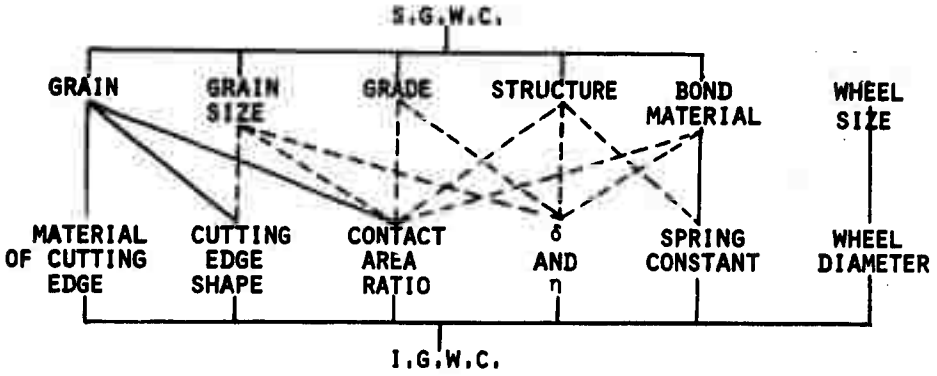

FIGURE IV-2 - RELATION BETWEEN SGWC AND IGWC

In summary, Figure IV-1 divides the wear process into four regions, and the mechanism of wheel wear which exists in each region is described in Table IV-1 . The grinding wheel characteristics have a completely different character depending upon whether the conditions of grinding occur in Region I and II, or Region III and IV. In Region I and II the wheel grade is more influential on the cutting performance, while in Region III and IV the cutting edge shape generated by dressing and the wear resistance of the grain are the sigrificant factors.

IV.2.3 I.G.W.C.

During the grinding operation the cutting performance of the grinding wheel changes with working time as the grinding wheel characteristics change. Accordingly, in order to analyze the cutting mechanism at each instant of time it is necessary to know the instantaneous grinding wheel characteristics which are the basic parameters of chip formation physics. These important instantanous characteristics are the following:

(1) Wheel diameter

(2) Successive cutting edge spacing or number of cutting edges.

(3) Cutting edge shape.

Statistical rake angle

Statistical clearance angle

Statistical cutting edge width

TABLE IV-1 - WHEEL WEAR CHARACTERISTICS

Region	Wear Mechanism		Force	Basic Character	Equilibrium Line
	Main	Secondary			
I	(c)	(a)	$I \rightarrow f_B$	Grade	Above OA
II	(a)	(c)	$II \rightarrow f_B$	Grade	Below OA
III	(a)	(b)	$III \rightarrow f_G$	Abrasive	Below AB
IV	(b)	(a)	$IV \rightarrow f_G$	Abrasive	Above AB
Point A	(c) (b) (a)		$f_B = f_G$	Grade, Abrasive	

TABLE IV-2 - TYPES AND STRUCTURES OF TESTED WHEELS

BOND	ABRASIVE	GRADE	V_G	V_B	V_P
Vitrified	WA36	K	6		
	WA60	H	.480	.106	.414
		L	.480	.177	.343
		P	.480	.247	.273
	WA120	K	6		
Resinoid	WA60	H	.470	.125	.405
		L	.470	.165	.365
		P	.470	.215	.315

TABLE IV-3 - DRESSING CONDITIONS

	t_d (in.)	V_{fd} (in/rev. of G.W.)	RPM
a	.0001	.002	1800
b	.0008	.008	1800
c	.0016	.016	1800

(4) Contact length or contact area ratio

(5) Cutting edge mounting condition

(6) Wear resistance of cutting edge.

Some of the values tabulated above cannot be measured practically or can only be measured with great difficulty. The I.G.W.C. are defined as follows with the present state of the art of grinding technology.

(1) Wheel diameter (2) Average δ and n

(3) Cutting Edge Shape (4) Contact area ratio

(5) Spring Constant (6) Cutting edge material

In Figure IV-2 the relationship between I.G.W.C. and S.G.W.C. are shown where the solid line indicates a direct relationship and the dotted line an indirect relationship.

IV.2.4 F.G.W.C.

In order to analyze the grinding process the I.G.W.C. are the most important values, however, these are not fixed values of the grinding wheel. Therefore, in order to specify a grinding wheel, some type of fixed specifications (F.G.W.C.) which show the variation of the I.G.W.C. are needed. As mentioned in the previous sections the grinding wheel action in Regions I and II is really different than the action in Regions III and IV. Therefore, a different set of F.G.W.C. are important in these regions.

In Regions I and II the steady state value of the cutting edge conditions which have been defined as I.G.W.C. are functions of f_B. In this case the grade effect on I.G.W.C. is

very important, so for this case the S.G.W.C. may be used as the F.G.W.C.

In Regions III and IV the initial values of I.G.W.C. are determined by the dressing method and conditions of the wheel. The time change of I.G.W.C. is influenced by the attritious wear characteristics of the grain. As a result, the F.G.W.C. in these regions should be defined in a much different manner than S.G.W.C. Practically, the F.G.W.C. must be defined from the cutting edge generation method.

IV.3 Physical Properties of Grinding Wheel

IV.3.1 Introduction

As the first step to basically investigate scientific grinding wheel characteristics, several physical properties of a grinding wheel which are closely related to the wheel-work interaction will be discussed.

VI.3.2 Volumetric Composition

The complicated structure of a grinding wheel composed of grains, bond and pores has been represented with only a single number. In this paragraph, the interrelation between three kinds of volumetric parameters will be discussed based on conventional structure and grade grinding wheel designations.

The volumetric composition of a grinding wheel is given by:

$$V_K + V_B + V_P = 100\%$$

where V_K = Volume of grain/total apparent volume x100%

V_B = Volume of bond material/total apparent volume x100%

V_P = Volume of pore/total apparent volume x100%

The volumetric relation is shown on a ternary diagram in Figure IV-3 .

Contained in this figure are many interesting points. First note that there is only a small region of practical interest. This region is bounded by packing densities of the abrasive and bond properties. The maximum packing density is fixed due to the size and shape of the grain and the lower packing density conforms to a requirement that abrasive grains have some contact in order to maintain shape during the firing of the wheel. The lower bond equivalent is determined by strength considerations in the grinding wheel. The maximum bond equivalent is a practical value determined by experience.

The lines of constant grade of existing grinding wheels are of various shapes. As an example, a relationship between grade and structure is shown in Figure IV-4 .

IV.3.3 Modulus of Elasticity

Modulus of elasticity of work material is one of the most basic characteristics of the material. Using this basic parameter it is possible to investigate deformation, stress wave propagation and grindability of the material.

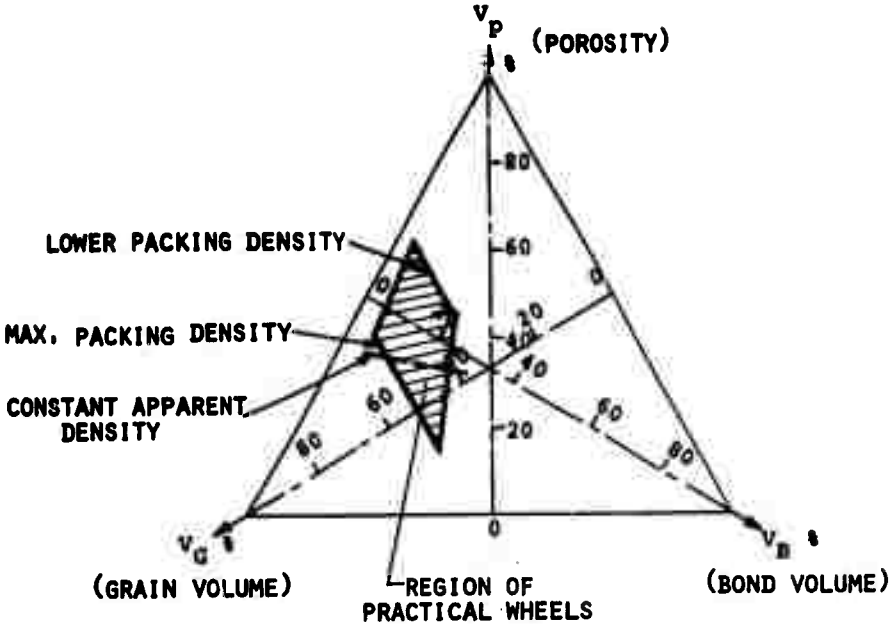

FIGURE IV-3 - TERNARY DIAGRAM OF VOLUMETRIC COMPOSITION

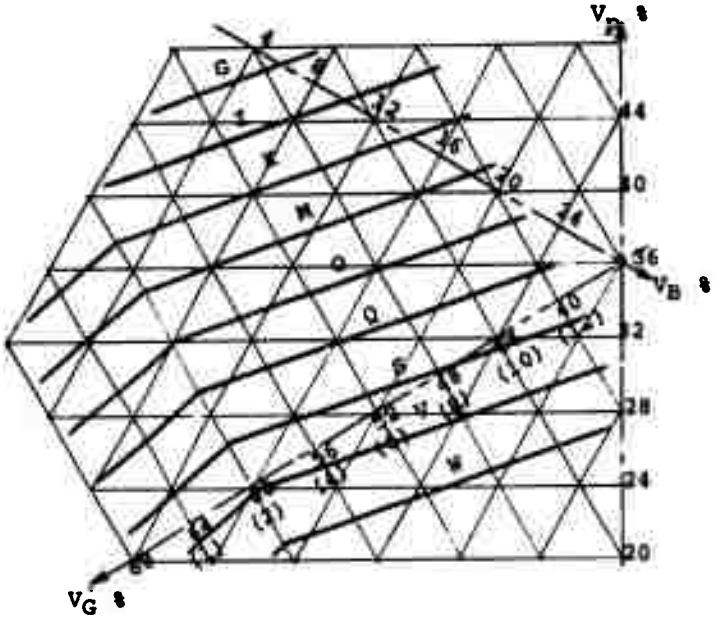

FIGURE IV-4 - AN EXAMPLE OF CONSTANT GRADE LINES ON THE TERNARY DIAGRAM

The Young's modulus of the grinding wheel is also expected to be important, and can be measured by a sonic method. The sonic method can be used to determine the natural frequency of the grinding wheel. The natural frequency of a wheel of particular shape is related mathematically to the modulus of elasticity.

Figure IV-5 shows one example of the experimental results on the relation between modulus of elasticity of grinding wheel and the natural frequency together with the grade indicated on the wheel. As can be seen in this figure, the modulus of elasticity of a grinding wheel increases from 2×10^6 psi to 9×10^6 psi with the change of grade from G to Q. This is 1/3 to 1/10 of that of conventional steel.

IV.3.4 Spring Constant of Grain Mounting

As mentioned in Section II, the properties of the grinding wheel should be described by the amount of elastic displacement of the grain incurred during the grinding process. Therefore, the spring constant of the grain mounting will be more useful to the grinding process in terms of basic chip formation than the modulus of elasticity of the wheel. In the next paragraph the three-dimensional distribution of cutting edges which is important in the analysis of the spring constant will be discussed and the spring constant of a grain under various boundary conditions is presented.

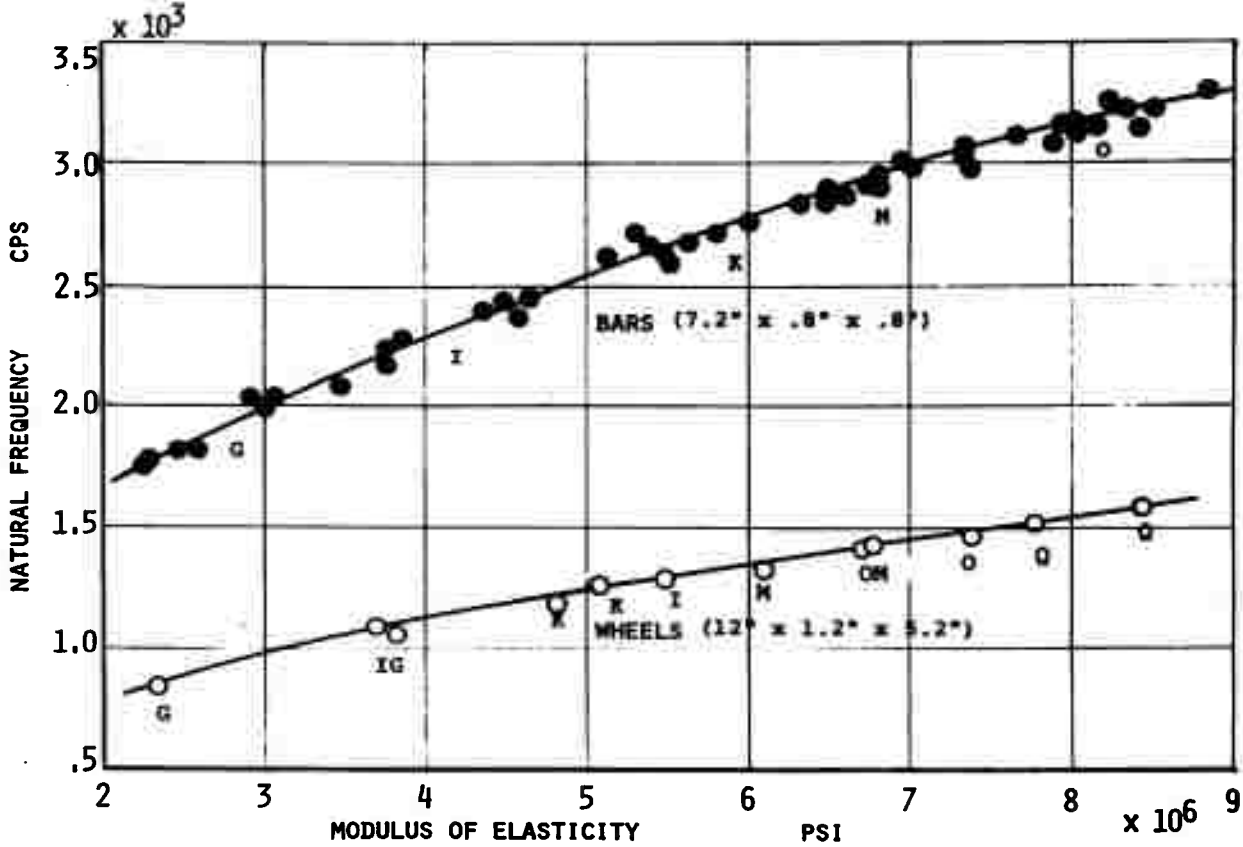

FIGURE IV-5 - SOME EXAMPLE OF MODULUS OF ELASTICITY FOR GRINDING WHEELS

(1) Three-dimensional distribution of cutting edges.

The distribution of cutting edges on the surface of wheel has been measured in many different ways by many researchers on the assumption that the cutting edges are distributed uniformly over the surface of the wheel. In actual wheels, the cutting edges are not uniformly distributed and, in fact, the distribution of cutting edges is a function of the depth from the surface of wheel.

The three-dimensional density of cutting edges can be calculated statistically from a profile curve obtained by measuring the surface of the wheel with a roughness measuring instrument. Tables IV-2 and IV-3 show the wheels and dressing conditions used throughout the following experiments. The density of cutting edges $\lambda(u)$ at the depth u from the surface of wheel can be obtained from the equation

$$\lambda(u) = \frac{3}{2[3d_o(u+\delta)-2(u+\delta)^2]} \left\{ \int_o^u g(u)du \right\}^2 \qquad \text{(IV.3.1)}$$

where d_o is the average grain size and δ is the amount of grain diameter removed by dressing and calculated from the average initial area in the clearance surface. The distribution function g(u) can be determined statistically. The histograms in Figure IV-6 show the normalized distribution of cutting edges calculated from the profiles of the surface of the wheel dressed under three different conditions a, b and c. From this figure it can be seen that the value of the curve g(u) increases rapidly near the surface of the

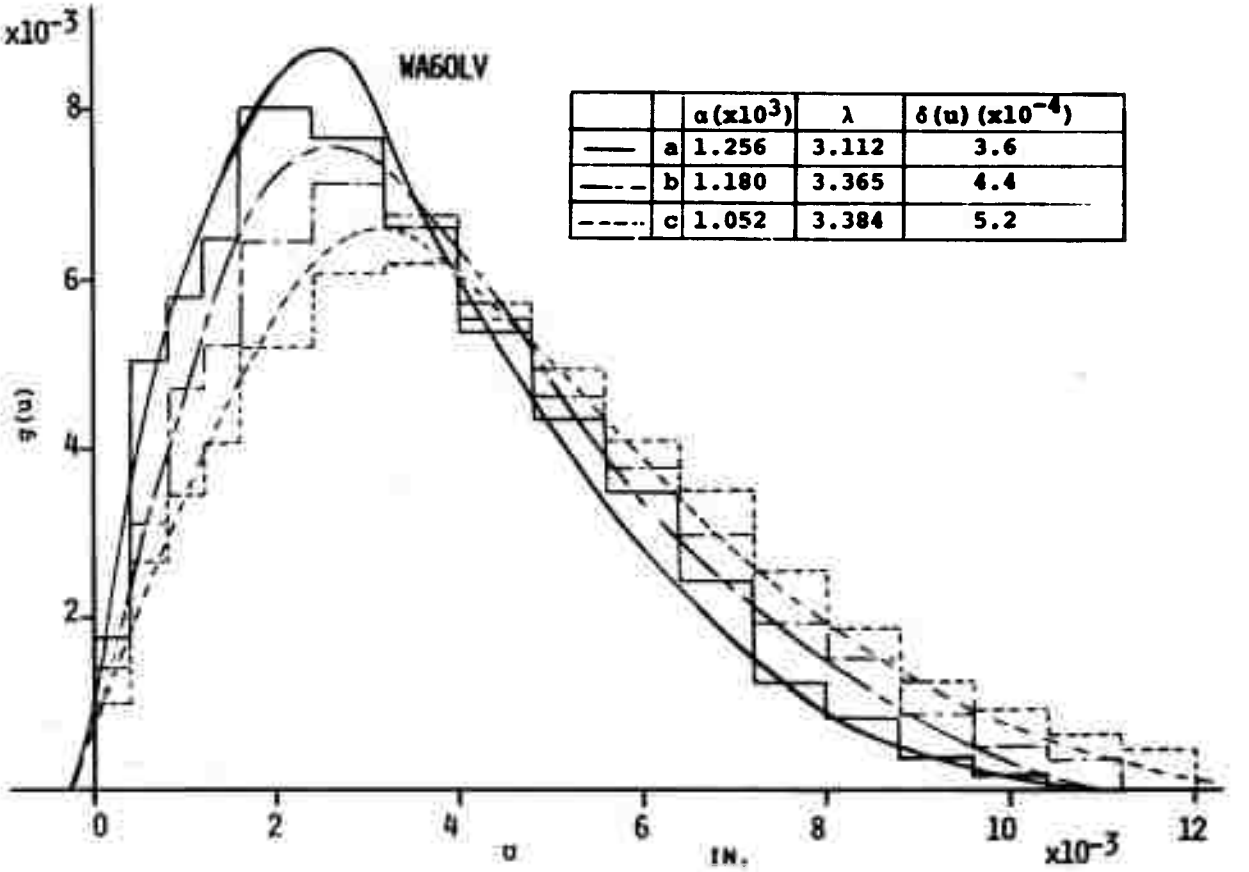

FIGURE IV-6 - NORMALIZED CUTTING EDGE DISTRIBUTION

wheel, becomes maximum at a certain point and then decreases. Therefore, the analytical form of the distribution curve g(u) may be represented by the modified Γ distribution function. That is,

$$g(u) = \frac{\alpha\lambda}{\Gamma(\lambda)} \quad (u+\delta)^{\lambda-1} \; e^{-\alpha(u-\delta)} \qquad \text{(IV.3.2)}$$

where α and λ are characteristic values by which the Γ distribution can be described and can be found from the mean value $\bar{X}$ and the variance S^2 of the g(u) distribution as follows:

$$\alpha = \bar{X}/S^2 \quad , \quad \lambda = \bar{X}^2/S^2 \qquad \text{(IV.3.3)}$$

The curves in Figure IV-6 show the value calculated by Equation (IV.3.2). From the comparison of the curves with the histogram it can be seen that the Γ distribution function (IV.3.2) can be adopted for the analytical form of the distribution curve g(u). Therefore, if the characteristic values α, λ and δ are statistically estimated, the three-dimensional density of cutting edges at the depth u from the surface of wheel can be calculated by Equations (IV.3.1) and (IV.3.2). Figure IV-7 shows the variation of the characteristic values α and λ with the bond ratio for vitrified bond, and Figure IV-8 shows the variation of the value δ with the bond ratio as examples.

Figures IV-9 and IV-10 show the three-dimensional density of cutting edges for the grinding wheels WA60LV and WA60LB dressed under three different conditions a, b, and c respectively. In these figures, the points show the density

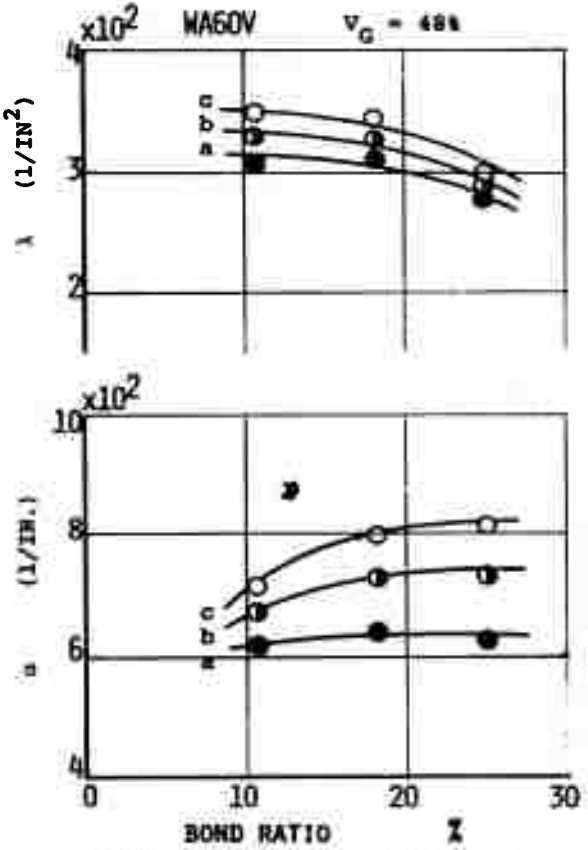

FIGURE IV-7 - VARIATION OF a, λ, WITH BOND RATIO

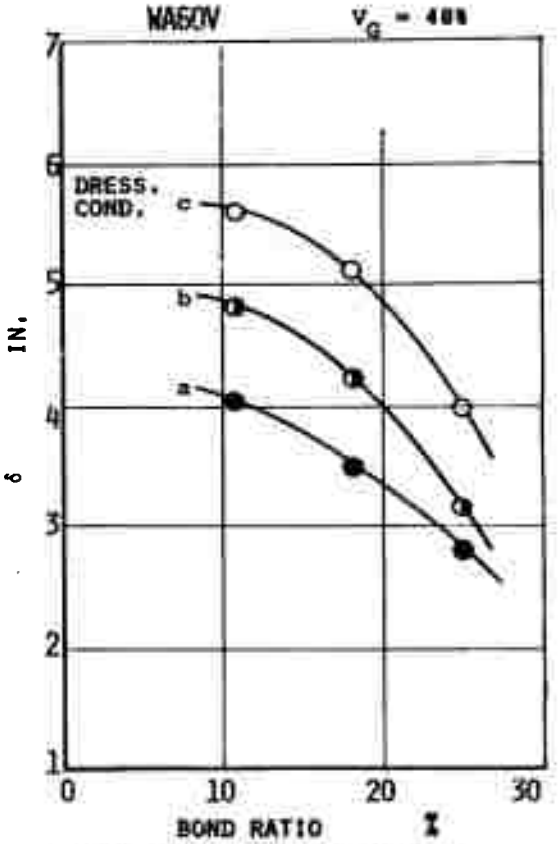

FIGURE IV-8 - VARIATION OF δ WITH BOND RATIO

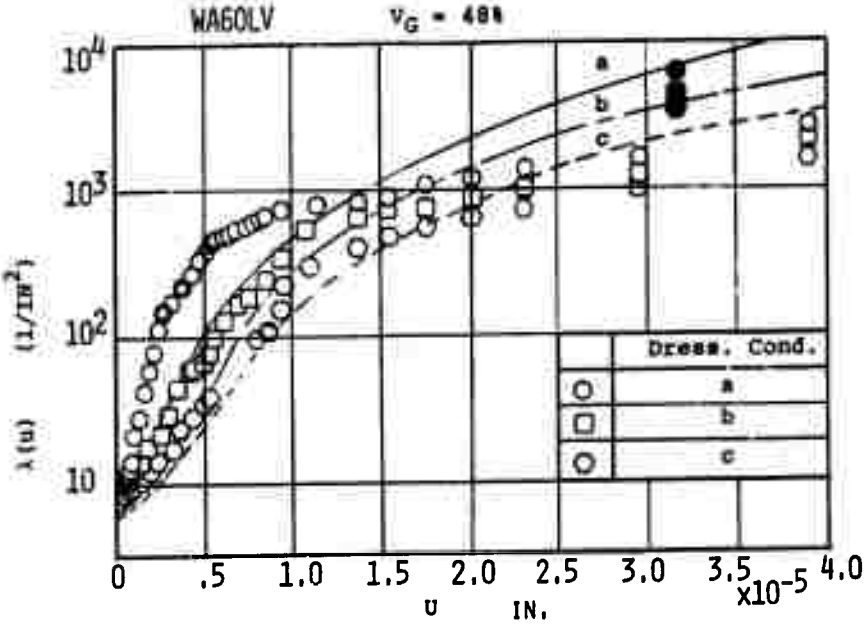

FIGURE IV-9 - CUTTING EDGE DENSITY FOR V BOND WHEEL

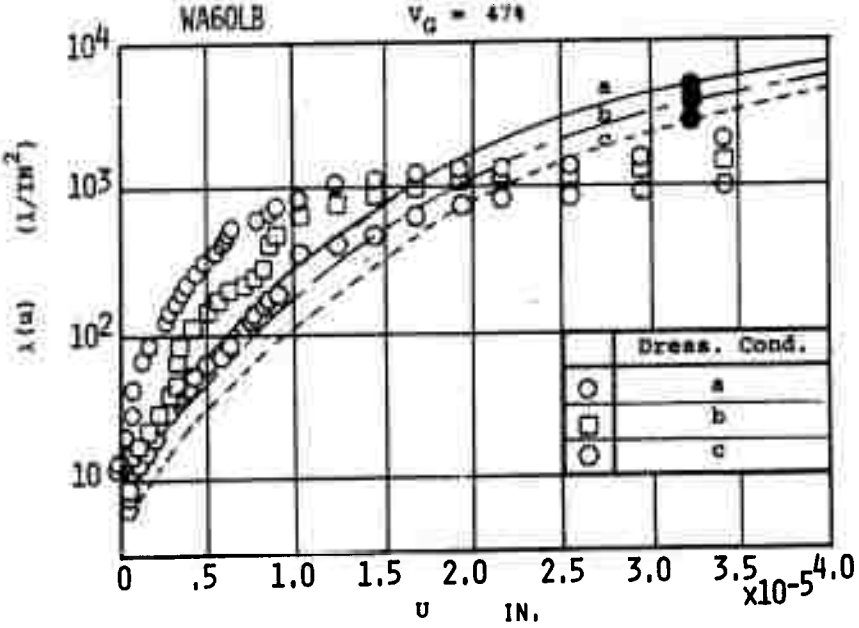

FIGURE IV-10 - CUTTING EDGE DENSITY FOR B BOND WHEEL

counted directly, the smooth curves are calculated by Equation (IV.3.1) and (IV.3.2), and three black points at the depth u = .003" are obtained from the copies of the surface of the wheel by a direct contact method.

(2) Static Spring Constant of Grain Mounting

In practical grinding each grain in the interference zone supports part of the grinding load and displaces almost separately. Therefore, the spring constant of the grain mounting has a strong physical meaning to the cutting process of abrasive grain. The spring constant of the grain mounting will be measured based on the three-dimensional distribution of cutting edges.

The density $\lambda(u)$ of the cutting edges increases with an increase of the depth u from the surface of wheel and, therefore, the spring constant of the grain mounting will become larger with increasing depth u.

Now assuming that the cutting edges are mounted resiliently on non-linear springs, the initial spring constants at a depth u before deformation are also equal to k(u). As shown in Figure IV-11, when the push bar of cross section area s is indented into the surface to a depth u, all of the cutting edges between 0 and u under the push bar will displace to a position of depth u. Then the spring constant of all cutting edges at a depth u are equal to k(u) and, therefore, the increment of force dP necessary to displace the push bar further by an infinitesimal depth du is given by the equation

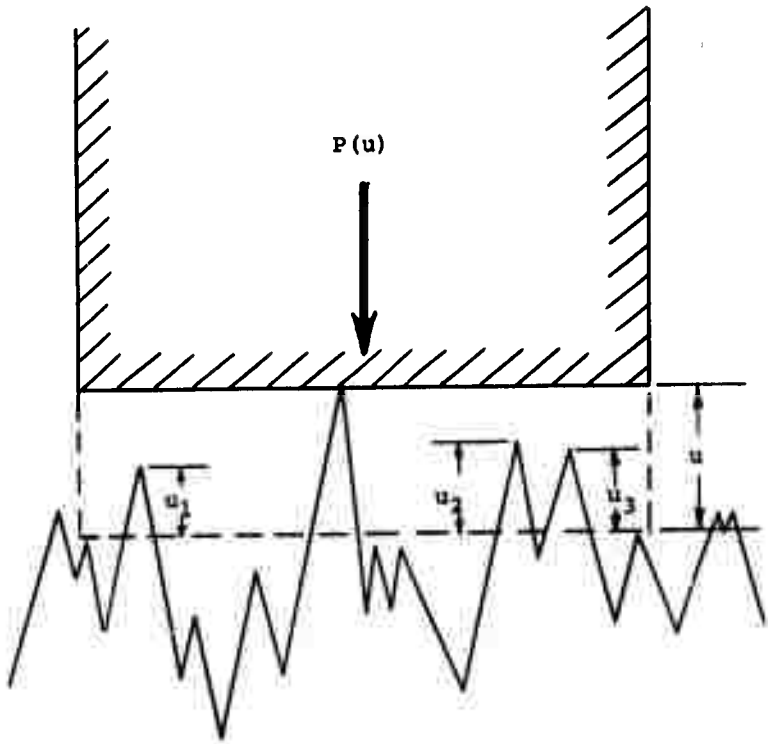

FIGURE IV-11 - PUSH BAR ACTING ON A WHEEL

$$dP = s \cdot k(u) \cdot \lambda(u) \cdot du \qquad \text{(IV.3.4)}$$

Then

$$k(u) = \frac{1}{\lambda(u)} \frac{d}{du}\left(\frac{P}{s}\right) = \frac{1}{\lambda(u)} \frac{dp}{du} \qquad \text{(IV.3.5)}$$

where $p = \frac{P}{s}$

The three-dimensional density of cutting edges $\lambda(u)$ can be calculated by Equations (IV.3.1) and (IV.3.2). Consequently, if the slope $\frac{dp}{du}$ of the force-displacement curve can be experimentally evaluated, the spring constant of grain mounting k(u) will be determined by Equation (IV.3.5). The slope $\frac{dp}{du}$ of the force-displacement curve is, therefore, the fundamental value required to evaluate the spring constant of grain mounting.

The spring constant of grain mounting can be calculated from Equation (IV.3.5) by the increment $\frac{dp}{du}$ shown in Figures IV-12 and IV-13 and the density $\lambda(u)$ of cutting edges. Figures IV-12 and IV-13 show variations of the slope of the force-displacement curve with dressing conditions and grade respectively.

Figures IV-14 and IV-15 show the effect of dressing conditions on the spring constant of vitrified and resinoid bond wheels respectively. In these figures it can be seen that the spring constant k(u) becomes larger with depth from the surface and for finer dressing for both the vitrified and resinoid bonded wheels.

Figures IV-16 and IV-17 show the relation between the grade and the spring constant under a fixed dressing

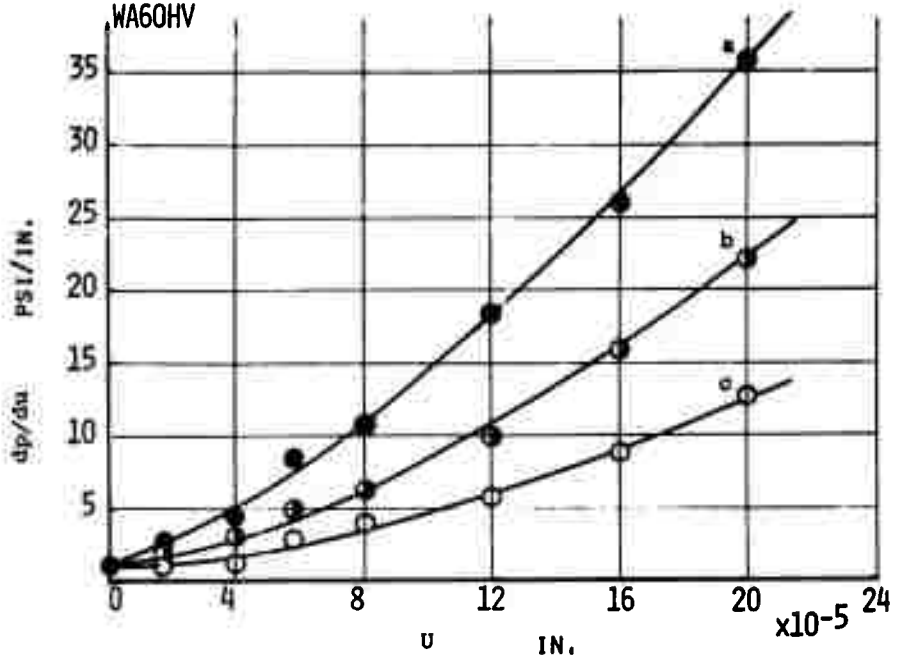

FIGURE IV-12 - VARIATION OF dp/du FOR V BOND WHEEL

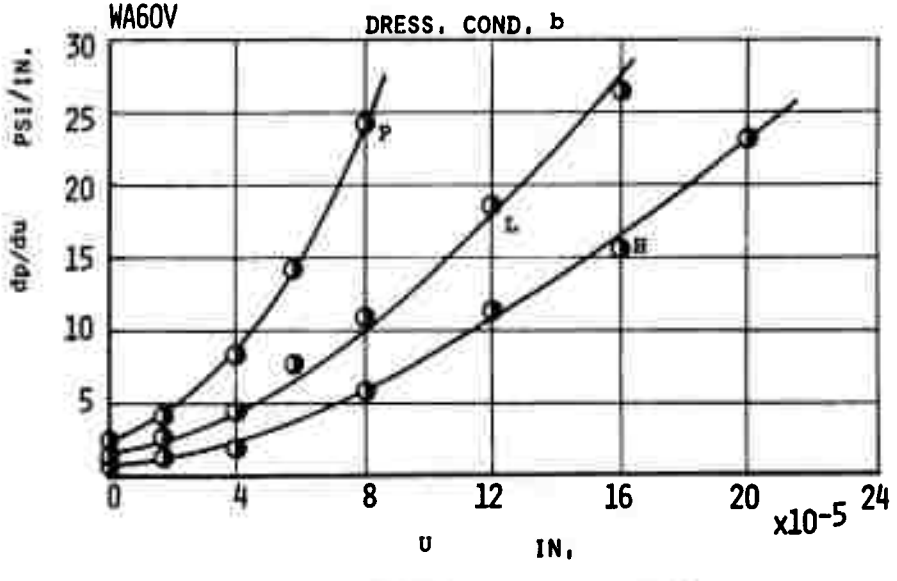

FIGURE IV-13 - VARIATION OF dp/du WITH GRADE

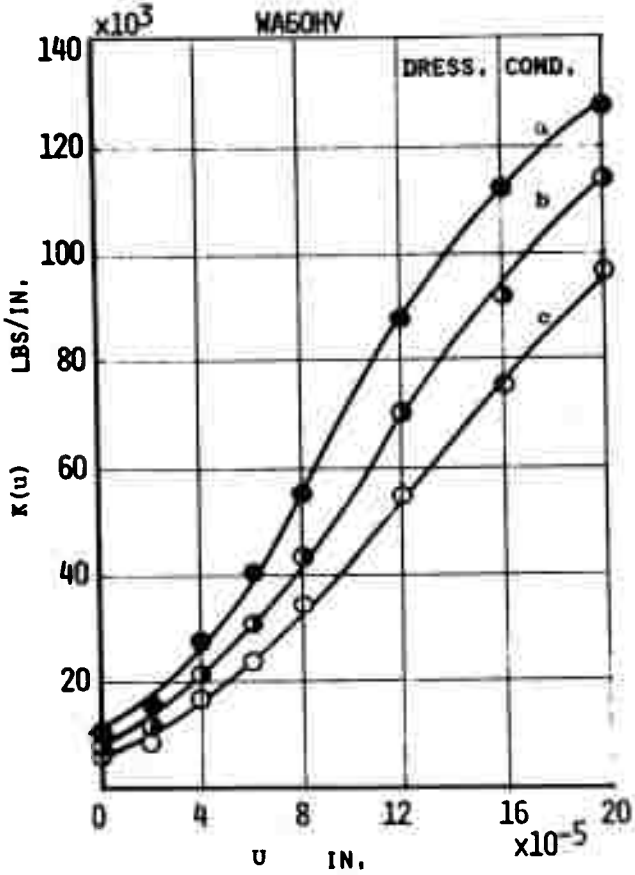

FIGURE IV-14 - EFFECT OF DRESSING CONDITION ON SPRING CONSTANT FOR V BOND WHEEL

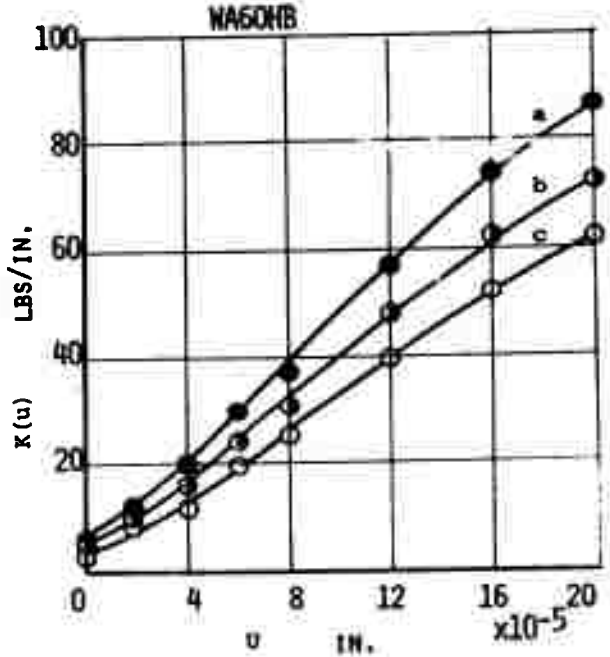

FIGURE IV-15 - EFFECT OF DRESSING CONDITION ON SPRING CONSTANT FOR B BOND WHEEL

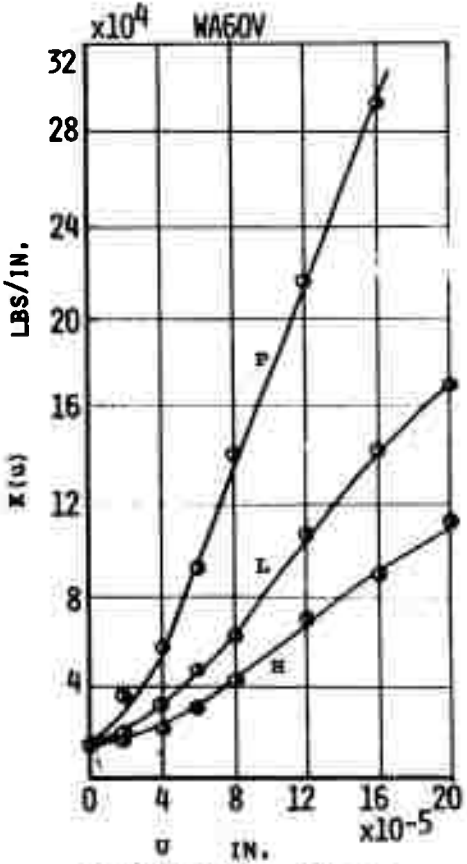

FIGURE IV-16 - SPRING CONSTANT FOR V BOND WHEEL

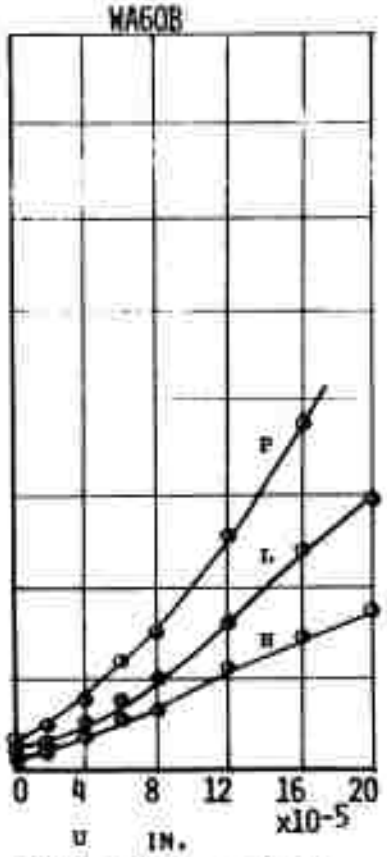

FIGURE IV-17 - SPRING CONSTANT FOR B BOND WHEEL

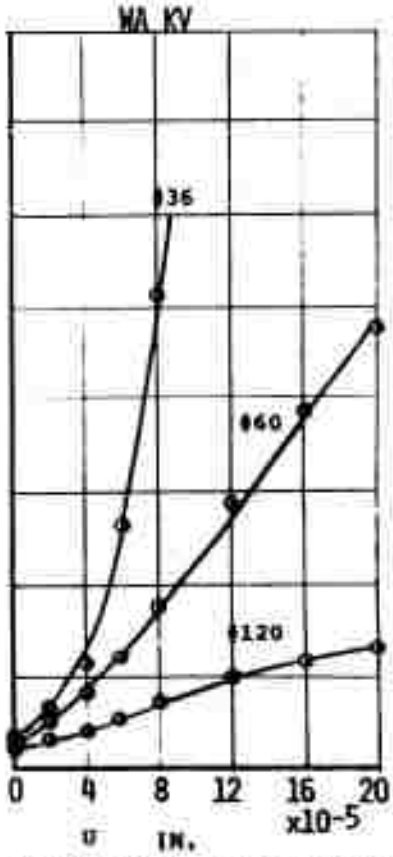

FIGURE IV-18 - RELATION BETWEEN SPRING CONSTANT AND GRAIN SIZE

condition for vitrified and resinoid bonded wheels respectively. These figures show that the spring constant of grain mounting becomes larger with a higher value of the grade for the case of constant grain ratio. Figure IV-18 shows variations of the spring constant with grain size for vitrified bond wheels with fixed dressing conditions.

IV.4 Vibration Dressing

IV.4.1 Introduction

In order to better utilize the grinding process especially for HSTR materials it is necessary to use a cutting tool (grinding wheel) with better cutting capabilities. An advantage can be obtained by using a new method to dress the present wheel since in this way no new wheels are necessary. A new method for producing many sharp cutting edges on the working surface of the grinding wheel was developed and tested.

IV.4.2 Theoretical Cutting Edge Generation

In this section discussions of an ideal cutting edge, the properties of the grinding wheel components, a practically realizable cutting edge, and methods of generating cutting edges are presented.

IV.4.2.1 Characteristics of an Ideal Tool in Grinding.

The ideal properties of a single cutting edge in grinding are nearly the same as any cutting tool. These properties include resistance to wear (hardness), resistance to breakage (toughness), low frictional coefficient, uniform

spacing, stiff mounting, chemical inertness and good geometrical configuration. The geometrical configuration of a tool includes such parameters as rake angle, clearance angle and flank area.

For grinding, the ideal cutting edge would have no flank area, that is the rubbing area or "contact area" as it is commonly called in grinding terminology should be close to zero. Note that this is only true from the point of view of metal removal. From the point of view of polishing or lapping, a large contact area is needed since the rubbing of the contact area is a mechanism which yields smooth surface finish. Ideally there should be as many cutting edges as possible in order to rapidly remove metal. The only limitations on the maximum number of cutting edges would be clearance for the grinding chip.

IV.4.2.2 Wheel Constituents

The abrasive materials used presently in grinding are diamond, silicon carbide (SiC), and aluminum oxide (Al_2O_3). All three of these materials are very hard crystalline materials and have the ability to hold sharp edges, therefore they satisfy most of the requirements of an ideal cutting tool. To satisfy the rest of the requirements it is necessary to space, mount and form the materials.

The process of forming the cutting edge on the abrasive utilizes the anisotropic properties of crystals. For example, in aluminum oxide crystals the strength of the stronger

direction is on the order of 30% greater than that of the weaker direction. Aluminum oxide crystals are hexagonal and are described as having almost perfect cleavage parallel to the base and faces of the unit rhombohedron. The crystals form into hexagonal sheets which can be split apart similar to mica. Thus there are four directions in which Al_2O_3 may cleave or split.

The bond in a grinding wheel is the agent that holds the cutting edges together and is the "mounting" for the grain. The hardness of the wheel and the stiffness of the mounting of the grain are dependent upon the amount of bond in the wheel.

The grain-bond system is of prime importance since it is this system that is the cutting "tool." For dressing considerations the interest is in what happens to this system when it is acted upon by a force. Namely the interest is in the fracture characteristics of the overall system. Knowing that the grain has strength orientations and the bond is uniform, the interesting property is the relative magnitude of the strength of the grain versus the strength of the bond.

If the strength of the bond is weaker than the grain strength in the abrasive's cleavage direction, any dressing force large enough to affect the wheel would only break out grains. This is a possible method of retaining sharpness but not as economical as others, since grinding forces would

break the wheel down very quickly. This would also have detrimental effects on the surface finish and dimensional accuracy of the workpiece. A more practical scheme would be for the bonding force to be somewhere between the two strengths of the grain. This would lead to a continuously sharp wheel because unless the grain broke, the force of the dressing tool would break the supporting bond, tearing the entire grain out of the wheel. (Refer to Figure IV-1) The most practical case is for the bond strength to be greater than the grain strength, because of the greatly increased life of the grinding wheel. However, because of the strength of the bond, it is now possible for the dressing tool to machine the grain rather than break it. It is this characteristic that causes wear areas on the surface of a freshly dressed wheel.

IV.4.2.3 Actual Cutting Edge

An actual cutting edge differs from an ideal one in some respects. Because of the random manner in which the grain is oriented in the wheel at manufacture there is no control over clearance angle, rake angle, or area on the surface of the wheel, and the grain wears and breaks to a much greater extent than other cutting tools. The breakage of the abrasive grain during grinding can expose new sharp cutting edges to the metal, and under certain grinding conditions the wearing phenomena is advantageous to the grinding process. First the grain wears a flat area on the surface

of the wheel due to rubbing against the workpiece. This larger area is acted upon by an increasing normal force, a frictional force due to rubbing, and a cutting force. When the magnitude of the resultant force on the grain reaches either the bond strength of the wheel or the body strength of the grain, the flat area is broken away. Ideally a grain would cut until it obtained a certain wear area, then part of the grain would break away removing the wear area and leaving another sharp cutting edge. This phenomena is called "self sharpening." Good grinding conditions would be those that provide a balance between dulling and the self sharpening effect of the wheel. The practical cutting edge, since it is not already present on the surface of the wheel, must be formed there. The only method available to do this forming is the process of dressing.

IV.4.2.4 Force Considerations in Dressing

Due to the directional properties of grain, the direction of forces acting on the wheel play an important part in the action of the grinding wheel. The reason for the interest in the dressing force is that improvements of the observed parameters will occur if the dressing tool applies a force on the grain in such a manner that the grain breaks, leaving behind rough sharp cutting edges.

For conventional dressing, the direction of the force is influenced by some machine and dressing parameters such as traverse rate and dressing drag angle, but the direction

of force on the grain is nearly opposite the direction of motion of the grit. Tsuwa shows that there are flat areas on the surface of a freshly dressed wheel. The flat area is produced by the dressing tool machining the grain rather than breaking the bond or the grit.

To improve dressing conditions it is necessary to reduce the number of machined grains and increase the number of broken grains. A way to do this is to change the dressing configuration in such a manner that the dressing tool has a chance to hit the grain in more than one direction. This will increase the probability of breaking the grain. Two possible methods are tangential dressing and radial dressing.

(a) Tangential Dressing

The first method is to utilize an oscillatory motion in the same plane as the tangent plane of the grinding wheel's surface and parallel to the direction of traverse of the diamond. This method is called tangential dressing. The forces acting on the grain due to both conventional and tangential dressing have a direction close to that of the tangent plane to the wheel. This results in a high probability of a grain breaking nearly parallel to the tangent plane of the wheel. This would yield a decrease in the amount of rubbing area and would give a sharper overall dressed condition. Note however that the wheel would have a tendency to quickly regain the larger flat area due to the small angle formed between the grain cleavage surface and the tangent

plane of the wheel. (See Figure IV-19). This condition of blocky shaped grain should be kept in mind in the case of high grinding forces where a smaller cross section of the grain would break more easily.

(b) Radial Dressing

Another dressing configuration would be to impose a radial oscillation on the traversing diamond. This would tend to make the resulting dressing forces more perpendicular to the tangent plane of the grinding wheel thereby increasing the probability of grain fracture along a more vertical plane. (See Figure IV-20). This reduces the contact area as before but due to chipping and crumbling of the grain it makes it possible to obtain more than one cutting edge per grain. Note here the tendency to regain the contact area is not as great as in the previous two cases since the grain shape is now more narrow with steeper sides.

Note that the steeper sides mean a smaller rake angle on the grain. If metal cutting theory based on turning is valid for grinding, the smaller rake angle of the grain should make it easier for the grain to cut chips.

IV.4.2.5 Conclusions

From the consideration of dressing forces it can be seen that improvement in the grinding process can be gained by using either of the special dressing methods since they both reduce the contact area. However, considering also the angle of the forces, it can be seen that greater

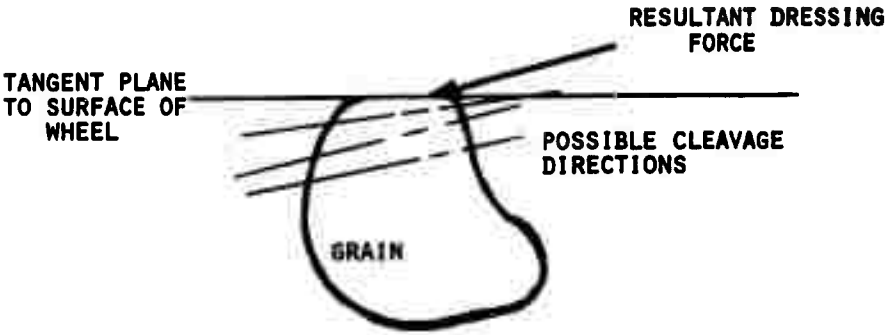

FIGURE IV-19 - LOW ANGLE CLEAVAGE OF CONVENTIONAL AND TANGENTIAL METHODS

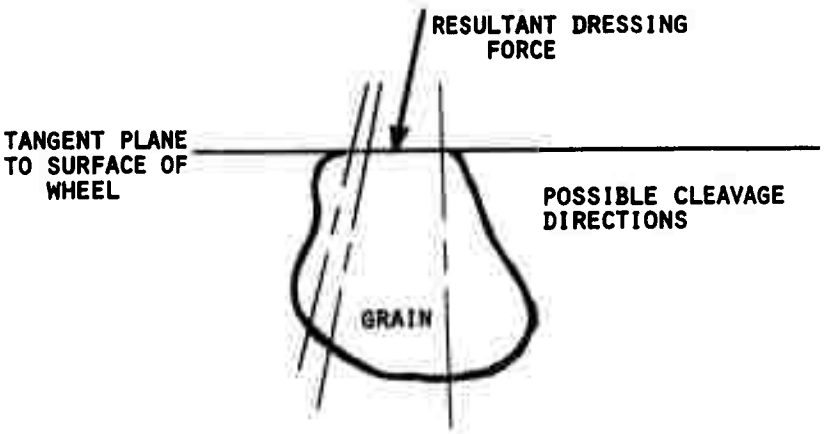

FIGURE IV-20 - VERTICAL CLEAVAGE OF RADIAL DRESSING METHOD

improvement is expected with the radial dressing method. Experimental procedure and equipment were developed to study the effects of the changed dressing configuration.

IV.4.3 Experimental Procedure and Equipment

Conventional dressing under the similar conditions of depth of cut and traverse rate were performed as the basis of comparison for the different dressing methods.

IV.4.3.1 Tangential Dressing

The tangential dressing method imparts a sinuosidal motion to the tip of the diamond. The dressing tool was mounted on the end of a cantilever beam arrangement in a fixture that could be vibrated with the hydraulic exciter. (See Figure IV-21). A compensating network utilizing a Bently inductance displacement probe as the feedback element was used to assure reliable amplitude and stable operation at a peak to peak amplitude of 1×10^{-4} inches and a frequency of 800 cycles per second. Some tests at 60 cycles per second at a larger amplitude were run for comparison.

IV.4.3.2 Radial Motion Dressing

Radial motion dressing has a small amplitude of vibration in a direction normal to the surface of the wheel imposed on the conventional dressing motion. This is accomplished by mounting the diamond in a cantilever type fixture in such a manner that the motion of the dressing tool can be controlled by a hydraulic exciter. (See Figure IV-21). The feedback

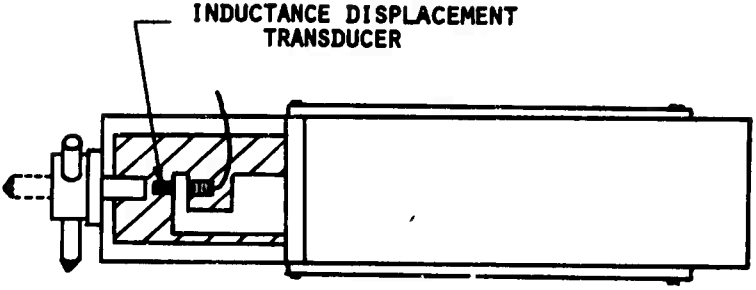

(A) Top View

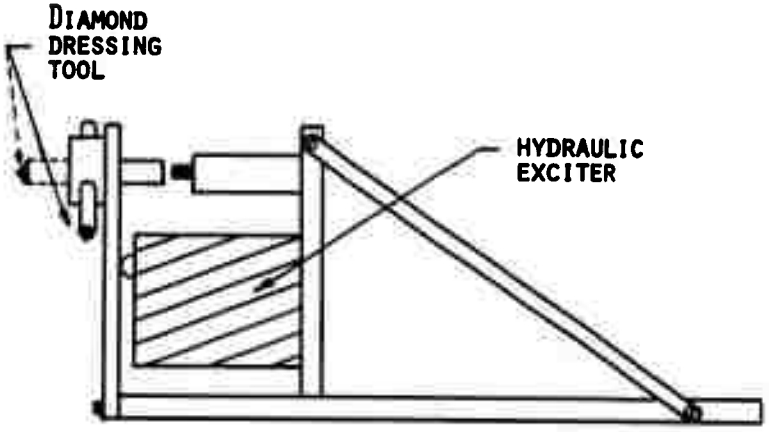

(B) Side View

FIGURE IV-21 - VIBRATION DRESSING FIXTURES

loop of the system was completed with a Bentley inductance proximity detector. Due to the necessity of carefully maintaining a static position of the diamond dressing tool so that no waves are dressed onto the wheel, a compensating network that attenuates signals higher in frequency than 40 cycles per second was used to eliminate low frequency motion.

IV.4.3.3 Test Procedure

The wheel is first dressed with a worn diamond until no evidence of loading is visible. Then the wheel is made very smooth by taking a very small depth of cut with the dressing tool and allowing the diamond to traverse across the wheel several times without removing further stock from the wheel. This operation is repeated several times. Then ten dressing passes are taken with another diamond. No sparkout passes are permitted during final dressing. The wheel is then touched up to the workpiece and a small amount of material is removed as the wheel sparks out against the workpiece. The touch up operation is performed so that loosened grains in the wheel will be knocked out and so that the rubbing area on the wheel will be polished to make it easier to observe through the microscope. After observations on the freshly dressed wheel are completed, ten grinding passes are taken to dull the wheel. During this grinding period the tangential grinding force is recorded. After the grinding period the number of cutting edges and amount of rubbing area is again observed through the microscope.

IV.4.3.4 Method of Observation of Grinding Wheel

A new method for directly observing the cutting edges on the surface of the grinding wheel was developed. A hole was cut in the grinding wheel housing and a microscope was mounted directly on the machine so that removal of the wheel from the machine for observation of the grain is unnecessary. The internal light of the microscope is polarized and then directed normal to the grinding wheel surface. The reflected light is then repolarized so that only light that has been immediately reflected back is visible. Imposed on this light is a non-polarized source of lower intensity light striking the wheel at an oblique angle. Due to the translucent properties of aluminum oxide grain, the result of the two light sources is to cause the worn contact area to stand out brightly and to ghost in the overall shape of the grain. The number of cutting edges are then simply counted and the contact area estimated by using a fine grid in the eyepiece of the microscope.

IV.4.3.5 Tangential Grinding Force Measurements

As a secondary indication of the effectiveness of the dressing condition a recording wattmeter was connected to the wheelhead motor. Calibration of the recording wattmeter was accomplished using a prony brake. While this method is not extremely accurate, the purpose of the force measurement is only to give a relative indication of the cutting ability. Previous work done on another machine using the same method gave good results.

IV.4.4 Experimental Results

IV.4.4.1 Summary of Test Results

All data was taken on a 12" Cincinnati universal grinding machine. The grinding wheel is a Cincinnati specification 4A60K4VPM and the dressing diamonds are 1.5 carat pyramidal stones having a vertex angle of approximately 100°. The eight conditions of infeed and traverse rate are shown in Table IV-4 .

TABLE IV-4 SUMMARY OF DRESSING TESTS

Test No.	Diamond Infeed x 10^{-3} in.	Dressing Lead in/rev. of wheel
1	0.25	.008
2	0.25	.016
3	0.5	.008
4	0.5	.016
5	1.0	.008
6	1.0	.016
7	2.0	.008
8	2.0	.016

For each test, the characteristics of the grinding wheel surface were observed under 42 power magnification at twenty random places around the periphery of the grinding wheel. This represents a total viewing area of 135 square millimeters.

To show the effects of dulling on the dressing condition a small amount of grinding was performed with each dressing condition. The procedure was to take ten passes across a 3" diameter 10" long bar of annealed 4340 steel with a depth of cut of .0005" per pass. The surface speed of the workpiece was maintained at 100 feet per minute and the traverse rate

was 28 inches per minute. The wheel rotational speed for all tests was 1750 RPM.

For the tangential data the amplitude of motion of the diamond in the horizontal direction was 1.0×10^{-4} inches at a frequency of 800 cycles per second. The amplitude of radial motion of the diamond for the radial dressing tests was also 1.0×10^{-4} inches at a frequency of 800 cycles per second.

IV.4.4.2 Data

The number of cutting edges and wear area data shown in Tables IV-5, IV-6, IV-7 is the average of twenty observations. The tangential grinding force is the average of the maximum tangential force recorded on the last nine dulling passes. The force of the first dulling pass was ignored due to the inaccuracy in setting the first depth of cut.

Figures IV-22 through IV-27 are plots showing relations between wheel surface characteristics and the effects of dressing on these characteristics. Due to the grouping of the data it can be seen that dressing methods do have a significant effect on the surface characteristics of the grinding wheel. It is also interesting to note that grinding, even for a short period of time, significantly changes the relations between the wheel surface characteristics.

Figures IV-22 and IV-23 show the relation between the number of cutting edges per unit area and wear area.

TABLE IV-5 - DATA FROM CONVENTIONAL DRESSING TESTS

Test No.	SHARP			WORN			Average Tangential Force (lbs)
	Cutting Edges / in^2	Area (%)	Area / Edge x10^{-6} (in^2)	Cutting Edges / in^2	Area (%)	Area / Edge x10^{-6} (in^2)	
1	1376	.815	5.92	1210	1.116	9.18	4.63
2	1471	.961	6.53	995	1.619	16.27	3.90
3	1305	.670	5.13	990	1.702	17.19	3.79
4	943	.435	4.61	1319	.926	7.02	3.20
5	1095	.708	6.47	1100	1.012	9.20	2.49
6	1081	.354	3.27	995	1.003	10.08	2.37
7	1019	.482	4.73	1271	.943	7.42	2.32
8	952	.426	4.47	910	.955	10.49	2.44

Wheel Diam. - 14"
Work Diam. - 3"
Wheel 4A60K4V

Wheel Speed - 1750 RPM
Work Speed - 100 ft/in.
Coolant - none

TABLE IV-6 - DATA FROM TANGENTIAL DRESSING TESTS

Test No.	SHARP			WORN			Average Tangential Force (lbs)
	Cutting Edges in^2	Area (%)	$\frac{\text{Area}}{\text{Edge}} \times 10^{-6}$ (in^2)	Cutting Edges in^2	Area (%)	$\frac{\text{Area}}{\text{Edge}} \times 10^{-6}$ (in^2)	
1	1510	.613	4.06	1695	.869	5.13	3.06
2	1690	.554	3.28	1952	1.164	5.96	3.59
3	1733	.688	3.97	1533	.961	6.27	3.35
4	1129	.571	5.06	1729	1.009	5.84	2.56
5	1619	.827	5.11	1719	.940	5.47	2.34
6	1576	.551	3.50	1838	.830	4.52	2.25
7	1510	.690	4.57	1681	.961	5.72	2.27
8	1833	.571	3.12	1533	.872	5.69	2.38
6*	2186	.440	2.01	2238	1.077	4.81	2.73

* Test run at .030 peak to peak displacement at 60 cycles/sec.

Wheel Diam. - 14"
Work Diam. - 3"
Wheel 4A60K4V

Wheel Speed 1750 RPM
Work Speed 100 ft/in.
Coolant - none

TABLE IV-7 - DATA FROM RADIAL DRESSING TESTS

Test No.	SHARP			WORN			Average Tangential Force (lbs)
	Cutting Edges / in²	Area (%)	Area / Edge x10⁻⁶ (in²)	Cutting Edges / in²	Area (%)	Area / Edge x10⁻⁶ (in²)	
1	1914	.619	3.23	1957	.708	3.62	2.35
2	2648	.887	3.35	2376	.875	3.68	2.48
3	1986	.729	3.67	2210	.750	3.39	2.29
4	2029	.655	3.23	1929	.696	3.61	2.23
5	2448	.946	3.86	2086	.598	2.87	2.17
6	2071	.533	2.57	1938	.536	2.77	1.57
7	2057	.560	2.72	1995	.583	2.92	1.94
8	1905	.932	4.89	1857	.667	3.59	1.76
6*	2357	.729	3.09	2114	.780	3.69	2.02
6**	1624	.693	4.27	1505	.744	4.94	1.82

* Test run at 400 cycles per second.

** Test run at 200 cycles per second.

Wheel Diam. - 14"
Work Diam. - 3"
Wheel 4A60K4V

Wheel Speed 1750 RPM
Work Speed 100 ft/in.
Coolant - none

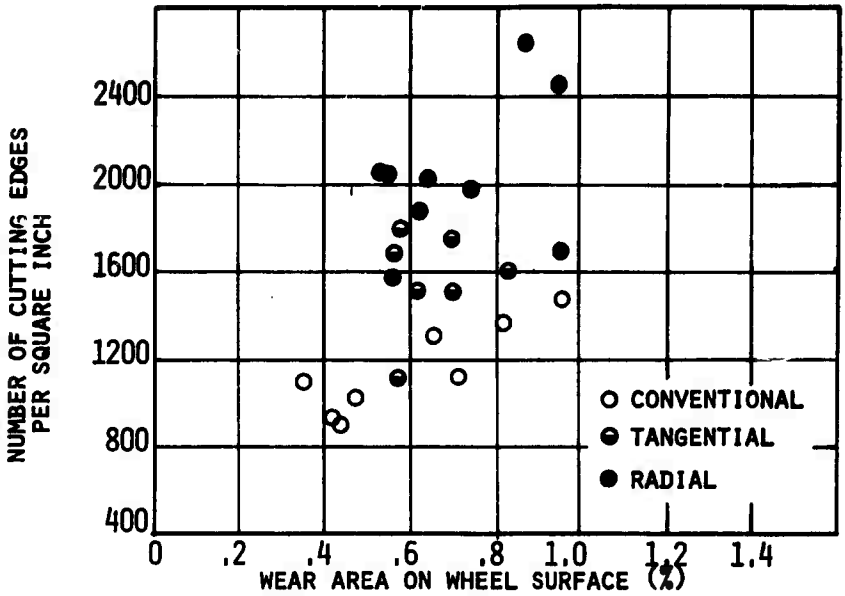

FIGURE IV-22 - NUMBER OF CUTTING EDGES vs. WEAR AREA FOR SHARP CONDITION

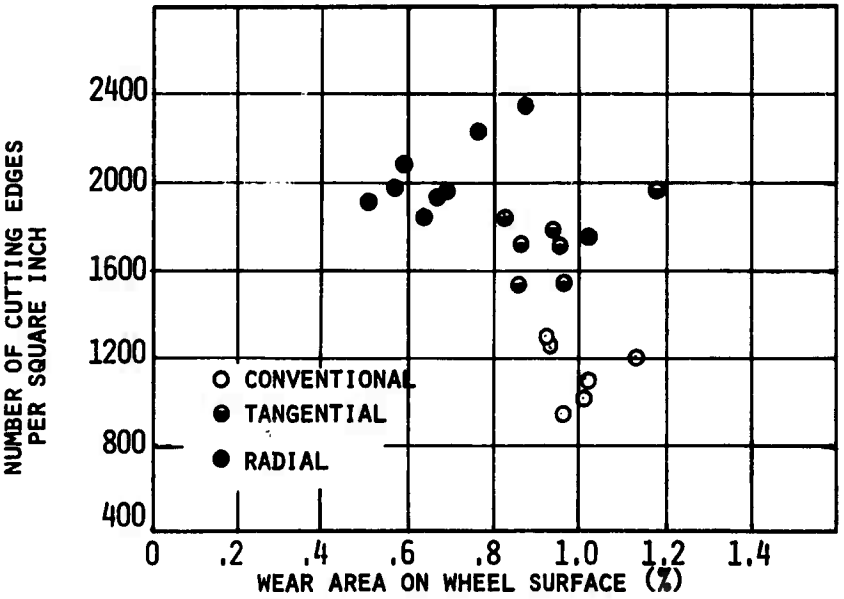

FIGURE IV-23 - NUMBER OF CUTTING EDGES vs. WEAR AREA FOR WORN CONDITION

In Section IV.4.2 it was pointed out that desirable wheel conditions are high number of cutting edges and low wear area. Both tangential and radial dressing methods show an improvement in both these areas over conventional dressing.

Figures IV-24 and IV-25 describe the relation between the area per cutting edge and the number of cutting edges. These figures show that the new dressing methods cause a decrease in the average wear area per grain. A wear phenomena can be inferred also. Comparing the change in wear area per grain between the freshly dressed wheel and the dulled wheel, it can be deduced that the wearing process increases the average wear area on a grain. This increase is more pronounced for conventional dressing than for the new methods. A possible explaination of this phenomena is the discussion involving grain shape below the surface of the grinding wheel in Section IV.4.2.4

Other effects of the dressing method on the grinding wheel are shown in Figures IV-26 and IV-27 . The effect of dressing method on properties just below the surface of the wheel is most pronounced in these figures. A logical conclusion derived from Figures IV-24 and IV-25 might be that the total wear area is constant. However, even though there are more cutting edges, Figure IV-27 shows that similar or smaller total area is obtained when the new dressing methods are used.

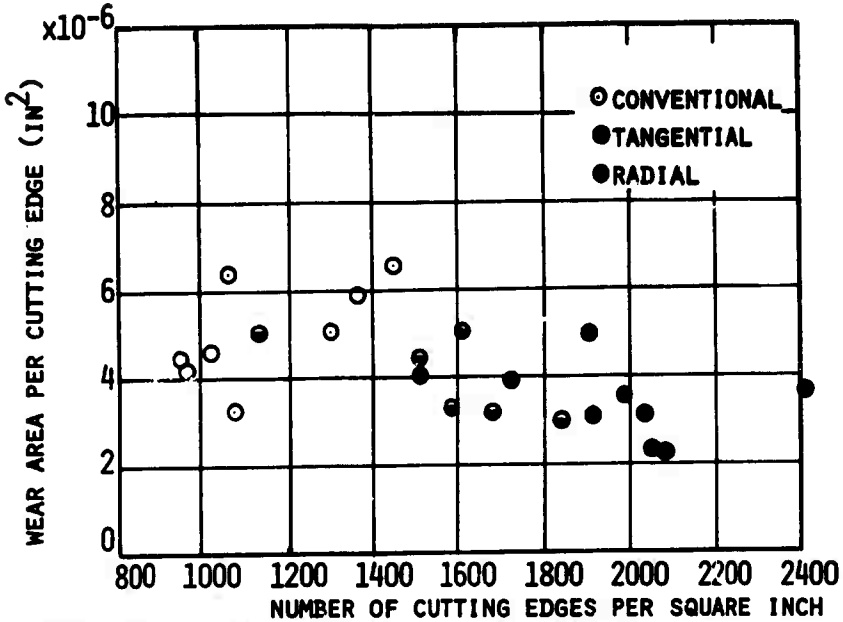

FIGURE IV-24 - WEAR AREA PER CUTTING EDGE vs. NUMBER OF EDGES FOR SHARP CONDITION

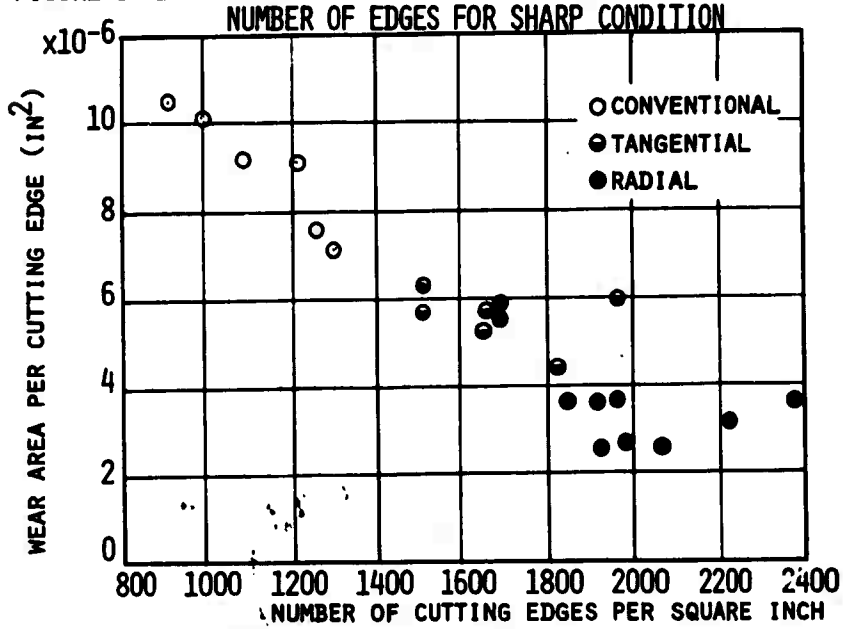

FIGURE IV-25 - WEAR AREA PER CUTTING EDGE vs. NUMBER OF EDGES FOR WORN CONDITION

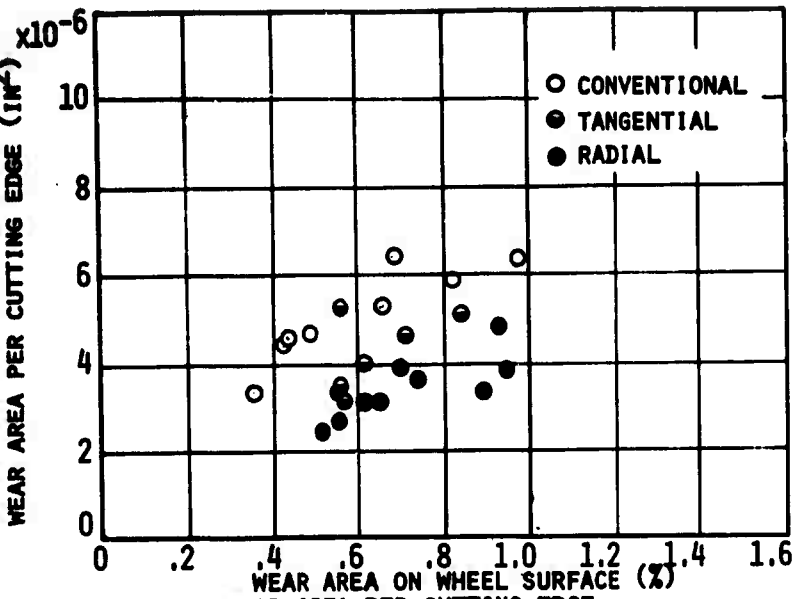

FIGURE IV-26 - WEAR AREA PER CUTTING EDGE vs. WEAR AREA FOR SHARP CONDITION

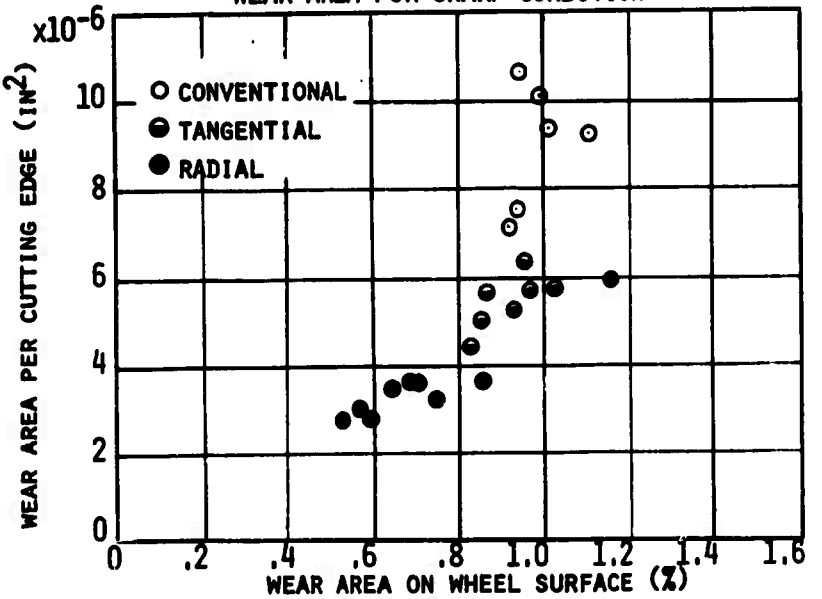

FIGURE IV-27 - WEAR AREA PER CUTTING EDGE vs. WEAR AREA FOR WORN CONDITION

Figure IV-28 showing the effect of wear area on tangential grinding force, indicates that a smaller wear area on the surface of the wheel yields a lower tangential grinding force.

IV.4.5 Conclusions on Dressing Method

This investigation was concerned with the effects of grinding wheel dressing methods on the surface characteristics of the grinding wheel. Two new methods of dressing the grinding wheel were developed. The new methods of dressing both had a small oscillatory motion imposed on the conventional motion of the dressing tool.

The effects of dressing conditions on the number of cutting edges and amount of contact area on the surface of the wheel were observed with polarized light. The results clearly indicate that a great effect on wheel surface parameters was obtained by changing the dressing method. The new dressing methods both resulted in a grinding wheel with more cutting edges and less contact area than obtained with conventionally dressed wheels.

IV.5. Conclusions

The studies of grinding wheel properties have resulted in enough basic information so that a good understanding of the variables of the grinding wheel is possible. The wear mechanism of the wheel has been described and new definitions of important variables of the wheel have been clearly

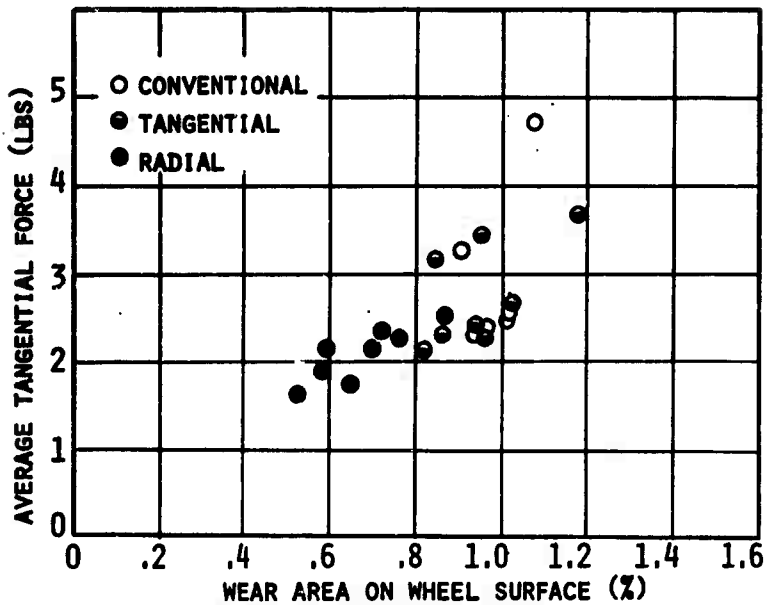

FIGURE IV-28 - AVERAGE TANGENTIAL FORCE vs. WEAR AREA

decided. The physical properties of the grinding wheel such as composition, modulus of elasticity and spring constant of abrasive grain mounting have been carefully described. It was shown that the modulus of elasticity is a good physical property of the grinding wheel that can describe many of the actions of the grinding process. The spring constant of grain mounting is important in the analysis of the chip formation physics of the grinding process.

The increased knowledge in this area of wheel properties was instrumental in the development of a new dressing process. This new process, utilizing vibratory motion, was designed to increase the cutting ability of the grinding process by introducing more and sharper cutting edges onto the surface of the grinding wheel. Experimental work with this type of dressing indicated that this method will work very successfully.

SECTION V

DYNAMIC ANALYSIS IN GRINDING

V.1 Introduction

The information reported in this section concerns vibrations during grinding and is a summary of the work reported in Section II of the Interim Engineering Reports.

The main concern under this contract has been *chatter vibration*. Chatter implies a mechanism whereby a pattern is produced upon the surface due to a mechanical vibration (in contrast to the marking which can result from geometrical effects such as those of a milling cutter).

Chatter in grinding is a serious problem. It adversely affects surface finish, dimensional accuracy, tool life and machine life. In addition, grinding chatter may cause high local heat sources due to variations in the depth of cut which can cause detrimental effects on the surface integrity.

Chatter can be separated into two categories: forced chatter and self excited chatter. Forced Chatter can result from unbalance of rotating members, drive train disturbances, bearings, impact of multi-tooth cutters and/or mounting disturbances. The violent vibration most often observed during metal removal processes is Self-Excited Chatter.

Many studies of machine tool chatter appear in the literature. This report, however, provides the most comprehensive approach to self-excited chatter in grinding proccesses at

the present time. It is an extension of work by Snoeys, and is a summary and reorganization of the work presented in the Interim Engineering Reports.

In Section V.2 the theory for self-excited chatter in grinding is developed. The development of this theory is carried out by postulating an appropriate model with a control systems approach. The equations describing the model are determined and requirements for dynamic stability of the grinding process are specified. The rate of growth of instabilities is also discussed.

In Section V.3 the parameters which are shown to be important from the theoretical analysis are discussed in terms of their effect on grinding process stability. In Section V.4 some important cases of instability which can occur in practice are discussed in a theoretical manner.

Section V.5 presents the results of experimental grinding chatter investigations, and conclusions are given in Section V.6.

V.2 Theory For Self Excited Chatter In Grinding.

V.2.1 Introduction

In this section a general theory is developed which can be used to describe self-excited vibrations. The approach is similar to the closed loop approach used by Cincinnati Milling in describing single point cutting. In fact, the current approach includes single point cutting as a special case.

This stability theory includes the regeneration of wave patterns on the workpiece and grinding wheel surfaces. The workpiece and grinding wheel contribute to mutual wear and/or stock removal and therefore it becomes a matter of convention to define the workpiece and grinding wheel, even though the nature of the mechanism of stock removal or wear is quite different. In other words, the roles of the wheel and workpiece should be interchangeable in the theoretical approach.

A second significant aspect which has to be included in the stability theory of the grinding operation is the role of the local deformation of wheel-work contact area. In single point cutting operations this is neglected because the local deformation is small compared to the depth of cut. In grinding, however, the deformation can be of the same order of magnitude as the depth of cut.

In introducing these two new aspects, a complete stability theory was developed which is suitable for describing chatter in grinding and yields an explanation and better understanding of practical chatter observations.

V.2.2 Basic Equations for the Grinding Operation

Figure V-1 shows two rotating bodies, w and s, in contact. Due to the cutting force F_c, the machine deforms an amount y_m and the contact area deflects an amount y_k.

The total elastic deformation at a given instant of time is

$$y_t(t) = y_m(t) + y_k(t) \qquad (V.2.1)$$

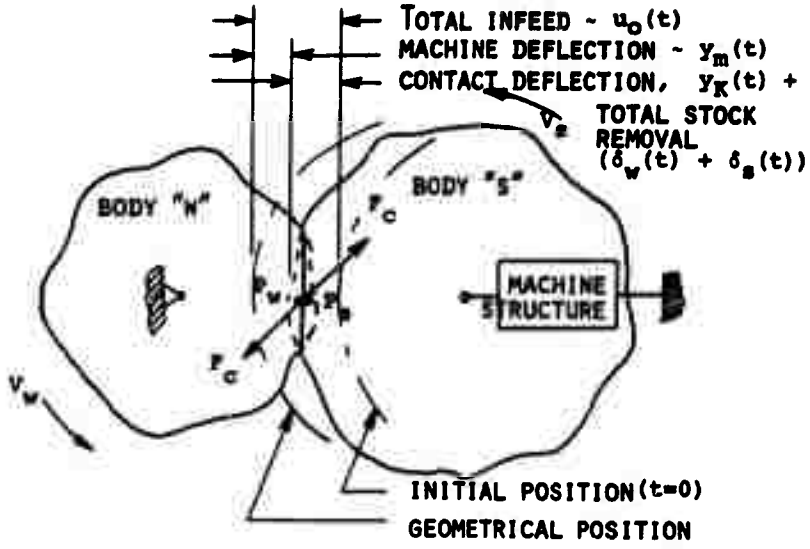

FIGURE V-1 - MODEL OF GRINDING PROCESS

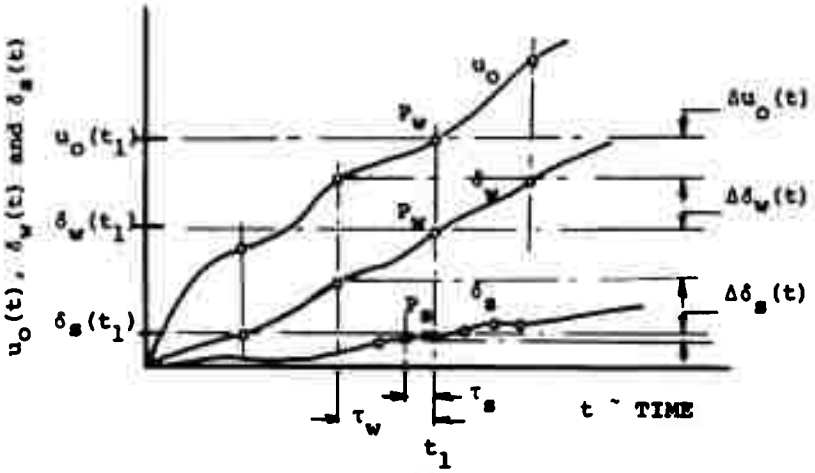

FIGURE V-2 - INFEED AND WEAR VERSUS TIME

The total infeed u_o can be some arbitrary function of time as shown in Figure V-2. The desired infeed Δu_o at the instant when point "P_w" is in contact with the body "s" is the increment of the total feed during the previous revolution of the body "w" or

$$\Delta u_o(t) = u_o(t) - u_o(t - \tau_w) \qquad (V.2.2)$$

which by Laplace transforming and rearranging yields

$$\frac{u_o(s)}{\Delta u_o(s)} = \frac{1}{1-e^{-\tau_w s}} \qquad (V.2.3)$$

Similar relations can be derived for the total wear of the body "w" and body "s":

$$\frac{\delta_w(s)}{\Delta\delta_w(s)} = \frac{1}{1-e^{-\tau_w s}} \qquad (v.2.4)$$

$$\frac{\delta_s(s)}{\Delta\delta_s(s)} = \frac{1}{1-e^{-\tau_s s}} \qquad (V.2.5)$$

From basic geometrical considerations at any instant of time, the sum of the total wear of bodies "w" and "s" must be equal to the total infeed minus the deformation of the contact area and machine (See Figure V-2). Therefore,

$$\delta_w(t) + \delta_s(t) = u_o(t) - y_k(t) - y_m(t) \qquad (V.2.6)$$

or in Laplace notation:

$$\delta_w(s) + \delta_s(s) = u_o(s) - y_k(s) - y_m(s) \qquad (V.2.7)$$

Combining the previous equations, the first basic equation for the grinding process is developed as follows:

$$\frac{\Delta\delta_w(s)}{1-e^{-\tau_w s}} + \frac{\Delta\delta_s(s)}{1-e^{-\tau_s s}} = \frac{\Delta u_o(s)}{1-e^{-\tau_w s}} - y_k(s) - y_m(s) \qquad \text{(V.2.8)}$$

A second set of basic equations concerning the cutting and wear process can be developed. It is assumed that the instantaneous depth of cut or wear amount is proportional to the cutting force as was assumed in the stability theory for single point operations, therefore:

$$F_c = k_s \Delta\delta_s = \text{(wear stiffness)(instantaneous wear)} \qquad \text{(V.2.9)}$$

$$F_c = k_w \Delta\delta_w = \text{(cutting stiffness)(instantaneous depth of cut)} \qquad \text{(V.2.10)}$$

The third set of basic equations relates cutting force to the machine dynamics and the contact area stiffness:

$$\frac{y_m(s)}{F_c(s)} = \frac{1}{k_m} G_m(s) \qquad \text{(V.2.11)}$$

$$\frac{y_k(s)}{F_c(s)} = \frac{1}{K} \qquad \text{(V.2.12)}$$

In Equations V.2.9, V.2.10, and V.2.12 the parameters k_s, k_w, and K may not be constant and could be frequency dependent. However, in order to simplify the instability consideration, they are assumed to be constant.

For steady state conditions, a linear relation has been measured between the stock removal, the rate of wheel wear and the cutting force intensity. This is illustrated by some results derived from Hahn's work and is shown in Figure V-3. Therefore the linear assumption for the wear and stock removal appears to be reasonable.

The contact stiffness K is not constant because the relation between force and contact area deformation is non-linear. However for small disturbances the local stiffness value can be utilized since the border-line of stability is the important consideration.

The basic transfer function of the grinding operation can be determined from the previous basic equations. It is the ratio of the instantaneous depth of cut to the instantaneous infeed: (*)

$$\frac{\Delta\delta_w(s)}{\Delta u_o(s)} = \frac{1}{[1 + \frac{k_w}{k_s}\frac{1-e^{-\tau_w s}}{1-e^{-\tau_s s}}] + (1-e^{-\tau_w s})[\frac{1}{K} + \frac{1}{K_m} G_m(s)]k_w} \qquad (V.2.13)$$

The interrelation between the basic equations can be illustrated by means of a block diagram (Figure V-4). The role of the grinding wheel and workpiece are interchangeable.

(*) For single point cutting, the contact deformation can be neglected, ($K \to \infty$) and the "wear stiffness" of the tool is assumed to be infinite ($k_s \to \infty$). Applying these to Equation V.2.13, the corresponding equations for single point cutting can be obtained.

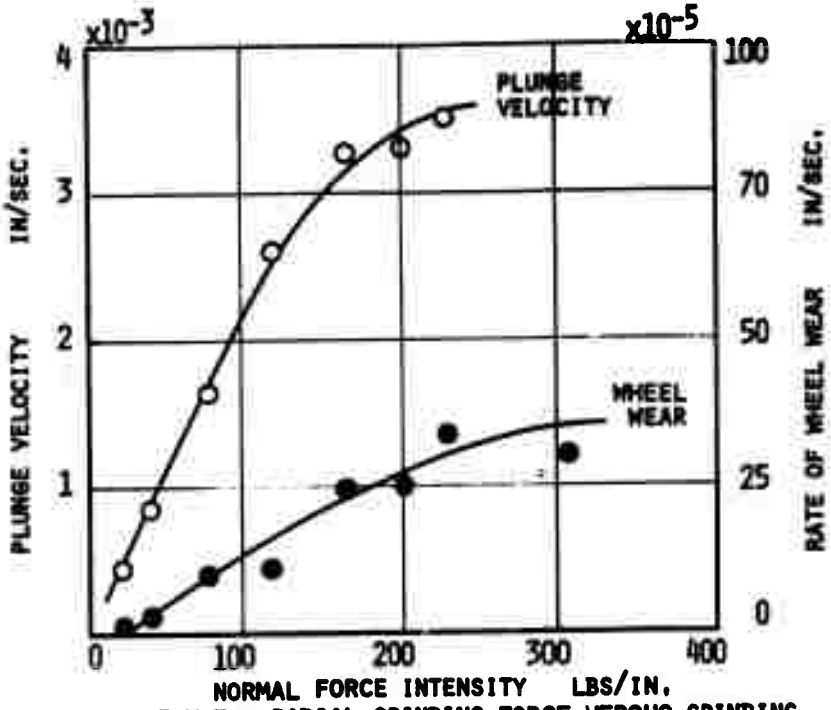

FIGURE V-3 - RADIAL GRINDING FORCE VERSUS GRINDING WHEEL WEAR AND STOCK REMOVAL

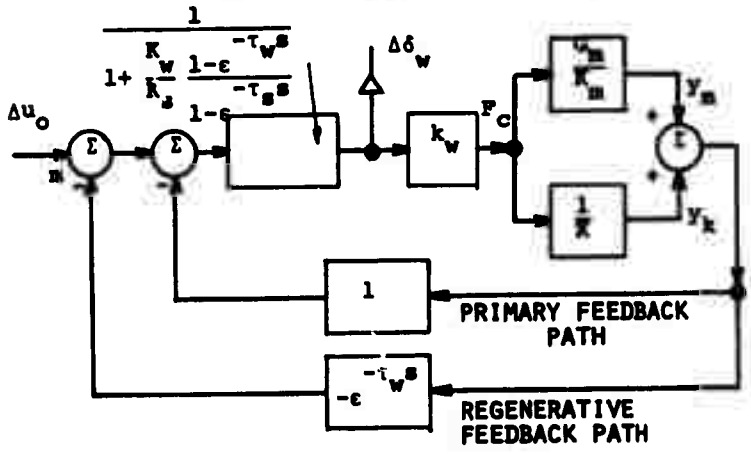

FIGURE V-4 - CLOSED LOOP REPRESENTATION OF PLUNGE GRINDING OPERATION

A similar diagram can thus be obtained by a mutual change of the indices w and s. Figure V-4 indicates the mathematical aspects of the problems. In order to develop a better physical understanding of the process, an analog model of the process is indicated in the Block Diagram of Figure V-5. This block diagram also indicates the fact that the process can be simulated using an analog computer if a time simulation is desired. For studing various methods of stabilization an analog simulation can be very useful.

The physical meaning of the block diagram shown in Figure V-5 can be very easily seen. The total infeed amount u_o causes a deformation of the contact area y_k and a contact force F_c builds up. This force will deflect the machine structure y_m and cause an instantaneous wear of the wheel $\Delta\delta_s$ and an instantaneous depth of cut $\Delta\delta_w$. The instantaneous depth of cut and wear must be subtracted from the form of the wheel and workpiece, which existed one revolution before. This in turn leads to the total wear of the wheel and workpiece which along with the deflection of the machine is subtracted from the total infeed of the machine yielding the deformation of the contact area, thereby closing the loop.

One of the basic assumptions implied in the formulation of the problem at this point is that a straight-in plunge cut is taken. If a traverse cut is taken, then the full effect of the regeneration is not realized. To account for this effect an overlap parameter is included in the analysis.

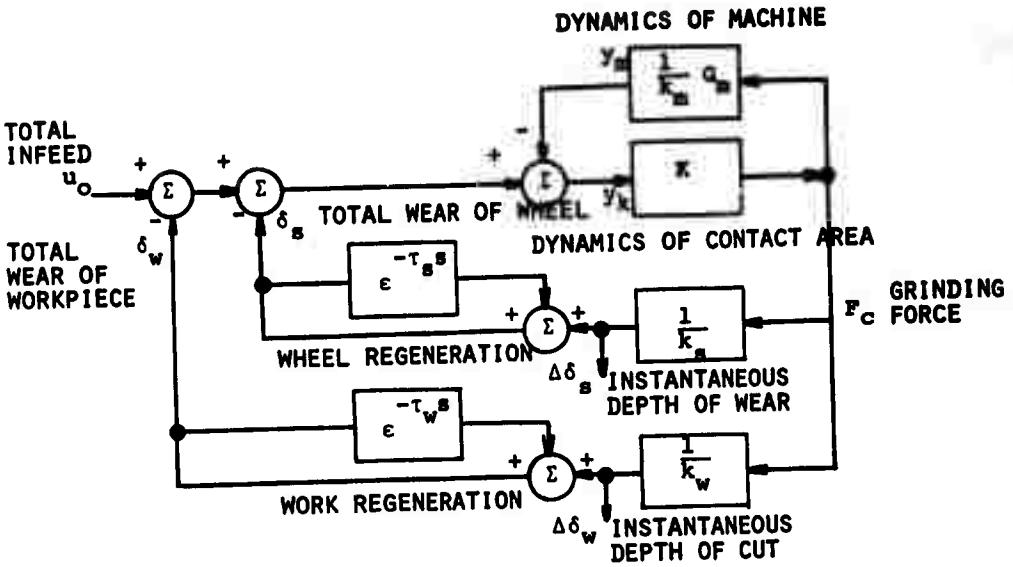

FIGURE V-5 - CLOSED LOOP REPRESENTATION OF GRINDING OPERATION

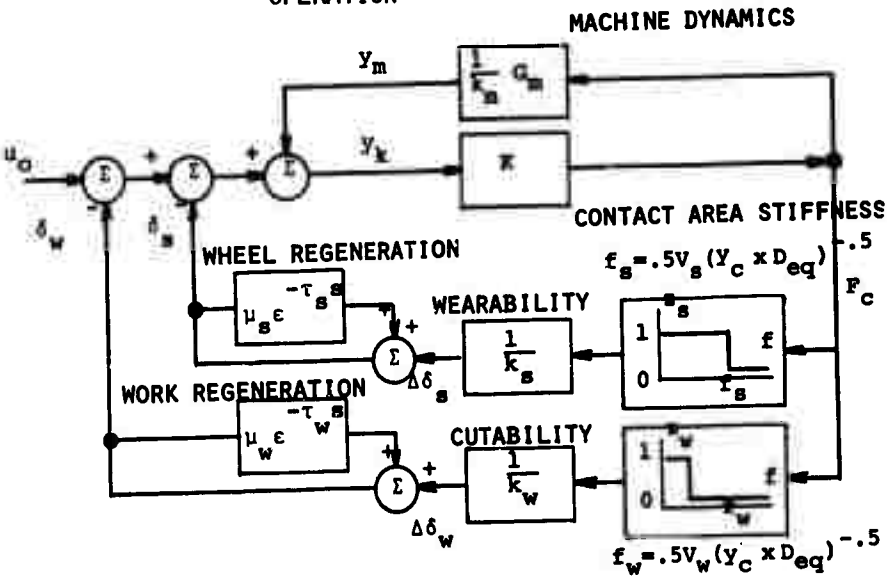

FIGURE V-6 - COMPLETED CLOSED LOOP REPRESENTATION OF GRINDING OPERATION

The overlap factor accounts for the overlapping of successive cuts, i.e. it defines the proportion of the previous cut which overlaps the present cut during traverse grinding. If this effect is included, the transfer-function for the grinding system becomes:

$$\frac{\Delta\delta_w(s)}{\Delta u_o(s)} = \frac{1}{[1 + \frac{k_w}{k_s}\frac{1-\mu_w e^{-\tau_w s}}{1-\mu_s e^{-\tau_s s}}] + (1-\mu_w e^{-\tau_w s})[\frac{1}{K} + \frac{1}{k_m} G_m(s)]k_w} \qquad (V.2.14)$$

where μ_w and μ_s are the overlap factors for the workpiece and grinding wheel respectively.

The overlap factor basically behaves as a filtering effect where the regeneration effect is increasingly filtered out as the overlap factor approaches zero. Another type of filtering effect is also possible. This is due to geometrical filtering occuring when the wave length of the chatter pattern approaches the length of contact between the grinding wheel and workpiece. When this occurs, the wave pattern can no longer be produced upon the surface of the body (workpiece and/or wheel). This effect was described in great detail in Section II.3.3 of the fourth Engineering Report and Section II.4.2 of the fifth Engineering Report and will be discussed more fully later in this report. The equation for the transfer function can be expanded to included this effect by introducing filter elements $Z_s(s)$ and $Z_w(s)$ into Equation V.2.14 as follows:

$$\frac{\Delta\delta_w(s)}{\Delta u_o(s)} =$$

$$\frac{1}{\left[1 + \frac{k_w Z_s(s)(1-\mu_w e^{-\tau_w s})}{k_s Z_w(s)(1-\mu_s e^{-\tau_s s})}\right] + (1-\mu_w e^{-\tau_w s})\left[\frac{1}{K} + \frac{1}{k_m} G_m(s)\right]\frac{k_w}{Z_w(s)}}$$

(V.2.15)

The effect of the filtering elements is made clear in the block diagram indicated in Figure V-6. The filtering effect is very important for many practical grinding cases.

Another important effect which has not been included in the analysis is the effect of wheel loading. This can be a very important consideration when grinding HSTRA material, especially the nickel base alloys (Rene'41, Waspaloy, etc.) The effect of loading on the feedback loop analysis of grinding will be discussed in Section V.4. The introduction of loading into the basic equation results in a time-varying coefficient which complicates the analysis. Therefore, for simplicity this effect is not included in this section.

V.2.3 Stability Requirements

A linear system is defined to be stable if its impulse response decays with time. This definition of stability can be translated into the following mathematical requirements: A linear lumped parameter system is stable if and only if all roots of its characteristic equation have negative real parts. If any or all of the roots have positive real parts,

then the system is unstable. If any of the roots have zero real parts, and if the remaining roots have negative real parts, the imaginary roots represent the *borderline* of stability and solutions of the characteristic equation are harmonic, (no increase or decrease of amplitude with time).

The characteristic equation of the system can be obtained directly from the transfer function, $\frac{\Delta\delta_w(s)}{\Delta u_o(s)}$, given in Equation V.2.15 and can be rearranged in the following form:

CHARACTERISTIC EQUATION

$$\frac{1}{k_w}\frac{Z_w(s)}{(1-\mu_w e^{-\tau_w s})} + \frac{1}{k_s}\frac{Z_s(s)}{(1-\mu_s e^{-\tau_s s})} + \left[\frac{1}{K} + \frac{G_m(s)}{k_m}\right] = 0 \qquad (V.2.16)$$

The general time solution of the above equation would be:

$$\Delta\delta_w(t) = \Delta u(t)\left[A_1 e^{s_1 t} + A_w e^{s_2 t} \ldots A_n e^{s_n t}\right] \qquad (V.2.17)$$

where

S_i = The complex roots of the characteristic equation.

A_i = Arbitrary constant determined by the initial conditions.

In the case of the border-limit of stability, the roots have no real parts consequently the roots are equal to $(j\omega_i)$ or purely imaginary, thus the following stability equation can be obtained:

$$\frac{1}{k_w}\frac{Z_w(j\omega)}{[1-\mu_w e^{-\tau_w(j\omega)}]} + \frac{1}{k_s}\frac{Z_s(j\omega)}{(1-\mu_s e^{-\tau_s(j\omega)})} + \left[\frac{1}{K} + \frac{1}{k_m}G_m(j\omega)\right] = 0 \qquad (V.2.18)$$

The term $G_m(j\omega)$ in the above equation is the normalized directional frequency response parameter of the grinding machine, where the displacement y_m is taken in the cutting depth direction and is due to a force acting in the cutting force direction. In general this is a complex relation. Furthermore, there are an infinite number of roots to the characteristic equation, therefore an analytic solution is impractical. For this reason a graphical procedure, similar to that used for single point cutting, will be utilized in determining the roots of Equation V.2.18. By assuming that the wear and deformation of the tool and the filtering effect of the contact zone can be neglected, the grinding system reduces to the single point cutting case:

CHARACTERISTIC EQUATION SINGLE POINT CUTTING

$$\frac{1}{k_w(1-\mu_w e^{-\tau_w s})} + \frac{1}{k_m} G_m(s) = 0 \qquad \text{(V.2.19)}$$

For single point cutting, a graphical solution was developed by H. Merritt which utilized a phase-gain plot of the machine in conjunction with the "Merritt Chart" to obtain a graphical solution to Equation V.2.19. For the grinding case, a similar type graphical solution was employed to solve Equation V.2.18. In this case a polar plot was more useful than a phase-gain plot.

Equation V.2.18 is rearranged in the following manner:

$$- \frac{k_m}{k_w} \frac{Z_w(j\omega)}{[1-\mu_w e^{-\tau_w(j\omega)}]} - \frac{k_m(j\omega)}{k_s(1-\mu_s e^{-\tau_s(j\omega)})} + \frac{k_m}{K} = G_m(j\omega) \qquad (V.2.20)$$

If the overlap factors μ_w, μ_s are equal to one (plunge grinding), the left side of Equation V.2.20 plots into a straight line parallel to the imaginary axis. The real and imaginary parts of the straight line are:

Real Part

$$- \frac{1}{2} \frac{Z_w k_m}{k_w} - \frac{1}{2} \frac{Z_s k_m}{k_s} - \frac{k_m}{K} = Re_\ell \qquad (V.2.21)$$

Imaginary Part

$$\frac{Z_w k_m}{k_w} \left[\frac{\sin \omega \tau_w}{2-2 \cos \omega \tau_w}\right] + \frac{Z_s k_m}{k_s} \left[\frac{\sin \omega \tau_s}{2-2 \cos \omega \tau_w}\right] = Im_\ell \qquad (V.2.22)$$

By letting $\omega\tau_{w;s} = 2 (n_{n;s} + \nu_{n;s})$ and noting for integer values of n that $\sin 2\pi(n+\nu) = \sin 2\pi\nu$; and likewise $\cos 2\pi(n+\nu) = \cos 2\pi\nu$; and also by using the series approximation for the sine and cosine terms, the expression for the imaginary part can be reduced to the following:

$$\frac{Z_w k_m}{2\pi k_w \nu_w} + \frac{Z_s k_m}{2\pi k_s \nu_s} = Im_\ell \qquad (V.2.23)$$

An intersection between the plot of the machine frequency response $G_m(j\omega)$ and the straight line corresponds to a solution

of Equation V.2.19 and represents a point on the border-limit of stability. If no intersection occurs, then the process is stable. The graphical procedure is indicated in Figure V-7 for a single degree of freedom system. The criteria for stability is that

$$Re_{\ell} < (Re_m)_{min} \qquad (V.2.24)$$

Where Re_{ℓ} = real part of line

$(Re_m)_{min}$ = minimum real part of machine normalized frequency response, $G_m(j\omega)$

or

$$-\frac{1}{2}\frac{Z_w k_m}{k_w} - \frac{1}{2}\frac{Z_s k_m}{k_s} - \frac{k_m}{K} < (Re_m)_{min} \qquad (V.2.25)$$

The asympotic stability requirement is defined as the condition $Re_{\ell} = (Re_m)_{min}$.

V.2.4 Border-Limit of Stability Diagram

In this subsection the procedure for obtaining a stability diagram which determines the stability characteristics of a grinding process is described.

In the previous section criteria for stability were obtained and illustrated in a polar plot of $G_m(j\omega)$, determined from the measured machine frequency response, and the real part of the right side of Equation V.2.20.

The example to be illustrated is the case where workpiece regeneration is filtered out by the contact zone; that is, $Z_w = 0$ (low workspeed case). It is also assumed that $Z_s = 1$.

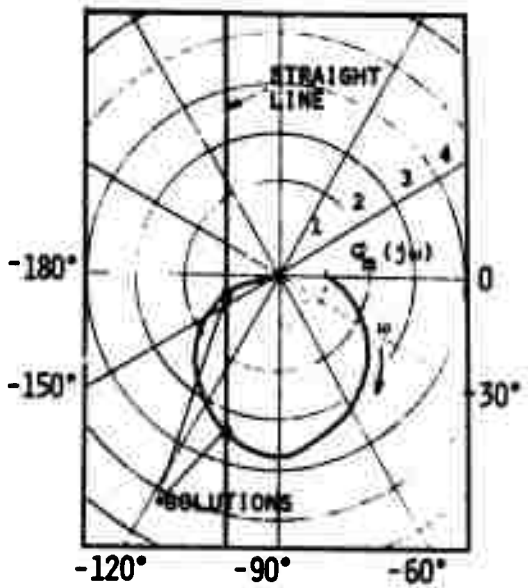

FIGURE V-7 - GRAPHICAL DETERMINATION OF THE BORDERLINE OF STABILITY

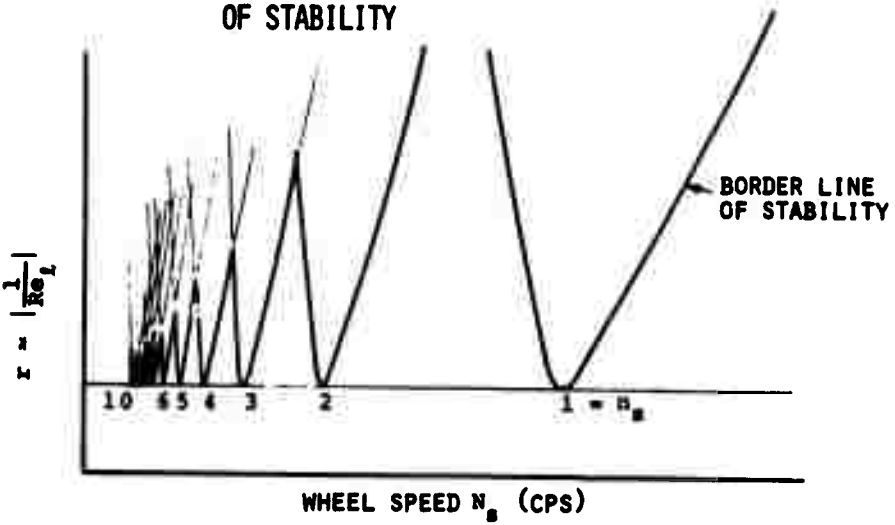

FIGURE V-8 - STABILITY DIAGRAM FOR SYSTEM INDICATED IN FIG. V-7

From Equation V.2.21 the effective "gain" of the system, r, is determined as

$$r = \left| \frac{1}{Re_f} \right| = \left| \frac{1}{\left(-\frac{1}{2}\frac{k_m}{k_s} - \frac{k_m}{K}\right)} \right| \qquad \text{(V.2.26)}$$

The stability diagram desired is a plot of r versus wheel speed N_s cycles per second, where N_s is related to the time delay τ_s by

$$N_s = \frac{1}{\tau_s} = \frac{\omega}{2\pi(n_s + \nu_s)} \qquad \text{(V.2.27)}$$

From the polar plot, Figure V-7, a particular intersection of a line with G_m defines two values of ω, and ν_s is determined either from the polar plot or by

$$\nu_s = \frac{k_m}{2\pi k_s Im_f} \quad \text{(from Equation V.2.23)} \qquad \text{(V.2.28)}$$

With the known values of ω and ν_s for a particular intersection, n_s is determined by Equation V.2.27 for integer values of n_s ranging from 0 to ∞.

The plot of $r = \left|\frac{1}{Re_f}\right|$ versus N_s is thus determined, and shown in Figure V-8. The border line of stability is indicated by the heavy line. If the grinding conditions correspond to a point "P" which is located above the border-limit of stability line, the process is unstable. If it falls above the lines which define each wave pattern, it is unstable for those patterns. For the example of Figure V-8, wave patterns with n_s = 5 and 6 are unstable.

The physical significance of n_s is that it corresponds to the number of waves which develop around the circumference

of the grinding wheel, likewise n_w indicates the number on the workpiece. In the case under examination, the actual wave form which would develop on the circumference of the grinding wheel is the summation of wave patterns with 5 and 6 cycles per circumference. The exact ratio of the *amplitude* of these patterns is not predicted.

The parameter ν_s used in calculating N_s has a very important physical significance. This parameter corresponds to the phase angle between wave patterns on successive revolutions of the grinding wheel. In other words the wave pattern moves on the circumference of the wheel at a rate which can be determined by this parameter. This parameter is also a measure of the growth rate of the wave pattern. The larger its value the greater the rate of growth. This will be discussed in greater detail in the next section.

It is very difficult to construct a complete stability diagram for the case where both wheel and workpiece regeneration are possible (i.e. $Z_w \neq 0$, $Z_s \neq 0$). The reason for the difficulty is that the stability diagram becomes a surface instead of a curve where the three ordinates are the reciprocals of the real part, $1/Re_\ell$; the wheel speed, N_s; and the workspeed, N_w. The procedure for describing this surface requires the simultaneous solution of seven equations, four of which are non-linear. Fortunately, with the following conditions:

$$\frac{k_m}{k_w Im_m} < 2\pi n_s \text{ or } 2\pi n_w$$

and $$\frac{k_m}{k_s Im_m} < 2\pi n_s \text{ or } 2\pi n_w$$

A reasonable estimate can be obtained by simply treating both the wheel and workpiece independently and constructing separate stability diagram

$$\frac{1}{Re_t} \text{ vs. } N_s$$

and $$\frac{1}{Re_t} \text{ vs. } N_w$$

From these diagrams particular values of the number of waves on the wheel (n_s) and workpiece (n_w) would be predicted for specified grinding conditions. The wave numbers that would exist in actuality would be only those that satisfy

$$n_s N_s \approx n_w N_w \qquad (V.2.29)$$

somewhat analogous to the meshing of gears.

V.2.5 Rate of Growth of Grinding Instablities.

In this section the analysis will be extended to consider the rate of growth of the grinding instablities for the unstable case.

For the case with only wheel regeneration, it is possible to grind under unstable conditions for extended periods of time before the amplitude of vibration becomes objectionable.

This is a fortunate circumstance since many practical grinding conditions are of this type. The stability requirement for the case of wheel regeneration is more severe than for the case with workpiece regeneration.

There are two common procedures which can be used to estimate the degree of instability in a feedback loop. The first is the root locus procedure in which the roots of the characteristic equation are determined. The second method is the construction of a Nyquist Plot from which the relative stability can be roughly estimated from the gain and phase margins. Unfortunately, due to the time delays in the feedback loop, both of these procedures are impractical since the characteristic equation has an infinite number of roots.

Instead of using these more standard procedures, a method similar to the method utilized in determining the limit of stability was employed.

This procedure is based on the assumption of roots of the form $S_i = x_i + jy_i$ instead of the form $S_i = j\omega_i$ assumed in the stability analysis (Section V.2.3). If roots of the form $S_i = x_i + jy_i$ are assumed, then the characteristic equation for the wheel regeneration case becomes:

$$-\frac{k_m}{k_s(1-e^{-\tau_s(x+jy)})} - \frac{k_m}{K} = G_m(x+jy) \qquad \text{(V.2.30)}$$

The same graphical procedure will be used to solve Equation V.2.30 as was utilized in solving the Equation V.2.20 for the border-limit of stability.

The left and the right hand side of Equation V.2.30 will be plotted separately in a polar plot and the intersection of the two curves will correspond to solution of Equation V.2.30. Due to the slow rate of growth of the instability, the value of x can be assumed very small. Therefore the right hand side of the equation reduces to the normalized frequency response of the machine $G_m(jy)$. The left hand side of the euqation plots into a straight line segment. (See Figure V-9) This was shown very clearly in the Sixth Interim Engineering Report

For x equal to zero, the right hand side of the equation plots into a line segment of infinite length as was indicated in the border limit of stability studies presented in Section V.2.3.

For the value of x not equal to zero, the line is of finite length and there are limiting intersection points (See Figure V-10) of the straight line segment with the plot of $G_m(jy)$. A limiting value is determined by the condition that the length of the line segment is equal to the imaginary component of $G_m(jy)$. For values less than this, no intersection will occur. Physically this limiting case corresponds to a maximum value of x that can occur under those conditions. The length of the line segment can be given by the following relationship.

$$I_{max} = \pm \frac{1}{4\pi} \frac{k_m}{k_s} \frac{y}{n_s x_c} \qquad (V.2.31)$$

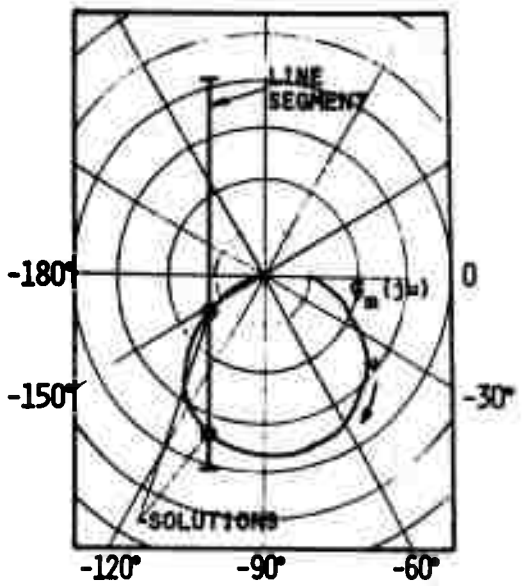

FIGURE V-9 - STABILITY RATE CONSTRUCTION METHOD

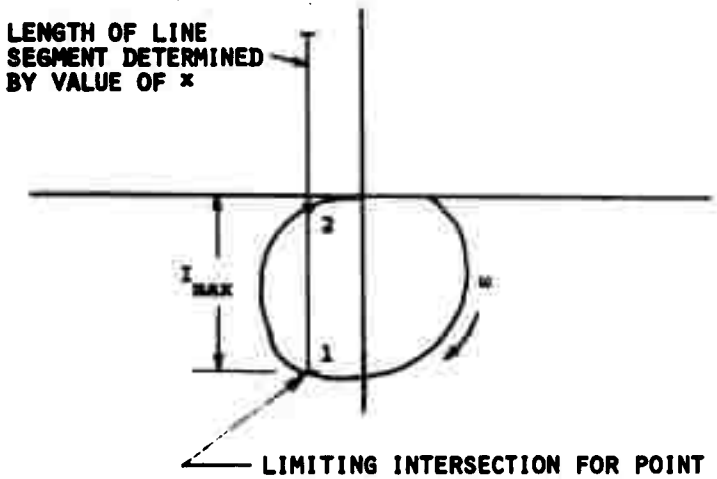

FIGURE V-10 - LIMITING INTERSECTION CONDITION

Where y corresponds to the frequency taken at the intersection point of the frequency response plot of the machine.

I_{max} = maximum length of the line segment.

x_c = critical value of x.

Therefore the maximum length of the line is then a function of the ratio of the machine static stiffness k_m, to the wheel wear stiffness, k_s; the number of waves on the grinding wheel circumference n_s, the frequency of the oscillation y, and the critical rate of growth of the oscillation x_c.

A stability diagram can be constructed which is very similar to the diagram constructed for the border limit of stability diagram. In fact, for x = 0 it reduces to the border limit of stability plot.

The plot is constructed by plotting the reciprocal of the real part of the straight line segment versus the wheel speed which can be determined from the frequency of oscillation, y (rad/sec), by the following relation:

$$N_s = \frac{1}{\tau_s} = \frac{y}{2\pi(n_s+\nu_s)} \approx \frac{y}{2\pi n_s} = \frac{f}{n_s} \quad (*) \qquad (V.2.32)$$

where f = frequency of oscillation - cycles/sec.

(*) In general the value of ν_s is very small for the wheel regeneration case and can be neglected with respect to n_s.

Also from the imaginary part of the machine frequency response curve the critical value x_c can be determined from Equation IV.2.31 by solving for x as follows:

$$x_c = +\frac{1}{4\pi}\ \frac{k_m}{k_s}\ \frac{y}{n_s I_{max}} \qquad (V.2.33)$$

where I_{max} equals imaginary part of the machine transfer function $G_m(jy)$ at the intersection point.

This critical value of x corresponds to the maximum value of x where the intersection between the straight line segment and the frequency response plot is still possible. By varying the location of the line segment along the negative real axis, a locus of points can be generated in the stability plot. One loop of this diagram is shown in Figure V-11, for $n_s = 1$. The critical value of x is indicated along the stability curve. The degree of instability can be estimated by dropping a vertical line down from the point which describes the grinding conditions to the stability line. The value of x at this point on the stability line is a measure of rate of growth of instability.

In Figure V-12 the stability diagram is shown for the first eight waves (n_s = 1 to 8). The limit of stability is indicated and lines which correspond to various values of x (rate of growth parameter) are drawn on the plot to indicate how the stability changes with the number of waves (n).

There are a number of ways of presenting the stability data. One method would be as shown in Figure V-11 where the degree of instability could be obtained by dropping a

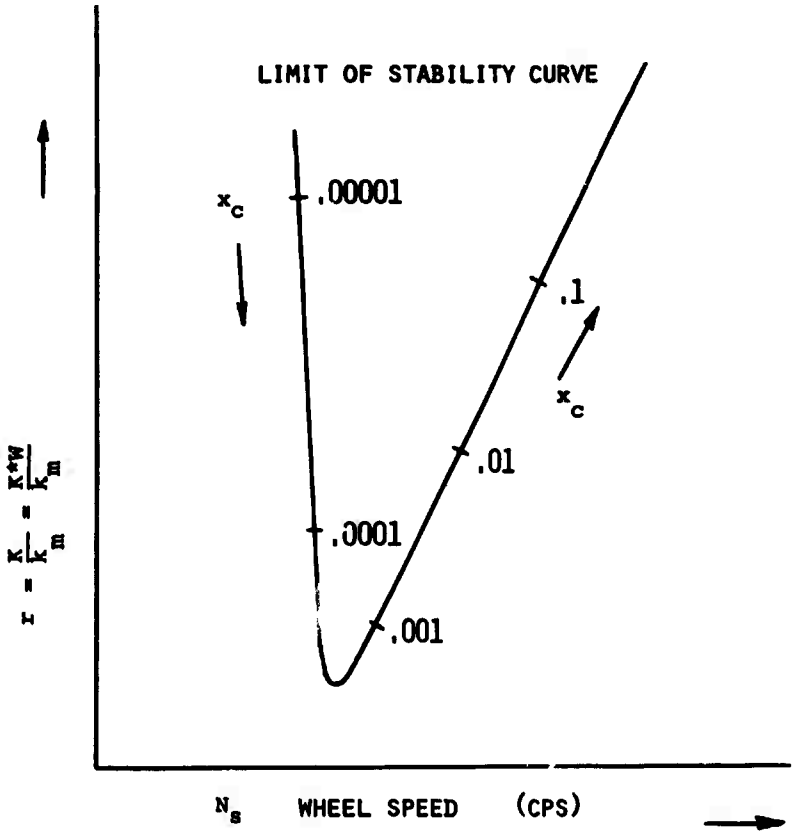

FIGURE V-11 - TYPICAL LOOP OF STABILITY RATE DIAGRAM

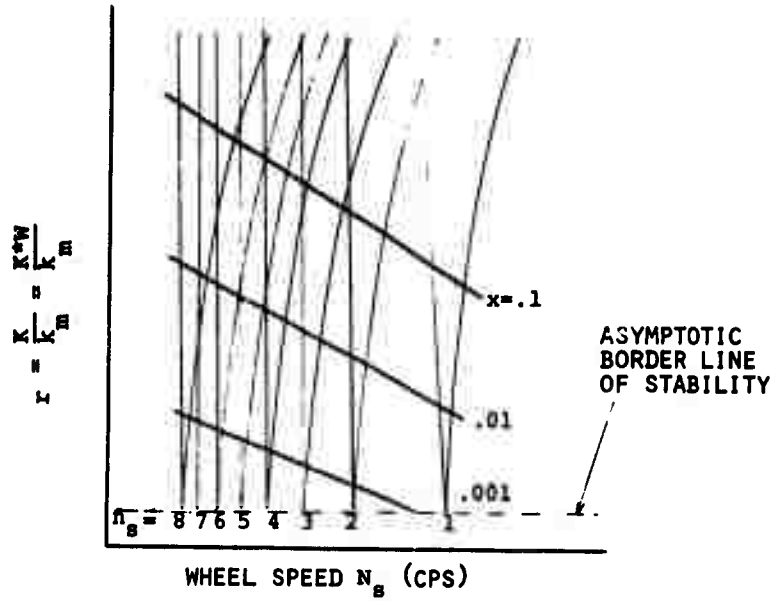

FIGURE V-12 - STABILITY DIAGRAM SHOWING CHANGE OF x WITH N_s

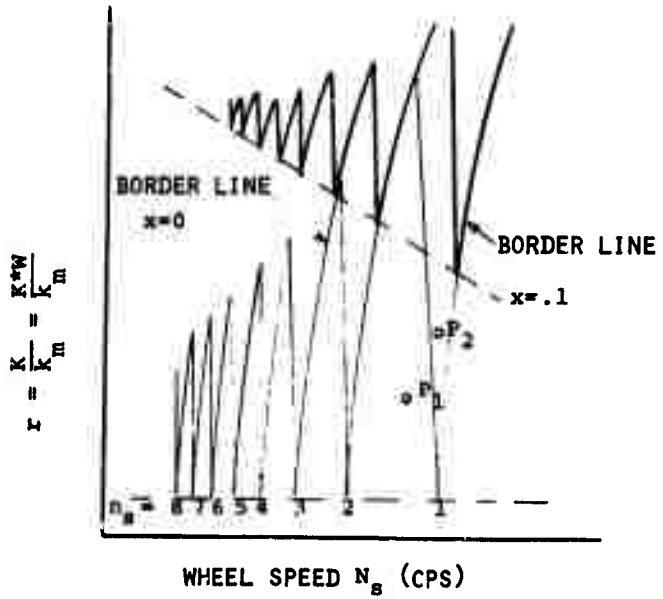

FIGURE V-13 - SECOND PROCEDURE FOR PRESENTING STABILITY RATE DIAGRAM

vertical line down from the operating point to the stability line. A second procedure would be to construct a diagram where the limiting line would be shown for various values of x. See Figure V-12 for an example. In Figure V-13 the limiting line is shown for x = 0 and x = .1. If the operating point lies below the x = 0 curve, the process is stable as indicated by point P_1. If the point lies between the two curves such as point P_2, the process is unstable and the instability grows at a rate less than x = .1. If the point lies above both lines the instability has a rate of growth greater than x = .1. The rate of growth of each wave (n_s = 0 to 8) can be estimated from this chart.

V.3 Discussion of Important Parameters.

V.3.1 Introduction

In this section the various important parameters which appeared in the stability analysis are described.

V.3.2 Machine Structure: $\frac{G_m(j\omega)}{k_m}$

The machine structure is an important factor in the stability consideration of the grinding process. The machine structure is described by the machine directional frequency response $\frac{G_m(j\omega)}{k_m}$.

It is obvious from Section V.2.3 on the stability requirements that in order not to have an intersection of the straight line segment with $G_m(j\omega)$, the machine must have a high static stiffness k_m and a small negative real

part of $G_m(j\omega)$, which implies high dynamic stiffness. Therefore high static and dynamic stiffnesses are requirements for stable operation. Thus, the machine structure is very important in the stability consideration.

V.3.3 Cutting Stiffness : k_w

The cutting stiffness, k_w, is a measure of the resistance to cutting of the workpiece and depends upon many different parameters such as the workpiece material, dressing conditions of the grinding wheel, the composition of the grinding wheel, and relative cutting speed between the cutting edge and workpiece. It is presently impossible to theoretically predict the influence of these various conditions upon the cutting stiffness. The importance of the chip formation physics studies upon the understanding of cutting stiffness is therefore clear. The ultimate goal of the basic chip formation investigations is to develop relationships between stock removal and various grinding parameters, one of which is the grinding force. At the present time it is necessary to measure k_w experimentally.

The effect of the cutting stiffness on the stability of the grinding process can be ascertained from Equation V.2.25.

$$-\frac{1}{2}\frac{Z_w k_m}{k_w} - \frac{1}{2}\frac{Z_s k_m}{k_s} - \frac{k_m}{K} < (Re_m)_{min}$$

where $(Re_m)_{min}$ is the minimum value of the real part of $G_m(jw)$. If this inequality is satisfied, the grinding process is stable. It is obvious that the larger the value of k_w the

less likely it is for the process to be stable. Large values of k_w indicate hard to grind materials and it is common knowledge that the chatter problem increases for hard to grind materials.

One example of the manner in which k_w depends on grinding conditions is discussed here.

The cutting stiffness was previously defined as

$$k_w = \frac{F_c}{\Delta\delta_w} \qquad \text{(V.3.1)}$$

The cutting stiffness is directly proportional to the width of cut w

$$k_w = k_w^* \; w \qquad \text{(V.3.2}$$

It is generally recognized that for a *constant stock removal rate,* the grinding forces are independent of the workspeed V_w in a broad speed range. The actual depth of cut, however, changes inversely with the workspeed, and the cutting stiffness is directly proportional to the workspeed. It has also been found that grinding forces decrease as grinding wheel speeds increase. This also means that the cutting stiffness is a function of the wheel speed. This situation of interdependence is quite different as compared to single tool cutting operations where the cutting stiffness may be considered constant in a broad cutting speed range.

In the range of common grinding practice ($K_v < .1$) the cutting stiffness is found to be a linear function of the speed ratio $K_v = V_w/V_s$:

$$k_w^* = k_c K_v \qquad (V.3.3)$$

or

$$k_w = w k_c K_v \qquad (V.3.4)$$

where k_c is a cutability coefficient depending on the work material characteristics, the composition of the grinding wheel, and the dressing conditions.

V.3.4 Wear Stiffness: k_s

The wear stiffness k_s, like the cutting stiffness, depends on many different grinding parameters and conditions. The wear stiffness is very important in determining the limit of stability and also the rate of growth of the grinding instabilities for the wheel regeneration case. (See Equation V.2.25 and V.2.33). The larger the value of k_s the less likely the process will be stable, as seen from Equation V.2.25.

However, the rate of growth of instability is smaller with large values of k_s (Equation V.2.33).

It is necessary to measure k_s experimentally for a particular grinding case since it is impossible to theoretically predict. This indicates a major problem. Before the stability theory can be applied, it is necessary to measure values of k_w and k_s for a particular grinding case. In the single point cutting theory it was necessary to determine k_c, the cutting stiffness of the work material, as a function of the work material and tool geometry. This was done experimentally and tabulated. This same sort of procedure must be done for grinding. The grinding case, however, is more difficult

since there are many more grinding parameters which affect k_s and k_w. This indicates the importance of developing a clear understanding of the cutting mechanism. The cutting mechanism is not only important in the analysis of the surface integrity of the workpiece, but it is also very important in dynamic considerations.

V.3.5 Contact Stiffness : K

The contact stiffness relates deformation in the contact area to the cutting force,

$$F_c = K\, y_k$$

where y_k includes both work and wheel deformation, although in most cases it is expected that the wheel deformation is much greater than that of the workpiece.

In the theory it has been assumed that K is constant. Actually K is a function of the grinding force.

Therefore the value of the contact stiffness used in the theory should correspond to the grinding force for the grinding conditions being investigated. This value should give a good estimate of the border-line of stability and should also give a reasonably good estimate of the chatter frequencies at the on-set of chatter. As the chatter amplitude builds, the effective contact stiffness will decrease resulting in a change in the chatter frequency. This result is very important in exploring the evalution of grinding chatter. This will be discussed in the section on the experimental studies.

The effects of the contact stiffness upon the grinding stability can be obtained from Equation V.2.25. For smaller values of K the grinding process is more stable.

V.3.6 Width of Cut w

Since the cutting force is proportional to the width of cut being taken, it is advisable to consider previously mentioned stiffnesses k_w, k_s, and K in terms of unit width.

The stability requirement, Equation V.2.25 is rewritten as

$$[-\frac{1}{2}\frac{Z_w k_m}{k^*_w} - \frac{1}{2}\frac{Z_s k_m}{k^*_s} - \frac{k_m}{K^*}] < w\,(Re_m)_{min} \quad (V.3.5)$$

(I) (II) (III) (IV)

where $k^*_w = \frac{k_w}{w}$, $k^*_s = \frac{k_s}{w}$, $K^* = \frac{K}{w}$.

The width of cut is one parameter which can be varied in order to increase stability. Decreasing w increases the likelihood that the process is stable.

V.3.7 Relative Importance of Terms in Stability Requirement.

Typical ranges of values of the terms in Equation V.3.5 are tabulated below:

$$-10^3 < I < -10^{-1}$$
$$-1 < II < -10^{-5}$$
$$-10^3 < III < -10^{-2}$$
$$-10^2 w < IV < -w$$

Terms I and III are generally of greater magnitude (large negative number) than term II. It is therefore concluded that the cutting stiffness k_w and contact stiffness K

have a more significant influence on stability than the wear stiffness k_s. However, the wear stiffness is important in determining the rate of growth of instability.

V.4 Important Cases of Instability

V.4.1 Introduction

In order to decide whether or not a particular type of instability is likely to be encountered, it is necessary first to consider the mechanism by which wave patterns can be filtered out.

V.4.2 Filtering Mechanisms

There are two different types of geometrical filtering elements which can prevent or eliminate wave patterns generated by unstable grinding conditions. The first type is due to the overlap factors μ_w and μ_s, resulting from the traverse feed of the workpiece with respect to the grinding wheel. In most cases this type of filtering element is limited to the workpiece since the grinding wheel is normally in contact at all times. The exception would be in the case of centerless grinding where the workpiece traverses across the grinding wheel. If the overlap factor is equal to zero then regeneration is not possible and the process is in general greatly stabilized. If μ_w equals zero in Equation V.2.20, and $\mu_s = 1$ then the stability requirement is given by

$$\underset{(I)}{-\frac{Z_w k_m}{K_w}} \underset{(II)}{-\frac{1}{2}\frac{Z_s k_m}{K_s}} \underset{(III)}{-\frac{k_m}{K}} \underset{(IV)}{<} (Re_m)_{min} \qquad (V.4.1)$$

rather than Equation V.2.25, obtained for the case of μ_w = μ_s = 1. The first term, involving cutting stiffness, is thus greater in magnitude for the case of μ_w = 0 than for the case of μ_w = 1. Consequently, the process is more likely to be stable if μ_w = 0. Since it was previously shown that first term is generally much greater than the second term, the case when μ_s = 0 is not expected to greatly affect the limit of stability.

The second type of filtering element is due to the geometrical length of the contact zone. If this length is greater than the wave pattern generated on the surface of the workpiece or the grinding wheel, the pattern will be filtered. This is illustrated by Figure V-14, shown for the case of wave generation on the workpiece. A similar situation would occur with wheel regeneration. This results in the wheel or workpiece term being dropped completely from the stability requirements. In other words either the value of Z_s or Z_w becomes zero in Equation V.2.25. The contact length filtering element has been studied in great detail and a complete analysis is presented in the fourth and fifth Interim Engineering Reports.

The values of Z_w and Z_s are functions of the workpiece and wheel speed and the chatter frequency.

The break frequency of the filtering element is given by (See Section II.4.2 of the fifth Engineering Report).

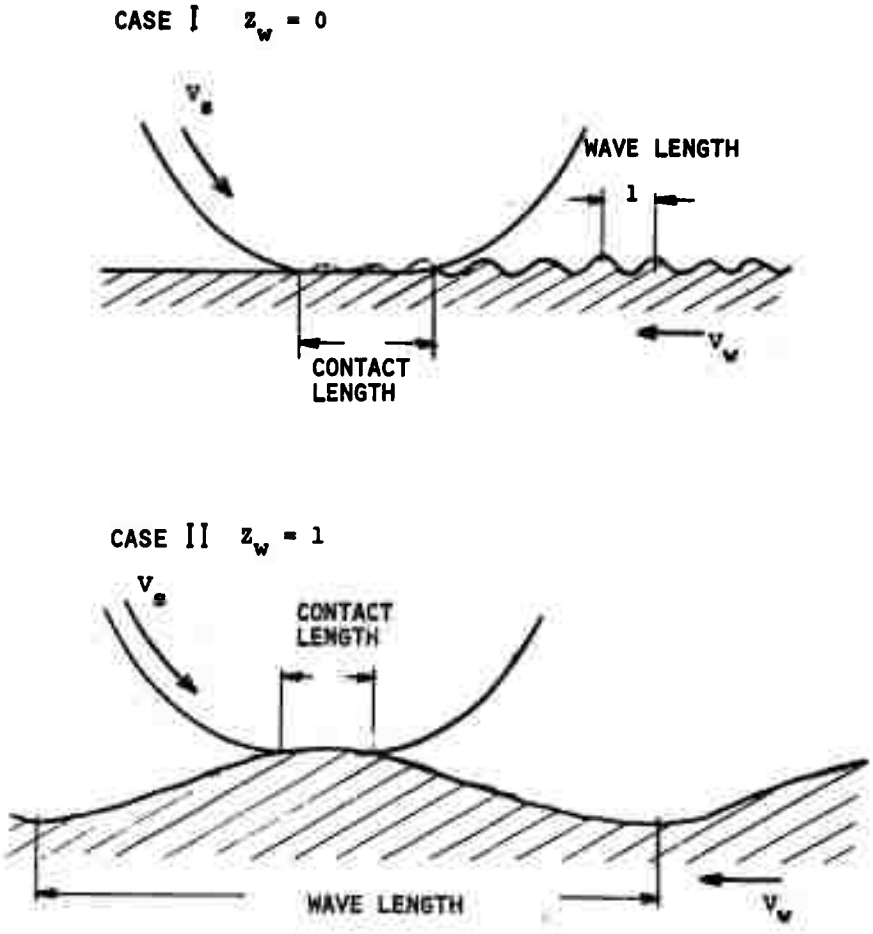

FIGURE V-14 - CONTACT LENGTH FILTERING ELEMENT

$$f_{w;s} = \frac{V_{w;s}}{2[y_c D_{eq}]^{.5}} \qquad (V.4.2)$$

The chatter frequency and break frequency are related to the filter element coefficient by (See Figure V-6):

$Z_w = 0$ if $f_c > f_w$

$Z_s = 0$ if $f_c > f_s$

$Z_w = 1$ if $f_c < f_w$

$Z_s = 1$ if $f_c < f_s$

where f_c = chatter frequency

From Equation V.4.2 it is evident that the break frequency for the grinding wheel is much higher than that for the workpiece since the surface velocity V_s is much greater than V_w for all practical grinding conditions. For example, if the typical values of

f_c = 400 cps, D_{eq} = 4 in., y_c = 100μ in.

are used in Equation V.3.7, a work velocity of 500 ft/min or more would be required to allow workpiece regeneration ($Z_w \neq 0$). This velocity is much higher than normal work speeds in grinding.

A summary of filtering effects of both types (μ,Z) is illustrated in Figure V-15.

V.4.3 Important Case of Grinding Instability - Wheel Regeneration

Since workpiece regeneration has been shown to be insignificant for many practical grinding conditions due to

STABILITY REQUIREMENT FOR Re_ℓ	STRUCTURAL DYNAMICS	BOUNDARY CONDITIONS
$-\frac{k_m}{w}\left(\frac{1}{2k_w^*}+\frac{1}{2k_s^*}+\frac{1}{K^*}\right)$	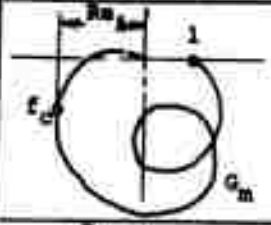	WORK REGENERATION $\mu_w = 1$ $\Sigma_w = 1$ $\mu_s = 1$ $\Sigma_s = 1$
$-\frac{k_m}{w}\left(\frac{1}{k_w^*}+\frac{1}{2k_s^*}+\frac{1}{K^*}\right)$	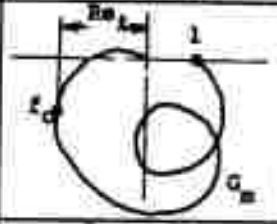	WHEEL REGENERATION $\mu_w = 0$ $\Sigma_w = 1$ $\mu_s = 1$ $\Sigma_s = 1$
$-\frac{k_m}{w}\left(\frac{1}{2k_s^*}+\frac{1}{K^*}\right)$	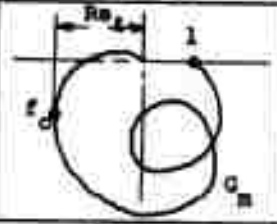	WHEEL REGENERATION $\mu_w = 1$ $\Sigma_w = 0$ $\mu_s = 1$ $\Sigma_s = 1$
$-\frac{k_m}{w}\left(\frac{1}{k_s^*}+\frac{1}{K^*}\right)$		NO REGENERATION $\mu_w = 1$ $\Sigma_w = 0$ $\mu_s = 0$ $\Sigma_s = 1$
$-\frac{k_m}{w}\left(\frac{1}{2k_s^*}+\frac{1}{K^*}\right)$	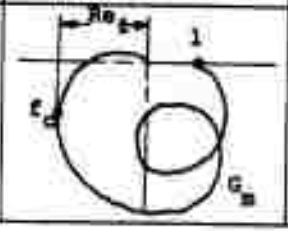	WHEEL REGENERATION $\mu_w = 0$ $\Sigma_w = 0$ $\mu_s = 1$ $\Sigma_s = 1$

FIGURE V-15 - STABILITY REQUIREMENTS FOR VARIOUS PRACTICAL GRINDING CASES

filtering, the case in which wheel regeneration occurs ($Z_w = 0$, $Z_s = 1$) is considered. The limit of stability was given by Equation V.2.25 (for the case of $\mu_s = 1$), and for the condition of $Z_w = 0$ that equation becomes

$$-\frac{1}{2}\frac{k_m}{k_s} - \frac{k_m}{K} < (Re_m)_{min} \qquad (V.4.3)$$

This corresponds to the model shown in Figure V-16, and the associated block diagram representation of Figure V-17.

Since $\left|\frac{k_m}{k_s}\right| << \left|\frac{k_m}{K}\right|$ in general (Section V.3.7), then the stability requirement becomes

$$-\frac{k_m}{K} < (Re_m)_{min} \qquad (V.4.4)$$

or

$$-\frac{k_m}{wK^*} < (Re_m)_{min}$$

As illustrated in Section V.2.4 and Figure V-8 the stability diagram can then be determined. In the case of wheel regeneration this stability diagram would consist of a plot of

$$r \equiv \left|\frac{1}{Re_\ell}\right| = \frac{wK^*}{k_m} \quad \text{vs.} \quad N_s$$

Furthermore, the rate of growth of instabilities can be investigated by means discussed in Section V.2.5 if k_s is known.

V.4.4 Effect of Wheel Loading

One further effect that could be considered is the case of wheel loading by chips of workpiece material. For a

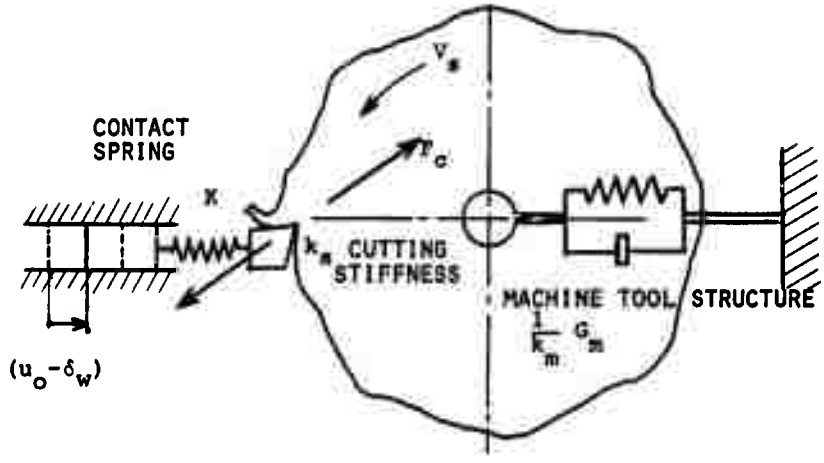

FIGURE V-16 - GRINDING CHATTER MODEL FOR SMALL WORK SPEED

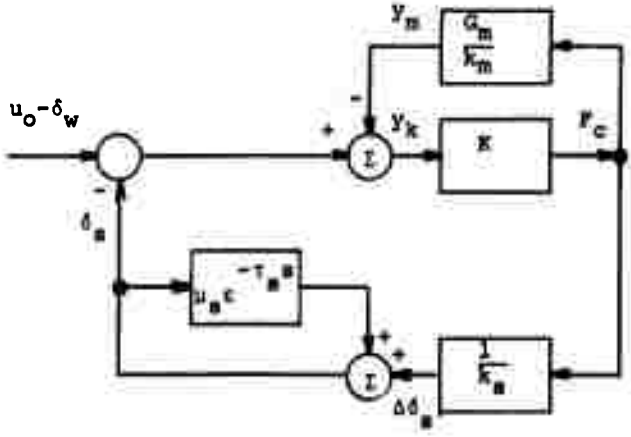

FIGURE V-17 - CLOSED LOOP REPRESENTATION OF THE GRINDING OPERATION FOR SMALL WORK SPEEDS

significant number of materials the loading of the wheel can be a major cause of grinding instability. Even where the loading of the pores of the grinding wheel occurs uniformly, the resulting cutting stiffness will increase and will move the grinding operation continuously closer to instability. However, observations often indicate that the loading of the wheel is not uniformly but rather periodically distributed.

This effect can be included in the dynamic model of the grinding operation by assuming that the instantaneous loading of the wheel is proportional to the cutting force and yields an instantaneous variation of the cutting ability

$$\Delta c_w(t) \equiv 1/\Delta k_w(t) = g\, Z_s(\omega)\, F_c(t) \qquad \text{(V.4.5)}$$

in Laplace notation

$$\Delta c_w(s) = \frac{1}{\Delta k_w(s)} = g\, Z_s(\omega)\, F_c(s) \qquad \text{(V.4.6)}$$

where

$\Delta c_w(t)$ = instantaneous variation of the cutability due to the instantaneous loading

g = proportionality factor

$F_c(t)$ = cutting force

$Z_s(\omega)$ = filter characteristic for grinding wheel which is a function of chatter frequency.

The variation of the cutability $c_w = \frac{1}{k_w}$, due to the loading effect of the grinding wheel, is equal to the cutability at time t minus the cutability at an instant of time $(t - \tau_s)$, just one revolution of the grinding wheel before:

$$\Delta c_w(t) = c_w(t) - c_w(t - \tau_s) \qquad (V.4.7)$$

Laplace transformation and rearranging yields:

$$c_w(s) = \frac{\Delta c_w(s)}{1 - e^{-\tau_s s}} \qquad (V.4.8)$$

Combining Equation V.4.8 and Equation V.4.6 leads to

$$c_w(s) = \frac{g\, Z_s(\omega)\, F_c(s)}{1 - e^{-\tau_s s}} = \frac{1}{k_w} \qquad (V.4.9)$$

This new relationship in the total dynamic model of the grinding operation is presented in Figure V-18. The factor g, relating the instantaneous variation of the cutability with the grinding force, can be positive, negative, or zero. If g is zero, the cutability does not change. For positive values of g the cutability increases as a function of time corresponding to a self-sharpening effect. Negative values of g yield a decreasing effect of the initial values of $1/k_w$ and introduce the influence of the loading effect.

The instantaneous depth of cut $\Delta\delta_w$ becomes a nonlinear function of the cutting force causing further difficulties in the mathmatical derivation of the stability criteria. A time simulation of this model can supply some interesting information about the dynamic performance of the system.

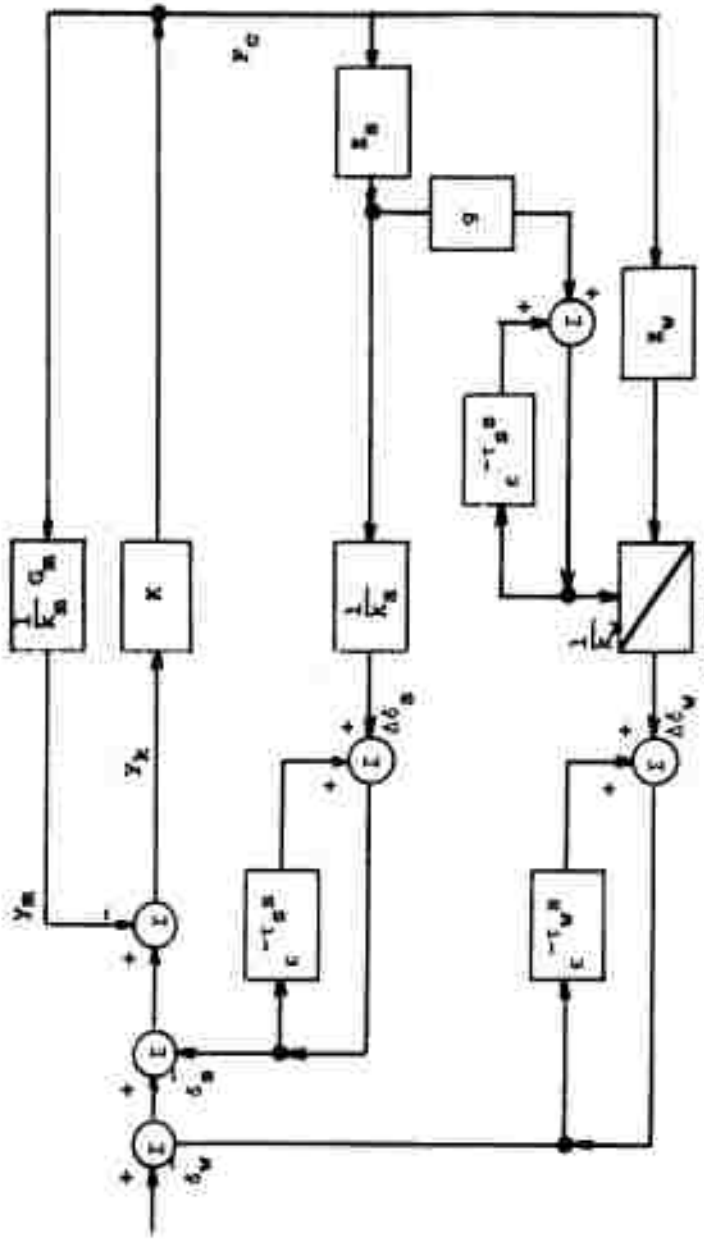

FIGURE V-18 - DYNAMIC MODEL INCLUDING LOADING EFFECT

V.5 Experimental Grinding Chatter Studies

V.5.1 Introduction

In order to verify the chatter theory developed under this contract, a carefully designed experiment was conducted. The characteristics of the grinding wheel and grinding machine were measured and a stability diagram was constructed for the machine. The cutting stiffness, wear stiffness, and constant spring stiffness were measured and then the chatter phenomena was predicted from the stability analysis. A set of grinding tests was performed to validate the chatter predictions. The results of the program were very successful.

V.5.2 Equipment

The main piece of equipment utilized during this program was a controlled force grinding machine, Figure V-19. This machine was particularly useful because it had the capability for long plunge-in cuts and also the normal force could be controlled. It was important to control the force so that the contact stiffness coefficient K remained constant, allowing the theory and experiment to be compared.

The grinding machine was slightly modified by adding a relatively weak workpiece holder on the head stock as shown in Figure V-20. The purpose of this was to provide a particular weak element so that $G_m(j\omega)$ is a relatively simple function. This enables a more accurate analysis of the role of the contact area compliance.

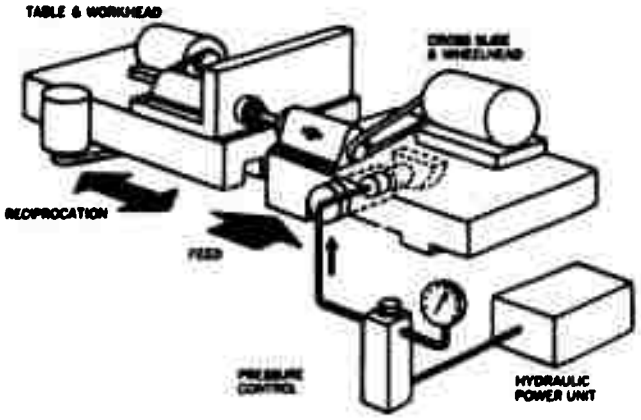

FIGURE V-19 - CONTROLLED FORCE GRINDER

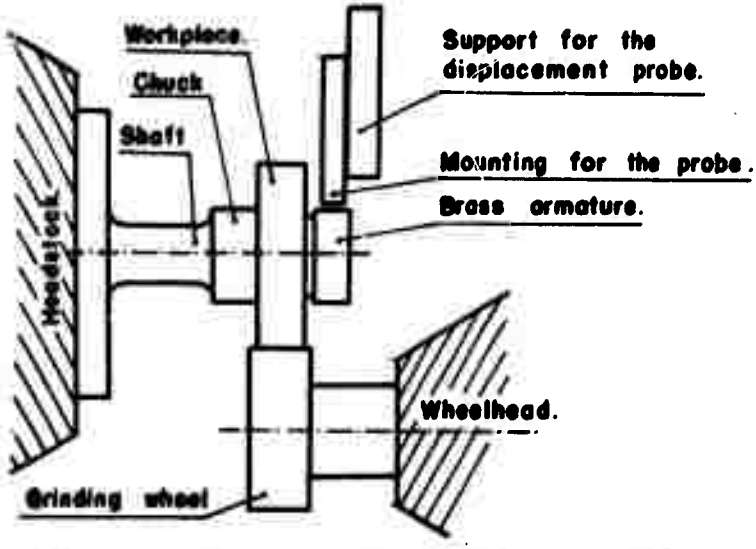

FIGURE V-20 - GENERAL SET-UP FOR CHATTER TESTING

The next important piece of equipment was the TFA (Transfer Function Analyser) which was used to measure the grinding machine frequency response. Two different measuring methods were used.

In the first a small hydraulic exciter was mounted between a special aluminum wheel (Figure V-21) and a specially designed work piece holder (Figure V-22). The displacement between the wheel and workpiece was measured using a small inductance pickup. The second method was to simultaneously excite the wheel spindle and the workpiece with a pair of electro-mechanical exciters (See Figure V-23).

A special piece of equipment was constructed to measure the contact area stiffness K. This equipment is shown in Figure V-24. This equipment is described in detail in the fifth and sixth Engineering Reports.

The cutting and wear stiffness (k_w and k_s) were measured during the grinding test by measuring the change in diameter of the grinding wheel and workpiece as a function of time and by also measuring the mean normal grinding force.

A tape recorder was used to record the chatter data from the TFA and a Fourier analysis oscilloscope was utilized in the data reduction.

V.5.3 Machine Frequency Response Plot.

The grinding machine frequency response was obtained using the set-up shown in Figure V-22 and V-23. The machine frequency response plot is shown in Figure V-25. In order

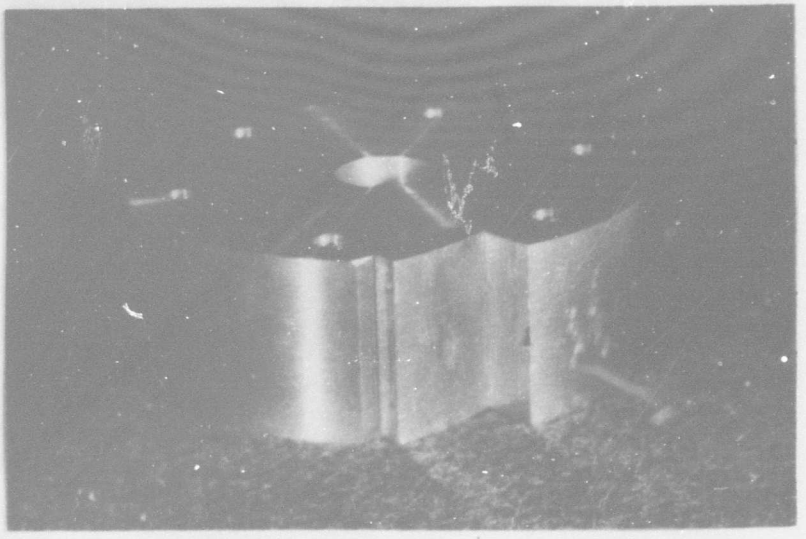

FIGURE V-21 - ALUMINUM GRINDING WHEEL SIMULATOR

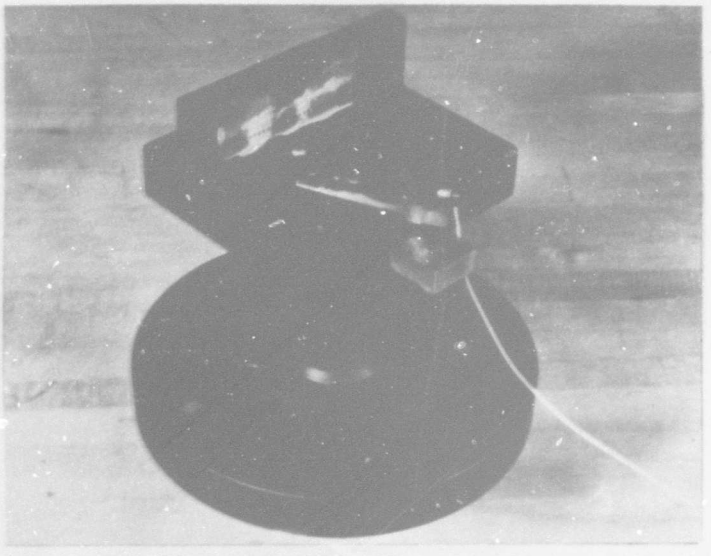

FIGURE V-22 - HOLDER FOR HYDRAULIC EXCITER WITH THE DISPLACEMENT PROBE MOUNTED

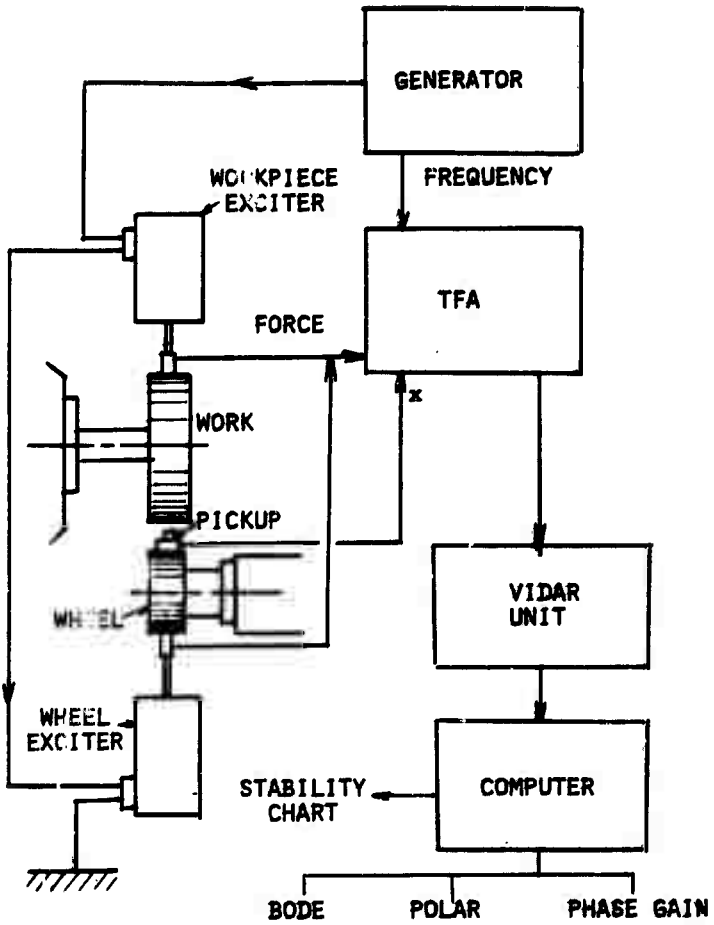

FIGURE V-23 - SECOND EXCITATION SET-UP OF THE GRINDING MACHINE

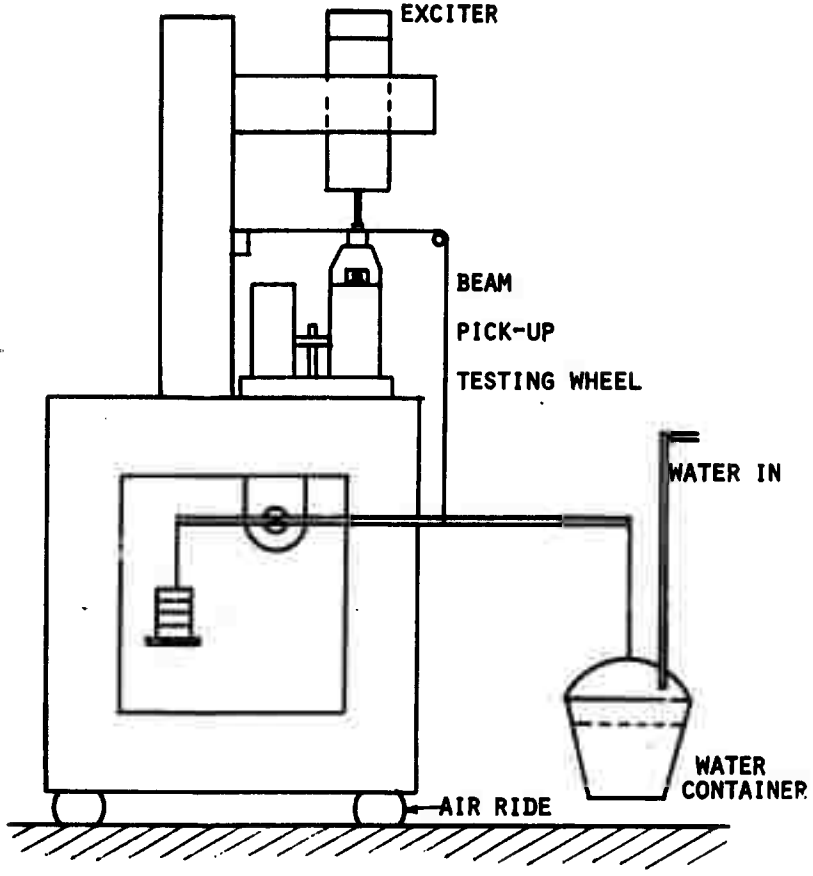

FIGURE V-24 - SCHEMATIC DIAGRAM OF THE SET-UP TO MEASURE THE CONTACT STIFFNESS

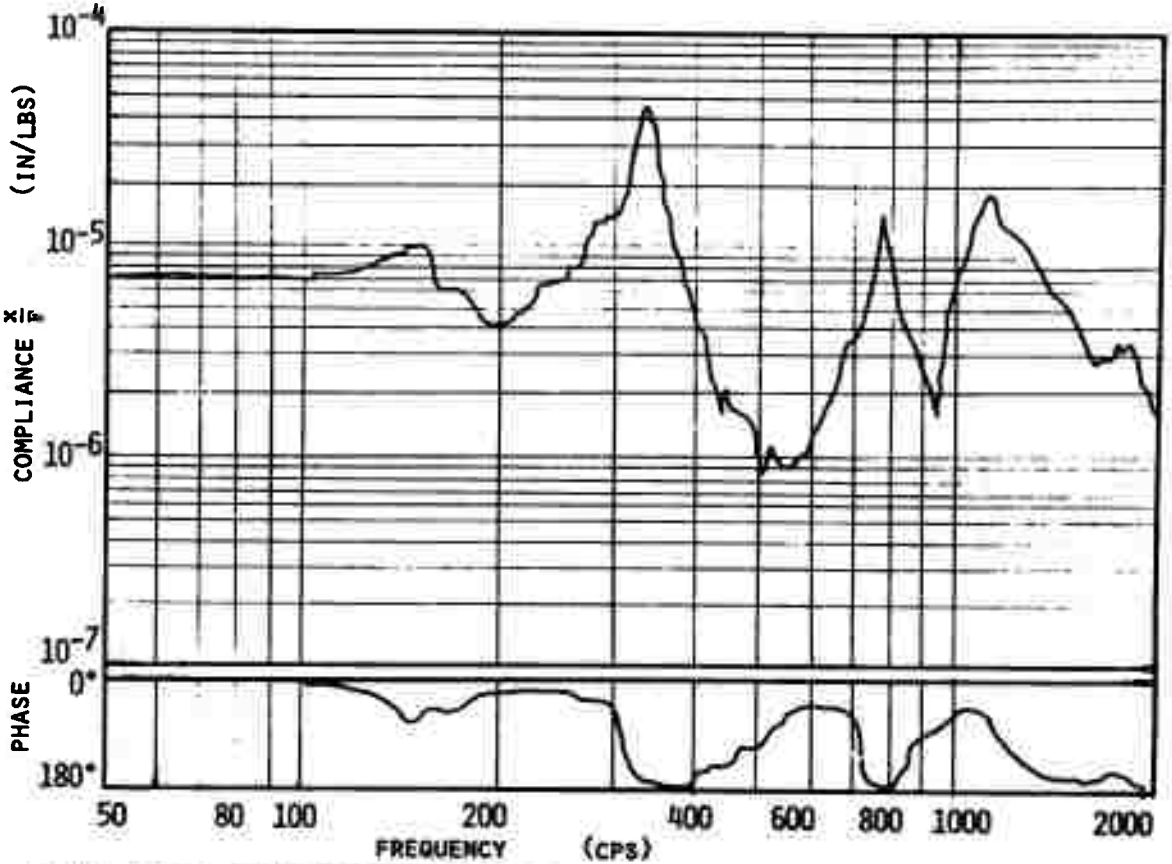

FIGURE V-25 - DRIVING POINT DIRECTIONAL FREQUENCY RESPONSE PLOT OF CONTROLLED FORCE GRINDER

to construct the stability diagram, the frequency response was plotted in polar form (See Figures V-26 and 27).

The modes of vibration which correspond to the resonance peaks in the frequency response plots are shown in Figure V-28. The 300 cps mode corresponds to the bending mode of the workpiece and is the predominate mode. The 800 cps mode corresponds to the rocking of the grinding wheel on the spindle. The 1140 mode corresponds to the bending mode of the wheel spindle. A forth mode at 145 cps was also measured but this mode was not important in the chatter phenomena.

V.5.4 Stability Diagram

Utilizing the method described in Section V.2.4 of this report a stability diagram for the controlled force grinding machine was constructed (See Figure V-29). Figure V-30 shows a more detailed view of Figure V-29 in the region of the operating wheel speed. It should be noted that the stability diagram of Figure V-29 considers the wheel regeneration case. This same figure can be used for the work regeneration case if the y cordinate is changed to correspond to $(\frac{1}{Re_l})$ for the work regeneration case.

V.5.5 Theoretical Prediction of Actual Grinding Chatter

The contact stiffness characteristic of the grinding wheel was measured using the set-up shown in Figure V-24. The characteristic of the contact zone for the wheel used in this experimental study is shown in Figure V-31.

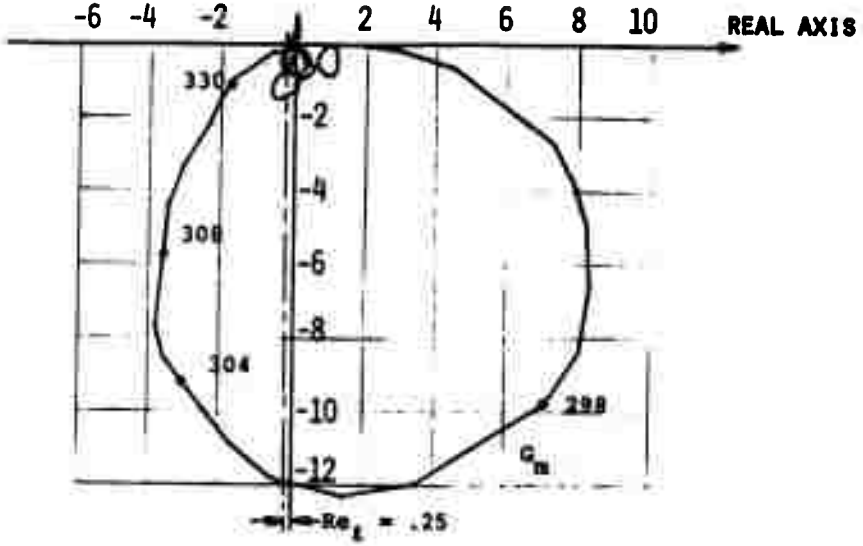

FIGURE V-26 - POLAR REPRESENTATION OF TRANSFER FUNCTION G_m OF THE GRINDING MACHINE

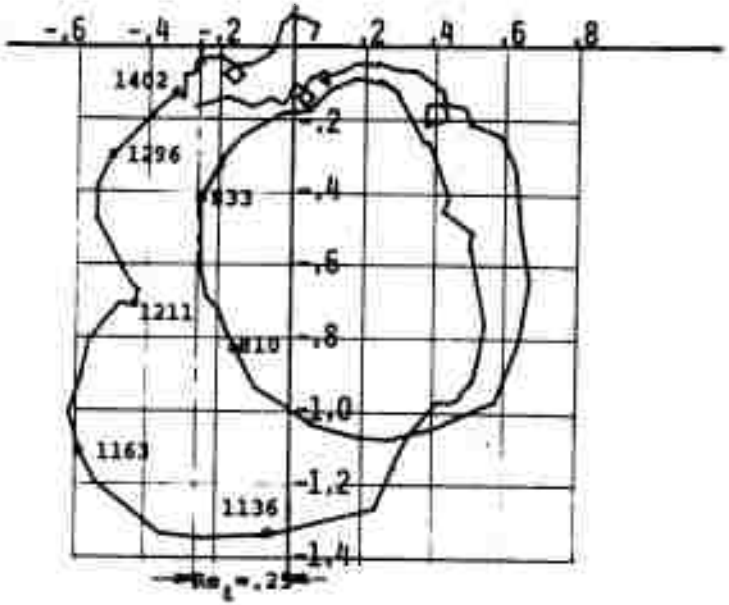

FIGURE V-27 - ENLARGEMENT OF HIGHER FREQUENCY MODES IN FIGURE V-26

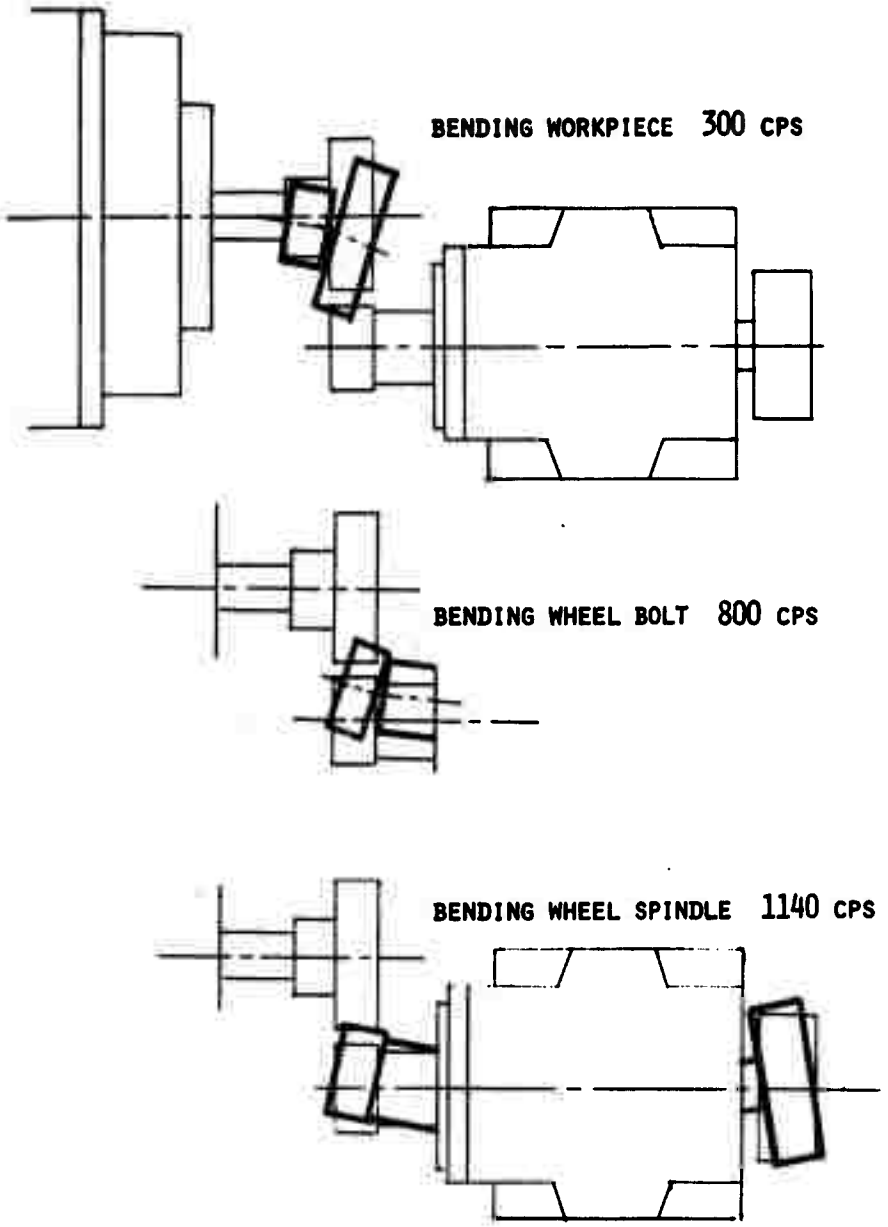

FIGURE V-28 - MODES OF VIBRATIONS

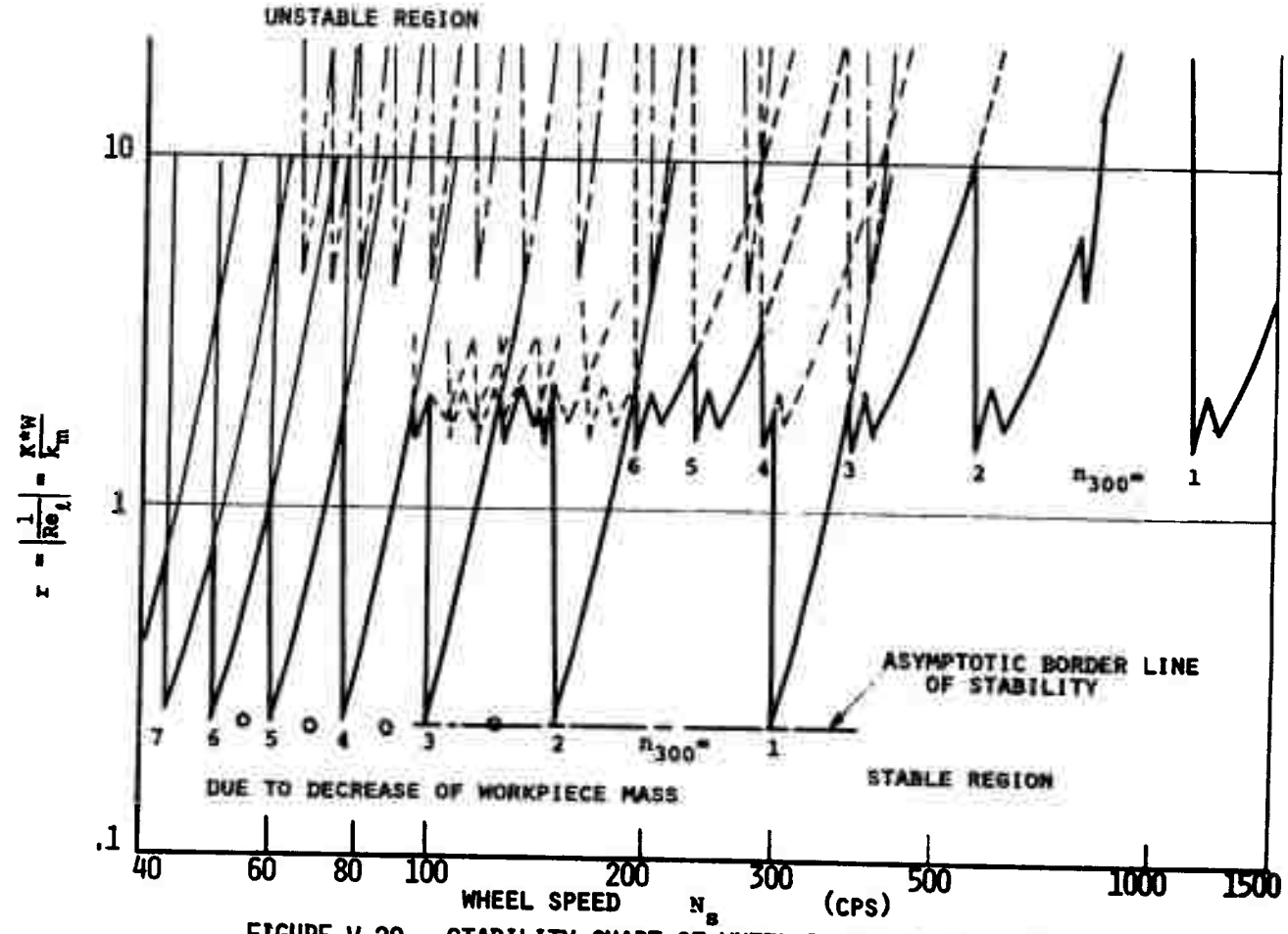

FIGURE V-29 - STABILITY CHART OF WHEEL REGENERATIVE CHATTER

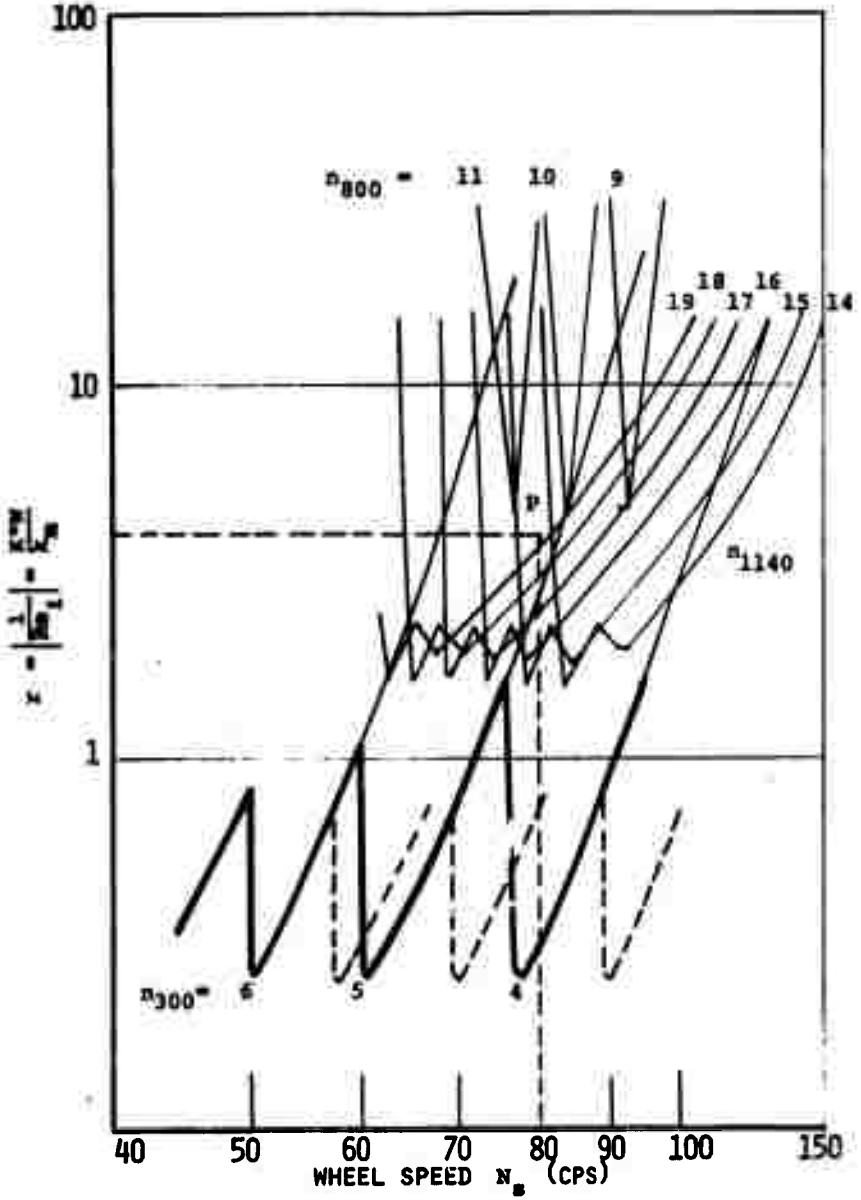

FIGURE V-30 - DETAIL OF STABILITY CHART

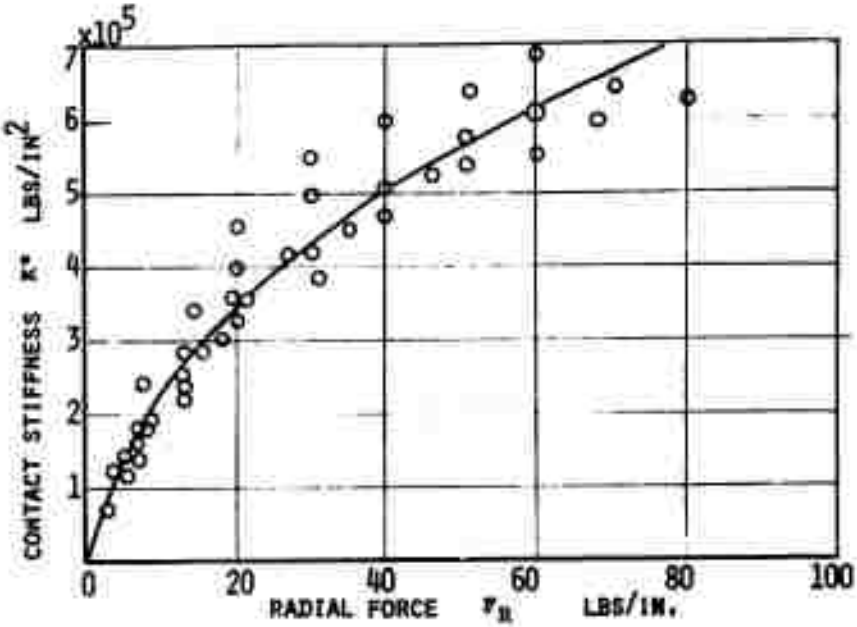

FIGURE V-31 - CONTACT STIFFNESS VERSUS RADIAL FORCE

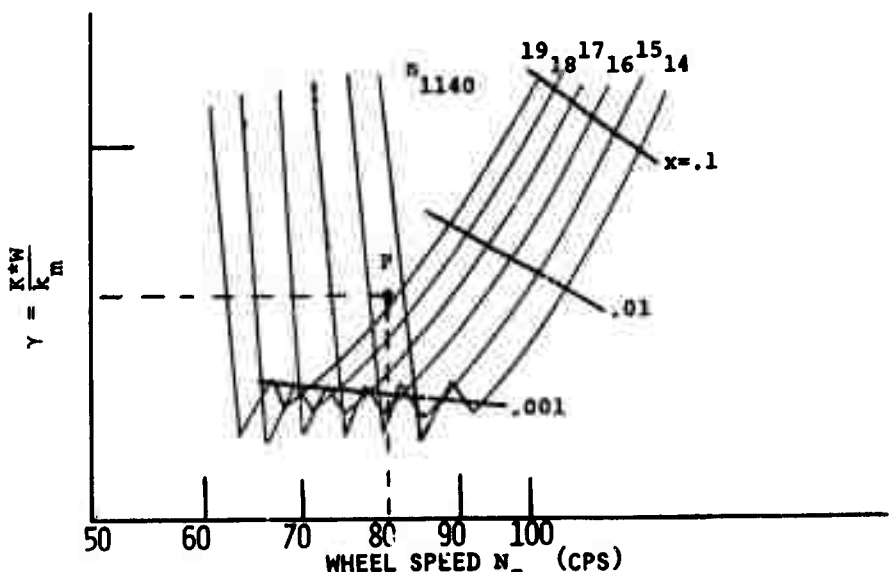

FIGURE V-32 - RATE OF GROWTH OF GRINDING INSTABILITY FOR THE 1140 CPS MODE

From the width of cut, the contact stiffness, and the stability diagram of the machine, a prediction concerning the chatter phenomena can be made. The grinding tests were performed with a width of cut w = 1.25 inch, contact stiffness K^*, corresponding to a normal grinding force of 20 lbs/in (approximately equal to 4×10^5 lbs/in, Figure V-31), and a machine static stiffness $K_m = 1.25 \times 10^5$ lbs/in.

The resulting value of r is

$$r \equiv \frac{1}{Re_\ell} = w\frac{K^*}{k_m} = 1.25 \times \frac{4 \times 10^5}{1.25 \times 10^5} = 4$$

The line defined by this value is shown in Figure V-26.

This is far above the asympotic borderline of stability value of $\frac{1}{(Re_m)_{min}} = .25$. The number of waves that may be generated can be found from Figure V-30 the position of the operating point, P, at r=4 and N_s = 80 cps. The following number of waves on the circumference of wheel are possible: 4, 5, 6 and 15 through 19. The 4 and 6 case depend upon the mass of the workpiece. Four and five waves can occur when the mass is large and five and six can occur when the mass is small.

Another point that should be noted is that the rate of growth is greatest for the largest number of waves (See Figure V-32). As the amplitude of vibration increases, the effective spring constant of the contact zone decreases due to its non-linear nature. When this occurs the point P drops on the stability diagram and the wave patterns with 19 and then 18

waves become stable and the lower number of waves begin to predominate. This explains the evolution of grinding chatter.

V.5.6 Chatter Test.

A set of chatter tests was performed on the grinding machine in order to verify the theoretical predictions of Section V.5.5. The tests were divided into different catagories, the high workspeed test and the low workspeed case. The high speed case included wheel and workpiece regeneration and the low speed case had only wheel regeneration. The chatter data was stored on magnetic tape along with timing marks which identified one revolution of the grinding wheel and one revolution of the workpiece. The cutting and wear stiffnesses were measured during the test.

The series of photographs shown in Figure V-33 give the time evolution of the chatter vibration. The speed of the workpiece is below the minimum speed $V_{w_{min}}$, and thus the tendency for work regeneration is strongly attenuated. It took several minutes before the chatter vibrations could be observed, indicating time rate of growth of the instability.

For the same work conditions, but at a higher workspeed, Figure V-34 gives the time evolution of the vibration signal. The time required to reach a high amplitude level is of the order of seconds, much more rapidly than for the case when only wheel regeneration is present.

The difference between the machined surfaces of both chatter cases shows up clearly in Figure V-35. The chatter

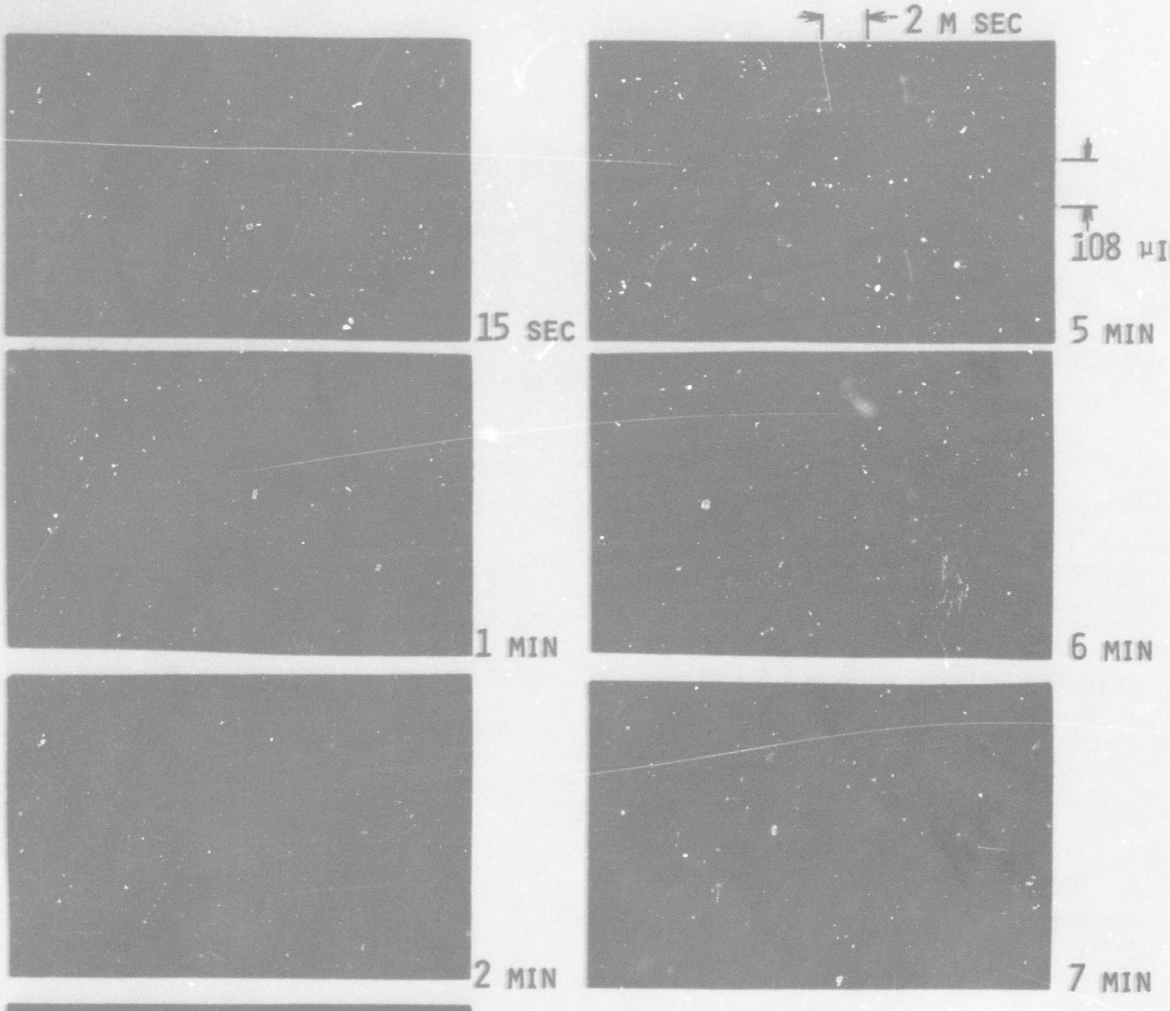

w: 1.25 in.
v_w: 169 sft/min.
v_s: 6.100 ft/min.
D_w: 4.1 in.
D_s: 4.8 in.
D_{eq}: 2.2 in.
F_R: 20 lbs/in.
R: 50
$\Delta\delta_w$: 2.6×10^{-5} in.
$\Delta\delta_s$: 1.4×10^{-8} in.
k_w: 7.8×10^{5} lbs/in^2
k_s: 1.4×10^{9} lbs/in^2
K_v: .027
k_c: 2.8×10^{7} lbs/in^2
z': .052 cu.in./min/in.
TEST: #10
MATERIAL: HARDENED STEEL 45 R_C
WHEEL: 2A60K6VLE

FIGURE V-33 - EVOLUTION OF VIBRATION FOR GRINDING CHATTER DUE TO WHEEL REGENERATION

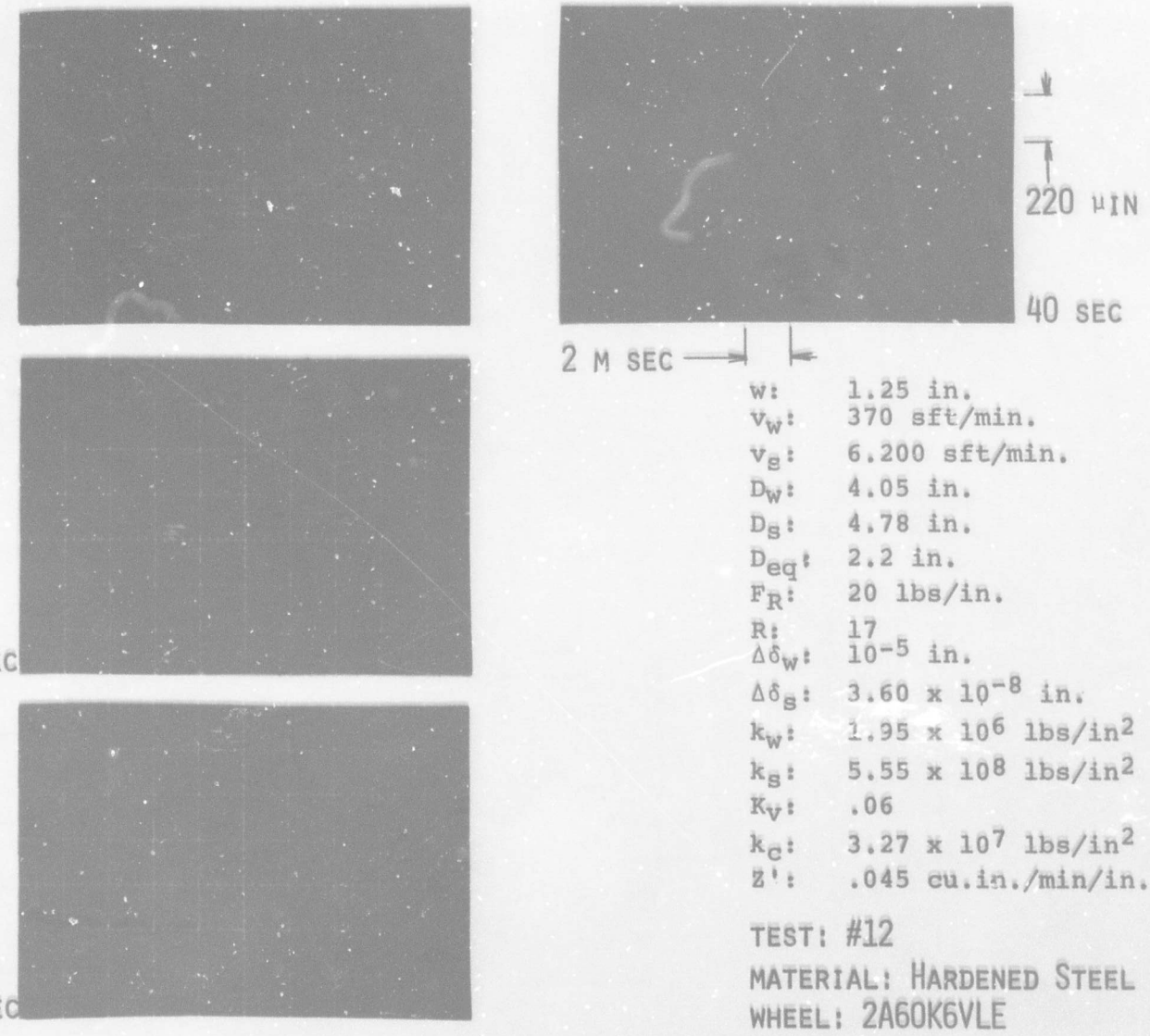

FIGURE V-34 - EVOLUTION OF VIBRATION FOR GRINDING CHATTER DUE TO WORKPIECE REGENERATION

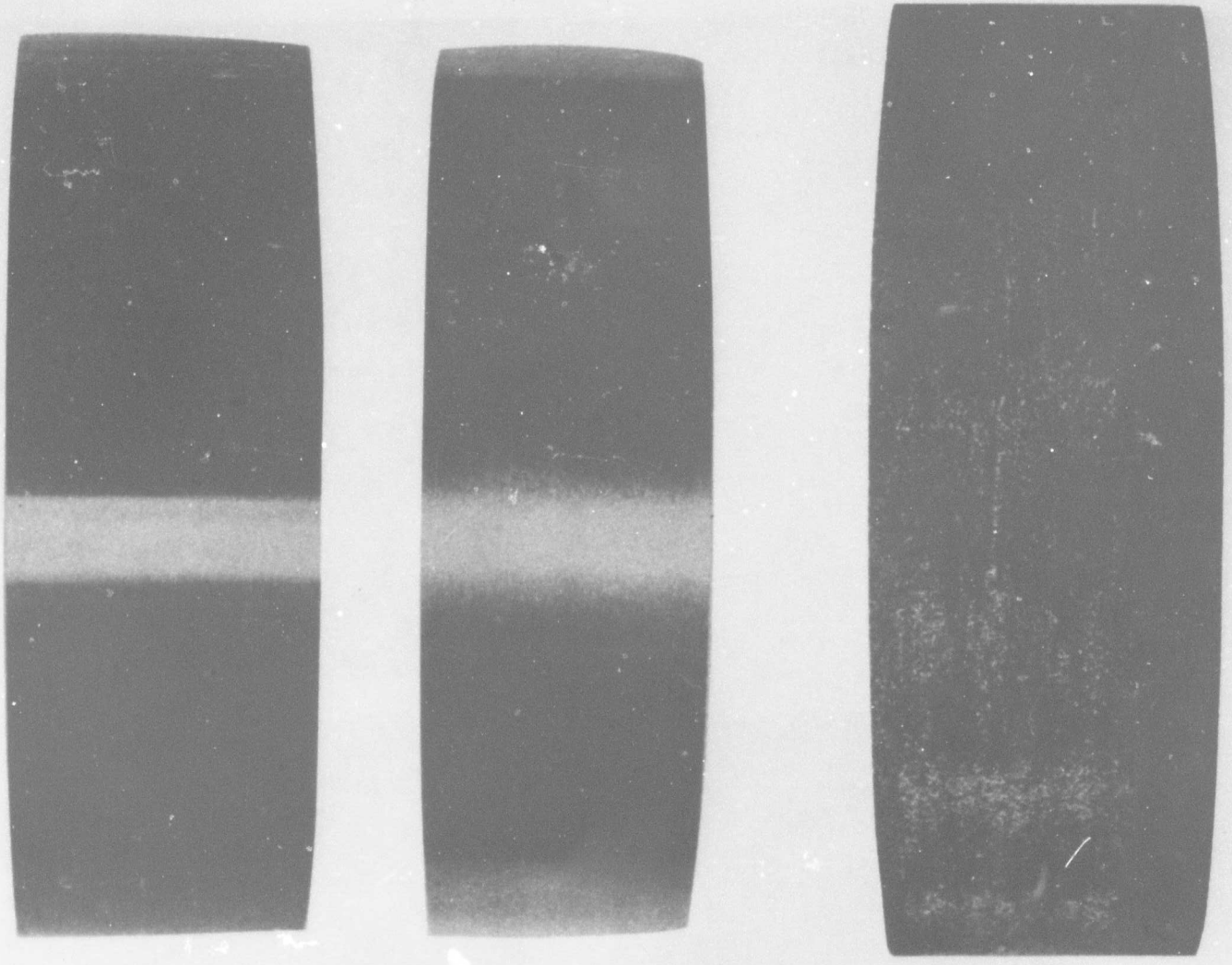

FIGURE V-35 - CHATTER MARKS ON GRINDING WHEEL AND WORKPIECE

marks on the workpiece are very deep for high workspeeds (work regeneration case) and are reduced to a more "optical" chatter pattern for low workspeeds. In the latter case, undulations occur on the wheel surface. The tops of these waves are indicated by a piece of chalk lightly pushed against the rotating wheel. For the two cases a Fourier frequency analysis of the vibration is made at different times during the tests. Figure V-36 shows the frequency analysis for the low workspeed case. The mean value of the frequency decreases as a function of time for chatter initiated at high frequencies. This is due to the nonlinear spring effect of the contact area. The average stiffness of a spring with a similar deformation characteristic decreases when the vibrational motion increases.

Figure V-37 concerns the work regeneration case. Chatter occurs in the lower frequency range and the amplitude grows very fast. Chatter is impossible in the high frequency range because of the filter characteristic in the workpiece regeneration feedback path.

To show that the developed undulations are really connected with either the grinding wheel or the workpiece, Figure V-38 was constructed. For the wheel regeneration chatter the vibration signal was repeated several times on an oscilli cope that was triggered with a reference impulse of the wheel rotation. A similar method is used for the workpiece regeneration. The same method was then applied to measure how fast the bumps on the wheel were travelling around the wheel (Figure V-39).

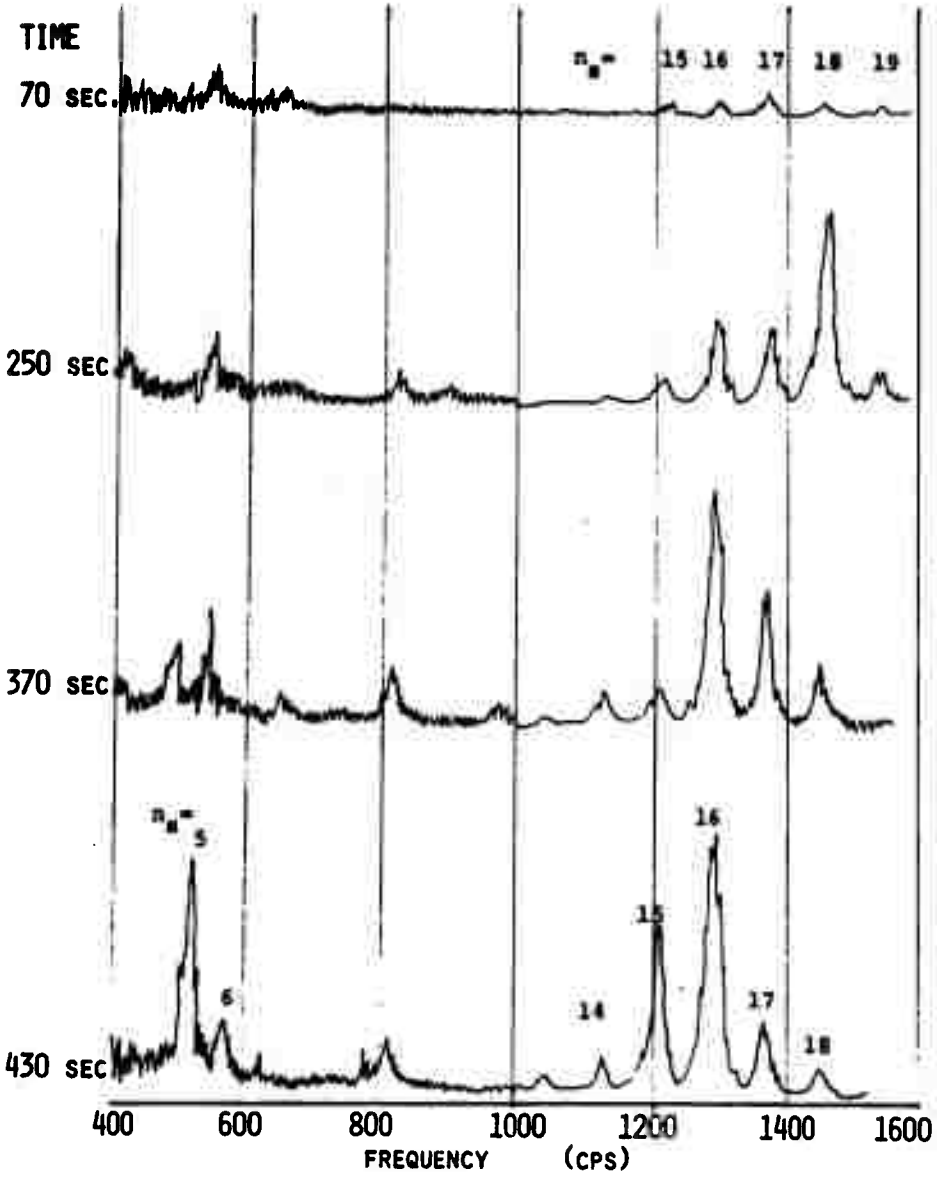

FIGURE V-36 - FREQUENCY ANALYSIS OF WHEEL REGENERATION

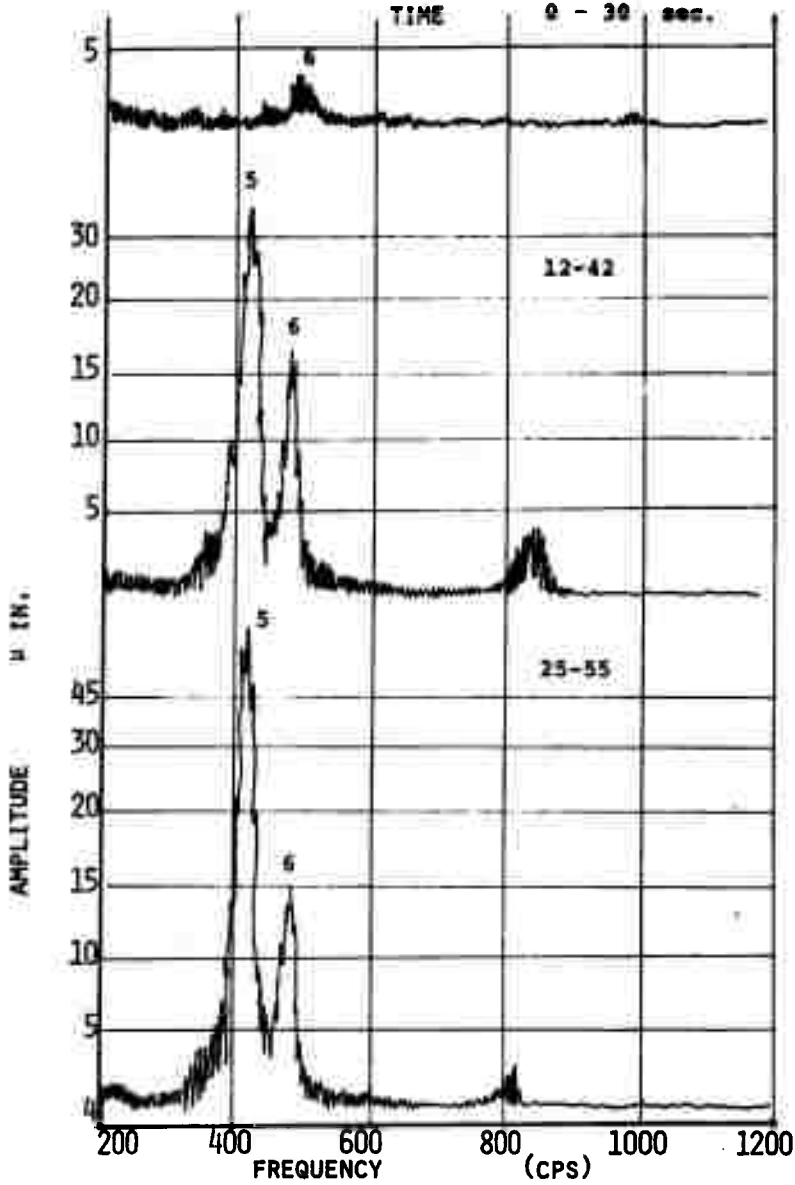

FIGURE V-37 - FREQUENCY ANALYSIS OF WORK REGENERATION

TRIGGERING WITH WHEEL ROTATION

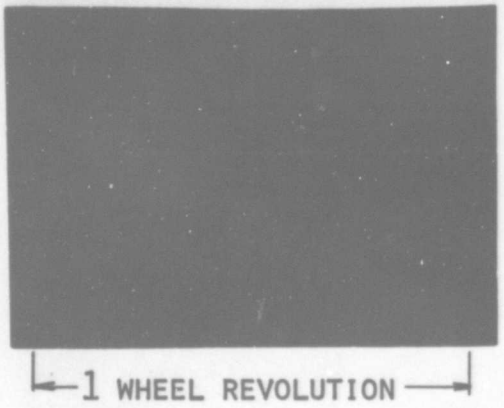

TRIGGERING WITH WORK ROTATION

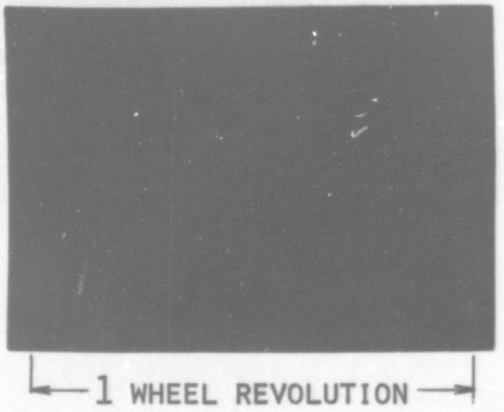

FIGURE V-38 - WHEEL AND WORK REGENERATION PATTERN

TRIGGERING WITH WHEEL ROTATION

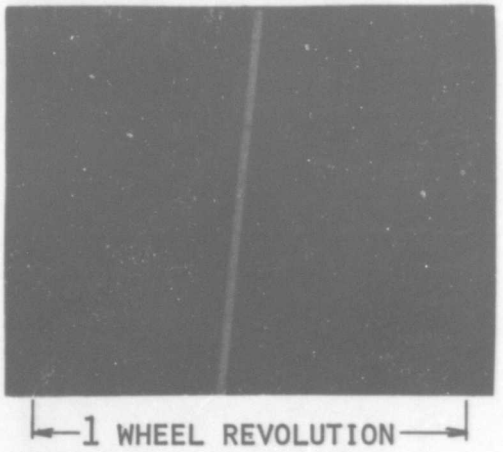

TRIGGERING WITH WORK ROTATION

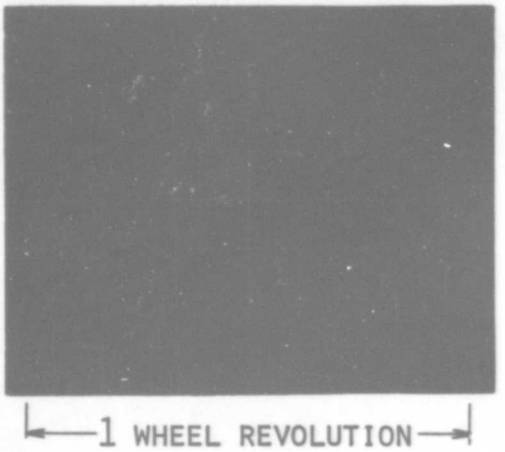

FIGURE V-39 - WHEEL AND WORK REGENERATION PATTERN

It was determined that it takes about 18,000 revolutions of the wheel, or 4 to 5 minutes, for the undulation pattern to travel around the wheel. This confirms the theoretically predicted small phase angle ν_s in wheel regenerative chatter cases. This is a direct indication that the wheel undulations are not caused by nonhomogeneity of the wheel, although nonhomogeneities greatly influence the initiation of chatter.

V.5.7 Discussion of Test Results.

The important results of the tests are that the experimental data agrees very well with theoretical predictions. For the wheel regeneration case the wave patterns which were predicted to be unstable are the patterns which were measured as unstable. The evolution of the chatter pattern behaved in the predicted manner with the higher frequencies appearing initially and shifting with time towards the lower frequencies.

The filtering element of the contact zone behaved in the predicted manner at low workspeeds since the regeneration of the workpiece was filtered out.

The wave pattern on the wheel moves around the wheel with the phase angle, ν_s. The magnitude of ν_s can be calculated from Equation V.2.28. This value corresponds to the borderlimit of stability value and for an unstable case the value is twice the value calculated from the border limit of stability analysis (See sixth Engineering Report). This value is approximately equal to $\frac{k_m}{k_s}$ which corresponds very closely to the measured value of about 10^{-3}. (See Figure V-37).

At higher workspeeds, regeneration of the workpiece occurred as was predicted. In this case the vibration developed very rapidly. The pattern which developed satisfies Equation V.2.29. The Fourier frequency analysis indicates only those harmonic frequencies primarily associated with the wheel because those associated with the workpiece are too close together for the filters to distinguish. The pattern is related to the workpiece, however, as indicated by Figure V-39.

V.6 Conclusions

A feed back loop approach for analyzing self-excited grinding chatter has been formulated and experimentally verified with excellent results. The theory lends great physical insight into the grinding chatter problem. Many chatter phenomena observed during grinding can now be explained by the theory. For example, one special case which has often puzzled grinding investigators is the one in which there is no chatter during rough grinding but it occurs during finish grinding. The reason for this phenomena is that the length of contact is great enough during rough grinding to filter out regeneration of the workpiece. As the infeed of the grinding machine is reduced, the contact length is likewise reduced and workpiece regeneration becomes possible thereby causing workpiece regeneration chatter.

From the theory it is possible to predict the influence of the grinding parameters upon the stability. In general

there were several new vibration grinding parameters defined by the theory. There parameters are the wear, cutting and contact stiffnesses. The conventional grinding parameters such as velocity ratio, infeed ratio, etc., can be related to those new parameters defined by the theory and the effects of the conventional parameters can be predicted.

The influence of the parameters used in the feedback loop theory are:

1). Machine structure, $\frac{1}{k_m} G_m(j\ )$, - The stiffer the machine, both statically and dynamically, the greater the stability of the grinding process.

2). Cutting Stiffness, k_w - The smaller the cutting stiffness the more stable the grinding process; thus the easier the material is to cut, the greater the stability.

3). Wear stiffness, k_s - The smaller the wear stiffness, the greater the stability of grinding process. This parameter usually has a very small effect upon the limit of stability in comparison to the other variables such as the machine structure, cutting stiffness and contact stiffness. It does, however, have a major effect upon the rate of development of the instability for the grinding wheel regeneration case. The larger the value of k_s, the smaller the rate of development.

4). Contact stiffness, K - The smaller the contact stiffness, the more stable the process.

5). Width of cut, w - If the cutting, wear and contact stiffnesses are defined for a unit width of the grinding wheel, the width of cut can be introduced into the basic equations. The smaller the width of cut, the more stable the process. The width of cut is a very important parameter since it can be easily controlled during grinding.

6). Filtering element, $\mu_{w;s}$, $Z_{w;s}$ - Increased filtering effects result in increased stability.

7). Modes of vibration - The modes of vibration of the grinding machine structure can be related to the chatter phenomena and appropriate means can be taken to eliminate the important modes, thereby, increasing stability.

Several of the more important grinding parameters often used in grinding work can be related to the parameters used in the theory and the effects of these parameters upon the stability can be evaluated as follows:

1). Velocity ratio, K_v - Decreasing velocity ratio $K_v=\frac{V_w}{V_s}$ decreases the cutting stiffness and therefore increases the stability.

2). Work and wheel speeds, $V_{w;s}$ - The work and wheel speeds effect the stability through a change in K_v. There is also a filtering effect when the wave pattern which develops has a wave length smaller than the contact length. This effect is directly related to work and wheel speeds. In this case very low speeds increase the filtering effect.

3). Infeed rate, $\Delta u_o(t)$ - Decreasing the infeed will decrease the static grinding force which decreases the contact stiffness due to its non-linear nature. This will increase the stability of the grinding process. However, as the infeed rate increases the contact length will also increase with a correspondence increase in the filtering effect, which has a stabilizing influence. The infeed rate also effects the cutting and wear stiffness, however these effects are not clear.

Some of these trends are common knowledge, again indicating the validity of the theory. Important, however, is the fact that a definite relationship has been established between the parameters.

Another significant benefit of this work is that a better physical understanding of the chatter phenomena has been developed and this understanding can be used to improve the process. For example, it appears that for many grinding conditions it is unlikely that theoretical stability can be

achieved because great increases in the static and dynamic stiffness of the machine are required. The extent of these increases is also limited by the stiffness of the workpiece. Therefore it is extremely important that methods be developed and applied which will delay the wave pattern development on the wheel and workpiece. Thus, the emphasis is not on how to stabilize the operation, but rather on how to increase the time of grinding under unstable conditions. A time simulation of the complete dynamic model of the grinding machine would be very useful for evaluation and optimizition of methods for retarding the rate of growth of chatter vibrations. The best stablizing or retarding process is to destroy or disrupt the regeneration pattern which develops on the wheel and/or workpiece. The time simulation will be important in investigating these methods. Several of the methods that may tend to improve the grinding process are tabulated below:

1). Use of controlled mechanical impedance, controlled force vibrations, and periodic variations of the machine transfer functions.

2). Improve the design of the machine including better performance of the workpiece support.

3). Application of passive absorbers and active dampers.

4). Programmed wheel and workpiece speed variations.

5). Elimination of the generation of certain numbers of waves on the wheel circumference by grinding two or more workpieces simultaneously (mechanical filter).

6). Use oil jet cleaning devices to keep the wheel from loading and using abrasive jet techniques to continuously reshape the wheel.

In order to make the theory developed in this section generally useful it will be necessary to generate data concerning the cutting stiffness and the contact deformation for different material and wheel combinations. This indicates the importance of the work in Section II of this report where the cutting problem is examined in great detail.

V.7 Nomenclature

$D_{(w;s)}$	in	Diameter (workpiece or grinding wheel)
D_{eg}	in	Equivalent diameter = $\frac{D_w D_s}{D_w + D_s}$
f_c	cps	Chatter frequency
f	cps	Frequency
F_R	lbs	Radial force
F_c	lbs	Cutting force
$G_m(j\omega)$	-	Directional normalized frequency response of machine structure
g	in/lbs^2	Proportionality factor relating cutting force and cutability variation
Im	-	Imaginary part
I_{max}	-	Maximum imaginary part
Im_ℓ	-	Imaginary part straight line
Im_m	-	Imaginary part of machine
k_c	lbs/in	Cutting stiffness coefficient of workpiece ($k_c = k_w^*/K_V$)
k_w	lbs/in	Cutting stiffness of workpiece

k_w^*	lbs/in/in	Cutting stiffness per unit contact width
k_s	lbs/in	Wear stiffness of grinding wheel
k_s^*	lbs/in/in	Wear stiffness per unit contact width
k_m	lbs/in	Static stiffness of machine structure
K	lbs/in	Static stiffness of contact area
K*	lbs/in/in	Static stiffness of contact area per unit width of contact
K_v	-	Speed ratio
ℓ	in	Contact length
$N_{s;w}$	rev/sec	Rotational speed (Wheel or workpiece)
$n_{s;w}$	-	An integer equal number of wave of circumference of wheel or workpiece
Re_ℓ	-	Real part of straight line
Re_m	-	Real part of grinding machine frequency response, $G_m(j\omega)$
$(Re_m)_{min}$	-	Minimum real part of machine normalized frequency response, $G_m(j\omega)$
r	-	Reciprocal of real part of straight line
s	-	Complex variable
(s)	-	Subscript denoting grinding wheel
t	sec	Time
$u_o(t)$	in	Total infeed
$\Delta u_o(t)$	in	Infeed per revolution of workpiece
$V_{(w,s)}$	in/sec	Surface speed (Workpiece or grinding wheel)
(w)	-	Subscript denoting workpiece
x	-	Rate of growth parameter
y	rad/sec	Frequency of ocillation
y_c	in	Depth of wheel - workpiece interference
y_m	in	Deformation of machine structure

y_k	in	Deformation of contact area
y_t	in	Total deformation ($y_t=y_m+y_k$)
w	in	Width of contact
$Z_{w;s}$	-	Filter characteristic coefficient
ε	-	Instantaneous wear to depth of cut ratio
$\delta_w(t)$	in	Total depth of cut
$\Delta\delta_w(t)$	in	Depth of cut per revolution of workpiece
$\delta_s(t)$	in	Total amount of wear
$\Delta\delta_s(t)$	in	Depth of wear per revolution of grinding wheel
ω	rad/sec	Frequency of ocillation
$\tau_{s;w}$	sec	Time delay - revolution time (grinding wheel or workpiece)
$\nu_{s;w}$	-	Phase shift of wave (on grinding wheel or workpiece) and cutting force
ν_c	-	Critical phase shift
$\mu_{s;w}$	-	Overlap factor (on wheel or workpiece)

SECTION VI

HSTRA GRINDING TEST RESULTS

VI.1 Introduction

Experimental analysis in grinding has, in general, been developed by varying only one parameter selected from many grinding conditions, holding the other parameters constant, thus determining the optimum condition for the parameter in the range of the experiment. In this case the problem is to select the parameter. In the past, parameters limited by the configuration of the grinding machine, such as wheel speed, work speed, infeed speed, and table speed, etc., have been selected. The many experiments conducted under programs such as this have never significantly improved grinding processes. To significantly improve the grinding process it is necessary to select input parameters which have a direct effect on the wheel-work interaction and whose influence on grinding results can be directly observed from the experiment. The planning of such experiments can only be made based on the results of the basic studies which have been developed under this contract. In this section the method of selection of proper grinding test conditions for experimentally determining which parameters can significantly improve the efficiency and the surface integrity in HSTRA grinding will be discussed. Then several examples of the results of experiments conducted

with carefully selected grinding conditions will be explained. From these examples it will be easy to understand the overall conclusions of the work done under the contract.

VI.2 Experimental Equipment

VI.2.1 Grinding Machine

Under this research three grinding machines have been used. Specifications of these grinders are shown in Table VI-1 and photographs of the grinders in Figure VI-1 to VI-3 .

Machine #2 has mainly been used for grinding tests of HSTRA materials. The work-head and the wheel-head of the grinding machines were modified so that speeds twice as great as those of conventional grinding machines could be obtained. Furthermore a microscope was mounted on the wheel cover for observation of the cutting edges on the wheel. (See Figure VI-4).

VI.2.2 Items To Measure

In order to scientifically develop experimental research on grinding, several items should be measured before, during, and after the experiment. Accuracy in measuring these items is directly related to the accuracy in selecting boundary conditions which affect the wheel-work interaction and the standard for estimating grinding results. Therefore scientific understanding of the grinding process is necessary in order

TABLE VI-1 - SPECIFICATION OF GRINDING MACHINE

Machine Number		Machine No. 1	Machine No. 2	Machine No. 3
Machine Name		Filamatic 10" Hydraulic Universal Grinding Machine	Cincinnati 12" Hydraulic Universal Grinding Machine	Heald Controlled-Force Internal Grinding Machine Centri-Matic 1CF70
Capacity	Max Work Dia.	10"	12"	4"
	Max Work Length	24"	36"	2-1/4"
Speeds	Wheel Size	12" x 1" x 5"	14" x 1" x 5"	5"
	Work Speed	40 - 450 rpm	59 - 750 rpm	0 - 1000 rpm
	Wheel Speed	2060, 2480 rpm	1730 rpm	8000 rpm
	Infeed Speed	0 - 0.04 in/min	By hand	Controlled Force
	Traverse Speed	0 - 20 ft/min	0 - 24 ft/min	
Special Feature		Plunge Grinding	High Work Speed	Normal Force 30 - 300 lbs

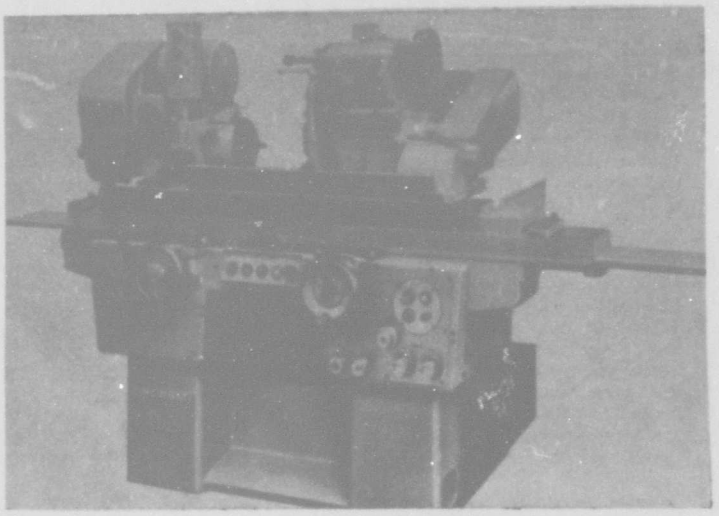

FIGURE VI-1 - PHOTOGRAPH OF GRINDING MACHINE #1

FIGURE VI-2 - PHOTOGRAPH OF GRINDING MACHINE #2

FIGURE VI-3 - PHOTOGRAPH OF GRINDING MACHINE #3

FIGURE VI-4 - MOUNTING THE MICROSCOPE ON THE WHEEL COVER

to select items to measure. The items of greatest importance are tabulated in Table VI-2 .

In the work under this contract, only a few items have been measured due to the limits of experimental equipment and only a few primary tests have been completed due to financial reasons. For this same reason metallurgical results, such as residual stress distribution, metal flow under the ground surface, fatigue life and stress corrosion which had been planned to be measured as standards for estimating the grinding results were not completed. However, in order to clearly describe the essential factors which have direct relations to input and output variables in grinding, the selection of grinding test conditions is more important than the measuring technique.

Surface roughness measuring equipment and the microscope shown in Figures VI-5 and VI-6 respectively have been utilized at the University of Cincinnati as measuring devices. Other measuring equipment is described in other sections of the report.

VI.3 Selection of Testing Conditions

VI.3.1 Introduction

Experimental studies of grinding where the grinding results are measured by changing easily-varied parameters of the grinding machine are not useful in improving the grinding process. This kind of grinding experiment has,

TABLE VI-2 - MEASUREMENT ITEMS

	Items	Before(B) During(D) After (A)	Measuring Method
Cutting Edge Condition (Wheel Charac.)	Contact Area	B, D, A	Special Microscope*
	Successive Cutting Edge Spacing (Number of Cutting Edges)	B, A	Special Microscope*
	Wheel Wear	A	Step Method
	Wheel Surface Condition	D	Microscope
	Wheel Life	D	From Contact Area & Grinding Force Information
Machine Tool Condition	Dynamic Stiffness	D	TFA
	Vibration & Chatter	D	TFA
Chip Formation Mechanism	Grinding Force	D	Dynamometer*
	Force Intensity	D	From Contact Area & Grinding Force Information
	Grinding Temperature	D	Pyrometer
Grinding Results	Stock Removal	A	Work Diameter Measurement
	Surface Roughness	A	Profilometer
	Grinding Action	A	From Wheel Wear & Stock Removal Information
	Chip Shape	A	Microscope
	Structure Deformation	A	Single Cutting Method
	Residual Stress	A	Special Beam Deflection Method

* SPECIALLY BUILT EQUIPMENT

FIGURE VI-5 - SURFACE ROUGHNESS MEASURING EQUIPMENT

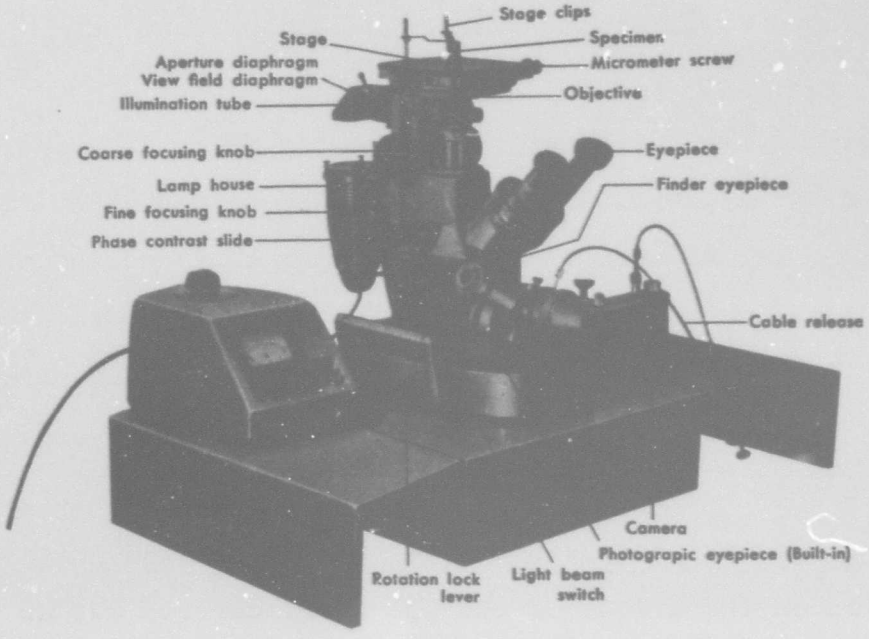

FIGURE VI-6 - PHOTOGRAPH OF MICROSCOPE

however, been tried again and again, and great amounts of complicated data have been obtained which serve only to confuse the process.

As described in Section II, which is the foundation of this report, the fundamental consideration for improving practical grinding is the cutting model in grinding as shown in Figure VI-7 . The analysis of a two-dimensional cutting model has resulted in some improvement of the single point cutting process. The analysis of the model of Figure VI-7 has resulted in some improvement of the grinding process, and *even more* improvements are expected to result in the future.

From the above mentioned point of view, grinding tests are first carried out by changing conventional variables and then carried out under the grinding test conditions which are selected based on the cutting model in grinding.

VI.3.2 Conventional Test Condition

Traditional experimental studies on HSTRA grinding have resulted in the conclusions that to improve the grinding process it is necessary to reduce the wheel speed and to increase the work speed.

The considerations of variables such as wheel, work and infeed speeds are also important in this study because this study is aimed at the improvement of grinding efficiency.

The conventional grinding tests of this study with special attention on the effect of the speed are carried out as follows:

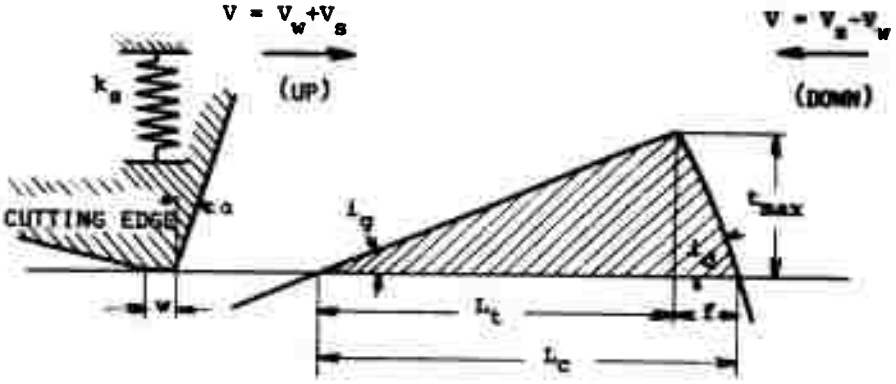

FIGURE VI-7 - GRINDING MODEL

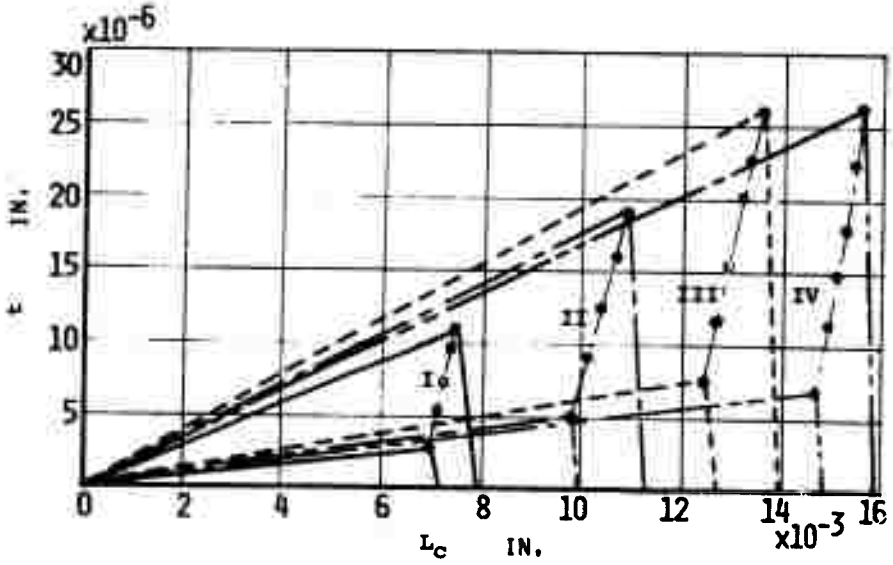

FIGURE VI-8 - UNDEFORMED CHIP GEOMETRY FOR TABLE VI-3

(1) Plunge grinding

(a) Work speed is changed in a certain range with constant depth of wheel.

(b) Work speed is changed in a certain range with constant infeed per unit time.

(2) Traverse Grinding

Work speed is changed in a certain range with constant depth of wheel.

An example of the grinding test conditions selected in the above mentioned way and the change of undeformed chip shape with the grinding test conditions are shown in Table VI-3 to VI-5 and Figure VI-8 to VI-10 as follows:

Table VI-3	(1)(a)
Table VI-4	(1)(b)
Table VI-5	(2)
Figure VI-8	From Table VI-3
Figure VI-9	From Table VI-4
Figure VI-10	From Table VI-5

It should be noted from these figures that the influence of the conventional grinding conditions on the undeformed chip shape, which is the basic consideration for wheel-work interaction, is very complicated and that the effects of speed on grinding results can not be analyzed by the conventional grinding conditions.

TABLE VI-3 - CONVENTIONAL TEST CONDITIONS FOR PLUNGE GRINDING
(CUTTING DEPTH OF WHEEL CONSTANT)

TEST NO.	WORKING CONDITION				UNDEFORMED CHIP SHAPE					RESULTS			
	WORK SPEED	IMPEED SPEED	CUTTING DEPTH OF WHEEL	$K_v=V_w/V_s$	i_g	t_{max}	L_c	T_c	H_{max}	F_t	F_t/d	F_t/t_{max}	$F_t/L_c t_{max}$
	V_w ft/min	f in/min	$dx10^{-5}$in	$x10^{-3}$	min	$x10^{-6}$in	$x10^{-3}$in	$x10^{-6}$sec	$x10^{-6}$in	lbs	lbs/µin	lbs/µin	lbs/in^{2}x10^{-9}
I	62	.0018	2	10.0	1.79	3.32	6.9	5.55	.038	1.9	.095	.57	.083
	72	.0020	2	12.2	2.20	3.94	6.9	5.70	.054	2.5	.125	.63	.091
	120	.0034	2	19.4	3.41	6.11	7.3	5.76	.139	2.9	.145	.48	.066
	171	.0050	2	29.0	5.07	8.53	7.4	6.07	.294	3.5	.175	.41	.055
	232	.0066	2	37.4	6.34	10.64	7.7	6.16	.499	5.1	.255	.48	.062
	269	.0080	2	45.6	7.72	12.20	7.9	6.35	.704	6.0	.300	.49	.062
	288	.0082	2	46.5	7.75	12.54	8.2	6.43	.757	4.8	.240	.38	.046
II	65	.004	4	10.3	1.84	5.03	10.0	7.85	.041	2.6	.065	.52	.052
	123	.007	4	19.5	3.42	9.16	10.4	8.06	.144	5.2	.130	.57	.055
	180	.010	4	28.6	4.95	12.94	10.7	8.26	.304	6.9	.172	.53	.049
	238	.013	4	37.8	6.40	16.45	11.1	8.46	.524	7.8	.195	.47	.042
	295	.016	4	46.8	7.79	19.61	11.4	8.66	.787	8.3	.207	.43	.038
III	74	.008	7	12.5	2.21	7.61	12.5	10.47	.055	5.0	.071	.66	.053
	108	.011	7	18.3	3.20	10.93	12.7	10.60	.117	10.5	.150	.96	.075
	158	.016	7	26.8	4.61	15.56	13.1	10.79	.247	13.1	.187	.84	.064
	210	.022	7	35.6	6.01	20.08	13.4	10.99	.428	15.8	.226	.79	.059
	243	.025	7	41.2	6.89	22.82	13.6	11.11	.568	18.6	.266	.81	.059
	276	.029	7	46.8	7.74	25.45	13.9	11.23	.724	20.8	.297	.82	.059
IV	57	.008	10	9.7	1.74	7.22	14.8	12.43	.034	7.3	.073	1.01	.068
	90	.013	10	15.2	2.69	11.13	15.0	12.55	.084	11.9	.119	1.06	.071
	124	.018	10	21.0	3.68	15.11	15.3	12.68	.154	13.9	.139	.92	.060
	157	.023	10	26.6	4.61	18.84	15.5	12.80	.245	15.9	.159	.85	.055
	191	.028	10	32.4	5.55	22.56	15.7	12.93	.360	17.3	.173	.77	.049
	234	.034	10	39.0	6.55	26.61	15.9	12.75	.522	19.3	.193	.72	.045

Wheel Speed V_s = 6000 ft/min.

TABLE VI-4 - CONVENTIONAL TEST CONDITIONS FOR PLUNGE GRINDING
(INFEED SPEED CONSTANT)

WORKING CONDITION				UNDEFORMED CHIP SHAPE					RESULTS
Work Speed	Infeed Speed	Cutting Depth of Wheel	K_v	i_g	t_{max}	L_c	T	H_{max}	Surface Roughness
ft/min	in/min	$x10^{-5}$in	$x10^{-3}$	(min)	$x10^{-6}$in	$x10^{-3}$in		$x10^{-6}$in	RMS
42	0.013	28.2	7.7	1.20	8.82	25.77	3.3	.019	
85		13.9	15.6	2.39	12.23	18.51	2.3	.071	18
130		9.1	23.9	3.61	14.75	15.39	1.9	.16	
150		7.9	27.5	4.11	15.49	14.54	1.8	.22	
200		5.9	36.7	5.39	17.27	13.01	1.6	.38	
260		4.5	47.7	6.87	18.63	11.89	1.5	.62	20
325		3.6	59.7	8.39	19.47	11.20	1.4	.96	
410		2.9	76.3	10.41	20.37	10.79	1.3	1.52	19
43	0.033	70.0	7.9	1.22	14.70	40.49	5.2	.02	
85		35.4	15.6	2.39	19.79	29.28	3.7	.071	25
150		20.0	27.5	4.11	25.30	22.68	2.8	.22	
200		15.0	36.7	5.39	28.56	20.15	2.5	.38	
260		11.6	47.7	6.87	31.55	18.3	2.2	.62	27
300		10.0	55.1	7.83	32.97	17.4	2.1	.82	
320		9.4	58.7	8.28	33.60	17.1	2.1	.93	
410		7.3	76.3	10.41	35.91	15.9	1.9	1.52	28

Wheel Speed V_s = 6000 ft/min. Grinding Fluid: CIMCOOL

Dressing Condition: Depth of Cut 0.0005"
Feed Speed 1.8 ft/min.

TABLE VI-5 - CONVENTIONAL TEST CONDITIONS FOR TRAVERSE GRINDING

WORKING CONDITION						UNDEFORMED CHIP SHAPE			
Work Speed RPM	Traverse Speed ft/min	Work Dia. in.	Work Speed ft/min	K_v $x10^{-3}$	$\frac{1}{K_R}$	i_g (min)	t_{max} $x10^{-6}$in	L_c $x10^{-3}$in	T microsec
59	1.22		32.6	5.1		1.33	12.0	30.5	23.5
75	1.56		41.5	6.5		1.70	15.2	30.5	23.5
120	2.50		66.3	10.3		2.67	23.8	30.9	23.7
190	3.96	2.1	105	16.4	6.7	4.20	37.1	31.3	24.07
300	6.25		166	25.9		6.55	57.4	31.9	24.51
460	9.59		255	39.8		9.74	85.4	32.9	25.16
720	15.05		397	61.0		14.34	124.9	34.3	26.19
59	1.22		42.4	6.6		1.36	14.7	26.2	20.1
75	1.56		54.0	8.4		1.73	18.5	26.2	20.1
120	2.50		86.3	13.4		2.73	29.0	26.5	20.3
190	3.96	2.75	136	21.3	5.1	4.28	45.1	26.9	20.7
300	6.25		216	33.7		6.61	68.8	27.6	21.1
460	9.59		331	50.9		9.66	99.1	28.4	21.7
720	15.05		509	81.0		14.53	144.8	30.1	22.9

Dressing Condition: Depth of Cut 0.0005"
Feed Speed 4 ft/min.

Grinding Fluid: CIMCOOL 1/60

TABLE VI-6 - THE GEOMETRICAL VALUES OF UNDEFORMED CHIP SHAPES

TEST SERIES	K_v	V_w fpm	K_d $x10^{-4}$	d $x10^{-3}$ in.	i_g $x10^{-4}$ rad.	f/R_s $x10^{-4}$	L_t/R_s $x10^{-2}$	f/L_c $x10^{-2}$	t_{max}/R_s $x10^{-6}$
T 1	.02	120	2.342	1.64	10.91	2	.917	2.13	10
2	.04	240	.647	.45	21.00	4	.476	7.74	10
3	.06	360	.327	.23	30.30	6	.330	15.38	10
4	.08	480	.214	.15	38.80	8	.257	23.70	10
L 1	.02	120	1.014	.709	10.91	2	.6	3.22	6.54
2	.04	240	1.008	.705	21.00	4	.6	6.25	12.58
3	.06	360	1.002	.702	30.30	6	.6	9.09	18.17
4	.08	480	.996	.699	38.80	8	.6	11.80	23.34
F 1	.05	300	.143	.1	25.73	5	.211	19.19	5.91
2	.05	300	.714	.5	25.73	5	.502	9.06	12.91
3	.05	300	1.428	1.0	25.73	5	.720	6.49	18.54
4	.05	300	2.857	2.0	25.73	5	1.029	4.69	26.46
C 1	.04	240	.378	.265	21.0	4	.360	10.00	7.53
2	.06	360	.820	.574	30.3	6	.540	10.00	16.35
3	.08	480	1.40	.98	38.8	8	.720	10.00	28.01
4	.10	600	2.11	1.48	46.8	10	.900	10.00	42.19

$K_p = \delta/R_s = .01$, $K_R = R_w/R_s = .214$

$R_s = 7.0$ in. , $V_s = 6{,}000$ fpm

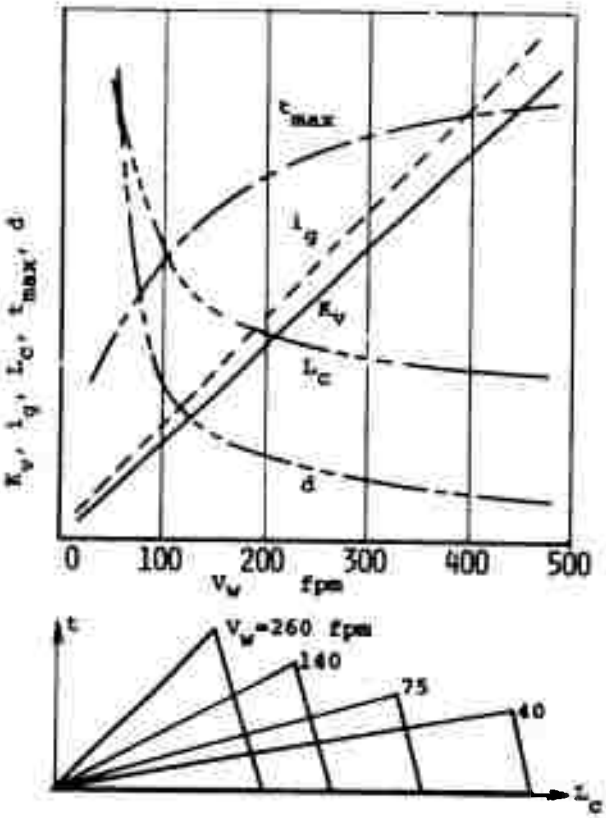

FIGURE VI-9 - CHIP SHAPE FOR TABLE VI-4

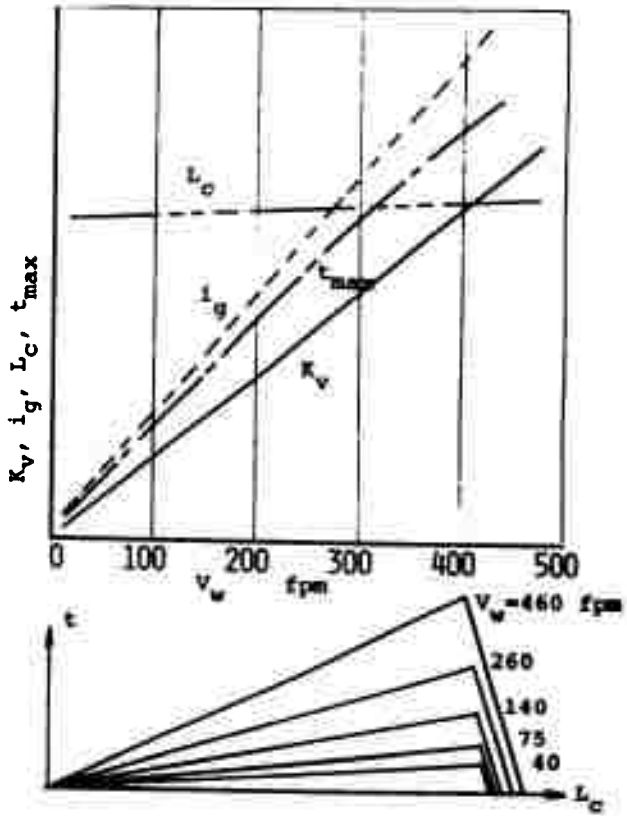

FIGURE VI-10 - CHIP SHAPE FOR TABLE VI-5

VI.3.3 Standard Grinding Test Condition (S.G.T.C.)

Grinding results are obviously produced as a result of wheel-work interaction. In order to describe the relation between input and output variables in grinding, the experimental grinding tests should be developed in such a way that the change of grinding results is analyzed by systematically changing the various values which determine the grinding model. From the above mentioned point of view, four sets of standard grinding test conditions have been selected as follows:

(1) T series	t_{max} constant
(2) L series	L_t constant
(3) F series	f constant
(4) C series	similar chip geometry

Figure VI-11 shows the relation between these four series series of grinding test conditions and the undeformed chip shape. In order to be able to select the range of the actual values of undeformed chip shape, and from these the conventional grinding conditions such as wheel speed, work speed, and depth of wheel, the detailed information on practical grinding and chip geometry in grinding are required. In this experiment the standard grinding test conditions have been determined for constant wheel speed, grinding wheel and dressing conditions such that the values of the undeformed chip shape change in the following range:

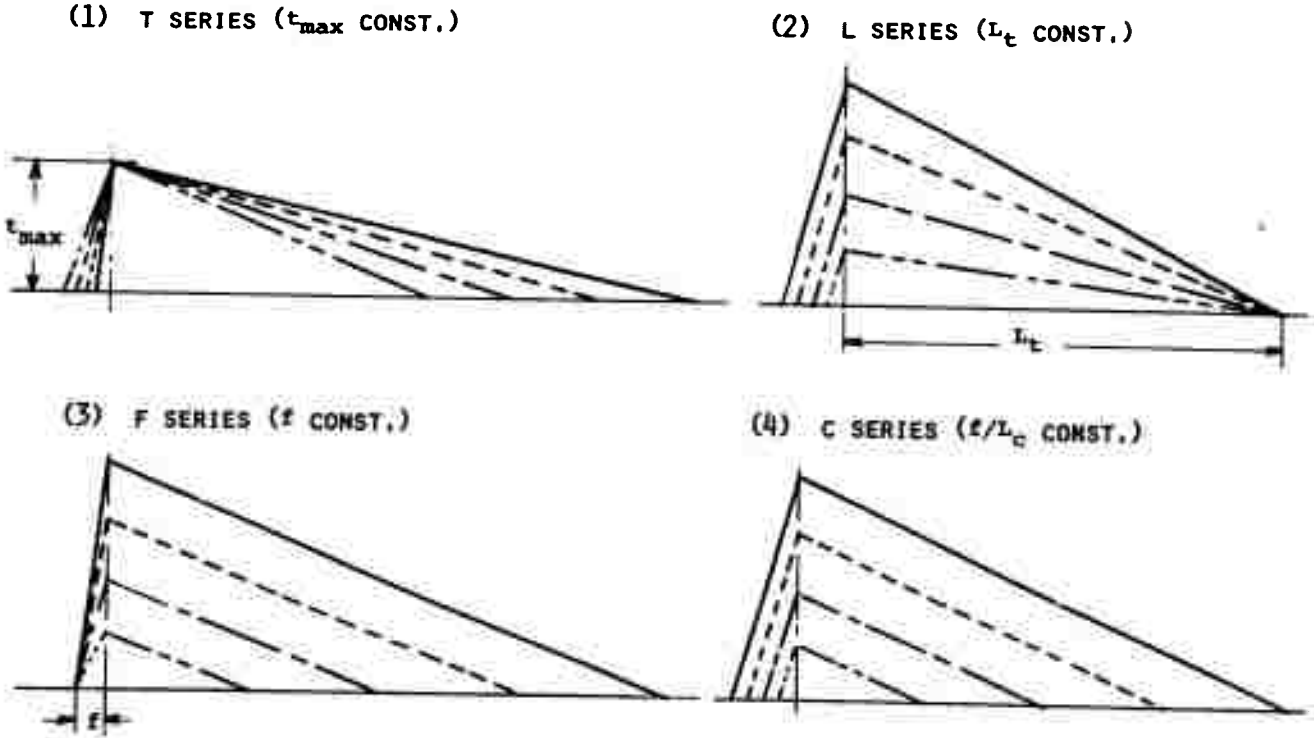

FIGURE VI-11 - CHIP SHAPE OF THE SGTC

$$t_{max}/R_s = 5 \sim 50 \times 10^{-6}$$

$$L_t/R_s = 2 \sim 10 \times 10^{-3}$$

$$f / R_s = 2 \sim 10 \times 10^{-4}$$

$$f / L_c = 2 \sim 25 \times 10^{-2}$$

In these cases the ratio K_v of the workspeed to the wheel speed is changed from .01 to .1. Consequently the changing range of the cutting depth of the wheel (d) and the work speed (V_w) is as follows:

$$d = 1 \sim 20 \times 10^{-4} \text{in}$$

$$V_w = 100 \sim 600 \text{ sfpm}$$

Figure VI-12 shows the relation between the speed ratio K_v and the cutting depth of the wheel d in the four series of the standard grinding test conditions.

As can be seen in this figure, the four series of standard grinding test conditions correspond to four different trends between the two physical values. In other words, the cutting depth of the wheel d increases in the C series, decreases in the T series and remains constant in the L series with an increase of the speed ratio K_v. Furthermore in the F series, the cutting depth of the wheel d changes and the speed ratio K_v remains constant.

In this kind of systematic grinding testing, the relation between grinding results and various variables can be directly analyzed.

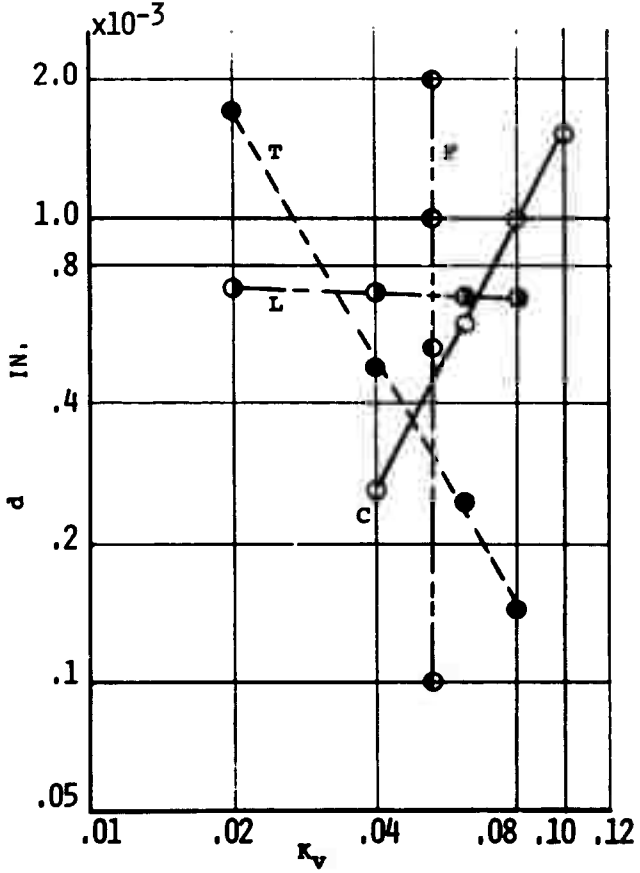

FIGURE VI-12 - RELATION BETWEEN d AND K_v IN SGTC

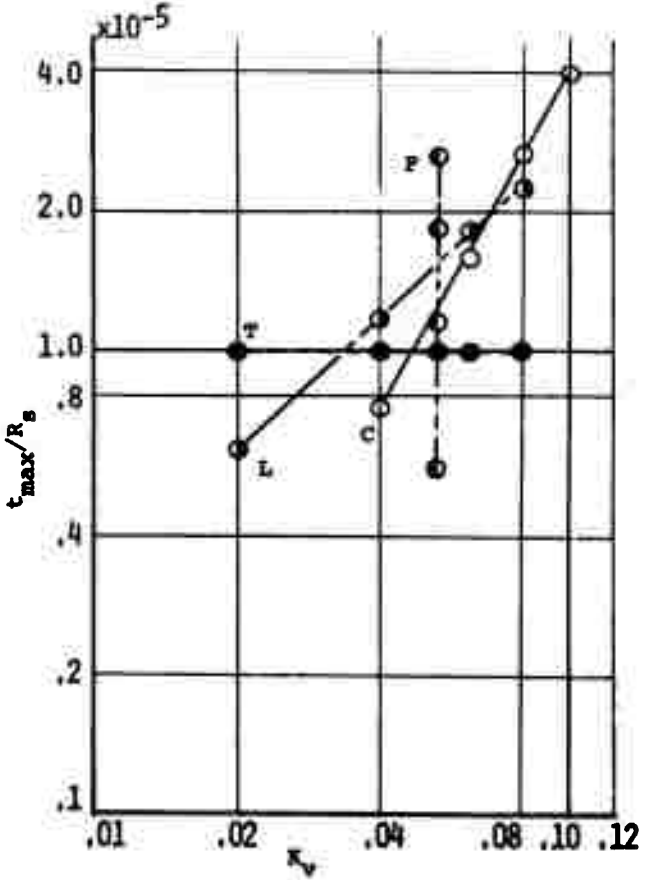

FIGURE VI-13 - RELATION BETWEEN t_{max}/R_s AND K_v IN SGTC

Figure VI-13 shows the relation between the standard grinding test conditions and the maximum cutting depth of grain. This quantity has been considered to be very important in traditional grinding tests.

VI.4 Experimental Results and Discussion

VI.4.1 Conventional Grinding Test

Conventional grinding test results are summarized in Table VI-3 to VI-5. Figure VI-14 shows variations of the tangential grinding force (F_t) with the work speed in plunge grinding under constant cutting depth of wheel. As generally known, the tangential grinding force (F_t) increases with increasing work speed.

In practical grinding operations if the wheel-workpiece interaction is similar to that predicted by the geometrical considerations explained in Section II, a value proportional to the specific grinding resistance can be obtained using the following assumptions:

The tangential grinding force (F_t) is made up by

$$F_t = \sum_{i-1}^{n} f_i = n\, f_{avg} \qquad \text{(VI.4.1)}$$

where:

n = number of cutting edges acting on the interference zone at one instant of time.

f_i = individual force on each grain.

f_{avg} = average cutting force per grain.

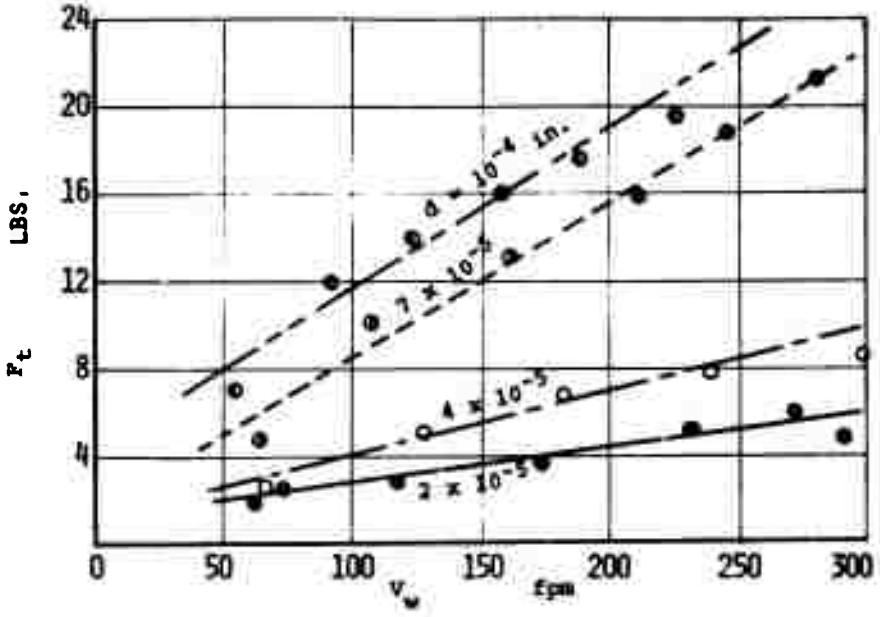

FIGURE VI-14 - VARIATION OF GRINDING FORCE WITH WORK SPEED

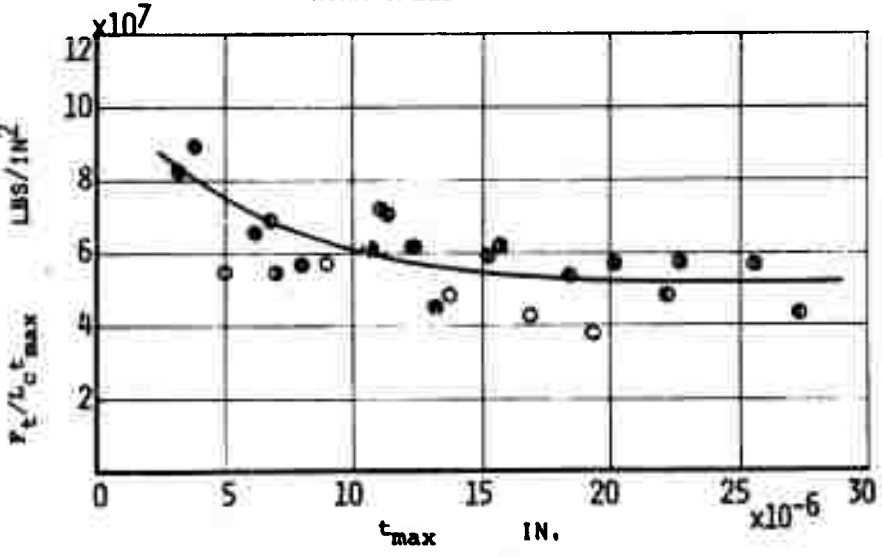

FIGURE VI-15 - RELATION BETWEEN t_{max} AND $F_t/L_c t_{max}$

The specific cutting resistance σ_t can be defined as follows:

$$\sigma_t = \frac{f_i}{s_i} = \frac{f_{avg}}{s_{avg}} = \frac{F_t/n}{s_{avg}} \qquad \text{(VI.4.2)}$$

where:

s_i = individual cutting sectional area

s_{avg} = average cutting sectional area

Assume that the number of cutting edges is linearly related to the area of the interference zone, since the wheel width B is constant, and therefore

$$= k_1 L_c \qquad \text{(VI.4.3)}$$

Also, assume that the cutting sectional area is proportional to the cutting depth of the grain:

$$s_{avg} = k_2 t_{max} \qquad \text{(VI.4.4)}$$

Then from Equations (VI.4.2,.3, and .4)

$$\sigma_t = K \frac{F_t}{L_c t_{max}} \qquad \text{(VI.4.5)}$$

The size effect can be shown as follows:

$$\sigma_t = f(t_{max}) \qquad \text{(VI.4.6)}$$

Figure VI.15 shows the relation between t_{max} and $F_t/L_c t_{max}$. In this grinding test F_t, L_c, and t_{max} varied in a wide range while $F_t/L_c t_{max}$ remained nearly constant, increasing slightly with decreasing t_{max}.

From these results, the wheel-workpiece interaction in practical grinding has been found to compare quite well with the geometrical theory.

VI.4.2 Standard Grinding Test

HSTRA grinding tests have been carried out under all series of the standard grinding test conditions which were selected based on the cutting model in grinding. In the HSTRA grinding tests, only three kinds of grinding results, that is, stock removal, wheel wear and surface roughness were measured. Therefore, the information obtained from the tests is insufficient to completely analyze all phenomena in grinding. However, the grinding tests performed under the standard grinding test conditions are sufficient to determine which variables control stock removal, wheel wear and surface roughness.

In these grinding tests, not only standard up grinding but also down grinding tests were carried out.

The grinding test results are summarized in Table VI-7 to VI-14 for each series, and for up and down grinding. Figure VI-16 to VI-18 show variations of stock removal, wheel wear and surface roughness respectively with conventional variables such as work speed and cutting depth of wheel, which have actually been changed in the grinding tests.

It should be noted from these figures that completely different trends can be obtained for each series. In other words stock removal, for example, increases with increasing work speed for some cases, decreases with increasing work speed for other cases and is independent of work speed for still other cases. This indicates that traditional grinding

TABLE VI-7 - UP GRINDING RESULTS FOR T-SERIES

TEST NO. & K_v,d	PASS NO.	INFEED $x10^{-3}$ in.	CUTTING LENGTH in.	STOCK REMOVAL $x10^{-3}$ in^3				WHEEL WEAR $x10^{-3}$ in^3				GRINDING RATIO				SURFACE ROUGHNESS R_{max} $x10^{-3}$ in.			
				4340	R.41	W	T	4340	R.41	W	T	4340	R.41	W	T	4340	R.41	W	T
UT-1	3	4.95	7.28	26.8	21.7	22.4	19.5	3.40	3.30	19.2	4.89	7.89	6.57	1.16	3.92				
.02	5	8.25	12.15	48.7	41.9	38.2	39.0	9.90	13.2	36.3	25.1	4.92	3.18	1.05	1.56				
1.64	10	16.50	24.3	105.0	99.5	92.1	79.4	17.9	33.0	91.0	116.5	5.87	3.00	1.01	.68				
	15	24.75	36.45	152.0	145.0	140.0	103.2	66.1	105.0	175.0	245.0	2.30	1.37	.80	.42				
	16,20	33.0	48.6	193.0	195.0	189.0	112.5	95.6	165.0	205.0	248.0	2.02	1.18	.93	.45	1.150	.550	.650	.725
UT-2	5	2.25	3.78	12.3	11.7	12.7	7.62	.69	3.25	3.25	3.77	17.8	3.60	3.91	2.02				
.04	10	4.50	7.55	31.8	25.6	26.1	21.7	2.13	19.5	13.0	12.6	15.0	1.31	2.00	1.72				
.45	20	9.00	15.1	61.5	48.4	53.3	48.6	4.23	32.5	30.7	25.1	14.5	1.49	1.74	1.94				
	30	13.5	22.65	97.6	83.0	83.0	71.8	6.50	56.0	52.0	43.9	15.0	1.48	1.60	1.84				
	50	22.50	37.8	163.0	142.0	139.0	131.8	11.4	91.0	91.0	87.8	14.3	1.56	1.52	1.49	.325	.350	.450	.200
UT-3	5	1.25	1.89	4.64	6.50	5.43	8.0	.37	3.54	1.93	3.14	12.0	1.83	2.82	2.55				
.06	10	2.5	3.78	-	15.9	13.7	16.7	-	9.32	6.43	6.27	-	1.70	2.14	2.68				
.23	20	5.0	7.56	35.6	33.9	31.1	34.9	3.94	24.1	12.5	12.4	9.05	1.38	2.48	2.81				
	30	7.5	11.34	50.3	50.9	43.4	51.3	7.13	37.1	20.9	21.9	7.05	1.37	2.08	2.35				
	50	12.5	18.9	87.7	86.4	76.6	84.4	15.4	51.5	33.7	40.8	5.70	1.67	2.28	2.07	.200	.150	.200	.122
UT-4	5	.75	1.26	5.32	3.59	3.59	4.14	.35	1.78	1.65	1.88	15.3	2.02	2.18	2.20				
.08	10	1.50	2.52	12.7	10.00	9.34	8.28	.70	6.38	5.40	5.00	18.2	1.57	1.73	1.66				
.15	20	3.00	5.04	19.8	18.7	19.4	18.1	2.10	11.1	12.8	9.42	9.40	1.69	1.52	1.92				
	30	4.50	7.56	31.2	29.5	30.2	25.6	4.85	22.3	20.7	18.8	6.43	1.32	1.45	1.33				
	50	7.50	12.6	51.7	49.6	50.8	45.9	6.25	31.3	28.7	25.1	8.23	1.58	1.74	1.80	.144	.100	.133	.100

TABLE VI-8 - UP GRINDING RESULTS FOR L-SERIES

TEST NO. & K_v	PASS NO.	INFEED $\times 10^{-3}$ in.	CUTTING LENGTH in.	STOCK REMOVAL $\times 10^{-3}$ in^3				WHEEL WEAR $\times 10^{-3}$ in^3				GRINDING RATIO				SURFACE ROUGHNESS H_{max} 10^{-3} in.			
				4340	T	W	R.41	4340	T	W	R.41	4340	T	W	R.41	4340	T	W	R.41
UL-1	5	3.55	12.0	26.55	18.92	22.20	17.61	1.23	12.25	13.48	7.35	21.6	1.54	1.65	2.40				
.02	10	7.09	24.0	52.01	37.85	43.67	36.65	2.45	24.50	29.40	14.70	21.3	1.54	1.50	2.50				
.709	20	14.18	48.0	103.66	82.59	85.16	79.04	4.90	53.90	49.00	34.30	21.0	1.53	1.73	2.30				
	30	21.27	72.0	155.67	124.79	129.20	126.11	7.35	83.30	77.18	58.80	21.3	1.49	1.67	2.14				
	50	35.45	120.0	256.42	206.65	215.82	214.49	12.03	138.43	139.65	112.70	21.3	1.48	1.54	1.90	0.300	0.175	0.275	0.250
UL-2	5	3.53	6.0	23.04	12.83	12.82	17.92	2.45	9.89	7.76	11.45	9.44	1.30	1.65	1.56				
.04	10	7.05	12.0	45.72	36.72	34.19	34.79	4.03	31.85	20.83	22.05	11.30	1.15	1.64	1.58				
.705	20	14.10	24.0	96.05	77.36	76.93	78.72	9.78	71.05	47.78	53.90	9.83	1.09	1.60	1.46				
	30	21.15	36.0	145.32	118.00	118.61	118.07	12.95	91.88	77.18	85.75	11.20	1.29	1.53	1.38				
	50	35.25	60.0	242.79	195.71	197.32	199.25	26.63	124.95	143.33	139.65	9.10	1.56	1.37	1.43	0.500	0.300	0.450	0.350
UL-3	5	3.51	4.0	22.11	16.42	15.00	11.69	2.45	7.35	9.80	7.25	9.04	2.23	1.55	1.60				
.06	10	7.02	8.0	44.92	37.02	35.93	26.47	4.90	18.38	19.60	20.83	9.15	2.02	1.83	1.28				
.702	20	14.04	16.0	92.92	76.14	75.00	68.06	9.35	56.35	46.50	42.88	9.40	1.35	1.61	1.59				
	30	21.06	24.0	140.28	114.56	114.41	107.94	16.50	95.55	90.65	72.28	5.72	1.21	1.26	1.49				
	50	35.10	40.0	235.29	190.35	191.15	183.56	29.40	186.20	171.15	116.38	8.00	1.02	1.11	1.57	0.550	0.300	0.450	0.400
UL-4	5	3.50	3.0	19.86	12.85	13.65	13.10	3.35	4.90	12.25	7.35	5.90	2.63	1.11	1.78				
.08	10	6.99	6.0	40.38	32.47	32.07	31.58	7.70	23.28	22.05	17.15	5.25	1.39	1.45	1.84				
.699	20	13.98	12.0	88.17	67.99	71.98	67.20	16.50	83.30	68.60	61.25	5.35	0.82	1.04	1.10				
	30	20.97	18.0	132.26	103.51	105.08	105.16	26.63	120.05	110.25	93.10	4.96	0.86	0.96	1.13				
	50	34.95	30.0	223.46	169.81	176.04	176.39	36.75	225.40	220.05	159.25	6.06	0.75	0.80	1.10	0.600	0.400	0.500	0.450

TABLE VI-9 - UP GRINDING RESULTS FOR F-SERIES

TEST NO.	PASS NO.	INFEED $x10^{-3}$ in.	CUTTING LENGTH in.	STOCK REMOVAL $x10^{-3}$ in^3				WHEEL WEAR $x10^{-3}$ in^3				GRINDING RATIO				SURFACE ROUGHNESS R_{max} $x10^{-3}$ in.			
				4340	T	W	R.41	4340	T	W	R.41	4340	T	W	R.41	4340	T	W	R.41
UF-1	5	1.0	2.51	2.23	1.86	0.75	1.12	0.40	1.58	2.11	2.30	5.64	1.18	0.35	0.49				
.05	10	2.0	5.02	8.93	7.46	5.98	8.23	0.79	3.30	7.92	4.35	11.28	2.26	0.76	1.89				
.1	20	4.0	10.04	23.44	20.50	19.42	24.33	1.85	6.60	14.65	14.91	12.69	3.11	1.33	1.63				
	30	6.0	15.06	37.95	33.18	31.75	35.55	5.94	14.83	21.24	22.51	6.39	2.24	1.50	1.58				
	50	10.0	25.10	70.70	60.39	56.03	62.87	15.17	34.17	36.07	49.08	4.66	1.77	1.55	1.28	0.215	0.135	0.150	0.150
UF-2	5	2.5	4.40	14.41	5.19	9.28	8.54	1.58	8.92	7.92	5.54	9.11	0.58	1.17	1.54				
.05	10	5.0	8.80	31.79	20.75	25.61	22.66	3.17	20.00	23.75	14.78	10.04	1.04	1.08	1.53				
.5	20	10.0	17.60	69.12	50.77	55.29	54.98	6.86	40.59	41.43	37.87	10.07	1.25	1.34	1.45				
	30	15.0	26.40	106.45	81.16	86.84	87.29	9.50	69.09	62.97	64.92	11.21	1.18	1.38	1.35				
	50	25.0	44.00	178.52	140.83	146.59	149.69	13.20	120.55	115.45	112.42	13.53	1.17	1.27	1.33	0.450	0.225	0.300	0.290
UF-3	5	5.0	6.15	30.14	20.06	21.95	14.65	2.55	12.47	12.29	7.38	11.84	1.61	1.79	1.99				
.05	10	10.0	12.30	65.36	46.69	51.95	42.85	5.34	37.92	40.46	42.75	12.23	1.23	1.28	1.00				
1.0	20	20.0	24.60	134.71	97.02	109.39	102.54	15.52	124.18	104.84	121.64	8.68	0.78	1.04	0.84				
	30	30.0	36.90	200.67	148.09	162.07	157.47	44.79	204.85	179.40	184.24	4.47	0.72	0.90	0.86				
	50	50.0	61.50	328.97	249.49	269.27	266.23	195.43	368.73	322.41	321.40	3.45	0.68	0.84	0.83	1.075	0.670	0.650	0.625
UF-4	5	7.5	7.50	38.64	28.78	31.68	30.63	7.35	25.70	28.25	49.62	5.25	1.12	1.12	0.62				
.05	10	15.0	15.00	79.03	58.28	70.47	70.53	17.1	118.71	69.22	102.81	4.60	0.49	1.02	0.69				
2.0	20	30.0	30.00	147.53	121.17	134.17	138.56	110.1	225.64	228.26	229.53	1.34	0.53	0.56	0.60				
	25	37.5	37.50	182.30	153.87	165.85	172.76	193.0	2 4.25	323.69	328.01	0.95	0.54	0.51	0.53	1.050	0.635	0.600	0.645

TABLE VI-10 - UP GRINDING RESULTS FOR C-SERIES

TEST NO.	PASS NO.	INFEED $x10^{-3}$ in.	CUTTING LENGTH in.	STOCK REMOVAL $x10^{-3}$ in^3				WHEEL WEAR $x10^{-3}$ in^3				GRINDING RATIO				SURFACE ROUGHNESS H_{max} $x10^{-3}$ in.			
				4340	T	W	R.41	4340	T	W	R.41	4340	T	W	R.41	4340	T	W	R.41
UC-1	5	1.33	4.0	7.17	3.75	2.67	4.12	1.32	3.96	6.60	4.35	5.43	0.95	0.41	0.95				
.04	10	2.65	8.0	15.84	12.38	10.69	14.99	2.64	11.88	11.88	8.71	6.00	1.04	0.90	1.72				
.265	20	5.30	16.0	34.70	29.63	27.11	33.74	6.60	23.75	18.47	18.21	5.26	1.25	1.47	1.85				
	30	7.95	24.0	56.20	49.51	43.53	49.48	10.56	29.03	29.03	23.75	5.32	1.71	1.50	2.08				
	50	13.25	40.0	93.92	77.64	74.45	81.72	18.50	47.50	42.22	38.26	5.07	1.63	1.76	2.14	0.225	0.110	0.165	0.150
UC-2	5	2.87	4.0	18.52	15.14	16.17	13.27	2.04	5.09	7.63	14.00	9.10	2.97	2.12	0.95				
.06	10	5.74	8.0	40.38	34.34	34.59	30.97	4.07	17.81	16.54	29.26	9.92	1.93	2.09	1.06				
.574	20	11.48	16.0	82.98	69.78	75.57	68.95	7.63	48.35	50.89	61.07	10.87	1.44	1.49	1.13				
	30	17.22	24.0	128.92	104.85	111.66	105.08	12.72	76.34	85.25	87.79	10.13	1.37	1.31	1.20				
	50	28.70	40.0	215.60	174.26	178.20	175.13	24.18	151.41	178.13	165.41	8.92	1.15	1.00	1.06	0.430	0.360	0.275	0.265
UC-3	5	4.90	4.0	29.27	21.77	21.47	19.26	2.36	11.78	14.73	11.78	12.4	1.85	1.46	1.63				
.08	10	9.80	8.0	52.55	45.33	48.41	46.72	5.89	47.12	38.29	41.23	8.93	0.96	1.26	1.13				
.98	20	19.60	16.0	110.40	89.95	96.45	95.93	22.4	143.73	132.54	135.48	4.92	0.63	0.73	0.71				
	30	29.70	40.0	163.65	129.22	143.03	141.57	69.5	239.15	221.48	217.95	2.35	0.54	0.65	0.65	0.575	0.500	0.475	0.325

TABLE VI-11 - DOWN GRINDING RESULTS FOR T-SERIES

TEST NO. & K_v,d	PASS NO.	INFEED $x10^{-3}$ in.	CUTTING LENGTH in.	STOCK REMOVAL $x10^{-3}$ in^3				WHEEL WEAR $x10^{-3}$ in^3				GRINDING RATIO				SURFACE ROUGHNESS R_{max} $x10^{-3}$ in.			
				4340	T	W	R.41	4340	T	W	R.41	4340	T	W	R.41	4340	T	W	R.41
DT-1	3	4.95	9.28	19.0	19.6	19.3	16.4	9.3	15.4	9.3	17.3	2.11	1.27	2.08	.932				
.02	5	8.25	12.15	39.0	39.2	40.4	29.6	12.2	37.1	27.8	52.0	3.25	1.05	1.45	.569				
	10	16.50	24.3	89.5	84.2	85.1	63.7	34.0	80.3	77.2	132.9	2.61	1.03	1.10	.483				
	15	24.75	36.45	131.0	129.9	121.1	96.9	114.2	142.0	157.6	242.3	1.15	.91	.77	.401				
	20	33.00	48.6	171.4	173.0	161.5	-	169.8	191.4	194.6	-	1.01	.90	.82	-	.875	.600	.600	.800
DT-2	5	2.25	3.78	11.0	9.5	8.80	9.30	3.08	6.50	6.73	5.77	3.90	1.46	1.30	1.61				
.04	10	4.50	7.55	23.9	20.0	18.6	20.4	6.74	16.5	12.3	17.3	3.55	1.21	1.51	1.18				
	20	9.0	15.1	55.8	45.7	45.4	50.1	12.3	36.8	30.7	31.8	4.53	1.22	1.48	1.57				
	30	13.5	22.65	87.3	71.3	71.3	72.9	29.5	49.1	36.8	52.0	2.94	1.45	1.93	1.40				
	50	22.5	37.8	146.8	124.2	127.2	129.9	44.8	98.0	73.6	86.6	3.25	1.26	1.73	1.49	.363	.400	.375	.250
DT-3	5	1.25	1.89	5.72	5.87	3.46	5.76	.71	2.14	1.5	2.9	8.01	2.74	2.40	1.99				
.06	10	2.5	3.78	14.1	12.4	11.1	12.6	2.38	8.31	3.00	8.66	5.92	1.50	3.70	1.46				
	20	5.0	7.56	30.6	28.6	26.4	29.2	6.55	17.8	7.45	17.3	4.58	1.61	3.54	1.69				
	30	7.5	11.34	48.8	43.8	43.3	43.2	8.56	35.7	15.20	26.0	5.71	1.23	2.84	1.66				
	50	12.5	18.9	81.4	73.8	70.4	74.5	17.3	53.6	28.2	40.4	4.70	1.38	2.50	1.84	.215	.200	.150	1.75
DT-4	5	.75	1.26	4.66	2.30	2.76	1.09	.74	.71	1.25	.31	6.30	3.24	1.65	3.52				
.08	10	1.5	2.52	8.31	7.55	6.87	5.44	2.98	6.60	4.17	2.90	3.09	1.14	1.65	1.87				
	20	3.0	5.04	20.3	15.8	14.8	14.9	7.48	14.8	14.8	8.65	2.62	1.07	1.00	1.70				
	30	4.5	7.56	28.9	24.7	24.0	23.6	8.86	20.6	20.6	17.3	3.26	1.19	1.17	1.38				
	50	4.5	12.6	49.5	44.3	38.6	45.4	13.6	29.5	26.6	23.1	3.63	1.51	1.45	1.90	.175	.187	.150	.100

TABLE VI-12 - DOWN GRINDING RESULTS FOR L-SERIES

TEST NO. & K_v	PASS NO.	INFEED $x10^{-3}$ in.	CUTTING LENGTH in.	STOCK REMOVAL $x10^{-3}$ in^3				WHEEL WEAR $x10^{-3}$ in^3				GRINDING RATIO				SURFACE ROUGHNESS H_{max} 10^{-3} in.			
				4340	T	W	R.41	4340	T	W	R.41	4340	T	W	R.41	4340	T	W	R.41
DL-1	5	3.55	12.0	23.30	20.74	20.03	16.34	1.30	18.73	10.66	7.35	18.00	1.11	1.90	2.17				
0.02	10	7.09	24.0	50.29	43.33	42.28	38.99	2.60	39.02	20.29	18.21	18.80	1.11	2.07	2.14				
	20	14.18	48.0	101.70	83.69	87.16	85.04	3.38	72.05	37.19	39.02	30.00	1.16	2.34	2.17				
	30	21.27	72.0	154.95	126.27	134.26	130.35	4.68	108.98	59.82	62.42	33.30	1.17	2.25	2.09				
	50	35.45	120.0	257.75	210.33	222.90	218.73	5.98	181.29	119.13	124.45	42.90	1.16	1.87	1.72	0.250	0.200	0.300	0.200
DL-2	5	3.53	6.0	19.84	17.41	16.70	15.28	1.85	13.01	10.48	11.61	10.70	1.33	1.60	1.31				
	10	7.05	12.0	45.46	39.54	38.13	37.10	4.68	35.63	25.49	29.39	9.70	1.10	1.50	1.27				
	20	14.10	24.0	97.05	81.99	80.98	77.85	7.28	71.53	48.90	57.22	13.30	1.14	1.65	1.36				
	30	21.15	36.0	147.57	120.44	125.64	118.96	13.79	118.40	85.31	99.10	10.65	1.01	1.47	1.20				
	50	35.25	60.0	246.42	198.44	204.81	198.29	16.39	188.57	156.84	158.14	15.00	1.08	1.30	1.25	0.550	0.225	0.400	0.400
DL-3	5	3.51	4.0	20.05	16.30	18.45	18.50	1.60	7.28	8.38	13.00	12.50	2.24	2.20	1.42				
	10	7.02	8.0	45.38	36.14	34.43	41.98	5.24	23.41	22.11	24.97	8.65	1.54	1.56	1.68				
	20	14.04	16.0	96.98	75.47	74.89	83.60	10.92	70.23	55.14	65.03	8.70	1.07	1.36	1.28				
	30	21.06	24.0	142.83	111.97	113.93	125.23	14.05	119.13	97.54	109.76	10.15	0.94	1.18	1.15				
	50	35.10	40.0	240.28	183.54	187.86	198.16	23.67	217.96	192.47	205.48	10.10	0.85	0.98	0.97	0.575	0.400	0.425	0.400
DL-4	5	3.50	3.0	18.17	17.34	10.42	10.09	2.08	7.80	6.50	14.05	8.73	2.22	1.60	0.72				
	10	6.99	6.0	40.79	36.07	33.01	28.18	5.20	29.13	26.27	23.41	7.84	1.24	1.25	1.20				
	20	13.98	12.0	87.40	69.03	70.53	65.76	8.50	88.43	70.49	81.41	10.30	0.78	1.00	0.81				
	30	20.97	18.0	132.65	100.59	122.99	98.82	14.83	143.06	120.95	140.19	8.90	0.70	1.02	0.71				
	50	34.95	30.0	217.65	168.92	174.06	170.15	46.04	266.86	237.99	238.77	4.73	0.63	0.73	0.72	0.800	0.400	0.500	0.400

TABLE VI-13 - DOWN GRINDING RESULTS FOR F-SERIES

TEST NO.	PASS NO.	INFEED $x10^{-3}$ in.	CUTTING LENGTH in.	STOCK REMOVAL $x10^{-3}$ in^3				WHEEL WEAR $x10^{-3}$ in^3				GRINDING RATIO				SURFACE ROUGHNESS R_{max} $x10^{-3}$ in.			
				4340	T	W	R.41	4340	T	W	R.41	4340	T	W	R.41	4340	T	W	R.41
DF-1	5	1.0	2.51	3.78	3.85	3.85	2.45	1.72	5.76	5.39	4.66	2.21	0.67	0.71	0.53				
	10	2.0	5.02	10.66	10.84	9.44	7.70	3.55	10.90	10.66	7.60	3.00	0.99	0.89	1.01				
	20	4.0	10.04	25.11	22.03	22.38	18.19	6.00	23.28	18.26	16.91	4.18	0.95	1.23	1.08				
	30	6.0	15.06	39.90	33.91	35.67	31.13	9.07	32.35	27.44	23.03	4.40	1.05	1.30	1.35				
	50	10.0	25.10	66.74	59.43	59.10	54.91	16.42	44.84	42.64	41.41	4.07	1.33	1.39	1.33	0.210	0.138	0.200	0.185
DF-2	5	2.5	4.40	15.02	12.50	11.11	8.00	1.59	3.92	9.80	6.13	9.43	3.19	1.13	1.31				
	10	5.0	8.80	31.06	26.04	25.01	21.90	3.19	16.17	19.60	12.25	9.75	1.61	1.28	1.79				
	20	10.0	17.60	69.91	56.94	54.18	53.18	5.64	37.61	53.30	39.82	12.40	1.51	1.02	1.34				
	30	15.0	26.40	100.70	85.06	82.66	84.12	7.72	72.16	70.20	62.61	13.05	1.18	1.18	1.34				
	50	25.0	44.00	168.97	141.31	134.41	136.26	11.03	121.17	137.59	116.39	15.32	1.17	0.98	1.17	0.360	0.300	0.350	0.300
DF-3	5	5.0	6.15	25.43	23.92	16.03	18.15	4.70	27.92	19.79	21.91	5.40	0.86	0.81	0.83				
	10	10.0	12.30	57.23	45.45	43.33	42.81	12.7	66.45	80.35	34.87	4.48	0.68	0.54	1.23				
	20	20.0	24.60	117.46	88.17	89.72	89.04	32.8	172.00	153.39	130.30	3.58	0.51	0.59	0.68				
	30	30.0	36.90	174.69	131.92	134.75	136.98	80.11	261.54	233.50	200.98	2.18	0.50	0.58	0.68		0.600		
	40	40.0	29.20			178.42	183.21			321.86	291.70			0.55	0.63				
	50	50.0	61.50	283.79				194.39				1.46				1.000		0.675	0.625
DF-4	5	7.5	7.50	33.65	27.25	25.04	29.15	10.3	40.86	44.44	63.51	3.24	0.67	0.56	0.46				
	10	15.0	15.00	66.34	82.77	53.09	53.94	20.67	118.90	112.72	128.55	2.98	0.70	0.47	0.42				
	20	30.0	30.00	128.79	101.01	104.51	112.56	138.0	295.89	295.89	301.96	0.95	0.37	0.35	0.37	1.250	0.875	0.750	0.685

TABLE VI-14 - DOWN GRINDING RESULTS FOR C-SERIES

TEST NO.	PASS NO.	INFEED $x10^{-3}$ in.	CUTTING LENGTH in.	STOCK REMOVAL $x10^{-3}$ in^3				WHEEL WEAR $x10^{-3}$ in^3				GRINDING RATIO				SURFACE ROUGHNESS H_{max} $x10^{-3}$ in.			
				4340	T	W	R.41	4340	T	W	R.41	4340	T	W	R.41	4340	T	W	R.41
DC-1	5	1.33	4.0	6.73	4.09	4.55	4.09	1.84	3.90	7.80	7.80	3.65	1.05	0.58	0.52				
	10	2.65	8.0	16.07	13.02	13.64	14.13	4.90	7.80	16.91	14.31	3.28	1.67	0.81	0.99				
	20	5.30	16.0	34.38	28.64	35.24	29.37	9.80	22.11	23.41	27.31	3.50	1.30	1.51	1.08				
	30	7.95	24.0	52.32	44.64	48.13	48.70	15.9	29.91	32.52	40.32	3.26	1.49	1.48	1.21				
	50	13.25	40.0	90.44	76.26	83.75	82.16	22.0	54.63	49.42	53.33	3.08	1.40	1.70	1.54	0.275	0.165	0.125	0.160
DC-2	5	2.87	4.0	18.87	13.79	10.71	9.42	3.83	16.58	7.65	3.83	4.93	0.83	1.40	2.46				
	10	5.74	8.0	44.27	32.31	25.86	26.45	7.65	26.78	15.30	22.95	5.79	1.21	1.69	1.15				
	20	11.48	16.0	88.17	67.52	62.81	61.23	11.48	77.79	51.01	54.83	7.68	0.87	1.23	1.12				
	30	17.22	24.0	130.63	101.28	94.58	94.92	17.85	108.39	98.19	104.57	7.32	0.93	0.96	0.91				
	50	28.70	40.0	216.98	168.07	151.11	154.34	20.40	190.01	214.23	209.13	10.64	0.89	0.71	0.74	0.575	0.400	0.280	0.325
DC-3	5	4.90	4.0	22.87	21.82	15.42	19.32	7.52	46.37	11.31	18.10	3.16	0.47	1.36	1.07				
	10	9.80	8.0	52.33	40.48	33.72	40.75	17.0	95.00	75.78	53.16	3.08	0.43	0.45	0.77				
	20	19.60	16.0	108.82	77.79	73.18	77.99	75.6	199.06	174.17	160.60	1.42	0.39	0.42	0.49				
	30	29.70	24.0	150.75	117.92	114.43	116.63	126.0	312.16	303.11	264.65	1.18	0.38	0.38	0.44	0.445	0.525	0.525	0.550

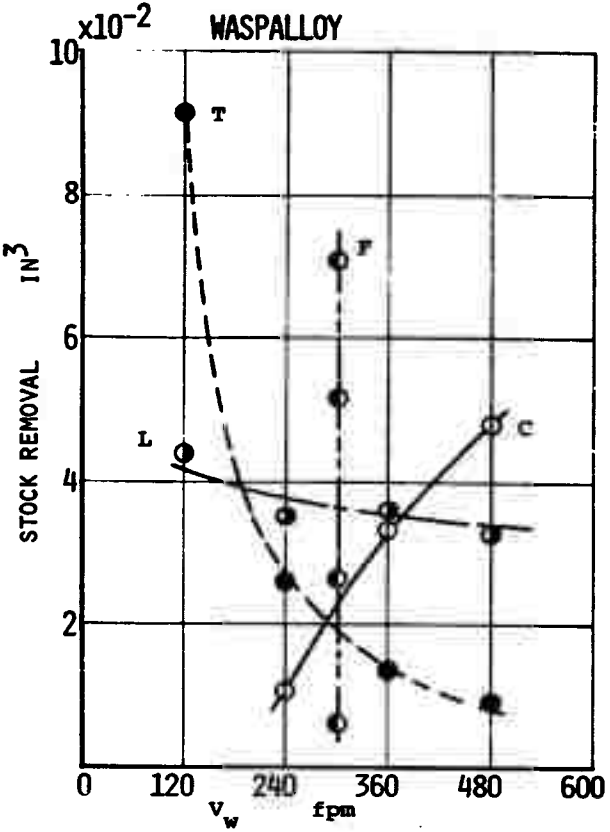

FIGURE VI-16 - RELATION BETWEEN WORK SPEED AND STOCK REMOVAL IN SGTC

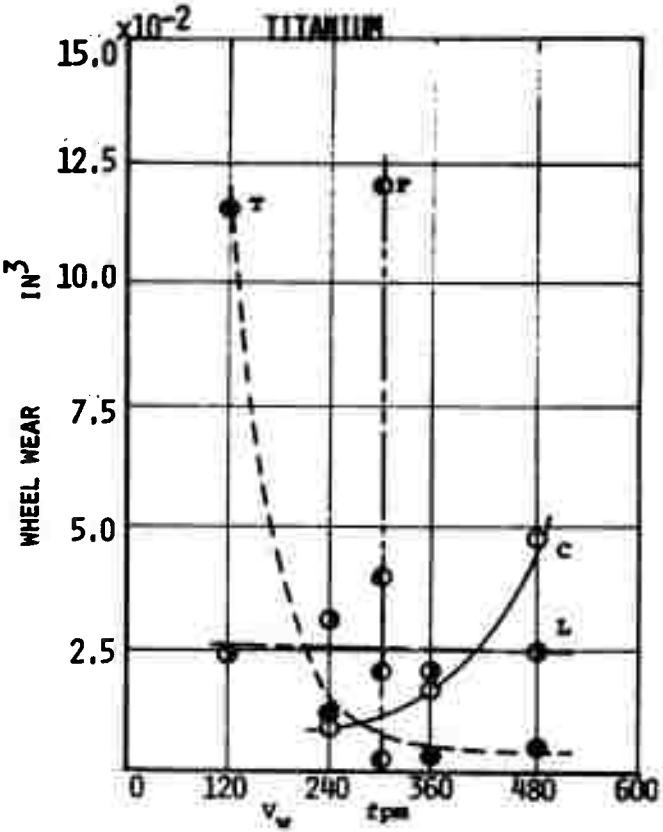

FIGURE VI-17 - RELATION BETWEEN WORK SPEED AND WHEEL WEAR IN SGTC

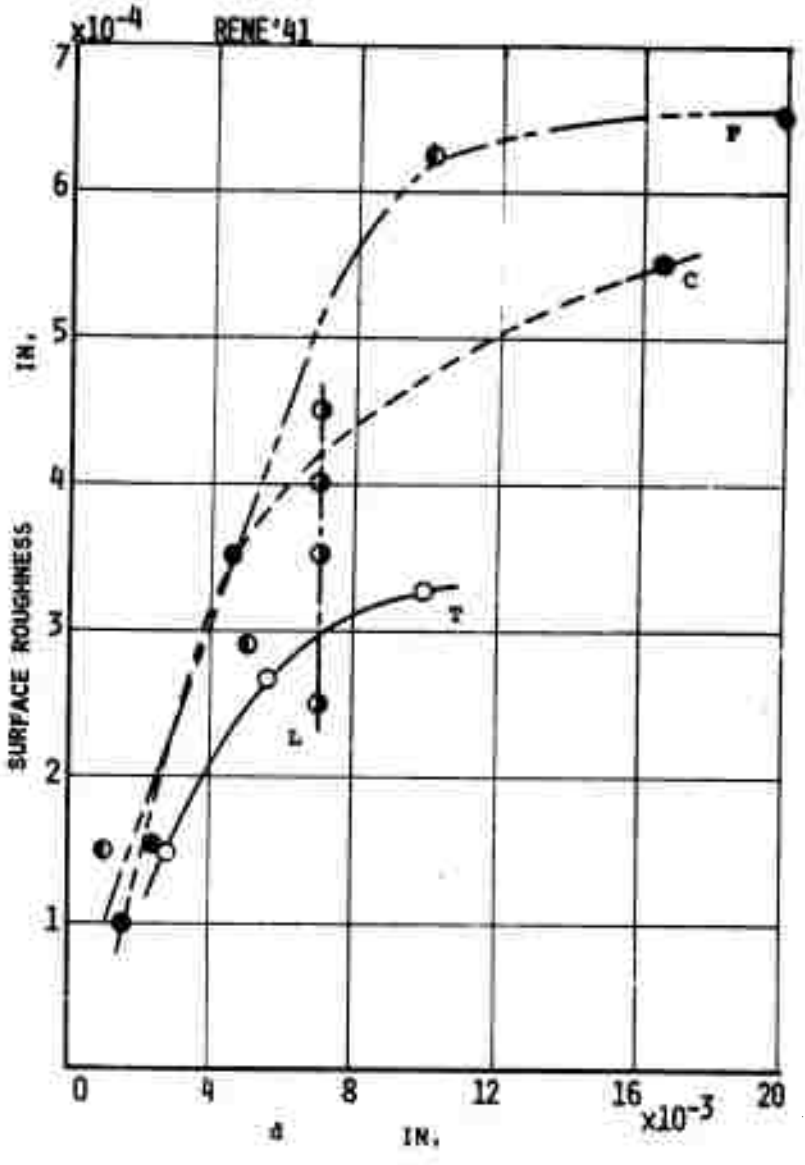

FIGURE VI-18 - RELATION BETWEEN WHEEL CUTTING DEPTH AND SURFACE ROUGHNESS IN SGTC

tests under easily-varied conditions are not useful to analyze and improve grinding processes. The standard grinding test conditions described in the previous paragraph are very useful to systematically find the parameters that have a direct relation to the grinding results. That is, various parameters have systematically been changed in these standard grinding tests, based on the undeformed chip shape which was analyzed in Section II. Therefore the relations between grinding results and various parameters can easily be found by correlation coefficients between them. Tables VI-15 and VI-16 show the correlation coefficients between grinding results and each parameter for up and down grinding respectively.

In Tables VI-15 and VI-16 it should be noted that the correlation coefficients were calculated from the data for different cutting lengths. The stock removal, wheel wear, and grinding ratio are functions of cutting length. Therefore, the correlation coefficients between the grinding results, which are functions of cutting length, and the values independent of cutting length (those which determine the undeformed chip shape), have no physical meaning.

On the other hand, the stock removal rate is not a function of the cutting length. Therefore, the correlation coefficients between the stock removal rate and total infeed (Σd) or the product $\ell.t_{max}$ have no physical meaning. Thus the correlation coefficients between the stock removal, wheel wear or grinding ratio, and the values independent of cutting length were

TABLE VI-15 - CORRELATION COEFFICIENTS (UP GRINDING)

		S.R.R.	S.R.	W.W.	G-Ratio	H_{max}	K_v	i_g	d	t_{max}	L_c	f	L_t	f/L_c	$L_c t_{max}$	ℓ	Σd	ℓt_{max}
STOCK REMOVAL RATE	4340		.5442	.6346	-.4494	.7262	.4305	.4267	.6267	.9717	.7612	.4305	.7046	-.4335	.9736	-.0148	.6969	.8099
	Titanium		.5081	.8114	-.8146	.7624	.4542	.4522	.6095	.9794	.7426	.4542	.6841	-.3904	.9871	-.0367	.6838	.7875
	Waspalloy		.5227	.8540	-.8853	.8917	.4055	.3436	.6820	.9628	.7976	.4055	.7426	-.4144	.9846	-.0321	.6686	.7708
	Rene'41		.5064	.8391	-.8520	.9313	.3873	.3825	.6999	.9575	.8078	.3873	.7543	-.4245	.9910	-.0399	.6682	.8035
STOCK REMOVAL	4340			.4763	-.4896	.4274	-.2589	-.2595	.5438	.3709	.6599	-.2589	.6701	-.7198	.4633	.6482	.9557	.8280
	Titanium			.6319	-.4673	.4010	-.1963	-.1922	.4379	.3864	.5749	-.1963	.5810	-.6509	.4851	.6605	.9491	.8295
	Waspalloy			.7939	-.6189	.5658	-.3043	-.1595	.6484	.3731	.7428	-.3043	.7532	-.7393	.3307	.6561	.9543	.8651
	Rene'41			.7193	-.3688	.5033	-.3496	-.3523	.6668	.3504	.7535	-.3496	.7702	-.7658	.4929	.6600	.9515	.8265
WHEEL WEAR	4340				-.6807	.8431	-.0300	.0313	.7616	.6079	.7307	.0300	.7124	-.3101	.7876	.2310	.6417	.8827
	Titanium				-.9139	.9059	-.0182	.0210	.8722	.7096	.9148	.0182	.8920	-.6096	.5845	.2206	.8365	.8625
	Waspalloy				-.8970	.8048	-.0113	.0457	.8371	.7373	.9051	.0113	.8848	-.6360	.7318	.2800	.8839	.8496
	Rene'41				-.8398	.8199	-.0151	.0179	.7943	.7119	.8474	.0151	.8279	-.5258	.8555	.2326	.8244	.8696
GRINDING RATIO	4340					-.5405	-.3391	-.3448	-.3796	-.4823	-.3228	-.3399	-.2840	.6210	-.5133	-.5685	-.0255	-.4334
	Titanium					-.8345	-.1386	-.2810	-.8791	-.7366	-.9235	-.3860	-.9002	.6222	-.8895	-.0968	-.6928	-.6875
	Waspalloy					-.8731	-.1457	-.1458	-.7771	-.7977	-.8468	-.1457	-.8151	.5726	-.8083	-.1197	-.7158	-.7380
	Rene'41					-.8478	-.3414	-.3424	-.6358	-.7955	-.6729	-.3414	-.5000	.1520	-.8062	-.0395	-.1829	-.4356
SURFACE ROUGHNESS	4340						.1107	.1185	.9641	.6178	.9494	.1107	.9395	-.5817	.8157	.0911	.6557	.5972
	Titanium						.0398	.0473	.9415	.6616	.9430	.0398	.9267	-.5581	.6186	.0464	.6397	.6341
	Waspalloy						.0934	.0606	.7890	.7790	.8689	.0934	.8416	-.5351	.6510	.0953	.6356	.7074
	Rene'41						.1641	.1560	.7759	.8334	.8490	.1641	.8155	-.4732	.9154	.0778	.6091	.7960

TABLE VI-16 - CORRELATION COEFFICIENTS (DOWN GRINDING)

		S.R.R.	S.R.	W.W.	G-Ratio	H_{max}	K_v	i_d	d	t_{max}	L_c	f	L_t	f/L_c	$L_c t_{max}$	t	Id	tt_{max}
STOCK REMOVAL RATE	4340		.4935	.5720	-.4362	.8683	.4567	.6102	.5810	.9691	.7286	.4567	.6702	-.4316	.9515	-.1189	.6568	.6504
	Titanium		.3783	.8795	-.7955	.7344	.4812	.5886	.5600	.9773	.7040	.4812	.6508	-.4098	.9522	-.1827	.6587	.6990
	Waspalloy		.4077	.9221	-.8162	.8682	.4052	.6711	.6463	.9552	.7804	.3970	.7265	-.4958	.9630	-.1279	.7057	.7130
	Rene'41		.4325	.9324	-.9154	.7904	.3913	.6900	.6720	.9548	.7982	.3913	.7445	-.4698	.9726	-.1465	.6924	.6999
STOCK REMOVAL	4340			.1534	-.4577	.3147	.2435	.5424	.4139	.2960	.5460	-.2435	.5572	-.6790	.3533	.6771	.9296	.8936
	Titanium			.4884	-.3333	.2840	.1931	.3460	.1996	.2125	.4117	-.1932	.3665	-.6013	.2194	.6988	.8531	.8660
	Waspalloy			.4939	-.2520	.3922	.1945	.5713	.4417	.1693	.5488	-.3945	.5741	-.7659	.2599	.7423	.9109	.8562
	Rene'41			.5750	-.2280	.2988	.3821	.6316	.5115	.2147	.6107	-.3822	.6335	-.7627	.3191	.7107	.9269	.8743
WHEEL WEAR	4340				-.4817	.8304	.2540	.7578	.8074	.5647	.7803	.0254	.7661	-.3585	.7269	.0664	.4921	.8737
	Titanium				-.9595	.8298	.2562	.8724	.8357	.7927	.9269	.0562	.9021	-.6909	.9014	.1391	.8024	.9000
	Waspalloy				-.8766	.9341	.2122	.7985	.7684	.8425	.8698	.2122	.8362	-.5704	.9238	.0643	.7988	.9241
	Rene'41				-.9006	.8179	.1355	.8203	.7893	.8359	.8889	.1355	.8573	-.6078	.9300	.0704	.8180	.9261
GRINDING RATIO	4340					-.3563	-.4303	-.1900	-.4227	-.3536	-.7950	-.4303	-.3750	.2420	-.3164	.8365	-.2229	-.4254
	Titanium					-.8702	-.0430	-.8866	-.8887	-.7154	-.9138	-.4300	-.9009	.7096	-.8503	.1538	-.7102	-.6774
	Waspalloy					-.0981	-.1968	-.6606	-.6670	-.7845	-.7301	-.2769	-.6891	.3750	-.8356	.1588	-.5657	-.6004
	Rene'41					-.0621	-.3611	-.6673	-.6827	-.8957	-.7578	-.3612	-.7078	.3718	-.9348	.3302	-.5305	-.5373
SURFACE ROUGHNESS	4340						.1714	.8288	.8447	.8445	.8942	.1714	.8590	-.5124	.9552	-.1126	.5963	.6554
	Titanium						.0401	.8552	.8859	.7106	.8629	.0408	.8738	-.4655	.8538	-.1781	.4259	.6171
	Waspalloy						.1083	.8589	.8440	.7845	.9121	.1083	.8872	-.5840	.9009	-.1046	.7060	.6912
	Rene'41						.0829	.7470	.7468	.7235	.8018	.0829	.7770	-.4331	.8161	-.1466	.5284	.6214

calculated for constant cutting length to investigate which of the values have the greatest effect on the grinding results.

The correlation coefficients for constant cutting length are shown in Tables VI-17 and VI-18 for up and down grinding, respectively. In these tables it can be determined which parameters of the undeformed chip shape strongly affect the grinding results.

(1) Stock Removal Rate.

From the correlation coefficients between the stock removal rate and the values which determine the undeformed chip shape in Tables VI-15 and VI-16, it can be seen that the stock removal rate is well correlated with the maximum chip thickness t_{max} , and the product $L_c t_{max}$ of the chip length by the maximum chip thickness.

From the physical point of view, the mean chip thickness (t_{mean}) should be taken for the maximum chip thickness t_{max} in the product. However, judging from the chip shape, the mean chip thickness will be about half the maximum chip thickness and thus the product $L_c \cdot t_{max}$ has the same physical meaning as $L_c \cdot t_{mean}$.

Figures VI-19 and VI-20 show variations of the stock removal rate with the increase of the maximum chip thickness t_{max}. The maximum chip thickness is an increasing function of the speed ratio K_v and the depth setting d, as described in Section II. Therefore, the speed ratio K_v and/or the depth setting d should be increased from the view point

TABLE VI-17 - CORRELATION COEFFICIENTS (UP GRINDING) WITH ℓ=20 in.

		K_v	i_g	d	t_{max}	L_c	f	L_t	$L_c t_{max}$	f/L_c
STOCK REMOVAL	4340	.7210	.7238	.2661	.8827	.3843	.7210	.3403	.7675	-.1324
	Titanium	.8302	.8303	.0621	.7809	.1850	.8302	.2183	.6066	.0711
	Waspalloy	.7874	.7885	.2017	.8601	.3150	.7874	.2779	.7275	-.0014
	Rene'41	.8005	.8044	.1675	.8372	.2716	.8005	.2423	.6988	.0324
WHEEL WEAR	4340	.6955	.6909	.3133	.7219	.3189	.6955	.1279	.6885	.1607
	Titanium	.4820	.4734	.6571	.9323	.7289	.4820	.5040	.9443	-.4220
	Waspalloy	.4825	.4755	.6697	.9454	.7304	.4825	.5320	.9630	-.3621
	Rene'41	.6963	.6996	.3950	.9490	.4725	.6963	.3450	.8750	-.0818
GRINDING RATIO	4340	-.5349	-.5391	-.0725	-.3290	-.0180	-.5349	.1008	-.2851	-.3776
	Titanium	.0851	.1009	-.8928	-.6190	-.9190	.0851	-.6227	-.7819	.6754
	Waspalloy	.0596	.0709	-.8348	-.6049	-.8484	.0596	-.6710	-.7511	.6266
	Rene'41	-.6595	-.6778	-.3239	-.8420	-.3788	-.6595	-.2847	-.7684	-.0157

TABLE VI-18 - CORRELATION COEFFICIENTS (DOWN GRINDING) WITH ℓ=20 in.

		K_v	i_d	d	t_{max}	L_c	f	L_t	$L_c t_{max}$	f/L_c
STOCK REMOVAL	4340	.6818	.6749	.2622	.8033	.3835	.6818	.3112	.6869	-.2306
	Titanium	.6952	.6951	.2544	.8440	.3854	.6952	.3687	.7154	-.1569
	Waspalloy	.6014	.5971	.4007	.8295	.5001	.6014	.3874	.7628	-.2935
	Rene'41	.5891	.5861	.4344	.8382	.5330	.5891	.4219	.7793	-.2156
WHEEL WEAR	4340	.4821	.4715	.3697	.6802	.3969	.4821	.2156	.6459	.0840
	Titanium	.5880	.5805	.5982	.9618	.5804	.5880	.4217	.9119	-.2348
	Waspalloy	.5726	.5670	.5340	.9524	.6025	.5726	.4300	.9195	-.2129
	Rene'41	.6153	.6107	.4685	.9522	.5426	.6133	.3759	.8981	-.1755
GRINDING RATIO	4340	-.3347	-.3430	-.0987	-.2412	-.0482	-.3347	-.0777	-.2312	-.3354
	Titanium	-.3270	-.3207	-.7263	-.9078	-.7768	-.3270	-.6348	-.9597	.4614
	Waspalloy	-.4437	-.4487	-.4613	-.7459	-.4999	-.4437	-.4394	-.7389	.1263
	Rene'41	-.6819	-.6985	-.2586	-.8472	-.3195	-.6819	-.2739	-.7538	0

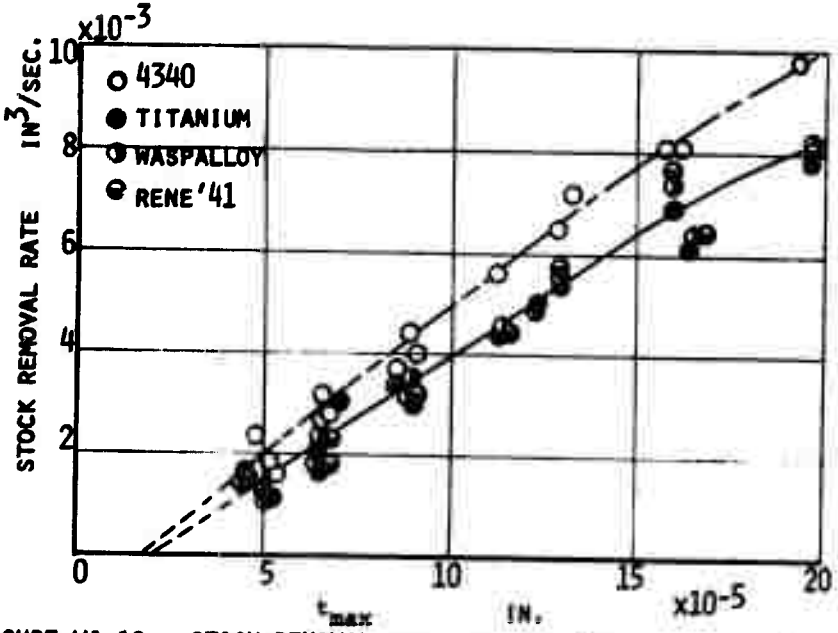

FIGURE VI-19 - STOCK REMOVAL RATE vs. MAXIMUM CHIP THICKNESS FOR UP GRINDING

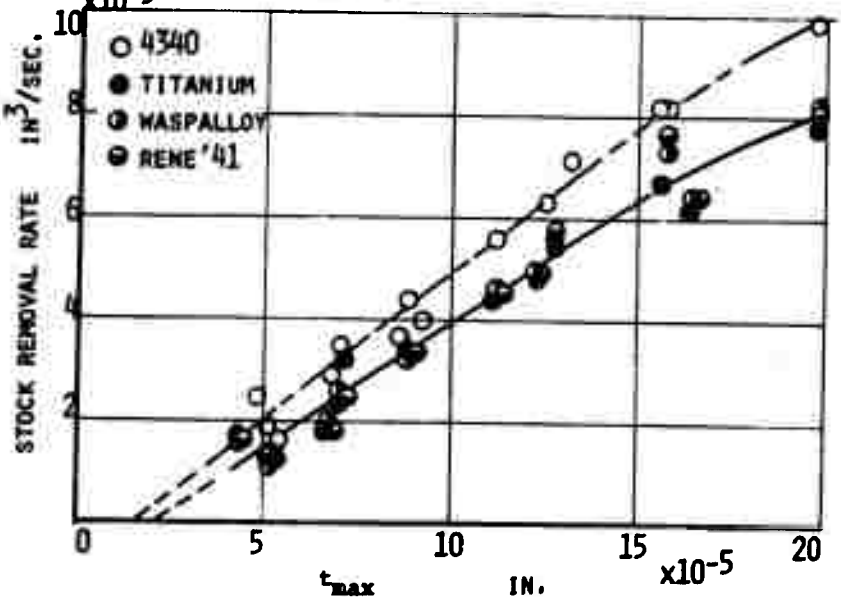

FIGURE VI-20 - STOCK REMOVAL RATE vs. MAXIMUM CHIP THICKNESS FOR DOWN GRINDING

of high production rate. In Figures VI-19 and VI-20, the critical values of maximum chip thickness at which the stock removal rate becomes zero are not zero. These critical values will be determined mainly by the sliding phenomena of the cutting edges on the surface of the workpiece. The critical values may correspond to the critical depth of cut of the plastic region as mentioned in Section II. Because cutting edges slide throughout the contact region without chip generation if the depth of cut is smaller than the critical one, there is no stock removal.

In order to indicate the difference between theoretical and practical stock removal rate, the stock removal rate is plotted with the product $K_v \cdot d$ of the speed ratio by depth setting, which is proportional to the theoretical stock removal rate in Figures VI-21 and VI-22. In these figures, the experimental curves are parallel to the theoretical curve only for the case of low $K_v \cdot d$. This fact indicates that the difference between the experimental and theoretical stock removal rate in this region may be due to the sliding phenomena of the cutting edges on the surface of workpiece. In Figures VI-19 to VI-22, the difference of stock removal rate between 4340 steel and the HSTRA materials can be found, but that between each of the HSTRA materials cannot be found. It should be emphasized that the increase of speed ratio K_v and/or depth setting d leads to higher production rate.

(2) Wheel Wear Characteristics.

In the wear mechanism of the grinding wheel, there are

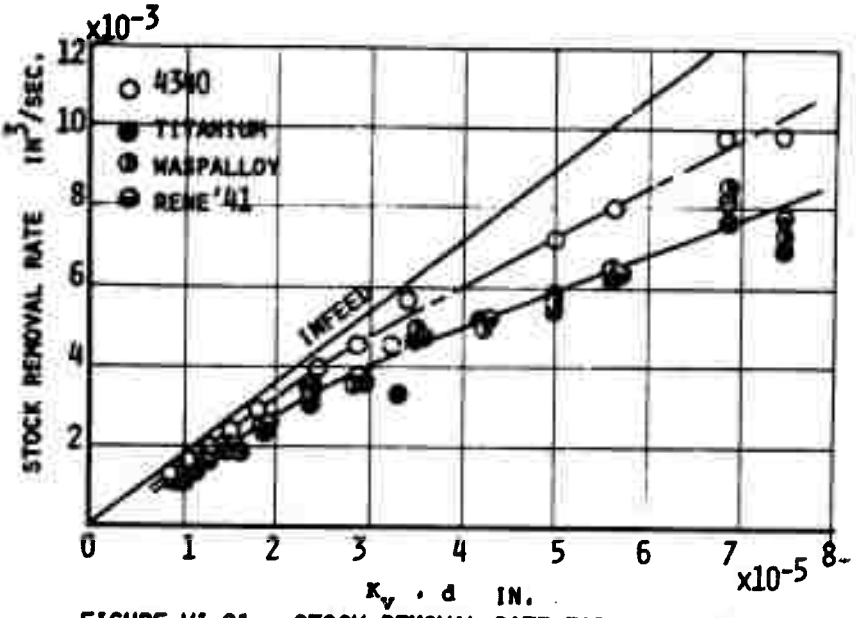

FIGURE VI-21 - STOCK REMOVAL RATE FOR UP GRINDING

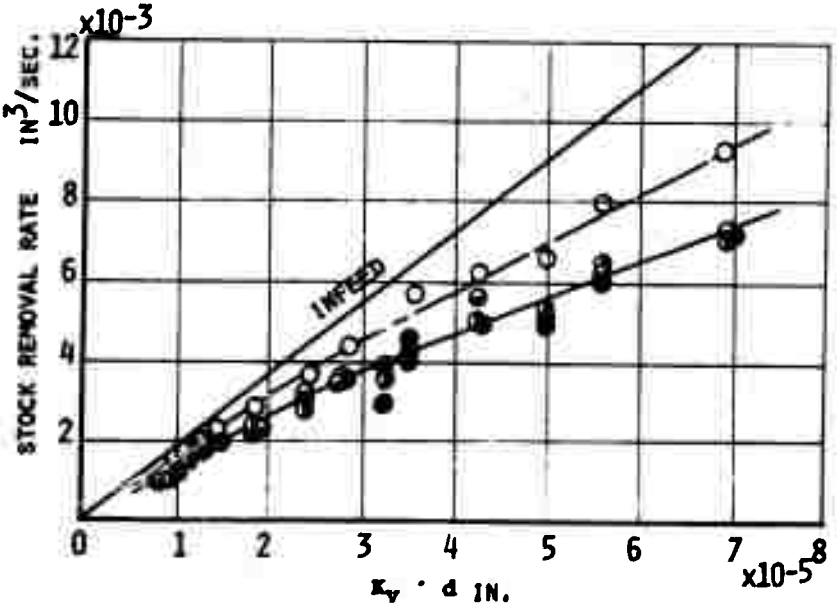

FIGURE VI-22 - STOCK REMOVAL RATE FOR DOWN GRINDING

three different types: attritious wear of grains under high temperature and pressure, mechanical fracture of grains, and fracture of bond bridges.

In discussing the relation between wheel wear characteristics and the values which determine the undeformed chip shape, Figures VI-23 and VI-24 show variations of wheel wear with the product $\ell.t_{max}$ for up and down grinding respectively.

In these figures, the wheel wear difference cannot be seen on the HSTRA material for up and down grinding. Furthermore, the facts noted in these figures are:

1. The wheel wear curves can be divided into two parts and are straight lines in each part.
2. The slope in Part I of the wheel wear curve is much smaller than in Part II.
3. The slope in Part I of the wheel wear curve for 4340 is different from that for HSTRA, but they are the same in Part II.
4. The slopes in each part of the wheel wear curve for up grinding are the same as for down grinding.
5. The critical value at the boundary point between the two parts is larger for 4340 than for HSTRA; and for down grinding it is smaller than for up grinding.
6. The scattering of data in Part II of the wheel wear curve is much wider than in Part I.

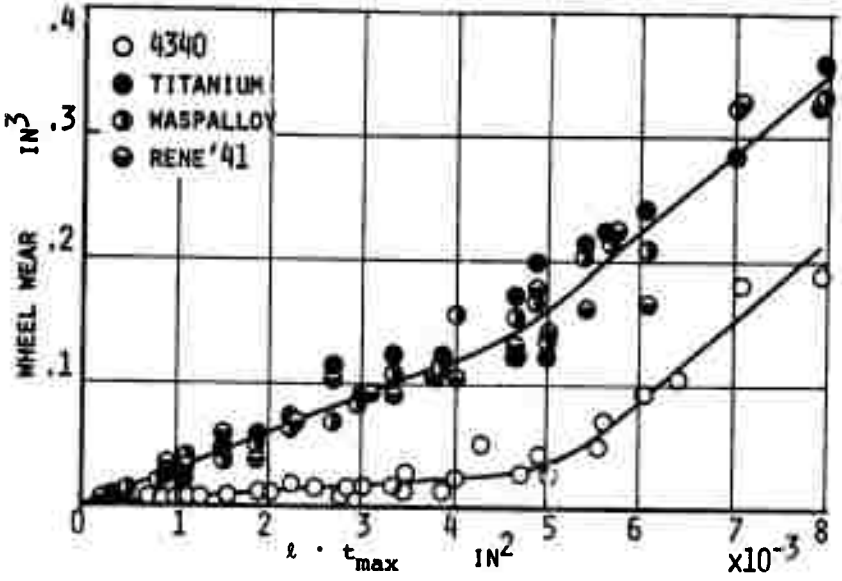

FIGURE VI-23 - VARIATION OF WHEEL WEAR WITH $\ell \cdot t_{max}$ FOR UP GRINDING

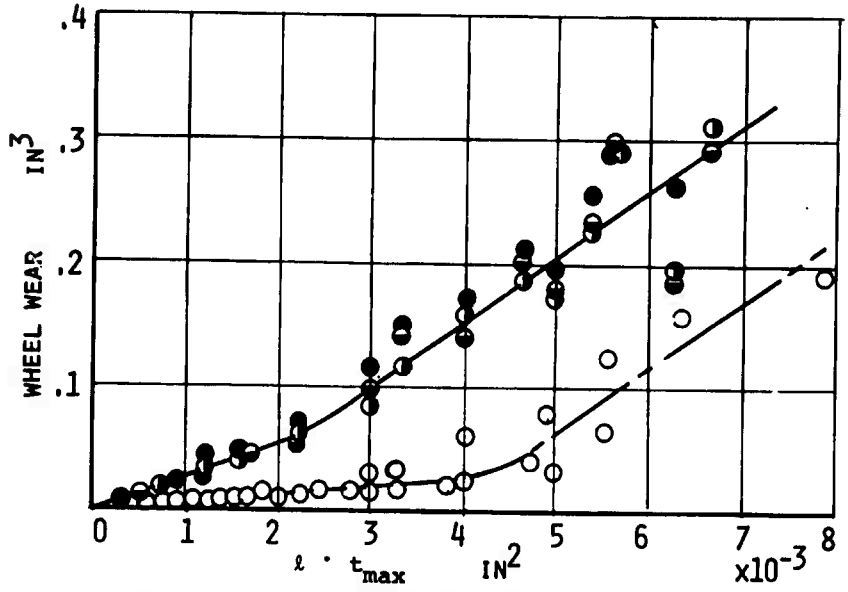

FIGURE VI-24 - VARIATION OF WHEEL WEAR WITH $\ell \cdot t_{max}$ FOR DOWN GRINDING

Judging from these facts, it may be considered that Parts I and II correspond to attritious wear and fracture respectively. In fact, almost all the facts listed above can be explained by this consideration.

First, consider why the wear mechanism changes from attritious wear into fracture with the increase of the cutting length for constant maximum chip thickness. Immediately after dressing each grain is sharp, and with an increase of cutting length, the wear area in the clearance surface of the grain gradually increases. This is due to chipping caused by stress concentrations at the sharp points and plastic and chemical wear under high temperatures and pressures. At the same time, the grain force increases gradually with the increase of the wear area in the clearance surface of the grain and then at a certain wear area the force increases abruptly. Mechanical fracture of grain or bond bridges, that is the fracture wear, may only occur when the grain force becomes equal to the grain strength or the bond strength. Once the fracture wear occurs, it will occur continuously because the positions of the top of the grains change causing a change of the number of cutting edges operating at a particular time and therefore the force acting on a grain becomes large. The above discussion may be the reason why the wear mechanism changes from attritious wear to fracture wear with the increase of cutting length.

The reason why variations of the wheel wear with the product $\ell.t_{max}$ are the same for different values of maximum chip thickness will now be discussed.

Figure VI-25 shows variations of the average wear area of a grain with cutting length and the product $\ell.t_{max}$ for different values of the depth of cut. The average wear area in the clearance surface of a grain was calculated from the reduction of the wheel radius on the assumption that grains are spheres distributed on the surface of the grinding wheel. In this figure, the increasing rate of the average wear area for the cutting length is higher for a larger maximum depth of cut, and the variation of the average wear area with the product $\ell.t_{max}$ is independent of the maximum chip thickness. Judging from this, the average wear area in the clearance surface of a grain at the point where the fracture wear begins to occur will be constant for different values of the maximum chip thickness.

On the other hand, grinding force is a function of the maximum chip thickness and grain force may also be a function of the maximum chip thickness. Therefore, the grain force at the starting point of fracture wear is larger for the larger maximum depth of cut. That is, the pressure necessary to break the grain is different for different values of maximum depth of cut. This can be explained as follows: in the case of a smaller depth of cut, the cutting length of a grain should be longer for the constant product $\ell.t_{max}$, and the

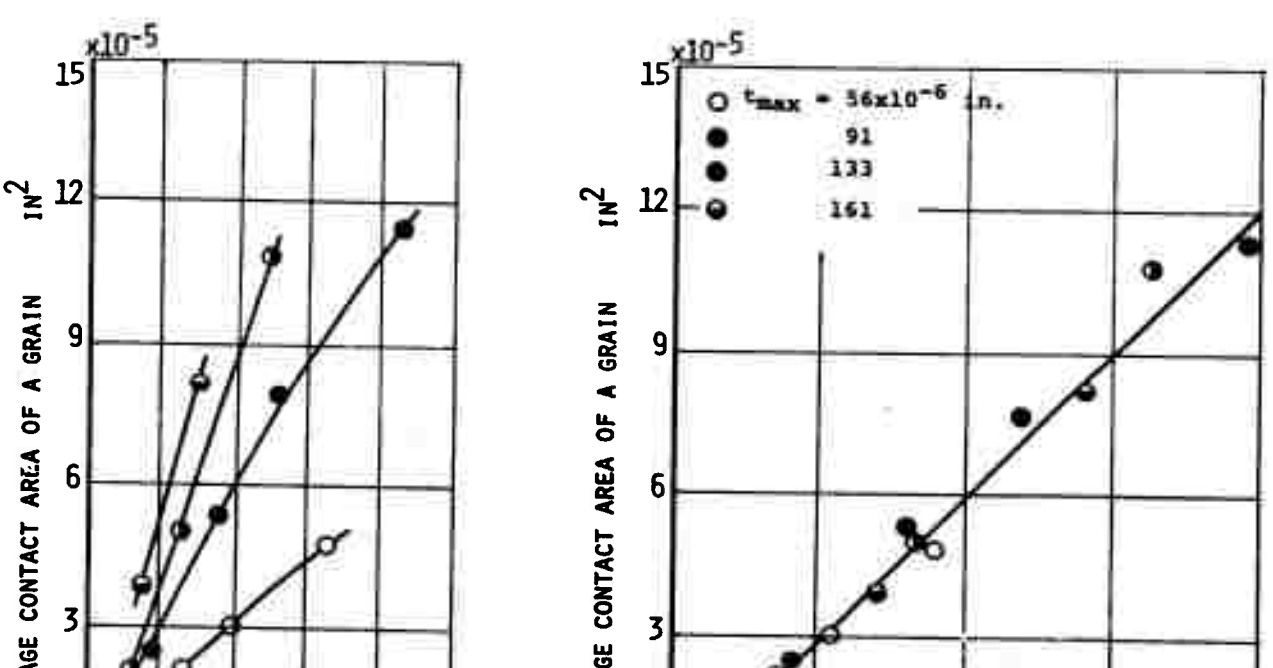

FIGURE VI-25 - VARIATION OF AVERAGE CONTACT AREA IN CLEARANCE SURFACE OF A GRAIN

number of grains contacting the workpiece in the case of the smaller depth of cut will be more.

In other words, an increase of the number of grains contacting the workpiece will lead to a decrease of the grain strength because of the repeated heating and cooling. This can explain why fracture wear begins to occur in spite of different values of maximum depth of cut.

Some conclusions derived are: the wheel wear is strongly affected by the product of the maximum depth of cut by the cutting length, which corresponds to the average energy given to a grain.

In a small range of the product $\ell.t_{max}$ attritious wear dominates the wheel wear and in a much larger range fracture wear dominates. The value of the product at the boundary point between attritious and fracture wear is constant for different grinding conditions considering the same workpiece material and grinding wheel.

The previous discussion was developed on the assumption that "fracture wear" meant the fracture of the grain, not the bond, because during these tests the grade of the grinding wheel used was high.(See Section IV)

(3) Surface Roughness.

Figures VI-26 and VI-27 show the relationship between the surface roughness and the product ($\ell.t_{max}$) for up and down grinding, respectively.

In these figures the surface roughness gradually becomes greater for small values of this product up to a certain

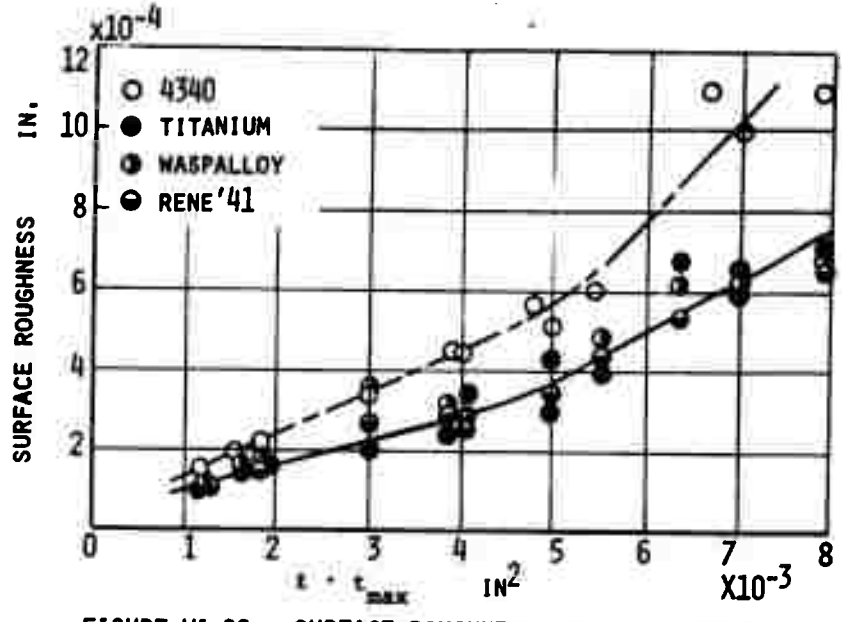

FIGURE VI-26 - SURFACE ROUGHNESS FOR UP GRINDING

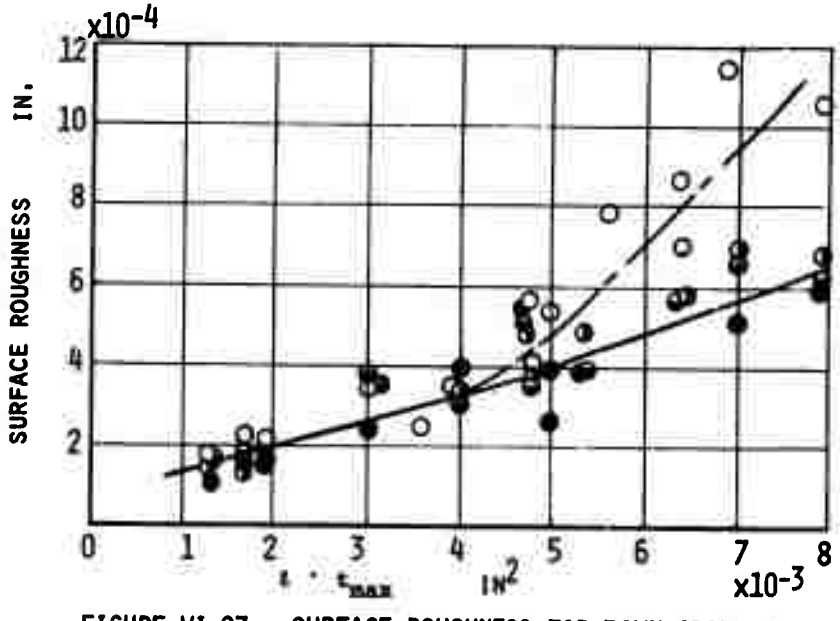

FIGURE VI-27 - SURFACE ROUGHNESS FOR DOWN GRINDING

point and then increases abruptly. The point where the surface roughness begins to increase rapidly corresponds to the boundary point between the attritious and fracture wear conditions of the grinding wheel. That is, the surface roughness increases slightly with an increase of cutting length of a grain. However the surface roughness abruptly becomes greater with the cutting length of a grain for the case of fracture wear. Therefore grinding should be carried out in the region of attritious wear of the wheel to keep the surface roughness low.

VI.5 Conclusions

Experimental studies on grinding under the easily-varied conditions imposed by the configuration of grinders has not been useful to improve grinding process. In order to find optimum grinding conditions for significantly improving grinding efficiency and surface integrity, grinding test conditions should be selected based upon the cutting model in grinding such that the relation between grinding conditions and results can be specified. In this section, four series of standard grinding test conditions have been set up from the above-mentioned point of view, based on the undeformed chip shape. Then the HSTRA grinding tests were carried out under the standard grinding test conditions. It has been shown that the essential parameters which have a direct relation to grinding results could easily be described in the grinding tests under standard grinding test conditions.

Furthermore several grinding results in conventional and standard grinding tests have been analyzed based upon all information obtained under this contract.

SECTION VII

RECOMMENDED HIGH EFFICIENCY GRINDING PROCESSES

VII.1 Introduction

The grinding studies under this contract have been aimed toward high grinding efficiency and good surface quality by scientifically analyzing various phenomena of the wheel-work interaction. The high efficiency grinding recommended in this section and proven by the efforts under this contract will significiantly improve grinding efficiency without damaging surface integrity not only for HSTRA materials, but also for most other materials. The recommendations for improvements in this section have never been presented in any other grinding report to the present time. If one has experience only with "trial and error" testing and does not understand the basic phenomena in grinding he may find it very difficult to believe the recommended high efficiency grinding.

The background for recommending the high efficiency grinding will therefore be described as clearly as possible. The paper entitled "High Efficiency Grinding" was reported by H. Opitz in 1967. The report concludes that efficient grinding conditions could be experimentally found by changing various grinding conditions one at a time. However the report doesn't explain why or how such grinding results could be obtained. His conclusions were presented that indicated high wheel speed grinding was beneficial. It is important to note, however, that grinding

tests were performed under conditions of constant work speed to wheel speed ratio $K_v = {}^{v}w/V_s$. Therefore, in these tests not only was wheel speed increased, but also work speed was increased. The report may not indicate the proper direction for maximum improvements in the grinding process which can be obtained in the future. The reason for this is that tests were performed in a conventional range of K_v and recommendations were based on grinding tests conducted with work speeds relatively low compared to wheel speeds (ie. low K_v).

Dr. K. Okamura, based on his investigations, has proposed the real direction for improvement of high efficiency grinding. The recommendations for high efficiency grinding have been theoretically and experimentally developed for two years under this contract and yield a significant benefit to HSTRA grinding. In this section the parameters that significantly affect the grinding efficiency are first discussed and then the discovery that the high efficiency may not decrease the surface integrity is presented. Finally the real direction for the high efficiency grinding is discussed and the benefits and important considerations for applying the recommended high efficiency grinding are presented.

VII.2 Most Important Parameter For Describing Grinding Efficiency

Cutting efficiency is affected only by the relative cutting speed in single point tool cutting. Efforts in the

studies of cutting theory have been concentrated on increasing the relative cutting speed for single point cutting. Tool life is the limiting factor for increasing the relative cutting speed, but improvements in cutting tool material have allowed a change of the allowable cutting speed as shown historically in Figure VII-1 . In grinding, the wheel and work have a relative cutting motion (not feed motion) and the work speed is conventionally about a hundredth of the wheel speed (K_v = .01). Grinding tests have been performed in which only the wheel speed was increased, under the assumption that the best way to increase the relative cutting speed is to increase the wheel speed. The results have indicated that the increase of the wheel speed alone yields only a detrimental effect on the ground surface integrity. However, the primary reason for not using high wheel speeds has not been the decrease in wheel life due to wear (tool life) or increased surface damage. The wheel speed has remained the same for a long time because of the increased possibility of breaking the wheel at higher speeds. The improved efficiency in single point tool cutting has been considered as resulting from increasing the relative cutting speed for a constant depth of cut. Since increased efficiency in single point cutting requires greater relative cutting speed for a specific depth of cut, the same factors are expected to be important in grinding. Thus, the cutting depth of a single grain and the relative cutting speed of the grain should be considered. From considerations of undeformed chip geometry it has been shown that, for a specified grinding

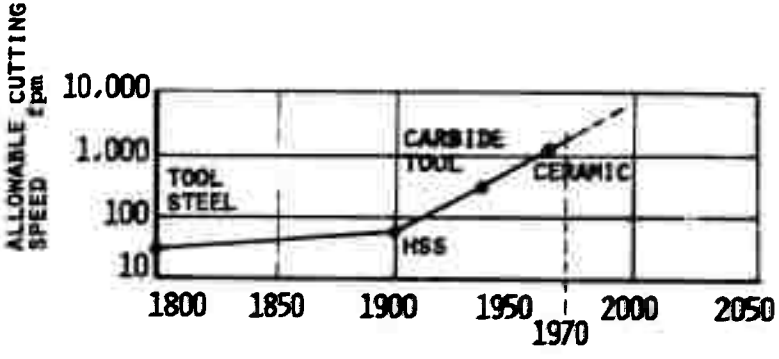

FIGURE VII-1 - HISTORY OF ALLOWABLE CUTTING SPEED FOR SINGLE POINT TOOL CUTTING

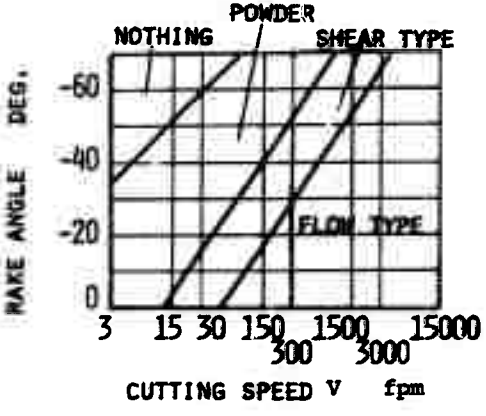

FIGURE VII-2 - RELATIVE CUTTING SPEED EFFECTS ON THE CHIP SHAPE

wheel, the undeformed chip shape depends on wheel cutting depth d and speed ratio K_V. Furthermore, the relative cutting speed V depends on V_w and V_s (for example $V = V_w + V_s$ for up grinding). In grinding experimentation, conditions of constant d and constant K_V should be considered so that changes in undeformed chip shape do not occur.

The measure of efficiency or productivity of the cutting operation can be represented by the stock removal per unit time. Then the grinding efficiency E_g for a unit width can be given by the equation

$$E_g = d \cdot V_w$$

Therefore the grinding efficiency increases proportionally with the work speed V_w for a constant cutting depth of the wheel. In this case, the wheel speed V_s should be increased proportionally with the work speed V_w since the speed ratio K_V is considered to be a constant. Furthermore all of the material shown by the undeformed chip geometry is not removed as a chip as described in detail in Section II. In other words, there are always rubbing and ploughing phenomena near the beginning of contact between a cutting edge and workpiece. Therefore the grinding efficiency can also be increased by decreasing the amount of rubbing and ploughing at the beginning of the cut.

The problem encountered is that the parameters which affect grinding efficiency are also the same ones which effect the rubbing and ploughing phenomena. It is therefore necessary

to understand chip formation physics in order to determine the optimum grinding efficiency.

VII.3 The Direction For Improving Ground Surface Integrity

Cutting processes are those in which a surface with a given dimensional accuracy is produced by removing a part of the workpiece as chips. Some amount of energy is supplied to the cutting operation and an affected layer due to this application of energy is produced on the finished surface.

The direction for improving the surface integrity in the cutting process is not an active one of using some kind of additional processes such as shot peening or stress relief by heat treating, but a passive one of finding some means of reducing the size of the affected layer. Two-dimensional cutting theory, which is a basis for analyzing single point tool cutting, yields no information on the finished surface in turning. However the cutting model in grinding introduced under this contract gives much information about the finished surface, as can be seen in Section II.

The means to improve the surface integrity in transitional cutting processes such as grinding and milling are summarized from some figures in Section II as:

(1) Decrease the plastic deformation region

(2) Make chip formation easier, that is, decrease the side flow in the cutting region.

Cutting with the above two conditions is called "free cutting".

The first condition is mainly affected by the undeformed chip shape. In other words, the plastic deformation region can be decreased and therefore the surface integrity can be improved by using a large interference angle i_g and greater speed ratio K_v. Obviously the surface integrity becomes better with sharper cutting edges and stiffer cutting edge mounting.

Furthermore the relation between cutting speed and surface integrity should be discussed from the viewpoint of efficiency.

VII.4 Relative Cutting Speed Effects

No effect of relative cutting speed on the chip formation mechanism has been considered in single point tool cutting. Only tool life changes have been studied for single point tool cutting under conditions of a constant depth of cut and variable cutting speed in a range higher than the built-up edge generating speed. It has, however, been found that a very high cutting speed, like that in grinding, significantly affects the chip formation mechanism of a cutting edge. Figures VII-2 to VII-4 show the relations between the relative cutting speed and chip formation mechanism of a pyramidal cutting edge which have been obtained from cutting experiments under the condition of constant depth of cut and varying the rake angle and cutting speed over a wide range. Figures VII-5 and VII-6 show several effects of the relative cutting speed on the transitional cutting process. From these figures the effects of increased

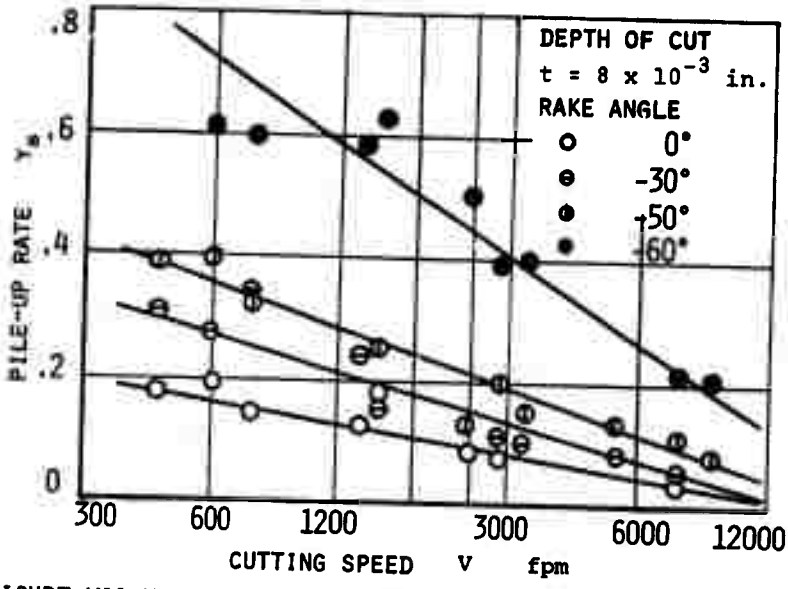

FIGURE VII-3 - RELATIVE CUTTING SPEED EFFECTS ON THE PILE-UP PHENOMENA

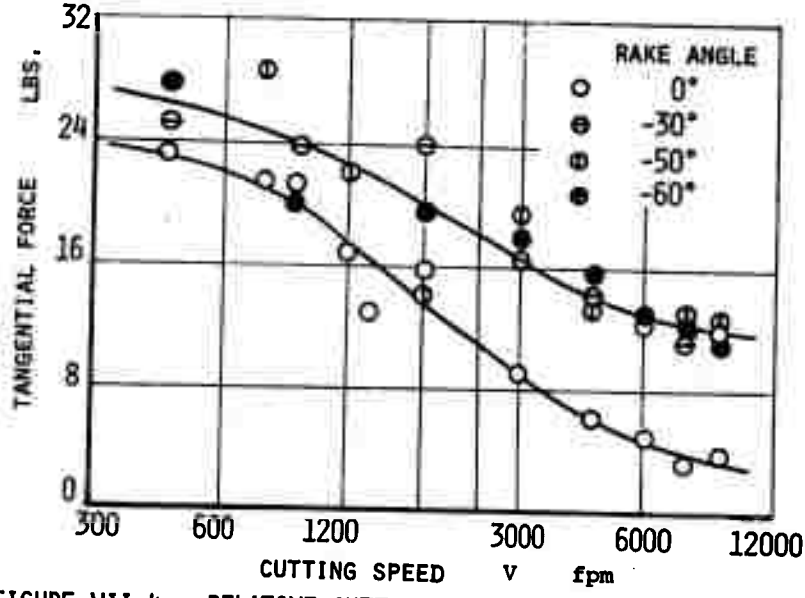

FIGURE VII-4 - RELATIVE CUTTING SPEED EFFECTS ON THE CUTTING FORCE

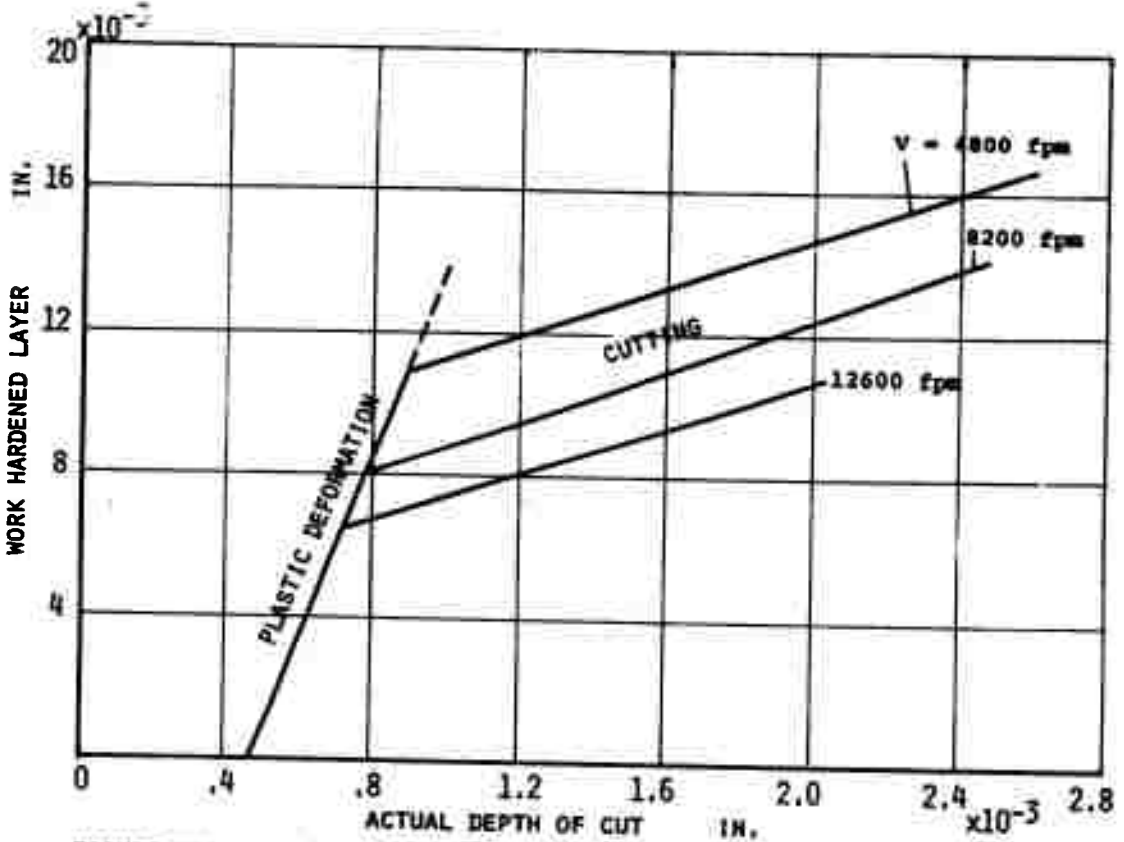

FIGURE VII-5 - RELATIVE CUTTING SPEED EFFECTS ON THE WORK HARDENED LAYER

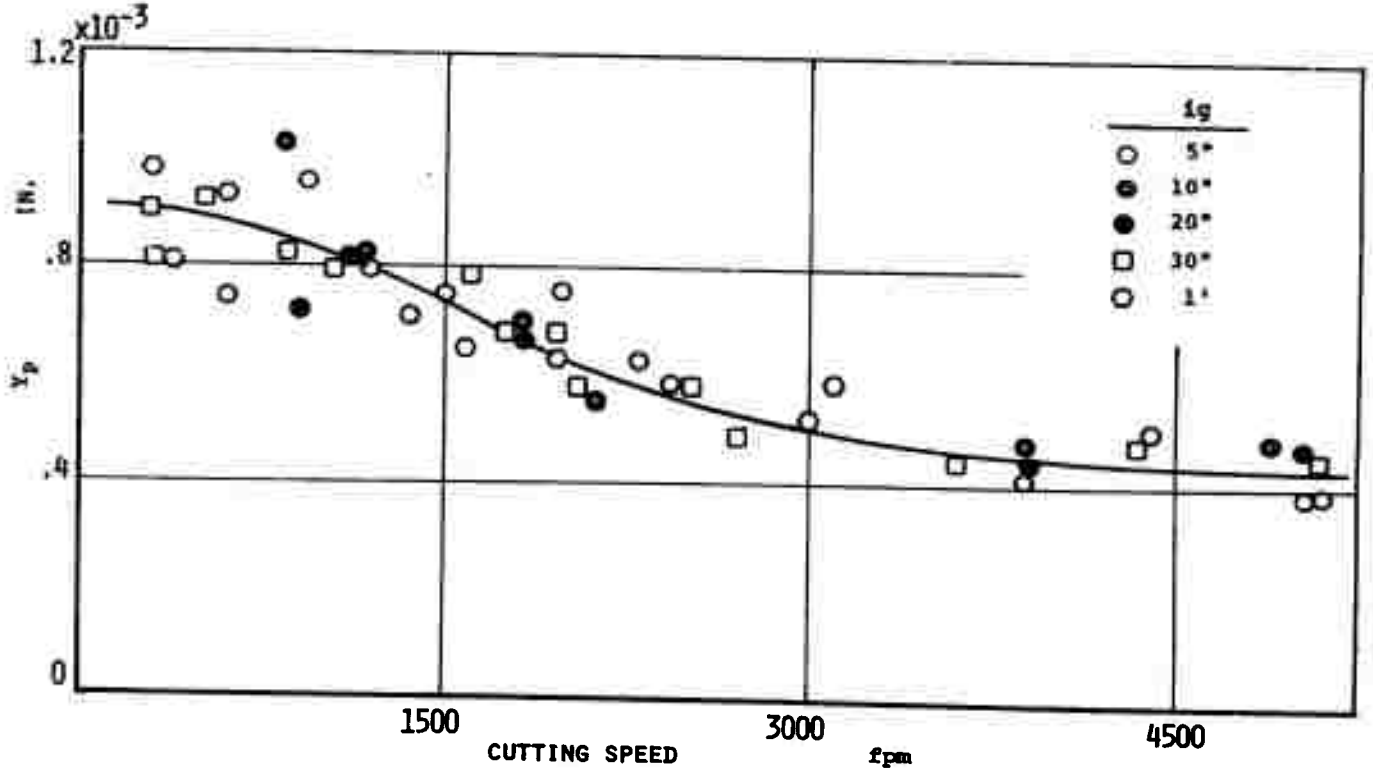

FIGURE VII-6 - RELATIVE CUTTING SPEED EFFECTS ON THE PLASTIC DEFORMATION

relative cutting speed upon the chip formation mechanism are summarized as follows:

(1) Decrease of pile-up phenomena and improvement of surface integrity due to cutting operation.

(2) Decrease of cutting forces and metal flow under cut surface.

(3) Change of chip type into flow chip and smooth formation of chip.

(4) Decrease of the depth of the work-hardened layer under the finished surface.

(5) Decrease of the plastic region at the beginning of the transitional cutting region and decrease of the critical depth of cut at which cutting operation occurs.

Considering all factors, the increase of relative cutting speed increases the free cutting operation in transitional cutting.

VII.5 Recommended High Efficiency Grinding Conditions

In the previous subsections the direction for high efficiency grinding has been clearly described. Fortunately the direction for improving surface integrity is the same as the direction for improving grinding efficiency. In summary, the direction for high efficiency grinding is as follows:

(1) Increase workspeed as high as possible

(2) Increase speed ratio Kv

(3) Increase relative cutting speed.

It is necessary for the wheel speed to be increased in order to satisfy the above three conditions. In conclusion, the grinding conditions recommended from the results of the work under this contract are "high relative cutting speed and high speed ratio".

The difference between the new conditions and the traditional recommended grinding conditions (high work speed and low wheel speed) is a reverse direction of the wheel speed. However, it should be noted that the conclusion of high work speed and low wheel speed in traditional studies indicates the importance of high speed ratio in grinding. Figure VII-7 shows the recommended direction for high efficiency grinding and the regions of high efficiency grinding testing by Dr. K. Okamura and those of Dr. H. Opitz. Point 0 in the figure represents the old HSTRA grinding condition under which HSTRA grinding is practiced in many air craft industries today.

The path of the change of grinding conditions for conventional materials to the point 0 may have been obtained by going first to low work speed because of the difficulty in grinding HSTRA materials and then by going in the direction of the arrow to improve grinding efficiency. The direction of the arrow is almost the same as the direction of increasing speed ratio K_V.

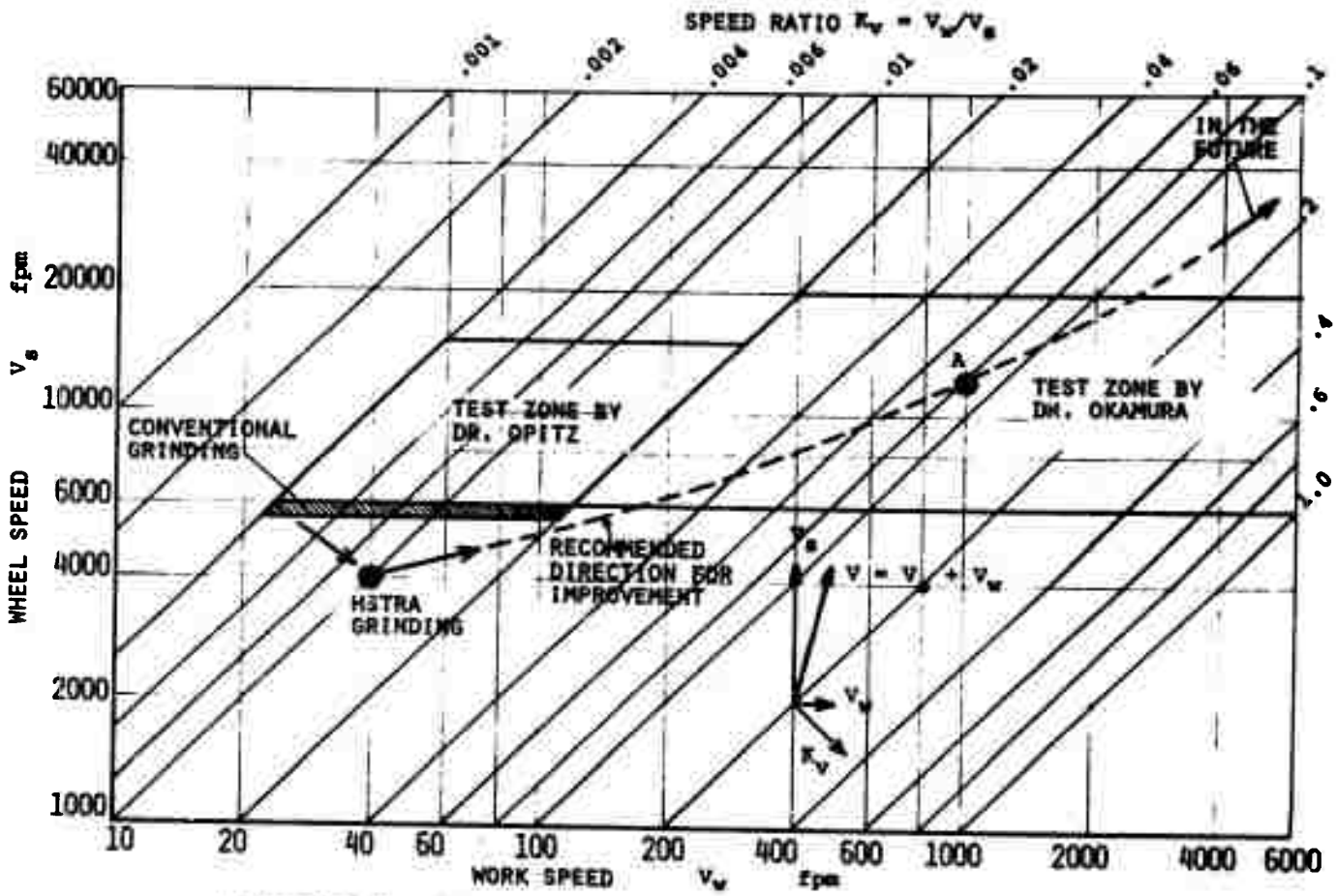

FIGURE VII-7 - RECOMMENDED HIGH EFFICIENCY GRINDING CONDITIONS

The direction recommended under this research is the direction shown as "recommended direction in the future" from point 0 through point A. This direction is the direction in which the three conditions for high efficiency grinding are best satisfied. The line at $K_v = 1$ may be the limit of further improvement of the process. The grinding investigations by trial and error have resulted in a valid conclusion that the speed ratio K_v, which has the most important effect on the surface integrity, should be increased. However in traditional grinding work there was no intention to actively improve the conditions of existing grinding machines. Furthermore traditional grinding efforts have been too particular about the finished surface integrity. Consequently the traditional conditions for HSTRA grinding are moving in a reverse way with respect to the relative cutting speed. It should be noted from this that a scientific study is very important.

VII.6 Difficulties In Practice Of The Recommended High Efficiency Grinding

It is very easy to start in the recommended direction of high efficiency grinding as described in Section VII.5 and even the first step will yield great benefits.

In order to significantly develop high efficiency grinding, several difficulties should first be overcome. The difficulties are concerned both with the machine and with the grinding wheel.

VII.6.1 High Efficiency Grinding Machine

High efficiency grinding machines should have capabilities of high work speed and high wheel speed. Many existing grinding machine wheel heads have a specially designed bearing capable of high rotational speeds so it is not so difficult to increase the wheel speed. On the other hand, the work head has been designed only for the purpose of turning at low revolution speeds and therefore needs more improvement than the wheel head in order to obtain the capabilitiey of grinding with high speed ratio K_v. A new type work head may be required for high efficiency grinding machine. One of the most basic difficulties is the stiffness of the high speed grinding machine. In precision grinding the machine stiffness or rigidity of the grinding system is very important. For some cases if no consideration of the decrease of the stiffness of the grinding machine due to the speed up is considered, the grinding results may be misinterpreted even under the improved grinding conditions. As a part of this study, high efficiency grinding tests have been carried out at high speed ratio with some simple modification of the grinding machines as shown in Figure VII-8 .

The differences between the metallurgical results shown in Figure VII-9 of the old and high efficiency grinding are not as remarkable as expected. Since modifications of the grinding machine resulted in low machine stiffness, this may have affected the resulting residual stress distributions. In conclusion, the grinding machine to be developed for high

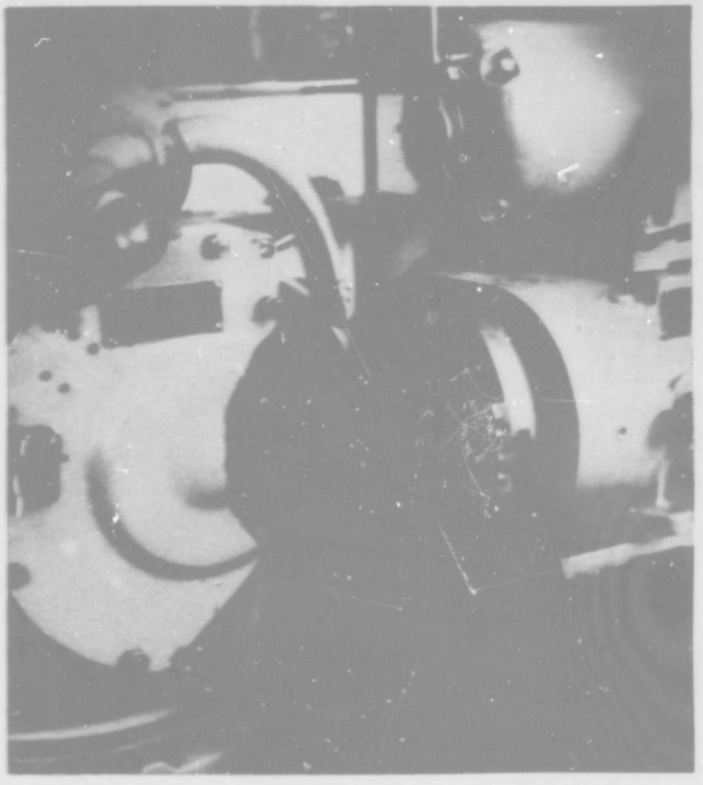

FIGURE VII-8 - PHOTOGRAPH OF HIGH WORK SPEED SURFACE GRINDING TEST SET-UP

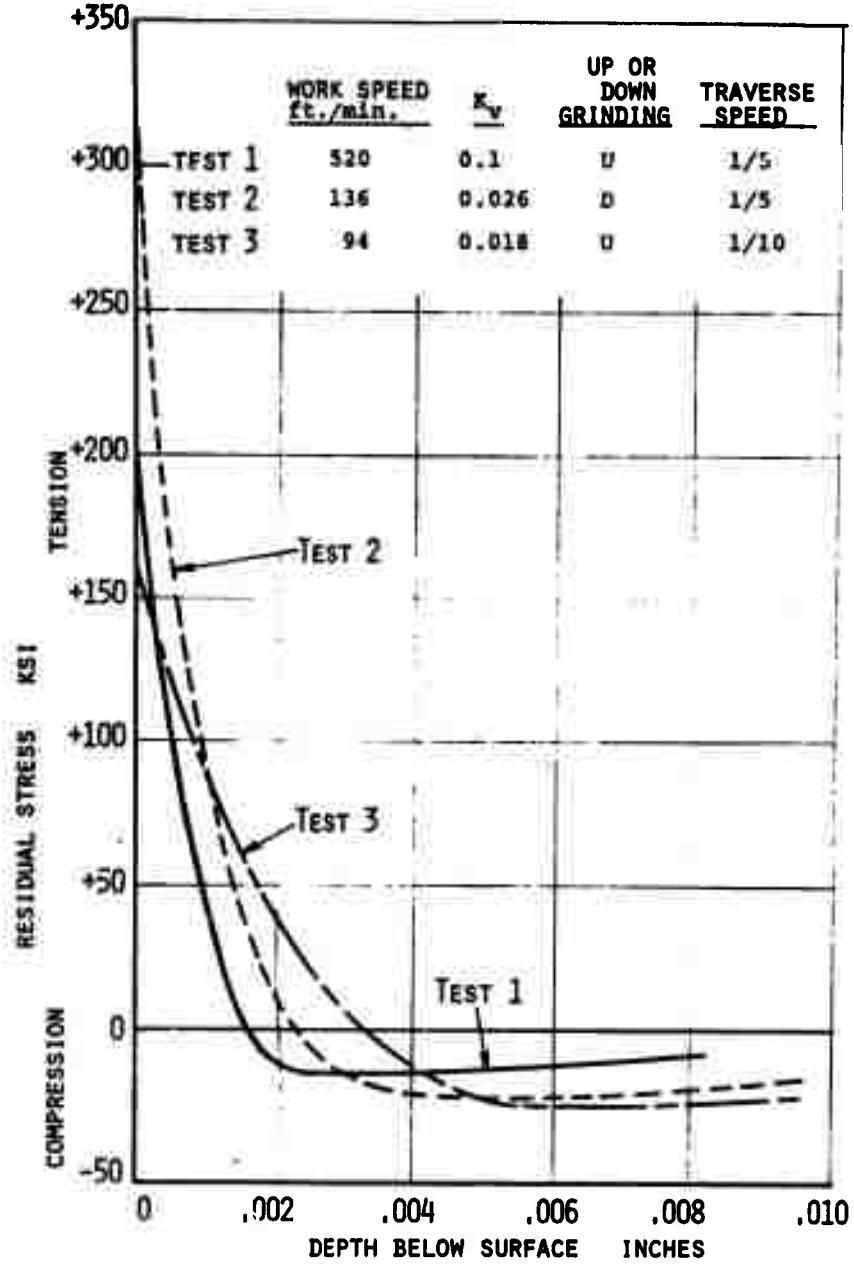

FIGURE VII-9 - RESIDUAL STRESS DISTRIBUTION

efficiency grinding must have the capabilities for high work speed, high wheel speed and high stiffness.

VII.6.2 Grinding Wheel

The essential problem of the grinding wheel at present is the limit of the allowable cutting speed. Most grinding wheel manufacturers speed test grinding wheels at two to three times greater speed than the recommended maximum speeds. From speed tests of this type it has been determined that allowable speeds for vitrified wheels are about 6000 ft/min. At a time when grinding machines with high stiffness based on the vibrations of the machine-grinding system can be made available, the allowable wheel speeds for present wheels can be made much greater. The breaking of the grinding wheel is due to centrifugal force. A reinforced grinding wheel, which can withstand much higher speeds than present ones, can be made by filling the pores in the inner part of the grinding wheel eliminating the breakage problem.

Another big problem is one of cutting edge generation method as pointed out in Section IV. The present dressing method is inadequate for good cutting edge generation. Judging from the fact that the contact area in the clearance surface of the cutting edge has a significant effect upon the ground surface integrity as analyzed theoretically in Section II, a special consideration should be made for the cutting edge generation method. The vibration dressing method described in Section IV is a good solution for this problem.

VII.7 Practical Example

The relation between grinding results and inputs will be discussed by considering for example, the effect of input variables on residual stress. The causes of residual stress can be classified as mechanical strain, thermal strain and crystallographic strain. Therefore the minimization of each type of strain will yield the minimum residual stress. Figure VII-10 schematically shows the process for finding the optimum grinding conditions for residual stress based on the theoretical and experimental analysis of the wheel-work interaction of the previous sections. The most important parameters involved in the minimization of residual stresses are relative cutting speed and speed ratio K_v.

The differences of grinding efficiency between the traditional grinding conditions (Point O in Figure VII-7) and one of the high efficiency grinding conditions (Point A in Figure VII-7) selected from the range where high efficiency grinding can be put into practice with existing techniques are calculated and shown in Table VII-1 . In this calculation it is assumed that the grinding efficiency is proportional to the workspeed. However the chip formation mechanism is improved with the increase of the relative cutting speed, and therefore the grinding efficiency under the new recommended condition is several percent greater.

Furthermore the calculation in Table VII-1 has been made on the following basic consideration. In rough grinding,

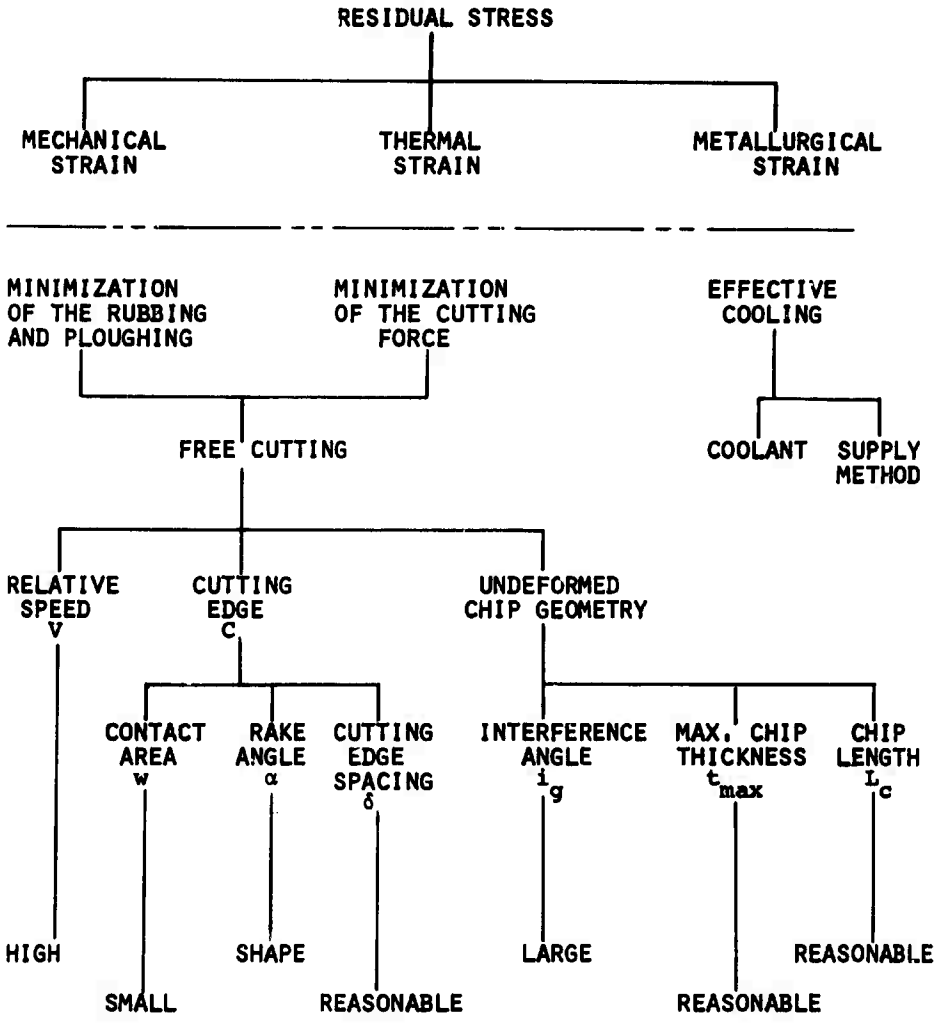

FIGURE VII-10 - RESIDUAL STRESS MINIMIZATION

TABLE VII-1 - GRINDING EFFICIENCY

ROUGH GRINDING		OLD HSTRA GRINDING COND. (Point 0 in Fig. VII-7)	NEW RECOMMENDED CONDITION (Point A in Fig. VII-7)
GRINDING CONDITION	Wheel Speed V_s (fpm)	4000	12,000
	Work Speed V_w (fpm)	40	1,000
	Speed Ratio K_v	.010	.083
	C.D.W. d (in/work rev.)	.001	.001
GRINDING EFFICIENCY	Time	1 (Standard)	.04
	E_G	1	25

FINISH GRINDING		OLD HSTRA GRINDING COND. (Point 0 in Fig. VII-7)	NEW RECOMMENDED CONDITION
GRINDING CONDITION	Wheel Speed V_s (fpm)	4000	12,000
	Work Speed V_w (fpm)	40	120
	Speed Ratio K_v	.010	.010
	C.D.W. d (in/work rev.)	.0003	.0003
STOCK FOR FINISH	in.	.010	.002
GRINDING EFFICIENCY	Time	1 (Standard)	.066
	E_G	1	15

the high relative cutting speed and the high speed ratio are utilized in order to remove most of the unnecessary part of the workpiece as chips in the free cutting range. The distribution of the residual stress on the finished surface in recommended high efficiency grinding is different from that in traditional grinding and is concentrated on a more shallow layer under the ground surface (a tenth of the depth of that for traditional grinding).

However the maximum value of the residual stress is larger than that of traditional grinding because the grinding forces increase with an increase of the speed ratio K_v in spite of the free cutting mechanism. Therefore only the small layer where the residual stress is concentrated need be removed with low K_v grinding for the finish operation. The stock that should be removed in finish grinding can be as small as a fifth of that for the traditional finish grinding because of the concentration of the residual stresses.

Grinding tests under the conditions shown in Table VII-1 were demonstrated at the University of Cincinnati in August, 1967. The demonstration for high efficiency grinding was attended by engineers from the aircraft industry and grinding machine industry. The significantly higher grinding efficiency and the much better surface finish under the new recommended grinding condition were of great interest to those who attended.

The grinding machine used for this demonstration was machine #2 and the reinforced grinding wheels were sent from Dr. K. Okamura's laboratory in Japan. The demonstration for high efficiency grinding was a preliminary test using the old grinding machine for high speed and the special grinding wheel. Remarkable improvements of HSTRA grinding can be obtained beyond the expectations presented in Table VII-1 with a specially designed grinding machine for high speed and a well-designed wheel.

VII.8 Conclusion

The purpose of investigations on cutting operations is to increase the efficiency of production. In this section high efficiency grinding with the improvement of the surface integrity has been discussed based on the theoretical and experimental analysis of the wheel-work interaction. Then the optimum direction for high efficiency grinding, which has never been obtainable from the traditional efforts, has been recommended. The recommended high efficiency grinding process has also been proven by experiment.

Furthermore the direction for improving grinding machines and wheels in order to put into practice the recommended high efficiency grinding has been pointed out.

In conclusion, grinding should be carried out at as high a relative cutting speed as possible and at a much higher

speed ratio than present practice. In other words, both the wheel speed and the work speed should be increased as high as possible with emphasis on the increase of the work speed. These increases yield much improved grinding efficiency and much better surface integrity.

SECTION VIII

GENERAL CONCLUSIONS

VIII.1 Conclusions

The method of study of grinding process as applied to High-Strength and Thermal Resistant Alloys under the contract AF33(615)-5412 has followed a carefully decided scientific plan rather than the traditional one in which HSTRA materials are ground under various grinding conditions changed at random. In this study the wheel-work interaction, which is basic and essential for describing the grinding process, has been analyzed theoretically and verified experimentally by using a simplified grinding model. This study of the wheel-work interaction has been divided into several phases which include chip formation analysis, thermal analysis, grinding wheel analysis and dynamic analysis. Conclusions pertaining to these specific phases of this program are presented in their corresponding sections of this report.

The application of this basic approach has made it possible to understand in general the grinding process and has led to the following results.

(1) Various phenomena in the wheel-work interaction were identified and described.

(2) Input variables which have a direct relation to grinding results were extracted from complicated grinding conditions.

(3) Analyzing the effects of the transitional cutting operation on the finished surface yielded means of grinding at high efficiency with improved surface integrity.

(4) Rubbing and ploughing phenomena in the grinding process were analyzed and then means of decreasing the effects of these phenomena were discussed.

(5) A grinding model sufficient for analyzing the grinding process was proposed based upon geometrical, elastic and plastic behavior in the wheel-work interaction.

(6) The usefulness of the grinding model to aid in the selection of fundamental parameters in grinding was verified by experimental tests.

(7) Thermal analysis determined the effect of coolants on temperatures in grinding. Furthermore, relations between temperatures in the region of a single grain and those at the finished workpiece surface were established through considerations of undeformed chip geometry.

(8) Investigation of grinding wheel characteristics pointed out parameters which are important in determining the effect of grinding wheels on grinding results.

(9) New wheel dressing techniques were devised and yielded significant improvements in the number and sharpness of cutting edges.

(10) Vibration analysis determined the parameters which govern stability of grinding processes, experimental

verification was accomplished, and criteria for improving grinding process stability were established.

VIII.2 Recommendations

The purpose of this study is to improve grinding technique for HSTRA materials. The direction of improvement of HSTRA grinding has been presented based upon the analyses of wheel-work interaction. Recommended high efficiency grinding is described in Section VII.

Traditional grinding methods (so called gentle grinding) for HSTRA specify low stock removal rates with low cutting speeds and small cutting depths of the wheel. These conditions result in longer grinding times (lower efficiency) and increased rubbing and ploughing of cutting edges. In rough grinding, the traditional grinding conditions can result in a deeper affected layer than would result from high efficiency rough grinding. The deeper affected layer therefore requires more time to be removed by finish grinding

High efficiency grinding recommended as a result of this work is based on the following principles:

(1) In rough grinding the affected layer should be made as shallow as possible and still maintain high grinding efficiency.

(2) In finish grinding only the shallow affected layer need be removed to obtain good surface integrity.

From the above point of view, rough and finish grinding conditions are recommended as follows:

Rough Grinding

(1) Make the workspeed as high as possible.

(2) Make the speed ratio K_v and cutting depth of *grain* as large as possible.

(3) Make the relative cutting speed as high as possible.

The exact values of speed ratio, relative cutting speed, and grain depth of cut are dependent on many factors in a particular grinding process and are limited in some cases, for example by machine capabilities. However, the above recommendations indicate the *direction* which should be taken to improve grinding processes.

Finish Grinding

(1) Reduce stock removal rate preferably by reducing infeed.

(2) Maintain a high relative cutting speed.

(3) Remove approximately a 0.002 in. layer of stock by finish grinding.

(4) Grind the workpiece in the opposite direction of rough grinding in order to offset plastic flow. This recommendation will require some design changes but in the future will yield further improvements in surface integrity.

It is now possible with new machines and wheels to perform grinding under the following conditions:

	K_v	Workspeed(fpm)	Wheelspeed(fpm)
Rough Grinding	.09	1100	12,000
Finish Grinding	.01	120	12,000

These conditions are recommended for use with machines and wheels designed for these speeds, which are now being made available by several companies. However, improvements in grinding efficiency can be realized on *present* machines by increasing K_v and relative cutting speed.

VIII.3 Future Development

VIII.3.1 Introduction

The ultimate goal of grinding process studies is the application of adaptive control methods to the grinding process, because this will allow maximum productivity and quality to be maintained under transient grinding conditions (for example, the wearing of the grinding wheel with time). The elimination of human errors from the machining process will result in consistent and repeatable quality of production parts.

In order to accomplish this work it is necessary to establish optimum working conditions. The criteria for defining optimum working conditions will be based on production efficiency (maximum stock removal rate and workpiece quality with minimum wheel loss and dressing time). The next step leading to the adaptively controlled grinding process is the choice of parameters to be measured in process, and the measuring equipment to be used (for example, in-process gaging of workpiece dimensions). Finally, a machine could be instrumented and tested.

VIII.3.2 Proposed Optimization Studies

Two basic approaches can be used for determining optimum working conditions. The first approach is to further extend

and unify the areas of chip formation physics, wheel characteristics, thermal analysis, and dynamic stability criteria to determine a complete, overall description of the wheel-work interaction zone. Then, with the use of computer simulation of the grinding process and overall grinding experimentation it will be possible to establish the optimum working conditions. This approach would ultimately provide the most thorough description of the grinding process and would be most likely to yield true optimum conditions. However, this method is also the most complicated and would involve a great deal of time before practical applications could be made.

The second approach is to perform optimization studies in specific areas and to combine the best conditions from each area in order to give the best input to wheel-work interaction zone. Then it will be possible to determine the best overall grinding conditions from grinding experiments.

This approach would yield results of immediate practical interest and could be accomplished in a shorter period of time. However, the results could not be expected to be completely comprehensive since all interrelated aspects of the different areas could not be considered. Several examples of proposed optimization studies in individual areas are discussed below.

From the thermal analysis performed under this contract it has been concluded that the desired lubrication and cooling properties of a grinding fluid may depend on the grinding time. Therefore, one area of investigation is to minimize grinding temperatures by either optimizing lubrication or cooling

functions of some grinding fluids, and specifying conditions under which one or the other of these functions is most important.

From the development of the vibration dressing technique it was possible to greatly increase the number of cutting edges and improve their sharpness. The conditions of optimum wheel surface properties would be determined. This requires comparison of vibration and crush dressing techniques, (Vibration and conventional dressing methods have already been compared) and then choosing the best dressing method and determining proper conditions for obtaining the optimum results by this dressing method.

Dressing time can be reduced and dynamic stability improved by retarding wheel loading. Therefore, an investigation of the effect and mechanism of high pressure oil jet wheel cleaning, particularly applicable in the case of HSTRA grinding, can yield optimum methods for cleaning the wheel and penetrating the wheel with lubricant.

The optimum wheel characteristics to give the best wheel-work contact stiffness from the standpoints of vibrational instabilities and the rate of growth of instabilities can be determined.

When the optimum conditions are determined for these cases, grinding experiments can be performed to determine the proper ranges of wheel speeds and work speeds for the best grinding results (efficiency and surface integrity).

From the basic knowledge developed under the present contract, the directions for performing various optimization

studies and for improving efficiency have been pointed out. Significant steps toward optimizing grinding processes can now be undertaken, which will lead to extensive development and practical improvement of grinding.

REFERENCES

Section I - General Description

1. Tarasov, L.P., Grover, H.J., Hyler, W.S., and Letner, H.R., "Effects of Grinding and Other Finishing Processes on the Fatigue Strength of Hardened Steel," Proceedings of ASTM, Vol. 50, 1950, Vol. 57, 1957, Vol. 58, 1958.

2. Tarasov, L.P., "How to Grind Titanium," American Machinist, Vol. 96, November 1952.

3. Letner, H.R., "Residual Grinding Stresses in Hardened Steel," Trans. ASME, October 1955.

4. Yang, C.T. and Shaw, M.C., "The Grinding of Titanium Alloys", Trans. ASME, July 1955.

5. Halverstadt, R.D., "Analysis of Residual Stress in Ground Surfaces of High-Temperature Alloys," Trans. ASME, May 1958.

6. Clorite, P.A. and Reed, E.C., "Influence of Various Grinding Conditions in Residual Stress in Titanium," Trans. ASME, Vol. 80, 1958.

7. Cadwell, D.E., Weisbecker, H.L., and McDonald, W.J., "Grinding a Titanium Alloy with Coated Abrasive," ASME Paper No. 58-SA-44, June 1958.

8. Olofson, C.T., Boulger, F.W., and Gurklis, J.A., "Machining and Grinding of Titanium and Its Alloys," NASA Technical Memorandum, NASA TMX-53312, August 1965.

9. Zlatin, N., Field, M., and Koster, W.P., "Machinability of Materials," Technical Report AFML-65-555, January 1966.

10. Hahn, R.S., "The Effect of Wheel Work Conformity in Precision Grinding," Trans. ASME, Vol. 77, No. 8, 1955.

11. Shaw, M.C., "The Role of Chip Thickness in Grinding," Trans. ASME, Vol. 78, No. 4, 1956.

12. Merchant, M.E., and Backer, W.S., "On the Basic Mechanics of the Grinding Process," ASME Paper No. 56-A-43, November 1956.

13. Hahn, R.S., "On the Nature of the Grinding Process," Proceedings of the Third International Conference on Machine Tool Design and Research, Sept. 1962.

14. Hahn, R.S., "On the Mechanics of the Grinding Process Under Plunge Cut Conditions," ASME Paper No. 65-Prod-7, July 1965.

15. Merchant, M.E., "Mechanics of the Metal Cutting Process," Journal of Applied Physics, Vol. 16, 1945.

16. "Machining Data Handbook," Published by Metcut Research Associates, Inc., 1966.

17. "Grinding Stress," Published by Grinding Wheel Institute.

Section II - Chip Formation Physics

1. Okamura, K., "The Cutting Mechanism of Abrasive Grain," Bulletin of JSME, Vol. 3, No. 12, 1960.

2. Takenaka, N., "A Study of the Grinding Action by Single Grit," C.I.R.P., Stressa, Italy, 1964.

3. Timoshenko and Goodier, Theory of Elasticity, McGraw Hill, 1951.

4. Alden, G.I., "Operation of Grinding Wheels in Machine Grinding," Trans. ASME, Vol. 36, 1914.

5. Manjoine, M.J., "Influence of Rate of Strain and Temperature on Yield Stresses of Mild Steel," Trans. ASME, 1944.

6. Davis, E.A., "The Effect of the Speed of Stretching and the Rate of Loading on the Yielding of Mild Steel," Trans. ASME, 1938.

7. Shaw, M.C., "The Size Effect in Metal Cutting," Trans. ASME, Vol. 74, January 1952.

8. Shaw, M.C. "Cutting Characteristics with Variable Undeformed Chip Thickness," CIRP-Annals, Vol. 10, 1963.

9. Kobayashi, S., Shabaik, A., "Chip Formation with Varying Undeformed Chip Thickness at Very Slow Speed." ASME Paper No. 64, Prod-8., 1964.

10. Field, M., Merchant, M.E., "Mechanics of Formation of the Discontinuous Chip in Metal Cutting." Trans. ASME., July 1949.

REFERENCES (Continued)

11. Chang Keng Lui, "Stresses and Deformations due to Tangential and Normal Loads on an Elastic Solid with Applications to Contact Stresses," Ph.D. Thesis, University of Illinois, May 1950.

12. Povitsky, H., "Stresses and Deflections of Cylindrical Bodies in Contact with Application to Contact of Gears and of Locomotive Wheels," Journal of Applied Mechanics pp. 191-201, June, 1950.

13. Weber, C., "The Deformation of Loaded Gears and the Effect on Their Load-Carrying Capacity," Institut fur Maschinenelemente Einzelbericht Nr102., Braunschweig, 1949.

14. Greenwood, J.A., Tripp, J.H., "The Elastic Contact of Rough Spheres," Trans. ASME - Series E, Vol. 34, March 1967.

15. Okamura, K., "The Cutting Mechanism of Abrasive Grain (2nd Report)," Bulletin of JSME, Vol. 3, No. 12, 1960.

16. Okamura, K., Nakajima, T., "Study on Cutting Mechanism of Abrasive Grain (6th Report)," Journal of JSPE, Vol. 33, No. 5, 1967.

17. Hertz, H., "On the Contact of Elastic Solids," Journal Math., Vol. 92, 1881, (See also H. Hertz's "Gesammelte Werke," Vol. 1, Leipzig, 1885).

18. Hertz, H., "On the Contact of Rigid Elastic Solids and on Hardness," Gesammelte, Vol. 1, Leipzig, 1895.

19. Mindlin, R.D., "Compliance of Elastic Bodies in Contact," Journal of Applied Mechanics, Trans. ASME, Vol. 72, 1950.

20. Smith, J.O., and Chang Kung Liu, "Stresses and Deformations Due to Tangential and Normal Loads on an Elastic Solid with Applications to Contact Stress Problems," Journal of Applied Mechanics, June, 1953.

21. Price, R.L., "Measurements of Stiffness Variations in Grinding Wheels," M.S. Thesis, Worcester Polytechnic Institute, May 1967.

22. Galin, L.A., Contact Problems in the Theory of Elasticity (Translated from the Russian by Mrs. H. Moss) Published by North Carolina State College, October 1961.

23. Muskhelishvili, N.I., Some Basic Problems of the Mathematical Theory of Elasticity (Translated from the Russian by J.R. Radok), Moscow, 1949.

24. Hill, R., The Mathematical Theory of Plasticity, Oxford University Press, New York 1950.

Section III - Thermal Analysis In Grinding

1. Malkin, S., "The Attritious and Fracture Wear of Grinding Wheels," ScD. Thesis, M.I.T., February 1968.

2. Sato, K., "Grinding Temperature," Bulletin Japan Soc. of Grinding Engineers, Vol. 1 (1961), pg. 31.

3. Jaeger, J.C., "Moving Sources of Heat and the Temperature at Sliding Contacts," Proc. Royal Soc. of New South Wales, Vol. 76, 1942, pg. 203.

4. Outwater, J.O., and Shaw, M.C. "Surface Temperatures in Grinding," Trans. ASME, Vol. 74, January 1952, pg. 73.

5. Mayer, J.E., and Shaw, M.C. "Grinding Temperatures" Journal of ASLE, January 1957, pg. 21.

6. Littman, W.E., and Wulff, J., "The Influence of the Grinding Process on the Structure of Hardened Steel." Trans. ASM, Vol. 47, 1955, pg 692.

7. Takazawa, K., "Effects of Grinding Variables on Surface Structure of Hardened Steel," Bulletin of Japan Soc. of Precision Engineering, Vol. 2, No. 1, April 1968.

8. Opitz, H. and Guhring, K., "High Speed Grinding," 17th C.I.R.P. General Assembly, Ann Arbor, Michigan, September 1967.

9. Whitehead, C.S., "On a Generalization of the Functions ber_x, bei_x, ker_x, kei_x," Quarterly Journal of Mathematics, Vol. 42, 1911, pg. 316.

10. DesRuisseaux, N., "Thermal Aspects of Grinding Process" Ph.D. Thesis, University of Cincinnati, August 1968.

REFERENCES (Continued)

Section IV - Grinding Wheel Characteristics

1. Peklenik, J., "Testing the Grade of Grinding Wheel" Microtechnic, Vol. 14, No. 5., 1960.

2. Kleinschmidt, B., "Schleif-und Poliertechnik", Bd. 1, 1950.

3. Spath, W., "Werkstattecnik und Machinenbau", Heft 9, 1951.

4. Imanaka, O., "Grade Test of Grinding Wheel," Kikaikosaku, 1963.

5. Spath, W., "Ind. Diamond Review", Vol. 16, No. 187., 1956.

6. Okamura, K., "The Cutting Performance Test of Abrasive Stone." Trans. JSME, Vol. 22, No. 122., 1956.

7. Asaeda, T., "Finishing Mechanism of Superfinish," Tokyo Institute Technology Report No. A-3., 1950.

8. Colwell, L.V., Lane, R.O., and Soderlund, K.N., "On Determining the Hardness of Grinding Wheels - I", Trans. ASME, Ser. B, Vol. 84., 1962.

9. Colwell, L., Lane, R.,Soderburg, K., "On the Determination of the Hardness of Grinding Wheels - II", ASME Series B, Vol. 85., 1963.

10. Colwell, L., "A Process for Determining the Hardness or Grade of Grinding Wheels," University of Michigan, March, 1962.

11. Peters, J. and Snoeys, R., "The E Modulus, A Suitable Characteristic of Grinding Wheels," Report CRIF MC 9, University of Louvain, August 1965.

12. Snoeys, R., "Recherche des Proprietes des Meules Abrasives," Report CRIF MC 3, University of Louvain, March 1964.

13. Peklenik, J., "Neue Statische und Dynamische Prufmethoden der Physicalisch - Mechanische Eigenschaften von Schleifkorpern" 18. Forschungs bericht, T.H. Aachen (Prof. Opitz), 1960.

14. Peklenik, J., Lane, R., Shaw, M., "Comparison of Static and Dynamic Hardness of Grinding Wheels," ASME, Series B, Vol. 86, August 1964.

REFERENCES (Continued)

15. Okamura, K., Nakajima, T., "Study on the Cutting Mechanism of Abrasive Grain (2nd Report)," JSPE, Vol. 32, No. 8 (1966), 551.

16. Munich, H., "Beitrag zur Sicherheit von unlaufenden Schleifhorpern," Diss. T.H. Hannover, (1965).

17. Krug, H., and Honica, G., "Die Elastische Verformung bei Schleifwerkzeugen," Werkstattlechnik 54, (1964), Heft 2, 553.

18. Yoshikawa, H., "Fracture Wear of Grinding Wheel," Scientific paper of I.P.C.R., Tokyo, Japan, Vol. 57, No. 4, 1963.

19. Frank, H., "Das Abrichten von Schleifsheiben mit Diamanten und der Einfluss auf das Schleifergebnis beim Assenrund-Einstechschleifen," Ph.D. Thesis, Aachen, Germany, 1963.

20. Okamura, K., "The Relation Between Wheel Life and Dressing Method," Japan Society of Grinding Engineers, Vol. 1, No. 1, 1964.

21. Tsuwa, H., "On the Behavior of Abrasive Grains in Grinding I," Journal of Society of Precision Mechanics, Japan, Vol. 26, 1960.

22. Malkin, S., "The Attritious and Fracture Wear of Grinding Wheels," Sc.D. Thesis, M.I.T., Feb., 1968.

23. Tsuwa, H., "An Investigation of Grinding Wheel Cutting Edges," ASME Engineering for Industry, Vol. 86, No. 14, 1964.

24. Yoshikawa, H., "Criterion of Grinding Wheel Tool Life," Bulletin Japan Society of Precision Engineers, Vol. 1, No. 1, October, 1963.

25. ... "Etude Sur La Rectification en Plongee et Les Conditions de Dressage," Centre de Rescherches Scientific et Techniques de L"Industrie des Fabrications Metalliques, Vol. 17, Sept., 1966.

26. Pahlitzch, G. and Appun, J., "Effect of Truing Conditions on Circular Grinding," Industrial Diamond Review, Vol. 14, No. 166, Sept., 1954.

27. Gerhardt, J., "Effects of Dressing Method on Grinding Wheel Properties," M.S. Thesis, University of Cincinnati, August 1968.

Section V - Dynamic Analysis In Grinding

1. Final Report on "Effect and Control of Chatter Vibrations in Machine Tool Processes," Project No. 7-771, Air Force Contract No. AF33(657)-9143, The Cincinnati Milling Machine Co., Cincinnati, Ohio.

2. "Research and Development on the Effect and Control of Chatter Vibrations in Machine Tool Processes," Interim Engineering Progress Reports I through IV, MMP Project Nr. 7-771, Air Force Contract No. AF33(615)-2661, The Cincinnati Milling Machine Co.

3. "Contributions to Machine Tool Chatter Research V," Survey of Chatter Research at Cincinnati Milling Machine Co. Proceedings of the 5th International Machine Tool Design and Research Conference, Birmingham, England, September 1964, Pergamon Press.

4. "Effect and Control of Chatter Vibrations in Machine Tool Processes," Scientific Report Number 1, Air Force Contract AF61(052)-966, Technischen Hochschule Aachen, Aachen, Germany.

5. "Effect and Control of Chatter Vibrations in Machine Tool Processes," Scientific Report Number 2, Air Force Contract AF61(052)-966, Technischen Hochschule Aachen, Aachen, Germany.

6. "Research on Control of Forced Vibration in Machine Tool/ Metal Cutting Systems," Interim Engineering Progress Reports I through V, MMP Project Nr. 8-364, Air Force Contract No. AF33(615)-2664, University of Cincinnati.

7. Merritt, H.E., "Theory of Self-Excited Machine-Tool Chatter," Trans. ASME, Series B, November 1965, pp. 447-454.

8. Snoeys, R., "Broutement en Rectification," C.I.R.P. Meeting, Paris, September 1966; MC14 Report CRIF, Louvain.

9. Snoeys, R., "Instabiliteit van het Slijpproces," CRIF Report MC13, Ph.D. Thesis (Prof. Peters), University of Louvain, July 1966.

REFERENCES (Continued)

10. Peters, J., and Vanherck, P., "Ein Kriterium fur die Dynamische Stabilitat von Werkzeugmaschinen," Industrie Anzeiger, Feb. 1963.

11. Peters, J., "La Determination Pratique des Conditions d'usinage Stable en Machine-outils," Mecanique Industrielle, September 1963.

12. Vanherck, P., "Quelgues Aspects Complementaires Concernants la Stabilite de Coupe Avec Outils a pas non Uniformes," CIRP, Paris 1966.

Section VII - Recommended High Efficiency Grinding

1. Okamura, K., and Nakajima, T., "Study on Ultra-high Speed Grinding." Research Report, Kyoto University, 1967.

2. Opitz, H. and Guhring, K., "High Speed Grinding," 17th C.I.R.P. General Assembly, Ann Arbor, Michigan, September 1967.

Security Classification

DOCUMENT CONTROL DATA - R & D

(Security classification of title, body of abstract and indexing annotation must be entered when the overall report is classified)

1. ORIGINATING ACTIVITY *(Corporate author)*

University of Cincinnati
Cincinnati, Ohio 45221

2a. REPORT SECURITY CLASSIFICATION

Unclassified

2b. GROUP

3. REPORT TITLE

STUDY OF GRINDING PROCESS AS APPLIED TO HIGH-STRENGTH AND THERMAL RESISTANT ALLOYS

4. DESCRIPTIVE NOTES *(Type of report and inclusive dates)*

Final Report, 1 July 1966 to 30 September 1968

5. AUTHOR(S) *(First name, middle initial, last name)*

Dr. Kenjiro Okamura, Toshikatsu Nakajima, David Brown
Dr. Neal R. DesRuisseaux, Dr. Raymond Snoeys, Jon S. Gerhardt

6. REPORT DATE	7a. TOTAL NO. OF PAGES	7b. NO. OF REFS
September 1968	382	94

8a. CONTRACT OR GRANT NO.	9a. ORIGINATOR'S REPORT NUMBER(S)
AF33(615)-5412	IR-9-711 (I thru VI)
8b. PROJECT NO. 9-711	
8c.	9b. OTHER REPORT NO(S) *(Any other numbers that may be assigned this report)*
8d.	

10. DISTRIBUTION STATEMENT DDC Release to CFSTI not authorized. This document is subject to special export controls and each transmittal to foreign governments or foreign nationals may be made only with prior approval of the Manufacturing Technology Division (MATF), WPAFB, Ohio 45433

11. SUPPLEMENTARY NOTES

12. SPONSORING MILITARY ACTIVITY

Manufacturing Technology Division
Air Force Materials Laboratory
Wright-Patterson Air Force Base, Ohio, 45433

13. ABSTRACT

This project is engaged in a program which is directed at the study of the basic understanding of the grinding process as applied to high-strength thermal-resistant alloys. Analytical methods and testing and specification techniques have been developed that should enable significant improvements in grinding efficiency and finished surface integrity to be accomplished. Grinding is an extremely complex process with many interrelated phenomena occurring simultaneously. For this reason an attempt is made to look at all aspects of grinding processes with the wheel-work interaction analysis taken as the basic standpoint for all of the analyses. The group of investigators is organized from many specialists in various technologies such as manufacturing, heat transfer, metallurgy and vibration. The chip formation mechanism in the grinding process has been clarified and the relationship between working conditions and grinding results are discussed from a scientific viewpoint. Thermal analyses have been presented which can be used to investigate the heat effect upon the finished surface. A set of scientific grinding wheel characteristics have been defined such that a better understanding of the grinding process when used as a cutting operation can be gained. The machine tool-grinding system has been investigated using vibrational analysis techniques to determine the effects of machine dynamics and to improve the grinding efficiency for HSTRA materials. In conclusion, new high efficiency grinding techniques which yield extremely high production rates for grinding HSTRA materials have been recommended from this study.

DD FORM 1 NOV 68 1473

Security Classification

14. KEY WORDS	LINK A		LINK B		LINK C	
	ROLE	WT	ROLE	WT	ROLE	WT
1. Grinding Process Cutting Mechanism						
2. Thermal Analysis in Grinding						
3. Grinding Wheel Characteristics						
4. Grinding Wheel Dressing Methods						
5. High Efficiency Grinding						